Universidad de Valladolid

TESIS DOCTORAL:

SIZING AND ENERGY MANAGEMENT FOR PHOTOVOLTAIC PUMPING

Presentada por Imene Yahyaoui para optar al
grado de
doctora por la Universidad de Valladolid

Dirigida por:
Fernando Tadeo Rico
& Maher Chaabene

To my parents Saída and Lamine

Summary

Over the last few decades, photovoltaic energy has become an effective source to produce electricity that will be used either in isolated sites or injected into the grid. In isolated areas in particular, photovoltaic installations are already being used for pumping water for agriculture or human purposes, since photovoltaic installations are easy to install and, after installation, the maintenance cost is low. However, the inherent variability of the sources means that the installation has to be carefully sized so as to provide an adequate energy management algorithm.

So, this thesis focuses on the sizing and energy management of an autonomous photovoltaic installation used to pump water for irrigation in an isolated site. Typically, this type of installation is widely used in arid and semi-arid regions, such as the Maghreb and the South of Europe, where in addition, there is an important availability of solar radiation. The correct operation of these installations is needed, not only to fulfil the water demand, but also to optimize the use of the photovoltaic energy and to extend the life of the components. These objectives can be ensured by a good sizing of the components and an optimum energy management, which represents the two main contributions of this thesis.

In fact, the first part of this thesis deals with the component sizing of the photovoltaic irrigation installation, namely the photovoltaic panels and the battery bank. Hence, an algorithm for the optimum sizing of the installation components has been established, based on the crops' water requirements, the site's climatic characteristics and the restrictions inherent to the components. For this, some models of the components are selected, which have also been validated experimentally. In addition, some techniques related to the maximum photovoltaic

power extraction have been studied. Then, the sizing algorithm has been validated using measured data of the target area (Medjez El Beb, Northern Tunisia).

The second part of the thesis deals with the energy management of the photovoltaic irrigation installation. Hence, a fuzzy logic based algorithm has been established, to manage the energy generated by the panels and stored in the battery bank. Fuzzy logic has been used, since it is easy to implement and our study is based on the knowledge of the user. The main idea behind the algorithm is as follows: depending on the photovoltaic power generated, the battery depth of discharge, the water level in the reservoir and the water flux, the connection and disconnection of the components is deduced by using some proposed fuzzy rules. The algorithm's efficiency has been firstly evaluated by simulation and validated secondly in a plant installed in the laboratory, with satisfactory results.

Hence, this thesis has satisfactorily contributed to the components sizing and energy management of photovoltaic irrigation installations.

Contents

Acknowledgments

Foremost, I would like to express my sincere gratitude and thanks to all the people and professors, who helped me, supported me and were with me since my primary school until my PhD candidature.

First, to my advisors Professors Fernando Tadeo and Maher Chaabene, for their continuous support during four years of my PhD study and research, for their patience, motivation, enthusiasm, and immense knowledge. Their guidance helped me in all the time of research and writing of this thesis.

Besides my advisors, I would like to thank the reviewers of the thesis, Professors Giuseppe Tina and Mohammed Faisal, for their time, feedback and nice comments. My sincere thanks also go to the member of the jury, for their willingness and feedback.

Thanks also to the professors and technician of Systems Engineering and Automatic Control department of the University of Valladolid: César, Felipe, Gloria, María Jesús, Jesús María, Smaranda, Rogelio, Teresa, Graciano, Teresa, Carlos, Santi and María.

My special thanks go also to professors and technicians of the Electric Conversion and Renewable Energy unity of the University of Sfax, Tunisia: M.B.A, Mohsen, Souhir, Khaled and Zied, for their help during my training.

My gratitude and thanks to the professors of the department of Electric, Electronic and Informatic of the University of Catania, Italy, for their kidness, help, advices and friendship: Marco, Antonio, Cristina, Valeria, Santi, Fabio and Giovani.

My thanks to Grundfus company for providing as with the necessary equipments, the Meteorological Nationnal Institute of Tunisia and the agriculture administry of Medjez El Beb, for providing as with climatic data of Medjez El Beb.

I thank my colleagues in ISA department of the University of Valladolid: Mohammed, Luis, Daniel, Ruben, Tania, Johana, Inès, Alvaro, María, Elena, Khaled, Daniel and Diego, for the nice time we spent during these four years.

I thank my colleagues in the chemistry department of the University of Valladolid, for their support and friendship: Daniela, Victoria, Araceli, Johanna and Daniel.

My special thanks go also to my colleagues in CMERP unit (Sfax, Tunisia): Sana, Mahmoud, Souleyman, Amal and Tarek.

To all the friends I made during these years in the nicest residences “Reyes Catolicos of Valladolid, Spain” and “Caraciuollo of Catania, Italy”, for the nice memories: Mayda, Rocio, Nuria, Elena, Isabel, Rosalia, Rodrigo, Elvira, Faustino, Juan, Carlos, Roberto, Miguel, Pilar and many others.

All my love, gratitude and thanks for my sister Ameni and my brothers Jawher and Wissem and for the Yahyaoui and Askri families.

Chapter 1: Introduction

Contents

1.1 Motivation

The production of electric energy using fossil fuels (oil, coal, natural gas, etc.) has traditionally provided adequate costs, but produce greenhouse gases. In fact, fossil power generation is responsible for 40% of global CO_2 emissions [1]. Nuclear power, which does not produce directly carbon dioxide, generally suffers from poor acceptance because of significant risks and costly waste storage [2, 3].

In this context, renewable energies are positioned as a solution to fossil fuel depletion [4, 5]. For remote sites, where the grid is not available, renewable energies provide an excellent solution, since the energy sources are abundant (namely, solar radiation and wind). Moreover, given the adequate attributed support, renewable energies can meet much of the growing demand at lower prices than those usually forecast for conventional energy (by the middle of the 21^{st} century, renewable sources of energy could account for three-fifths of the world's electricity market) [6]. Moreover, the electricity can be produced near the place of consumption and without producing greenhouse gases. Hence, autonomous installations based on renewable energies are used for different applications in remote sites.

For agricultural applications, the use of Renewable Energies [7] is a promising solution, especially for remote sites. In fact, much research has studied the efficiency of renewable energies in agriculture and other critical sectors for developing countries, as in our target country, Tunisia [8, 9]. Modern cultivation techniques require regular irrigation; especially in arid and semi-arid climates [10], for which, farmers generally use diesel engine water pumps. Although this solution was efficient in the past, the continuous increase in fuel prices and the requirement that the user be present are considered the main disadvantages of these installations [11]. Hence, renewable energies are considered a good solution for farmers without easy access to fuel or for remote sites, as in our case study. In fact, we focus on a specific implementation for a 10 ha of land in Medjez El Beb (latitude: 36.39°, longitude: 9.6°), planted with tomatoes (Figure 1.1). To irrigate the crops, a diesel engine is currently being used, which is complicated, since the

site is isolated. Given the significant solar radiation during the growing season, the solution proposed here is to use a photovoltaic installation for water pumping.

Figure 1. 1 Site of the studied land

The rest of the chapter is organized as follows: Section 1.2 gives some general ideas about the state of the art in renewable energies. Section 1.3 presents the objectives of the thesis, with a summary of the main contributions and organization presented in Sections 1.4 and 1.5. Finally, some conclusions are presented in Section 1.6.

1.2 Renewable Energies

Nowadays, most of the electric energy is obtained from fossil fuels like oil, coal and natural gas, or from nuclear energy [12]. Given the growing need for energy and the reduction in fossil sources, new energy resources are required to meet global energy needs. Renewable energies, such as photovoltaic, solar thermal, wind, hydro, waves and biomass, are the best placed to fill this gap [13]. In fact, these clean energy sources are inexhaustible. These sources are currently interesting thanks to the great technological progress, the huge investments for the development of the energy production systems, and the rapid growth in the use of renewable sources [14]. Figure 1.2 shows the distribution of the primary energy sources [12].

Renewable energies can be consumed directly by loads, transported to the distribution system or stored in storage components [14]. In fact, in grid-

connected areas, they can be used as supplementary sources.

In isolated installations, where autonomy is required, the difference between the renewable energies produced and the energy needed by the loads requires the diversification of the sources or the use of storage components, such as batteries [1]. Indeed, other technologies such as fuel cells could be used to store energy [13], although, they are not yet profitable due to their complexity. Hence, the majority of off-grid installations use lead-acid batteries.

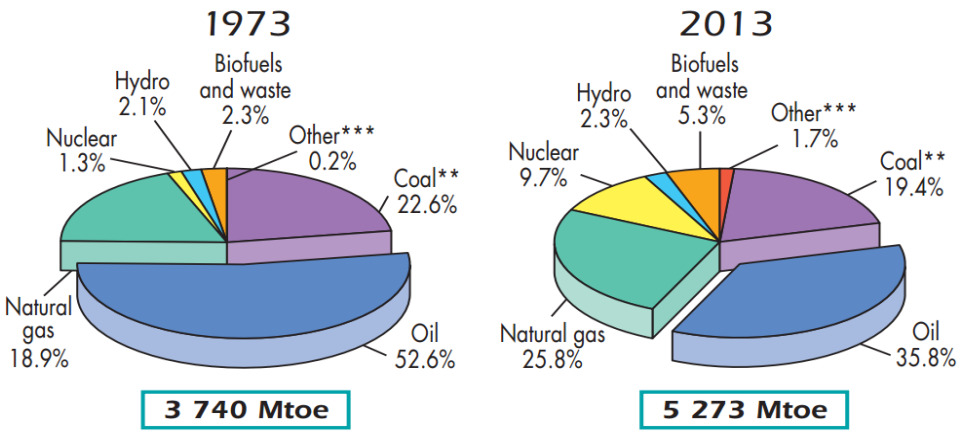

Figure 1. 2 Global primary energy [12]

Renewable energies production depends on the site and weather conditions. For instance, solar panels are effective if they are installed in well sunlit areas. Similarly, wind turbines are installed in regularly windy places [13]. The energy conversion can be classified into three main categories: electric (photovoltaic panels), thermal (solar thermal, geothermal, etc.) or mechanical (wind). Here, we give a brief description of the main energy sources currently in use (of course hybrid solutions have also been developed but they are outside the scope of this dissertation [15-17]).

1.2.1 Photovoltaic Energy

Each year, the Earth's surface receives 1.79 10^8 kWh, which is equivalent to a continuous power of 1.729 10^{17} W. It has been evaluated that 23% of this energy is reflected directly back into space, 29% is absorbed in the atmosphere and converted to heat radiated within the infrared spectrum, with the remaining 48% of the energy suppliying the hydrological cycles and photosynthesis [14]. Taking

into account the alternations of day and night and cloudy periods, the peak power is estimated to be 1kW [14].

The solar energy is converted to electricity by the junction charge carrier (contact between two different types of semi-conductors: p-type and n-type) [18, 19]. Although the material required for making the photovoltaic modules (Silicon) is abundant and inexpensive, the complexity of the construction techniques makes these modules relatively expensive [20]. However, technological advances are being made to enhance their competitiveness, such as the use of Maximum Power Point Tracking (MPPT) techniques [21, 22] and cells yield enhancement [23], which makes them a good solution, especially for isolated areas, thanks to their simplicity in installation. These facilities increase the worldwide photovoltaic energy use. Figure 1.3 describes the evolution of the global photovoltaic cumulative installed capacity between 2000 and 2013 [24].

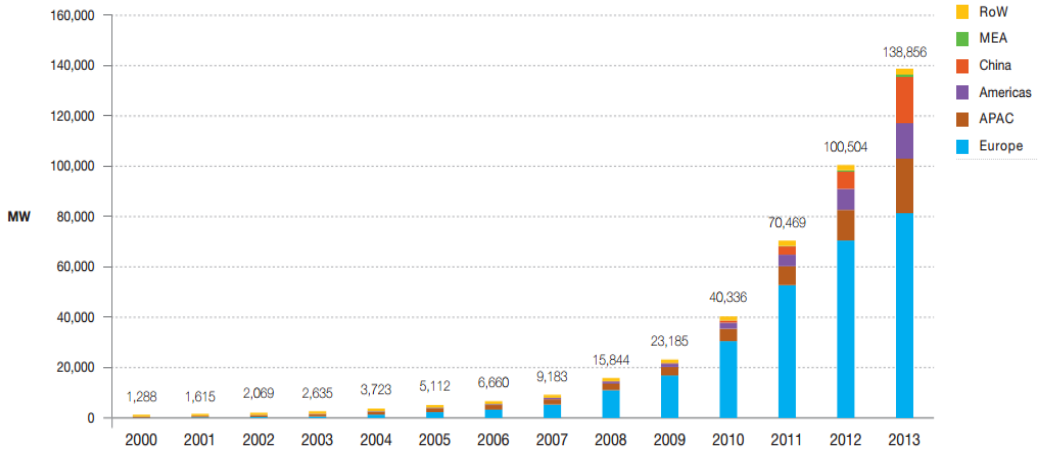

Figure 1. 3 Evolution of the global photovoltaic cumulative installed capacity 2000- 2013 [24]

The configuration of the components in the photovoltaic installations depends on the application. Some of them are now detailed:

a. Serial Configuration

In this case, all the photovoltaic energy produced passes through the battery bank, is converted from DC to AC by the inverter, and then transferred to the AC load (Figure 1.4) [13, 25].

This configuration is easy to install and can supply the load continuously. However, the excessive use of the battery bank decreases its lifetime. Moreover, it requires a large capacity to reduce its depth of discharge. Furthermore, the installation's efficiency is reduced, since all the energy flows through the battery bank and the inverter.

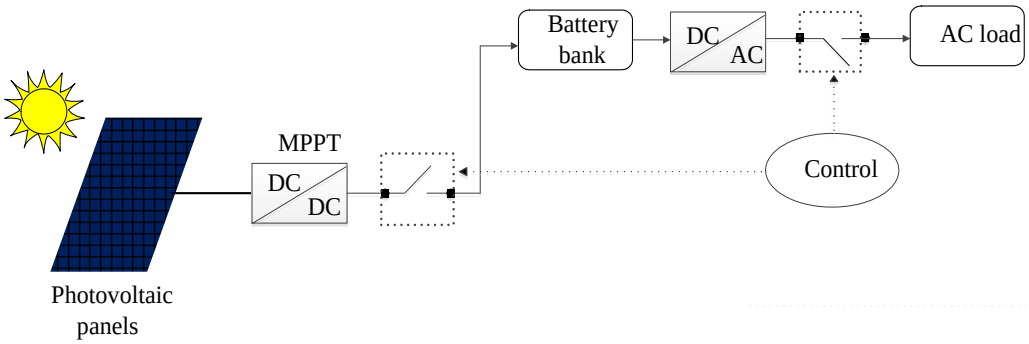

Figure 1.4 Serial architecture for photovoltaic installations

b. Parallel Configuration

The parallel configuration allows all energy sources to supply the AC load separately [25, 26] (Figure 1.5).

In the case of an excess in photovoltaic energy generation, the bi-directional converter charges the battery bank. Hence, the load can be met by the panel, the battery bank, or both. Moreover, a reduction in the rated battery bank capacities, inverter and photovoltaic panel is feasible, while also meeting the demanded load peaks and ensuring the installation's autonomy and the battery efficiency [26].

These objectives can only be met if the installed components are controlled by an "intelligent" energy management system. In fact, parallel systems include sophisticated controllers that include some of the following functions [13]:

- Control of the energy flow based on the load energy demand.
- Battery low voltage disconnection, to prevent excessive discharging.
- Battery charging control that ensures fast recharge, while avoiding overcharge.

- Controlled "boost-charging" of flooded electrolyte lead-acid batteries at regular intervals (2-6 weeks) to reduce the negative effects of electrolyte stratification.
- Battery management based on voltage measurements to estimate the batteries state of charge.
- Controlled bi-directional energy flow through the inverter to allow the load to be supplied, and to charge the battery bank from renewable resources, when excess energy is available from the photovoltaic panel, which is operated at its maximum efficiency.

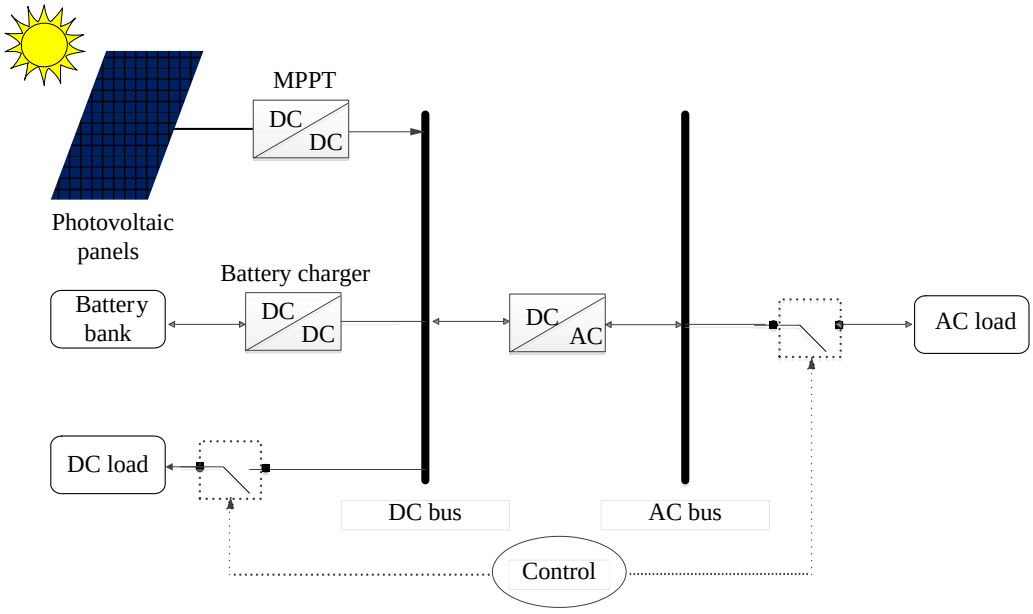

Figure 1. 5 Parallel architecture for photovoltaic installations

In both configurations, the use of MPPT is relevant to enable the panels to generate the maximum photovoltaic power. This is now detailed.

c. MPPT techniques

As is well known, the output power P_{pv} of the PV system T_a is nonlinear function crucially influenced by the solar irradiation G and the ambient temperature T_a [27]. Consequently, the PV system's operating point must change to maximize the energy produced. For this, MPPT techniques are used to maintain the PV array's operating point at its MPP [13].

Researchers have developed many methods for MPPT, such as the Look up Table [28], the Neuro-Fuzzy [29], the Incremental Conductance [29] and the Perturbation and Observation (P&O) [30] methods. They differ in complexity and tracking accuracy, but they all require the sensing of the photovoltaic current I_{pv} and voltage V_{pv} using off-the-shelf hardware. These techniques allow the MPP to be tracked thanks to the use of converters such as choppers, which are controlled by varying their duty cycle α [28] (Figure 1.6). We now briefly revise some of these methods.

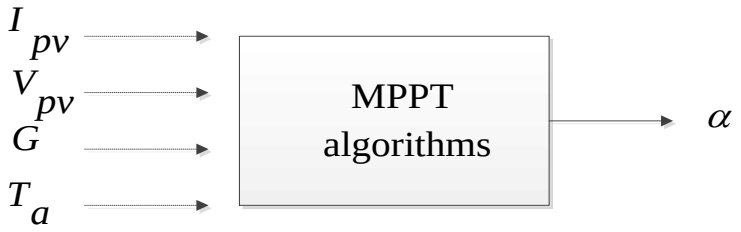

Figure 1. 6 General schematic diagram of inputs and output of MPPT algorithms

i. The Look up Table MPPT

The Look up Table MPPT method consists in dividing the possible solar radiation and ambient temperature into intervals, then attributing the minimum value of the corresponding interval for the measured climatic data [28]. Hence, each set of solar radiation and temperature intervals is assigned offline values of the photovoltaic voltage V_{mpp}, current I_{mpp} and power P_{mpp}. Then, a *PI* type controller adjusts the duty cycle α of the DC–DC converter to obtain these pre-determined values of current and power [28, 31].

This offline method allows the oscillations around the MPP to be reduced, with a rapid convergence [28], since it compares the duty cycle value, which corresponds to the operation in the maximum power point under predetermined climatic data, with the one stored in the control system [28, 31]. However, choosing the minimum value of each interval of G and T_a gives an operating point near but different from the MPP, which causes power loses.

ii. The Neuro-Fuzzy MPPT

The Neuro-fuzzy MPPT method is based on training a neuro-fuzzy tool using a solar radiation and ambient temperature database [13, 28, 32]. Then, the fuzzy rules that describe these relations are deduced. The training step is performed using an Artificial Neural Network (ANN), characterized by the ability to store experimental knowledge, which makes them well suited to tracking the maximum power point of PV panels [13, 32]. A multilayer perception network, trained by the back propagation method, is the most widely used technique to calculate the DC-DC optimal duty cycle α, considering the irradiation and the ambient temperature variation [28].

This method does not require a model for the panel and it can handle nonlinearities. However, it needs a continuous update for the database and a high performance processor.

iii. The Incremental Conductance MPPT

The Incremental conductance MPPT method uses the current ripple in the chopper output I_{pv} to maximize the panel power P_{pv} using the relation between the current and voltage continuously identified online [33, 34]. In fact, the incremental conductance for MPPT depends on the array terminal voltage V_{pv}, which is always adjusted according to the desired MPP voltage V_{mpp}, based on the instantaneous and incremental conductance of the photovoltaic module. Indeed, the algorithm tests the actual conductance $-\frac{I_{pv}}{V_{pv}}$ and the incremental conductance $\frac{dI_{pv}}{dV_{pv}}$ as follows [13, 28, 33]:

If $\frac{dI_{pv}}{dV_{pv}} \succ -\frac{I_{pv}}{V_{pv}}$, then the operating point is on the left of the MPP **(1)**

so, α is varied to increase V_{pv}.

If $\frac{dI_{pv}}{dV_{pv}} \prec -\frac{I_{pv}}{V_{pv}}$, then the operating point is on the right of the MPP, so **(2)**

α is varied to decrease V_{pv}.

If $\frac{dI_{pv}}{dV_{pv}} \approx -\frac{I_{pv}}{V_{pv}}$, then the operating point is in the MPP, so **(3)**

the value of α is maintained.

Hence, by comparing these conductance values following (1)-(3), at each sampling time, the algorithm tracks the maximum power of the photovoltaic module. This method allows the MPP to be tracked independently of the module characteristics [35]; when $dI_{pv} \succ 0$, the voltage at the MPP increases and, thus, the algorithm must increase V_{pv} to track V_{mpp}.

Although it has good efficiency, the complexity in implementation remains the main disadvantage of the Incremental Conductance MPPT method [32].

iv. The P&O MPPT

The P&O MPPT method uses the photovoltaic current and voltage measurements and compares their previous and present values. In fact, it consists in perturbing the panel voltage and comparing the photovoltaic power obtained with its previous value [36]. The increase in the photovoltaic power generates an increase of the perturbation voltage (Figure1.7) [36]. The P&O method is performed as follows [37]:

If $\frac{dP_{pv}}{dV_{pv}} \succ 0$, then the operating point is on the left of the MPP, so **(4)**

α is changed to increase V_{pv}.

If $\frac{dI_{pv}}{dV_{pv}} \prec 0$, then the operating point is on the right of the MPP, so **(5)**

α is changed to decrease V_{pv}.

If $\frac{dP_{pv}}{dV_{pv}} \approx 0$, then the operating point is in the MPP, so **(6)**

the value of α is maintained.

The oscillations that can be generated by P&O are considered the main drawback of this method [35]. However, it is easy to install and its cost is relatively low, so it is the most popular in practice [35].

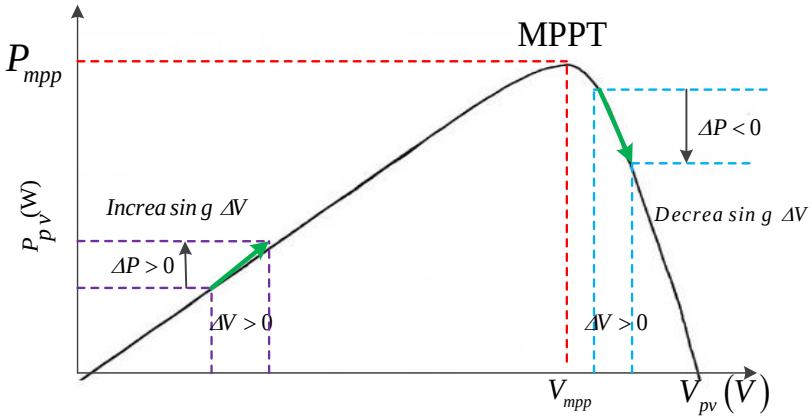

Figure 1. 7 Methodology to locate the Maximum Power Point using the Power versus Voltage curve

1.2.2 Thermal Energy

Thermal energy consists of the use of heat to produce electricity. The most popular sources are the thermal panels and concentrators (solar thermal) or the high temperature from the Earth (geothermal) [13].

a. Solar Thermal Energy

The thermal conversion in this case consists in absorbing solar energy to heat up dark surfaces placed in sunshine. Solar energy collectors working on this principle consist of sun-facing surfaces which transfer part of the energy absorbed to a fluid [38].

The possibility of generating high working temperatures (up to 4000 K) to operate conventional steam engines for electricity production in solar concentrators has been proven (Figure 1.8) [39]. Moreover, flat-plate collectors are used to generate low-temperature heat (<365 K), which is efficient for producing hot water or heating spaces [38]. However, the biggest disadvantages of the low temperature heat collectors are the inability to transport the energy for over long distances and the low efficiency if used to produce electricity [13].

Figure 1. 8 High temperature solar concentrator in Almeria (Spain)

b. Geothermal Energy

Geothermal energy consists in extracting the soil's energy on the basis of the temperature increase from the surface to the center of the earth [40], where the heat is produced by the natural radioactivity of the rocks.The geothermal energy, used to produce electricity, operates in very hot or very deep wells, geothermal sources, where water is injected under pressure into the rock.

Compared to other renewable energies, geothermal energy has the advantage of not depending on atmospheric conditions. It is therefore reliable and available over time [41, 42]. However, the energy extraction requires a high investment and sophisticated equipment.

1.2.3 Wind Energy

Wind energy is a renewable energy obtained from the pressure difference of natural warm and coolareas, which creates air masses in constant movement [43]. The electricity from wind is generated by a turbine that converts a portion of the kinetic energy from the wind into a mechanical energy available on a generator shaft [44].

World wind energy resources are substantial, and in many areas, such as the US and Northern Europe, could in theory supply all of the electricity demand. However, the remote or challenging locations, the intermittent character of the wind resources and the necessity of long distances for energy transmission are

considered the main drawbacks of wind energy. Figure 1.9 describes the wind power evolution in the world from 2005 to 2013 [45].

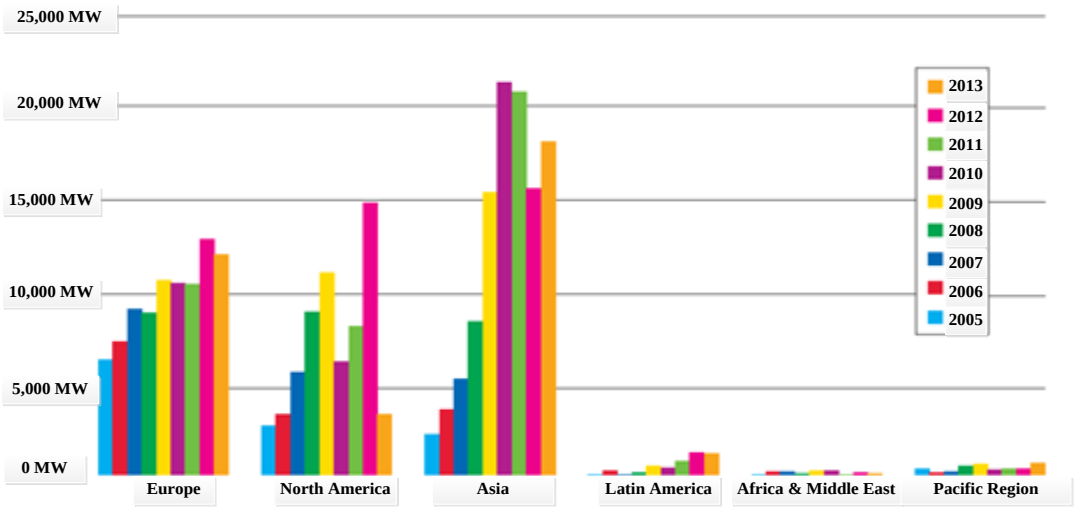

Figure 1. 9 Evolution of the installed wind power in the world [45]

1.2.4 Wave Energy

Produced by wind action, wave energy is considered as an indirect form of solar energy [46]. In fact, wind generates waves. When arriving at wave energy converters, these waves cede some of their energy that is converted into electricity. Similarly to wind energy, the main drawback of wave energy is its variability on several time-scales [47]: from wave to wave, with the state of the sea, and from month to month. Hence, unfortunately, the energy recovery is still not profitable.

1.2.5 Hydraulic Energy

Electricity is also produced from water flows, especially in dams constructed across rivers [48]. Since huge water volumes can be stored, dams produce important amounts of clean energy. The high stability of the source and the possibility of using small dams (less than 10 kW for isolated mini-grid sites) are considered a great advantage of hydraulic energy [13]. However, the

impossibility of constructing many dams is the most important disadvantage of this type of energy.

1.2.6 Biomass Energy

Biomass is one of the earliest sources of energy, with very specific properties. Biomass material (vegetable or animal) is transferred into electricity for example by burning waste in specific boilers [49]. Biomass is divided into three categories: dry biomass (wood, agricultural waste, etc.), biogas, and biomass wet (bioethanol, biodiesel, vegetable oil, etc.).

It has been found that using biomass in boilers offers many economic, social and environmental benefits, such as financial net savings, conservation of fossil fuel resources, and the reduction of Carbon Dioxide emissions. However, it requires a great harvesting and collection of material. Moreover, the transportation and storage costs are important [50].

1.3 Objectives of the Thesis

This thesis deals with the modelling, sizing and energy management of an autonomous photovoltaic installation destined to pump water needed to irrigate a plot of land planted with tomatoes.

The first objective of the thesis is to develop a sizing algorithm that gives the optimum sizes of the system's components, namely the surface of the photovoltaic panels and the battery bank capacity. To do so, we first develop and validate the models of the system's elements. These models are used to validate the sizing algorithm, using meteorological data for the target area in the months corresponding to the crop vegetative cycle.

The second objective of the thesis is to establish an optimal algorithm for the installation's energy management, based on fuzzy logic. The idea is to couple the energy demanded by the pump with the energy available from the panel and /or the battery bank, in order to fulfill the load requirements in energy and the crop's water needs. This is guaranteed using measured and predicted climatic data such as the solar radiation and the ambient temperature. The algorithm also decides

between storing energy in the battery or water in the tank, depending on the month and the crop's state of growth.

1.4 Contributions of the Thesis

This thesis provides several contributions on the sizing and optimal operation of a proposed photovoltaic water irrigation installation, as follows:

1. An optimum sizing algorithm that gives the adequate sizes of the installation's components to fulfill the irrigation requirements of the crops, and to optimize the use of the energy of the battery bank. The algorithm is validated using measurements of the target area. (This algorithm is presented in Chapter 2).

2. A fuzzy logic based algorithm for the optimal operation of the photovoltaic irrigation installation, balancing the energy consumption with the generation. The key idea is to manipulate the energy provided by the panels and the batteries to fulfill the water demand and safely operate the battery bank. For this, predictions of the climatic variables for the photovoltaic power generation and the irrigation requirements are used, together with current and water level measurements. The algorithm has been validated in a realistic plant in the laboratory. This algorithm is presented in Chapter 3.

1.5 Organization of the Thesis

The thesis is organized as follows:

Chapter 1: This chapter introduces the thesis content. Section 1.1 gives the motivation. Section 1.2 details the renewable energy situation in the world. The objectives, the main contribution and organization of the thesis are then summarized.

Chapter 2: This chapter deals with the sizing of the photovoltaic water pumping installation. First, Section 2.2 is dedicated to the renewable energies used for irrigation installations. Section 2.3 gives the description of the proposed installation. Section 2.4 presents a review on sizing algorithms, followed by the system elements modeling and validation (Section 2.5). Next, Section 2.6

details the proposed algorithm for the optimal sizing of the installation' components. Then, the algorithm efficiency is tested using measured climatic data of the target area.

Chapter 3: This chapter focuses on the energy management of the photovoltaic irrigation installation. A review of renewable energy management in irrigation is presented in Section 3.2, followed by the problem formulation in Section3.3. The proposed energy management algorithm is explained in Section 3.4 with some results presented in Section 3.5 and experimental validation illustrated in Section 3.6.

Chapter 4: This chapter summarizes the conclusions (Section 4.1), the publications derived from the thesis (Section 4.2) and the future work (Section 4.3).

Appendix A: This appendix is an extended abstract of the thesis in Spanish, and summarizes the objectives, contributions, organization and conclusions of the thesis.

Appendix B: This appendix presents the Tomatoes irrigation.

Appendix C: This appendix presents the panels and the batteries datasheets.

Appendix D: This appendix presents the induction machine modelling and control.

Appendix E, F, G, H and I: summarize respectively the MPPT methods and chopper modelling and control, datasheets of the sensors, the Programmable Power Supply, the inverter and the acquisition card.

Appendix J: This appendix includes the list of figures, tables, symbols, acronyms and internet links.

1.6 Conclusion

A study of the state of the art of renewable energies used for irrigation has been discussed. We have presented the situation of using renewable energies worldwide, namely photovoltaic, thermal, wind, wave, hydraulic and biomass energies, and the different photovoltaic installation architectures that can be used.

Knowing the specification of the studied site, we have decided to use a photovoltaic based installation to irrigate a plot of land planted with tomatoes. The installation's efficiency depends essentially on the system sizing and the energy management, which will be described, respectively in Chapters 2 and 3.

1.7 References

[1] Belakhal, Soltane. (2010). “Conception & Commande des Machines à Aimants Permanents Dédiées aux Energies Renouvelables”. Thesis presented at the University of Constantine, Algeria.

[2] Chapman, N. A; &Mc Kinley, I.G. (1987). “The geological disposal of nuclear waste’’. John Wiley and Sons Inc; New York, NY (USA); ISBN 0-471-91249-2.

[3] Lutze, W; &Ewing, R.C. (1988) “Radioactive waste forms for the future”. North Holland; Amsterdam (Netherlands); ISBN 0 444 87104 7.

[4] Henrik, Lund. (2007). “Renewable energy strategies for sustainable development”. Energy, 32, 912–919.

[5] Ibrahim, Dincer. (2000). “Renewable energy and sustainable development: a crucial review”. Renewable and Sustainable Energy Reviews, 4, 157-175.

[6] Johansson, Thomas B; Kelly, Henry; Amulya, Reddy. K. N; &Williams, Robert. H. (1992). “Renewable energy: sources for fuels and electricity”. Island press, ISBN 1-55963-139-2.

[7] Kumar, Atul; & Kandpal, Tara. C. (2007). “Renewable energy technologies for irrigation water pumping in India: a preliminary attempt towards potential estimation”. Energy, 32(5), 861-870.

[8] Purohit, Pallav. (2007). “Financial evaluation of renewable energy technologies for irrigation water pumping in India”. Energy Policy, 35(6), 3134-3144.

[9] Purohit, Pallav;& Kandpal, Tara. C. (2005). “Renewable energy technologies for irrigation water pumping in India: projected levels of dissemination, energy delivery and investment requirements using available diffusion models”. Renewable and Sustainable Energy Reviews, 9(6), 592-607.

[10] Rana, Gianfranco; Katerji, Nader; Lazzara, Paola; & Ferrara, Rossana. Monica. (2012). “Operational determination of daily actual evapotranspiration of irrigated tomato crops under Mediterranean conditions by one-step and two-step models: Multiannual and local evaluations”. Agricultural Water Management, 115, 285-296.

[11] Sumaila, Ussif. Rashid; Teh, Louise; Watson, Reg; Tyedmers, Peter;& Pauly, Daniel. (2008). "Fuel price increase, subsidies, overcapacity, and resourcesustainability". ICES Journal of Marine Science: Journal du Conseil, 65(6), 832-840.

[12] IEA-AIE. (2013). "Key World Energy Statistics 2013", International Energy Agency, www.iea.org, Rapport 2013.

[13] Ben Ammar, Mohsen. (2011). "Contribution à l'optimisation de la gestion des systèmes multi-sources d'énergies renouvelables". Thesis presented at the National Engineering School of Sfax, Tunisia.

[14] Chaabene, Maher. (2009). ''Gestion énergétique des systèmes photovoltaïques''. Master course at the National School for Engineers of Sfax, Tunisia.

[15] Nema, Pragya; Nema, Rajesh. Kumar; & Rangnekar, Saroj. (2009). "A current and future state of art development of hybrid energy system using wind and PV-solar: A review''. Renewable and Sustainable Energy Reviews, 13(8), 2096-2103.

[16] Bernal-Agustín, José. Luis; & Dufo-López, Rodolfo. (2009). "Simulation and optimization of stand-alone hybrid renewable energy systems". Renewable and Sustainable Energy Reviews, 13(8), 2111-2118.

[17] Deshmukh, Madhukar. K; & Deshmukh, Sudarshan. S. (2008). "Modeling of hybrid renewable energy systems". Renewable and Sustainable Energy Reviews, 12(1), 235-249.

[18] Green, M. A. (1982). ''Solar cells: operating principles, technology, and system applications''. Englewood Cliffs, NJ, Prentice-Hall, Inc.

[19] Yotaka, Harima; Kazuo, Yamashita; &Hitomi, Suzuki.(1984). "Spectral sensitization in an organic P-N junction photovoltaic cell". Applied Physics Letters, 45(10), 1144-1145.

[20] Chenni, Rachid; Messaoud Makhlouf, Mohammed; Kerbache, Taher; &Bouzid, Aissa. (2007). "A detailed modeling method for photovoltaic cells". Energy, 32(9), 1724-1730.

[21] Weidong, Xiao; &William, Dunford. G. (2004). "A modified adaptive hill climbing MPPT method for photovoltaic power systems". In the proceedings of the IEEE Conference on Power Electronics Specialists, 1957-1963.

[22] Aureliano Gomes de Brito, Moacyr; Galotto, Luigi; Poltronieri Sampaio, Leonardo; DAzevedo Melo, Guilherme; &Canesin, Carlos Alberto. (2013). "Evaluation of the main MPPT techniques for photovoltaic applications". IEEE Transactions on Industrial Electronics, 60(3), 1156-1167.

[23] Price, Samuel. C; Stuart, Andrew. C; Yang, Liqiang; Zhou,Huaxing;&You, Wei. (2011). "Fluorine substituted conjugated polymer of medium band gap yields 7% efficiency in polymer− fullerene solar cells". Journal of the American Chemical Society, 133(12), 4625-4631.

[24] EPIA. (2014), "Global market outlook for photovoltaic 2014-2018", European Photovoltaic Insustry Association, www.epia.org.

[25] Gules, Roger; De Pellegrin Pacheco, J; Hey, Héelio. Leãaes; & Imhoff, Johninso. (2008). "A maximum power point tracking system with parallel connection for PV stand-alone applications". IEEE Transactions on Industrial Electronics, 55(7), 2674-2683.

[26] Wang, Hong; &Zhang, Donglai. (2010). "The stand-alone PV generation system with parallel battery charger". In the proceedingsof the IEEE Conference on Electrical and Control Engineering (ICECE), 4450-4453.

[27] Faranda, Roberto; & Leva, Sonia. (2008). "Energy comparison of MPPT techniques for PV Systems".WSEAS transactions on power systems, 3(6), 446-455.

[28] Charfi, Sana; & Chaabene, Maher. (2014). "Acomparative study of MPPT techniques for PV systems. In the proceedings of the IEEE Conference on Renewable Energy Congress (IREC), 22-28.

[29] Veerachary, Mummadi; & Yadaiah, Narri. (2000). "ANN based peak power tracking for PV supplied DC motors".Solar Energy, 69(4), 343-350.

[30] Femia, Nicola; Petrone, Giovanni; Spagnuolo, Giovanni; & Vitelli, Massimo. (2005). "Optimization of perturb and observe maximum power point tracking method". IEEE Transactions on Power Electronics, 20(4), 963-973.

[31] Ghaisari, Jafar; Habibi, Mehdi; & Bakhshai, Alireza.R. (2007). "An MPPT controller design for photovoltaic (PV) systems based on the optimal voltage factor tracking". In the proceedings of the IEEE Conference on Electrical Power (EPC), 359-362.

[32] Salas, Vicente; Olias, Emilio; Barrado, Andrés;& Lazaro, Angel. (2006). "Review of the maximum power point tracking algorithms for stand-alone photovoltaic systems".Solar energy materials and solar cells, 90(11), 1555-1578.

[33] Oi, Akihiro. (2005). "Design and simulation of photovoltaic water pumping system". Doctoral dissertation, California Polytechnic State University, San Luis Obispo, USA.

[34] Hussein, K. H; Muta, I; Hoshino, T;& Osakada, M. (1995). "Maximum photovoltaic power tracking: an algorithm for rapidly changing atmospheric conditions". In the proceedings of the IEE Conference on Generation, Transmission and Distribution, 142(1), 59-64.

[35] Kurella, A;& Suresh, R. "Simulation of incremental conductance MPPT with direct control methods using cuck converter". IJRET, 2(9), 557-566.

[36] Esram, Trishan; & Chapman, Patrick. L. (2007). ''Comparison of photovoltaic array maximum power point tracking techniques''. IEEE transactions on Energy Conversion, 22(2), 439-449.

[37] Desai, Hardik. P; & Patel, Hiren. K. (2007). ''Maximum power point algorithm in PV generation: an overview''. In the proceedings of the IEEE Conference on Power Electronics and Drive Systems (PEDS'07), 624-630.

[38] Goswami, D. Yogi; Kreith, Frank;& Kreider, Jan. F. (2000). "Principles of solar engineering". CRC Press. ISBN 1-56032-714-6.

[39] http://outilssolaires.blog.ca

[40] Barbier, Enrico. (2002). ''Geothermal energy technology and current status: an overview''. Renewable and Sustainable Energy Reviews, 6(1), 3-65.

[41] Fridleifsson, Ingvar. B. (2001). ''Geothermal energy for the benefit of the people''. Renewable and Sustainable Energy Reviews, 5(3), 299–312.

[42] Fridleifsson, Ingvar. B. (2003). ''Status of geothermal energy amongst the world's energy sources''. Geothermics, 32(4), 379–388.

[43] Siegfried, Heier. (2014). "Grid integration of wind energy". John Wiley & Sons.

[44] Cavallo, Alfred. (2007). "Controllable and affordable utility-scale electricity from intermittent wind resources and compressed air energy storage (CAES)". Energy, 32(2), 120–127.

[45] GWEC (2013). "Global wind statistics". Global Wind Energy council.

[46] Pelc, Robin;&Fujita, Rod. M. (2002). “Renewable energy from the ocean”. Marine policy, 26(6), 471–479.

[47] Clément, Alain;McCullen, Pat;Falca, Antonio;Fiorentino, Antonio; Gardner, Fred; Hammarlund, Karin; Lemonis, George; Lewis, Tony; Nielsen, Kim; Petroncini, Simona; Pontes, M.-Teresa; Schild, Phillippe; Sjo Stro, Bengt-Olov; Sorensen,Hans Christian;&Thorpe, Tom. (2002). “Wave energy in Europe: current status and perspectives’’. Renewable and Sustainable Energy Reviews, 6(5), 405–431.

[48] Chanson, Hubert. (1994). “Comparison of energy dissipation between nape and skimming flow regimes on stepped chutes”. Journal of Hydraulic Research, 32(2), 213-218.

[49] Demirbas, Ayhan. (2005). ‘‘Potential applications of renewable energy sources, biomass combustion problems in boiler power systems and combustion related environmental issues’’. Progress in Energy and Combustion Science, 31(2), 171–192.

[50] Saidur, Rahman; Atabani, Abdelaziz; Demirbas, Ayhan Hilel; Hussein, Mahmud; &Mekhilef, Saad. (2001). ‘‘A review on biomass as a fuel for boilers’’. Renewable and Sustainable Energy Reviews, 15(5), 2262‑2289.

Chapter 2: Sizing of the Photovoltaic Irrigation Components

Contents

2.1 Introduction

Following the discussion in the previous chapter, a photovoltaic based installation is a promising solution for our irrigation problem, since the isolated site is characterized by a good solar insolation throughout the year [1- 3]. After studying the renewable energies used for irrigation (Section 2.2) and presenting the adopted installation (Section 2.3), we will describe the sizing problem (Section 2.4) and present and validate some of the system components models (Section2.5), which will be used to define the optimum components size (Section 2.6).

2.2 Irrigation using Renewable Energies

The need to save water and energy is a serious issue that has increased in importance over the last years and will become more important in the near future [4]. The low price of fuel was the reason why renewable energy sources are not widely used in several applications, including water pumping. So, pumping systems based on renewable energies are still scarce, even though they have clear advantages, namely, low generating costs, suitability for remote areas, and being environmentally friendly. Nowadays, the price of electric energy is rising constantly, investing in more efficient solutions is increasing [5].

2.2.1 Renewable Energies for Irrigation

Renewable Energies have been used in water pump applications, especially in remote agricultural areas, thanks to the potential of renewable energies. The renewable energies' use depends on the user's propensity to invest in renewable based pumping systems, his /her awareness and knowledge of the technology for water pumping, and also on the availability, reliability, and economics of conventional options [6]. Moreover, the evaluation of the groundwater volume required for irrigation and its availability in the area are also relevant in determining the profitability of renewable energies.

Photovoltaic Powered Electric Water Pumping Systems (PPEWPS) and Wind Powered Electric Water Pumping Systems (WPEWPS) are the most common installations used for water pumping [6]. PPEWPS are promising solutions,

Especially in small scale installations in regions characterized by good amounts of solar energy over the year [7, 8]. In fact, it is recommended that, for installing Solar Photovoltaic (SPV) pumps, the average daily solar radiation in the least sunny month should be greater than 3.5 kW/ m^2 on a horizontal surface [4]. Thanks to their efficiency and cost-efficiency rate, PPEWPS have been very popular and they have been developed to appear in these following categories [8]:

- *Directly coupled PPEWPS*:
  These systems pump water only when the photovoltaic modules capture the solar radiation.
- *Maximum Power Point PPEWPS:*
  These installations include MPP trackers to enhance the panels efficiency and thus increase the pumped water volume.
- *Batteries PPEWPS:*
  These systems include batteries to supply pumps when the panels power generation is not sufficient.
- *Sun trackers PPEWPS:*
  These installations include sun trackers to maximize the solar energy received. They are considered expensive and complicated [6].

  WPEWPS have been used in windy sites and can be classified as:

- DC *type WPEWPS:*
  This category of WPEWPS produces AC energy via wind turbines, which is then rectified to DC and used to supply DC loads [9].
- AC *type WPEWPS:*
  These installations generate AC energy used directly to supply AC loads [10, 11]. Moreover, they can take the form of a DC type when they are small size WPEWPS. For instance, permanent magnet synchronous generators (PMSG) with embedded rectifiers are used in small size and fixed pitch wind turbines, which have a simpler construction and are less expensive than DC type WPEWPS.

Some installations combine solar panels and wind turbines to compensate the solar radiation and the wind velocity fluctuations. These sources act in a

complementary way, since, generally, when the solar radiation is high, the wind velocity is low. This combination may result in a more reliable but complex water pumping, since electric power generated by wind turbines is highly erratic and may affect both the power quality and the planning of power systems [12].

Hence, as has been shown, there is a multitude of systems based on renewable energies. However, the choice of the energy source for the pump supply depends essentially on the site characteristics and the water needed by the crops. For our target application, photovoltaic system with MPPT and batteries will be selected. The irrigation methods are now detailed.

2.2.2 Irrigation Methods for Tomatoes

Generally, drip and furrow irrigation are the most used methods for tomatoes irrigation [13, 14]. Although mulching irrigation contributes to crop production by way of influencing soil productivity and weed control [15, 16], drip irrigation, characterized by its suitability for small and frequent irrigation applications [14], is selected here, since it only requires a small water volume and it allows the fruit production to be increased [13]. Small but frequent water applications enable the plant to grow well, without any effect from water-stress, thanks to the frequent water applications between consecutive irrigation periods [14].

Indeed, several researchers have focused on the yield improvement by drip irrigation of various crops (especially tomato). In fact, it has been reported that drip irrigation allows 30-50% higher tomato yields [14] and its use, either alone (or in combination with mulching methods), increases the tomato yield over the normal method of irrigation, which represents 44% savings in irrigation water [14]. Thus, the irrigation method generally affects the yield production.

2.3 Target System

As Tunisia's climate is considered semi-arid [18] and many crops need to be irrigated regularly [14] (Appendix B), the use of an autonomous installation for water pumping is required. The characteristics of the installation selected (presented in Figure 2.1) are now explained.

- *Choice of the Renewable Energy*:

  Since the land is characterized by a good amount of solar energy during the year [18], we choose a PPEWPS installation that includes the MPPT technique and batteries.

- *Choice of the components*:

  The installation is composed of photovoltaic panels (Appendix C). Since the installation autonomy is required, a lead-acid battery bank is used, as it is efficient and economic (Appendix C). These components supply a centrifuge water pump driven by an induction machine (Apepndix D), as our application is characterized by a constant flux and a moderate head (Figure 2.1). The regulator is composed of three relays that allow the components to be connected and disconnected. For the reservoir, we just consider its volume, which is the maximum volume needed by the crops in the most critical month (*July*).

- *Choice of the architecture*:

  Since our objective is to optimize the system components size, and control the installation, a specific parallel configuration for these components has been chosen. The installation cabling is done by DC bus.

- *Choice of the MPPT technique*:

  Based on the study done in 1.2.1.c, the P&O method for MPPT is chosen, since it is easy to implement and gives good performance [19] (Appendix E).

- *Choice of the irrigation method*:

  Thanks to its advantages in enhancing the production yield and saving waterand money [13-14], the drip irrigation method has been chosen for irrigating tomatoes (Appendix B).

After choosing the system characteristics, an adequate sizing of the installation components is relevant to the optimum use of the energy generated. In the following section, we focus on sizing algorithms proposed in the literature, for renewable energies applications.

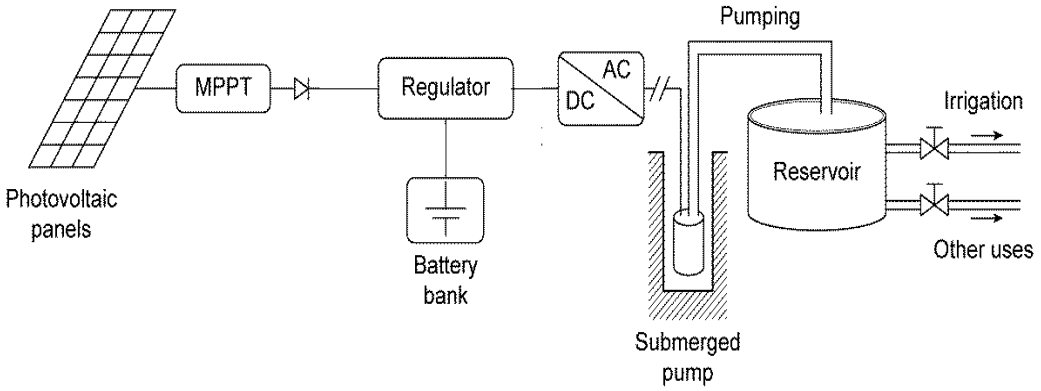

Figure 2. 1 Proposed photovoltaic irrigation system

2.4 A Review of Sizing Algorithms

As the sizes of the photovoltaic installation components affect its autonomy [20, 21], it is necessary to define some adequate values for the components parameters, such as the photovoltaic panel surface and the number of batteries [22, 23].

During the months that correspond to the vegetative cycle of the crops, the values selected must guarantee the water volume needed for the crops irrigation, the system autonomy and the battery bank safe operating [22]. In fact, knowing the water volume needed for irrigating the crops, the site characteristics, the solar radiation and the photovoltaic panel type, the algorithm that is proposed in this chapter provides the optimum values of the panel surface, the number of batteries and the reservoir volume. The idea consists in calculating the values that guarantee, on the one hand, the balance between the charged and discharged energy in the battery bank, and on the other hand, the pumping of the water volume needed. It is important to point out that the components size chosen must fulfill the irrigation requirements for all the months of the crops vegetative cycle (*March* to *July*).

Hence, researchers have established various methods to optimize the components sizes of these installations, essentially the photovoltaic panels surface and the battery bank capacity [24]. For instance, some works have focused on developing analytic methods based on a simple calculation of the panels surface and battery bank capacity using the energetic balance [25-27]. Other works have concentrated on the cost versus reliability question [28]. Moreover, some researchers have proposed sizing algorithms based on the minimization of cost functions, using the Loss of Load Probability (LLP) concept [29-33]. This LLP

approach has also been combined with artificial neuronal networks and genetic algorithms [28, 29].

However, these methods may result in an oversized system for one location and an undersized one for another location [34]. The oversized case results in high installation costs. With an undersized case, the installation is unable to supply the load with the energy needed. Moreover, the installation lifetime is shorter, due to the excessive use of batteries. For these reasons, the sizes must be carefully selected for each specific application and location [34].

In this context, several tools for photovoltaic installation sizing are available. For instance, HOMER [35], COMPASS [36], PVsyst [37], RAPSim [38] and RETscreen International [39] optimize the photovoltaic component size. Table 2. 1 summarizes the references for these tools and gives comments on their design methodologies.

Table 2. 1 Summary of sizing software [40]

Software	Organism	Observations
HOMER [35]	NREL: National Renewable Energy Laboratory, USA	Components classified by the cost and life cycle
COMPASS [36]	Global Headquarters and Technology Center, Hamburg, Germany	Batteries are not included in the software library
PVsyst [37]	University of Geneva, Switzerland	Sizing efficiency is done by years
RAPSim [38]	Murdoch University Energy Research Institute, Australia	Sizing is based on the evaluation of the installation yield using different components configurations
RETscreen International [39]	The Ministry of Natural Resources Canada	The conception is based on statistical models to evaluate the economic and energetic balance

The tools presented in Table 2.1 optimize the size of the PV installation components by taking into account the energetic, economic and environmental aspects [40]. However, some softwares (such as COMPASS) do not include batteries. Hence, in the case of water pumping, it is limited to pumping over the

sun. Moreover, HOMER is a good tool for sizing. Despite it guarantees the installation autonomy, it may give an oversized sizing, since it concentrates in the system autonomy. PVsyst is a good tool for sizing since it takes into account the Load Loss Propability. However, the evaluation of the sizing efficiency can be done by years. RAPSim focuses on modeling alternative power supply options. Using costs calculation throughout the lifespan, this tool is very adequate to predict the system performance and economic parameters of hybrid PV–Wind–Diesel–Battery systems [41]. RETscreen is an excel tool that assists the user in determining the energy production, life-cycle costs and greenhouse gas emission reductions for various types of renewable energy [41]. This tool allows the electricity produced to be determined using statistical sizing (provided by the user), models and climatic data of the target site [40].

Hence, these tools may give a good sizing for the installation autonomy, but they may result in oversized components. In this context, based on the load demand and the climatic data, an algorithm to determine the optimum size of our photovoltaic installation components is proposed in Section 2.6, using models of the panels, the battery bank and the pump, which are now presented and validated in Section 2.5.

2.5 System Modelling and Validation

In order to size and control the system elements, an essential step consists in modeling the installation components. Hence, we now present some models for the photovoltaic panels, the batteries and the pump, some of which will be experimentally validated and then used for sizing (Section 2.6) and management (Chapter 3).

2.5.1 System Modelling

In this section, we describe the installation components models, except the regulator (which is detailed in Chapter 3).

a. Photovoltaic Panels Models

In autonomous photovoltaic installations, panels are the source that generates the electric energy for the rest of the components. To better understand the

panel behavior, an essential step consists in studying the parameters affecting the photovoltaic power generation. These parameters are essentially the solar radiation G, the ambient temperature T_a and the panel characteristics [40], which are detailed below:

i. Solar Radiation Model

Solar radiation data provide information on how much of the sun's energy strikes a surface at a location on the Earth during a time period. These data are needed for effective research into solar energy utilization. Solar energy consists of two parts; extraterrestrial solar energy, which is above the atmosphere and global solar energy, which is under the atmosphere [43]. The global solar energy incidence on a tilted panel is generally evaluated using the Liu and Jordan relations [43, 44]. In this model, the solar radiation depends essentially on the position of the sun, which is determined by using the declination and the hour angle of the sun [40]:

❖ *Solar declination*

The sun's declination δ, needed to determine its position, is the angle between the sun's direction at the solar noon and its projection on the equatorial plane (Figure 2.2). In fact, it reaches its maximum (23.45º) at the summer solstice (21 *June*), and its minimum (-23.45º) at the winter solstice (*December* 21). It is described by Cooper's equation [40, 45- 46]:

$$\delta = 23.45 \sin\left(2\pi \frac{284 + d}{365}\right) \quad \textbf{(7)}$$

where d is the day number in the year.

❖ *Hour Angle of the Sun*

The hour angle of the sun w is the sun's East to West angular displacement around the polar axis. The value of the hour angle is zero at noon, negative in the morning and positive in the afternoon and it is increased by 15 º per hour.

The hour angle of the sun w_s at sunset is given by [47]:

$$\cos w_s = -tg\varphi \; tg\delta \qquad \textbf{(8)}$$

where:

δ is the declination (°) calculated from (1) and φ is the site's latitude (°).

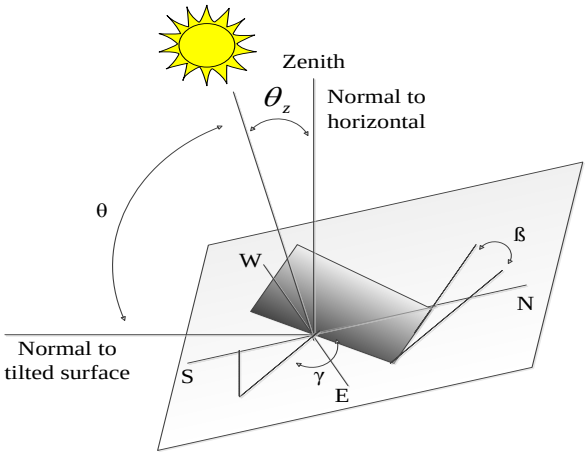

Figure 2. 2 Solar radiation angles

❖ *Extraterrestrial Radiation and Clearness Index*

The extraterrestrial solar radiation H_0 is the solar radiation outside the Earth's atmosphere. The extraterrestrial radiation (J/m^2) on a horizontal surface for the day d is obtained using the following equation [48]:

$$H_0(d) = \frac{24\times 3600}{\pi} G_{sc}\left(1+0.033\cos\left(2\pi\,\frac{d}{365}\right)\right)\left(\cos\varphi\cos\delta + w_s \sin\varphi\sin\delta\right) \qquad \textbf{(9)}$$

where G_{sc} is the solar constant (Table 2.2).

The solar radiation is attenuated by the atmospheric layer and clouds before it reaches the Earth's soil. The clearness index K_t is the ratio between the ground and the extraterrestrial radiations. The monthly average of this index is defined by [48, 49]:

$$\overline{K_t} = \frac{\overline{H}}{\overline{H_0}} \qquad \textbf{(10)}$$

where:

$\overline{H}$: the monthly average of the solar radiation on a horizontal plane,

$\overline{H_0}$: the monthly average of the extraterrestrial radiation on a horizontal plane.

❖ *Solar Radiation Calculation*

The total solar radiation on a tilted photovoltaic panel is calculated as follows:

1) Calculation of the diffused, the global and the direct solar radiation in a horizontal panel following (5-13).

2) Calculation of the global solar radiation corresponding to a tilted panel following (14).

3) Sum of the hourly values of the solar radiation folowwing (17).

These two steps are now presented in detail:

1) Calculation of the diffused and global solar radiation

In the literature, several models have been used to determine the diffused solar radiation $\overline{H_d}$. For instance, [44] used models that classify the daily diffused solar radiation based on the daily clearness index intervals. Other works proposed a seasonal relation for $\overline{H_d}$ that depends on the sun hour angle at sunset at the month mean day [51, 52]. The monthly diffused solar radiation has also been developed using the monthly clearness index [53].

In our case, the diffused and global solar radiations are deduced using the monthly average global solar radiation in a horizontal panel, since a monthly radiation average is needed for the sizing of the installation components. The diffused insolation $\overline{H_d}$ is a function of the hour angle at sunset. It is described as follows [48-49, 53-54]:

- If w_s is less than 81.4°:

$$\overline{H_d} = \overline{H}\left(1.391 - 3.56\overline{K_t} + 4.189\overline{K_t}^2 - 2.137\overline{K_t}^3\right) \quad \textbf{(11)}$$

- If w_s is higher than 81.4°:

$$\overline{H_d} = \overline{H}\left(1.311 - 3.022\overline{K_t} + 3.427\overline{K_t}^2 - 1.821\overline{K_t}^3\right) \quad \textbf{(12)}$$

The hourly diffused and global insolation H_d and H are respectively obtained using (7) and (8) [53]:

$$H_d(t,d) = r_d(t,d)\overline{H_d} \quad \textbf{(13)}$$

$$H(t,d) = r_t(t,d)\overline{H} \quad \textbf{(14)}$$

where r_d is the ratio of the hourly to daily total diffuse solar radiation expressed by [48-49, 53]:

$$r_d(t,d) = \frac{\pi}{24}\frac{\cos w - \cos w_s}{\sin w_s - w_s \cos w_s} \quad \textbf{(15)}$$

where:

w: the hour angle of the sun,

w_s: the hour angle of the sun at sunset (following (2)).

$r_t(t,d)$: the ratio of the hourly to the daily total global solar radiation, expressed by [48-49, 53]:

$$r_t(t,d) = \frac{\pi}{24}\frac{\cos w - \cos w_s}{\sin w_s - w_s \cos w_s}(a + b\cos w) \quad \textbf{(16)}$$

where:

$$a = 0.409 + 0.501 \sin\left(w_s - \frac{\pi}{3}\right) \quad \textbf{(17)}$$

$$b = 0.6609 + 0.4767 \cos\left(w_s - \frac{\pi}{3}\right) \quad \textbf{(18)}$$

Hence, the direct solar radiation $H_b(t,d)$ is obtained using the following equation [49, 53]:

$$H_b(t,d) = H(t,d) - H_d(t,d) \quad \textbf{(19)}$$

2) Calculation of the hourly radiation on a tilted panel

The total daily solar radiation H_t in a tilted panel is evaluated by varying the hour angle that corresponds to the length of the day. It is expressed by [40, 48, 49, 53]:

$$H_t(t,d) = R'_b\, H_b(t,d) + \left(\frac{1+\cos\beta}{2}\right) H_d(t,d) + \rho\left(\frac{1-\cos\beta}{2}\right) H(t,d) \quad \textbf{(20)}$$

where:

ρ: the albedo of the soil,

β: the panel declination (°),

R'_b: the ratio of the direct radiation on the tilted panel and the direct radiation on the horizontal panel, expressed by [40, 47- 49]:

$$R'_b = \frac{\cos\theta}{\cos\theta_z} \quad \textbf{(21)}$$

where:

θ: the radiation incidence angle (°),

$$\cos\theta = \sin\delta\sin\varphi\cos\beta - \sin\delta\cos\varphi\sin\beta\cos\gamma + \cos\delta\cos\varphi\cos\beta\cos w + \cos\delta\sin\varphi\sin\beta\cos\gamma\cos w + \cos\delta\sin\beta\sin\gamma\sin w \quad \textbf{(22)}$$

θ_z: the zenith angle of the sun (°), given by:

$$\cos\theta_z = \sin\delta\sin\varphi + \cos\delta\cos\varphi\cos w \quad \textbf{(23)}$$

3) Sum of the hourly values of the solar radiations

The evaluation of the solar energy W_{pv} is performed by summing the solar radiation received. Hence, it is assumed that during the hour, the solar radiation is constant [54]. The solar energy (Wh) is expressed by:

$$W_{pv} = \sum_{t_{sr}}^{t_{ss}} H_t(t)\,dt \quad \textbf{(24)}$$

where:

t_{sr}: the time of sunrise,

t_{ss}: the time of sunset.

ii. Ambient Temperature Distribution Model

The distribution model used to forecast the ambient temperature $T_a(t,d)$ of the day d at the hour t depends on the minimum and the maximum temperatures $T_{min}(d), T_{max}(d)$. Thus, $T_a(t,d)$ is expressed by [40]:

$$T_a(t,d) = \frac{T_{max}(d)+T_{min}(d)}{2} + \frac{T_{max}(d)-T_{min}(d)}{2} cos\left(\pi \frac{t-13}{24}\right) \quad \textbf{(25)}$$

iii. Photovoltaic Panels Model

In the literature, several models for the PV panels are used [53]. Since a photovoltaic panel is the parallel association of photovoltaic modules constituted of serially connected photovoltaic cells, modeling a photovoltaic panel consists first in modeling the photovoltaic cells and then applying the effect of the series and parallel connections [40]. In this sense, various models have been established to describe the photovoltaic current, which is a function of the photovoltaic voltage.

In fact, many works have been dedicated to the collection of a number of I–V characteristics in different environmental conditions. These data are arranged in a database, and then a relation between the solar radiation, the ambient temperature at the cell surface, and the photovoltaic current produced is deduced [55]. Despite the simplicity of this method, it remains practical only for the studied module and cannot be generalized for other modules' types.

Hence, researchers use general models, namely non-linear models. In this context, some works concentrate on the one (or two) diode based model, which associates a current source in parallel with one (or two) diode to describe the current generated by the cell [56, 57].

Moreover, more generalized models have been developed, such as the yield based panel model [53]. This yield is evaluated using the cell parameters values (the temperature coefficient for the panel yield, the panel yield at the reference temperature, etc.), and the cell temperature module, which depends

on the Nominal Operating Cell Temperature (NOCT) and the clearness index [53].

For our application, we use the yield based model for the sizing algorithm, and the one-diode non-linear model for the management. In fact, since the proposed sizing algorithm uses only the power curve of the PV modules, a yield based model has been selected. On the other hand, the management algorithm is performed dynamically, so it requires a precise real-time knowledge of all the panels variables (currents, voltages, etc.); thus, a one-diode model is selected.

❖ *Panel Yield-Based Model*

This simplified model, used for sizing, is based on few parameters. The panel yield model is given by:

$$\eta_{pv}(t) = \eta_r (1 - \beta_{pv}(T_c(t) - T_{a\,ref})) \quad \textbf{(26)}$$

where:

η_r : the panel yield at the reference temperature,

β_{pv} : the temperature coefficient for the panel yield ($°C^{-1}$),

$T_c(t)$: the cell temperature (ºC),

$T_{a\,ref}$: the reference temperature (°C).

The cell temperature $T_c(t)$ can be calculated as follows [53]:

$$T_c(t) = T_a(t) + H_t(t,d)\frac{NOCT - T_{ref}}{800} \quad \textbf{(27)}$$

where:

T_a : the ambient temperature (°C),

$H_t(t,d)$:the solar radiation on the tilted panel (W/ m^2),

NOCT: the Normal Operating Cell Temperature (ºC).

T_{ref} : the reference ambient temperature (°C),

Finally, the photovoltaic power can be evaluated as follows [53]:

$$P_{pv}(t) = S\, H_t(t,d)\, \eta_{pv}(t) \quad \textbf{(28)}$$

where S is the panel surface (m^2).

❖ *Panel Non-linear Model*

A one-diode based non-linear model is used for the management algorithm, using an ideality factor to describe the diode's performance [58, 59]. The model uses the radiation $G(t)$, the ambient temperature $T_a(t)$ at the panel surface, and the panel parameters to evaluate the photovoltaic current $I_c(t)$: see Figure 2.3 [57]. The model is described by (29)-(33) [59- 60]:

$$I_c(t) = I_{ph}(t) - I_r(t)\left(exp\left(\frac{V_c(t)+R_s I_c(t)}{V_{t\_T_a}} \right) - 1 \right) - \frac{V_c(t)+R_s I_c(t)}{R_p} \quad \textbf{(29)}$$

$$I_{ph}(t) = \frac{G(t)}{G_{ref}} I_{sc}(t) \quad \textbf{(30)}$$

$$I_{sc}(t) = I_{sc\_T_{ref}}\left(1 + a\left(T_a(t) - T_{ref}\right)\right) \quad \textbf{(31)}$$

$$I_r(t) = I_{r\_T_{ref}}\left(\frac{T_a(t)}{T_{ref}} \right)^{\frac{3}{n}} exp\left(\frac{-qV_g}{nK_B}\left(\frac{1}{T_a(t)} - \frac{1}{T_{ref}} \right) \right) \quad \textbf{(32)}$$

$$I_{r\_T_{ref}} = \frac{I_{sc\_T_{ref}}}{exp\left(\frac{qV_{c\_T_{ref}}}{nK_B T_{ref}} \right) - 1} \quad \textbf{(33)}$$

where:

$I_c(t)$: the estimated photovoltaic cell current (A),

$I_{ph}(t)$: the generated photo-current at a given irradiance G (A),

$I_r(t)$: the reverse saturation current for a given temperature T_a (A),

$V_c(t)$: the open circuit voltage of the photovoltaic cell (V),

R_s: the serial resistance of the photovoltaic module (Ω),

$V_{t\_T_a}$: the thermal potential at the ambient temperature (V),

R_p: the parallel resistance of the photovoltaic module (Ω),

G_{ref}: the solar radiation at reference conditions (W/m^2),

$I_{sc}(t)$: the short circuit current for a given temperature T_a (A),

$I_{sc\_T_{ref}}$: the short circuit current per cell at the reference temperature (A),

a : the temperature coefficient for the short circuit current (K^{-1}),

$T_a(t)$: the ambient temperature at the panel surface (K),

T_{ref} : the reference temperature at the panel surface (K),

$I_{r\_T_{ref}}$: the reverse saturation current for the reference temperature T_{ref} (A),

n : the quality factor,

q : the electron charge (C),

V_g : the Gap energy (e.V),

K_B : the Boltzmann coefficient (J/K),

$V_{c\_T_{ref}}$: the open circuit voltage per cell at the reference temperature (V).

The photovoltaic power P_{pv} generated by the panel is then described as follows [40]:

$$P_{pv}(t) = n_s n_p V_c(t)\left(I_{ph}(t) - I_r(t)\left(exp\left(\frac{V_c(t) + R_s I_c(t)}{V_{t\_T_a}} \right) - 1 \right) - \frac{V_c(t) + R_s I_c(t)}{R_p} \right) \quad \textbf{(34)}$$

where:

n_s : the number of serial photovoltaic cells,

n_p : the number of parallel photovoltaic modules.

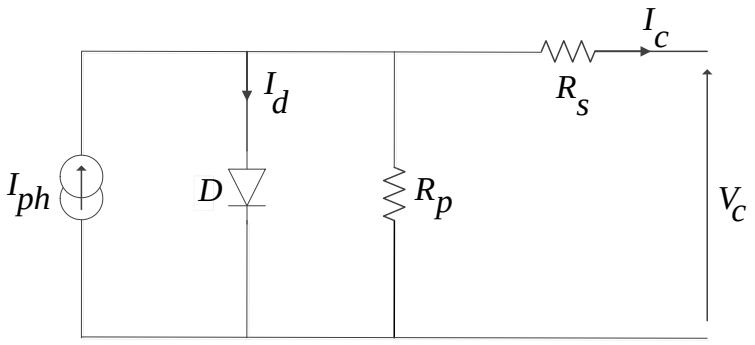

Figure 2. 3 Equivalent circuit for the photovoltaic cell

b. Battery Bank

The photovoltaic panel produces electric energy only when the solar radiation is available. Hence, the use of a battery bank is necessary to complete the remaining power to the load supply, and to store the excess photovoltaic energy.

A battery, composed of positive and negative electrodes separated by an electrolyte, converts the chemical energy to electric energy thanks to oxidoreduction reactions [61, 62]. The battery type most used in this type of stationary applications is the lead-acid battery since the relation between its cost and its life time is acceptable [53]. Some researchers have concentrated on developing models for the battery characteristics using linear modeling methods, namely the coulometric [53], the open-circuits voltage methods [63, 64], and the dynamic modeling method, which uses the battery voltage to model the battery's behavior [65].

Here, we concentrate on a non-linear model for modeling the lead- acid battery [66]. In addition to its simplicity, this model has the advantage of using both the battery current and voltage to describe precisely the battery behavior when charging or discharging. Its performance is then evaluated from its voltage V_{bat}, its capacity C_p, and its depth of discharge dod. In fact, the battery model adopted is composed of a resistance R_t in series with two parallel branches [53, 63] (Figure 2.4). The first branch represents the battery storage capacity using a capacitor C_{bulk}, in series with a resistance R_e. The second branch is composed of a capacitor C_s, which represents the diffusion phenomena within the battery, in series with a resistance R'_s. The battery equivalent resistance is described as follows [63, 64]:

$$R = R_t + \frac{R_e R'_s}{R_e + R'_s} \qquad \textbf{(35)}$$

where:

R_t is the terminal resistance (Ω), R_e is the end resistance (Ω) and R'_s is the surface resistance (Ω).

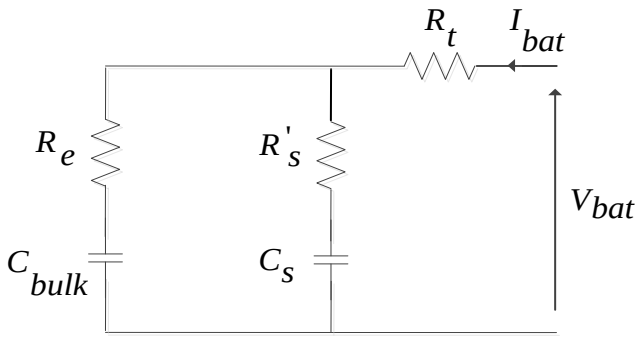

Figure 2. 4 Equivalent circuit of a Lead-acid battery

The stored charge in the battery C_R is described as follows [66, 67]:

$$C_{R_{(k)}} = C_{R_{(k-1)}} + \frac{\partial k}{3600} I_{bat_{(k)}}{}^{k_p} \quad \textbf{(36)}$$

where ∂k is the time between instant $k-1$ and k and k_p is the Peukert.

The depth of discharge dod is given by the following equation [66, 67]:

$$dod_{(k)} = 1 - \frac{C_{R_{(k)}}}{C_p} \quad \textbf{(37)}$$

where:

C_p : the Peukert capacity, considered constant (A.h).

c. Inverter

As in most research related to water pumping, the motor pump adopted is an induction machine (IM) (Appendix D), for its simplicity when control and its encouraging price. For this, the IM is supplied by an inverter, which is composed of six IGBT switches each shunted in antiparallel by a fast free wheeling diode, in order to return the negative current to the filter capacitor provided at the input of the converter (Figure 2.5).

The inverter is controlled by analog values. T_i and T_i' are the ideal switches of the same inverter arm, for which are associated the logic control signals S_i and $\overline{S_i}$ respectively, where $S_i = 1$ if T_i is switched on and $S_i = 0$ if T_i is switched off.

Hence, the composed and simple voltages vectors, and the currents vector, which depends on the control signals and the input voltage V_c are used to define the composed voltage vectors U_{s1s2}, U_{s2s3} and U_{s3s1} relative to the common point ***N*** of the load or the ground ***M*** as follows (38) [2]:

$$\begin{cases} V_{s1} - V_{s2} = V_{s1M} - V_{s2M} = V_{s1N} - V_{s2N} \\ V_{s2} - V_{s3} = V_{s2M} - V_{s3M} = V_{s2N} - V_{s3N} \\ V_{s3} - V_{s1} = V_{s3M} - V_{s1M} = V_{s3N} - V_{s1N} \end{cases} \quad \textbf{(38)}$$

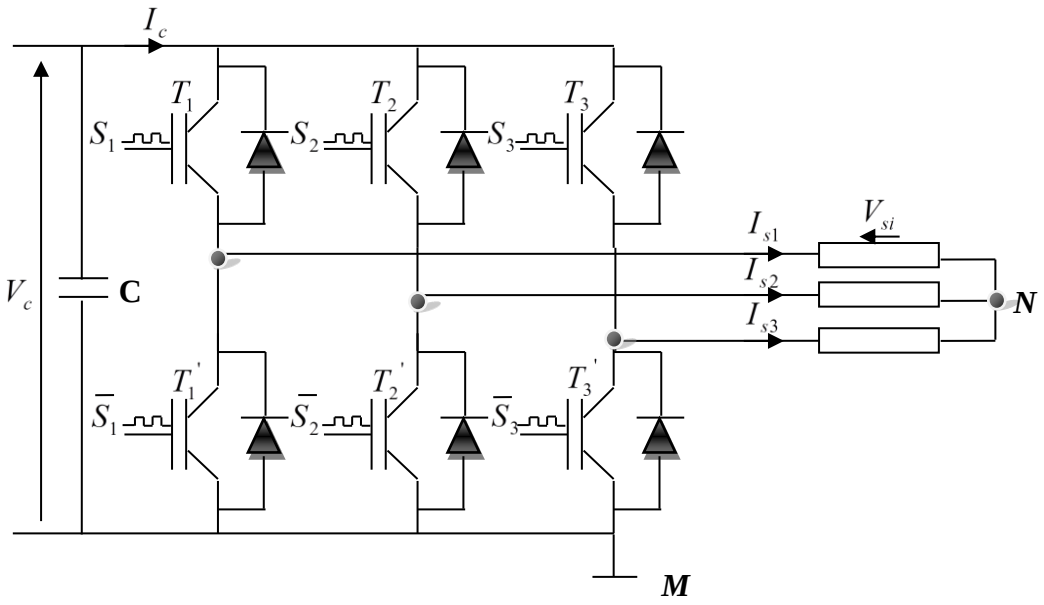

Figure 2.5 Schema of the inverter

Since $V_{iM} = V_c S_{i/i=s1,s2,s3}$ and the load is balanced, the stator voltage ensure that $V_{s1} + V_{s2} + V_{s3} = 0$.

Hence:

$$\begin{bmatrix} V_{s1} \\ V_{s2} \\ V_{s3} \end{bmatrix} = \frac{V_c}{3} \begin{bmatrix} 2 & -1 & -1 \\ -1 & 2 & -1 \\ -1 & -1 & 2 \end{bmatrix} \begin{bmatrix} S_{s1} \\ S_{s2} \\ S_{s2} \end{bmatrix} \quad \textbf{(39)}$$

The input current I_c can be expressed by (40):

$$I_c = S_{s1} I_{s1} + S_{s2} I_{s2} + S_{s3} I_{s3} \quad \textbf{(40)}$$

The sinusoidal PWM allows the control signals S_{s1}, S_{s2} and S_{s3} to be deduced. In fact, this modulation obtained (see [67] for details) by comparing a referential sinusoidal signal called modulating wave, characterized by the frequency f_r and the amplitude V_r) with a triangular signal (called carrier wave, characterized by a frequency $f_p \gg f_r$, and the amplitude [67] V_p. When two signals take the same value, IGBTs change the state, so the PWM signals are generated, with the frequency f_p.

d. Pump

A pump uses the power (in our case given by the panel and/or the battery) to provide a mechanical energy to the water (Figure 2.1). In the literature, these pumps are either positive displacement ordynamic pumps. Positive displacement pumps are used in applications characterized by a constant discharge speed, or at high heads and low flow rates, since this type of pump delivers periodic flows. In our application, dynamic pumps are used, as they are adequate when the application needs a variable discharge speed, or at high flow rate and low or moderate heads [68].

In this context, centrifugal pumps are commonly used, since they require less torque to start, and produce more head than other dynamic pumps at a variable speed [69]. Moreover, in addition to their simplicity and low cost, they are characterized by their low maintenance; and centrifugal pumps are available for different flow rates and heads [68]. Hence, in our application, we choose to use a centrifugal submerged pump.

As it has been previously mentioned, the centrifuge pump is supplied by an IM. To model it, the vector transformation (Appendix D) has been used, and gives the following dynamic model of the IM in a (*d*, *q*) frame (41) [66, 67]:

$$\begin{cases} v_{sd} = R_{ss} I_{sd} + L_s \dfrac{d}{dt} I_{sd} + m \dfrac{d}{dt} I_{rd} - w_s \left(L_s I_{sq} + m I_{rq} \right) \\ v_{sq} = R_{ss} I_{sq} + L_s \dfrac{d}{dt} I_{sq} + m \dfrac{d}{dt} I_{rq} + w_s \left(L_s I_{sd} + m I_{rd} \right) \\ 0 = R_{rr} I_{rd} + L_r \dfrac{d}{dt} I_{rd} + m \dfrac{d}{dt} I_{sd} - w_g \left(L_r I_{rq} + m I_{sq} \right) \\ 0 = R_{rr} I_{rq} + L_r \dfrac{d}{dt} I_{rq} + m \dfrac{d}{dt} I_{sq} + w_g \left(L_r I_{rd} + m I_{sd} \right) \end{cases} \quad \textbf{(41)}$$

with:

v_{sd} : the stator voltage in the direct axe (V),

v_{sq} : the stator voltage in the quadrature axe (V),

I_{sd} : the stator current in the direct axe (A),

I_{sq} : the stator current in the quadrature axe (A),

I_{rd} : the rotor current in the direct axe (A),

I_{rq} : the rotor current in the quadrature axe (A),

R_{ss} : the stator resistance per phase(Ω),

R_{rr} : the rotor resistance per phase(Ω),

L_s : the cyclic stator inductance per phase (H),

L_r : the cyclic rotor inductance per phase (H),

m: the mutual inductance stator-rotor (H),

w_g : the rotor pulsations (rad. s^{-1}).

The electromagnetic torque C_{em} is given by (42) [66, 67]:

$$C_{em} = \mathrm{p} \frac{m}{L_r} \left(\varphi_{rd} I_{sq} - \varphi_{rq} I_{sd} \right) \quad \textbf{(42)}$$

where:

p: the number of poles pairs,

φ_{rd} : the rotor flux in the direct axe,

φ_{rq} : the rotor flux in the quadrature axe.

The mechanic equation is (43) [66, 67]:

$$\frac{d}{dt} w_m = \frac{1}{J} \mathrm{p} \left(C_{em} - C_r \right) \quad \textbf{(43)}$$

In our case, the IM is coupled to a centrifuge pump whose torque is given by (44) [66, 67]:

$$C_r = k w_m \quad \textbf{(44)}$$

where:

$$k = \frac{C_{em\,max}}{w_{m\,max}} \quad \textbf{(45)}$$

where:

$C_{em\,max}$ is the maximum torque and $w_{m\,max}$ is the maximum speed.

During the pump operating, the rotor flux is positioned in a privileged position ($\varphi_{rd} = \varphi_r$ and $\varphi_{rq} = 0$), thanks to the Rotor Field Oriented Control (RFOC) (Figure 2.6). This method consists in controlling, independently, the flux and the current at a constant speed, by acting on the mechanic speed w_m and the rotor flux φ_r, using the direct and the quadrature components of the stator current I_{sd} and I_{sq}, respectively. In this sense, the flux and the current are controlled independently to impose the electromagnetic torque C_{em}. Hence equation (42) becomes [66, 67]:

$$C_{em} = \mathrm{p} \frac{M}{L_r} \varphi_r I_{sq} \quad \textbf{(46)}$$

Since the rotor flux is not accessible, it is estimated using the direct current component I_{sd} as follows [66, 67]:

$$\varphi_{rd} = \frac{M}{1+\tau_r s} I_{sd} \quad \textbf{(47)}$$

In the RFOC, the regulation of the current, flux and the speed is done via PI regulators. The mechanic power of the IM coupled to the pump is [66, 67]:

$$P_L = C_r w_m \quad \textbf{(48)}$$

Coupled to the IM, the total mechanical power is expressed by [66, 67]:

$$P_L = \frac{V\ g\ \rho\ H_h}{\eta_p\ \Delta t} \quad \textbf{(49)}$$

where:

V : the pumped water volume (m^3),

g : the gravity acceleration (m/s^2),

ρ : the water density (Kg/m^3),

H_h : the head height (m),

η_p : the pump efficiency,

Δt : the pumping duration (h).

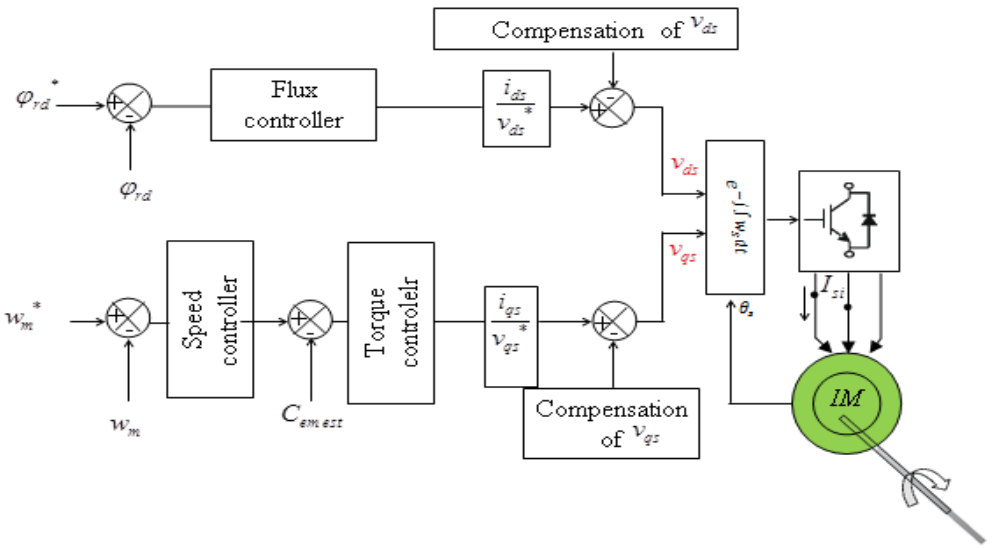

Figure 2. 6 Bloc diagram of the rotor field oriented control

2.5.2 Experimental Validation and Modeling Results

We shall now validate the models of the two main components: the photovoltaic panels and the battery bank, and present the inverter and the IM modeling results.

a. Photovoltaic Panels Models

The experimental validations of the panels models are based on varying the resistance used as a load (Appendix C). Using a solar radiance sensor and a PT1000, the solar radiance G and the photovoltaic cell temperature T_c were measured and used to draw the panel characteristics that correspond to the panel models previously presented in Section 2.5.1, equations (26)-(34) (Figures 2.7 and 2.8).

The validation was carried out by varying the resistance, directly connected to the panels. Current, voltage, radiation and panel temperature were measured, and the results compared with those obtained following the models (26)-(34), using the numerical parameters, presented in Table 2.2, obtained from datasheets of the TE500CR and Sunel panels (Appendix C), and from the literature.

The Sunel module has been divided in three substrings in serial. Hence, we consider the models validation for one Sunel substring. The experimental characteristics of the yield based panel model (26)-(28) are presented in Figures 2.9 and 2.11. The characteristics of the non-linear model (29)-(34) are presented in Figures 2.10, 2.12 and 2.13. The efficiencies of the proposed models are evaluated by calculating the NMBE and the NRMSE, using equations (50) and (51) [40]: they are presented in Tables 2.3 and 2.4.

$$\mathrm{NMBE}(\%) = \frac{\sum_{i=1}^{N} \tilde{X}_i - X_i}{\sum_{i=1}^{N} X_i} * 100 \qquad \textbf{(50)}$$

$$\mathrm{NRMSE}(\%) = \frac{\sqrt{\frac{1}{N}\sum_{i=1}^{N}\left(\tilde{X}_i - X_i\right)^2}}{\frac{1}{N}\sum_{i=1}^{N} X_i} * 100 \qquad \textbf{(51)}$$

Table 2. 2 Numerical parameters for TE500CR and Sunel panels

Parameters	Values (TE500CR)	Values (Sunel)
V_c	22.3 V (Appendix C)	36.7 V (Appendix C)
$I_{sc\_T_{ref}}$	4.2 A (Appendix C)	8.6 A (Appendix C)
n_s	36 cells/ module [40]	60 cells/ module
a	0.095 %/K [40]	0.039 %/K
V_g	1.12 V [40]	
η_r	13% [53]	
β_{pv}	0.4% [53]	
T_{ref}	25ºC [53]	
NOCT	45ºC [53]	
K_B	1.3806×10^{-23} J/ K [40]	
q	1.6×10^{-16} C [40]	
G_{sc}	1367 W/ m^2 [59]	
G_{ref}	1000 W/ m^2 [53]	

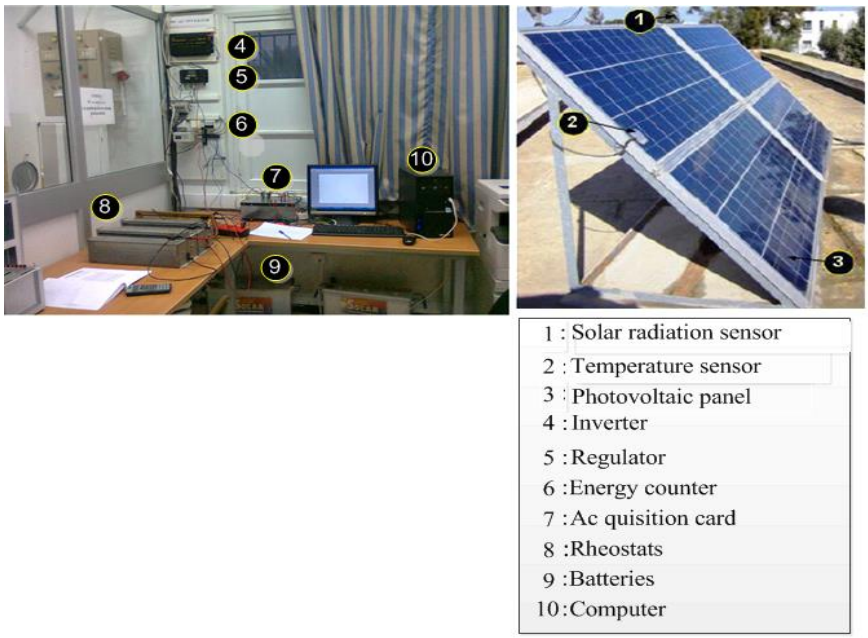

Figure 2. 7 Laboratory system used for validation of the TE500CR model

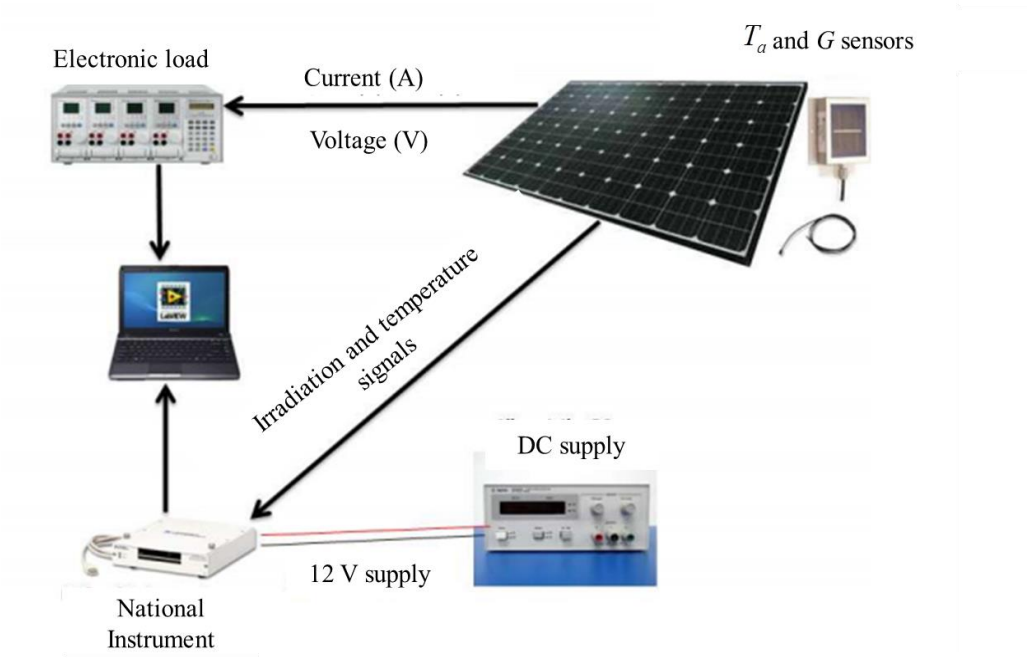

Figure 2. 8 Laboratory system used for validation of the Sunel model

The results show that the characteristics obtained for the models are very similar to those obtained in the experimental validation, for both panels. In fact, for the yield based model (Figures 2.9 and 2.11), the experimental and model results are similar. For example the NMBE for both TE500CR and Sunel panels are 3.77 % and 2.26 %, respectively (Tables 2.3 and 2.4). The difference between the corresponding curves can be attributed to measurement errors [60]. Hence, the use of this yield-based model for sizing is adequate. Figures 2.10 and 2.12 show that there are small differences in I_{sc} and V_c obtained by the non-linear panel model and experiments for both panels. These differences are demonstrated by the NMRSE values for both panels (6.89% for TE500CR and 5.77% for Sunel). Indeed, the change in the solar radiation affects the measurement: in reality, it is not possible to get the exact PV current and voltage values that correspond to one solar radiation when changing the load resistance, due to the solar radiation's rapid change. In addition, some differences between the model and the measured values of the PV current and power are due to the uncertainty in the selection of the parameters values and to simplifications adopted when modeling [60]. For example, there is a small difference between the values of the temperature coefficient a of the short

circuit current I_{sc}, given by the manufacturer and the value calculated (Table 2.5), as follows [40]:

$$a = \frac{I_{sc\,T_2} - I_{sc\,T_1}}{I_{sc\,T_1}} * \frac{1}{T_2 - T_1} \quad \textbf{(52)}$$

where:

$I_{sc\,T_2}$: the short circuit current at the temperature T_2 (A),

$I_{sc\,T_1}$: the short circuit current at the temperature T_1 (A).

Both the model and experimental characteristics of the PV currents show that the increase in the solar radiation *G* implies an increase in the generated current. Instead, the temperature increase at the module surface T_c decreases the open-circuit voltage V_c (Figures 2.12 and 2.13).

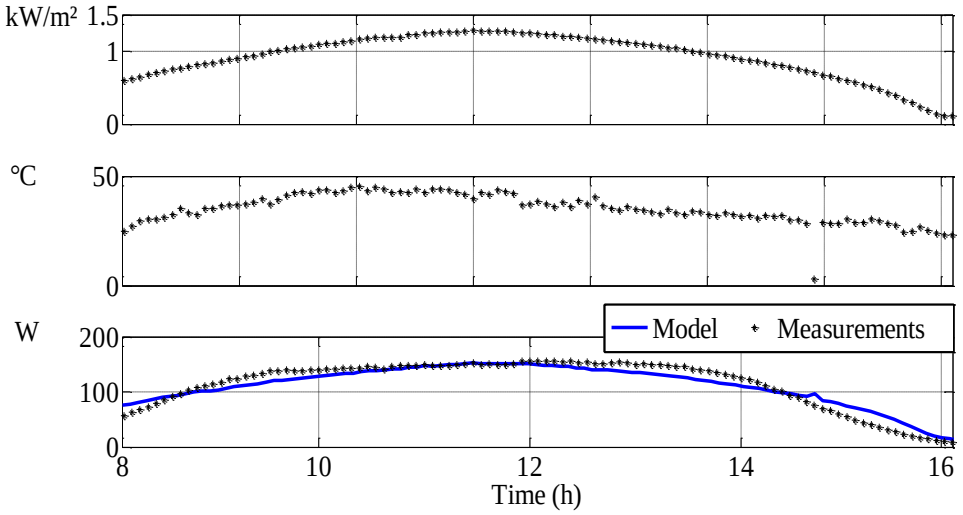

Figure 2.9 Yield based panel model validation for the TE500CR panel

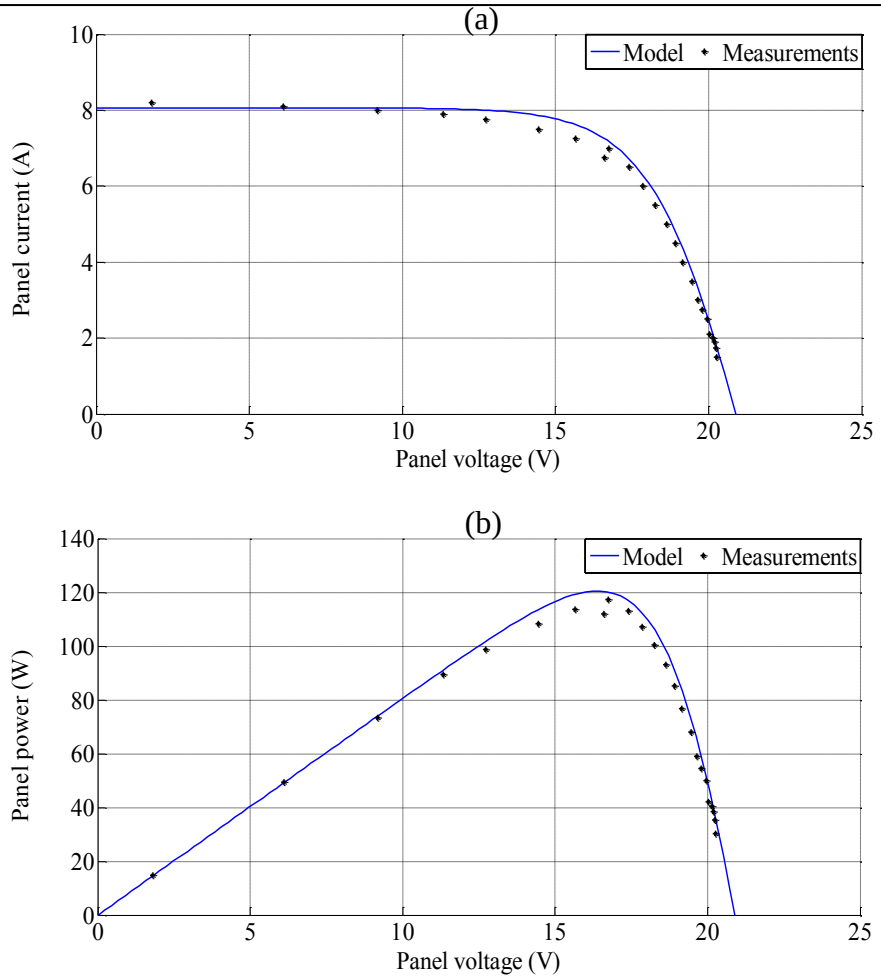

Figure 2. 10 TE500CR Photovoltaic Panel I-V (a) and P-V (b) curves at $G \approx 480\ \mathrm{W}/m^2$ and $T_c \approx 25°\mathrm{C}$

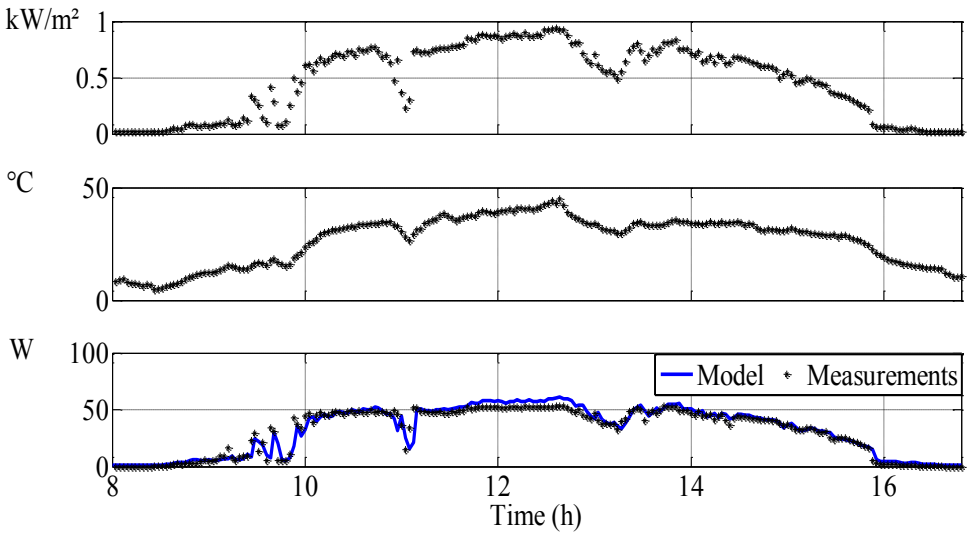

Figure 2.11 Yield based panel model validation for the Sunel panel

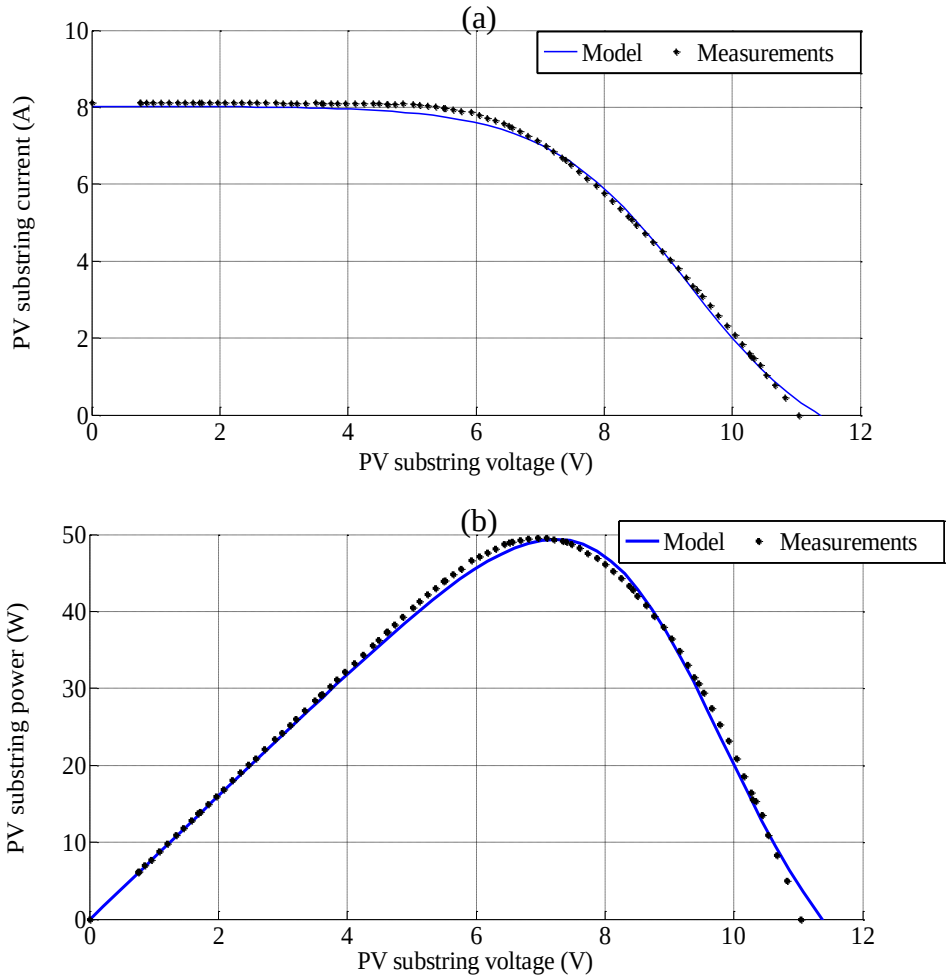

Figure 2. 12 Sunel Photovoltaic substring I-V (a) and P-V (b) curves at $G \approx 864$ W/m^2 and $T_c \approx 45$°C

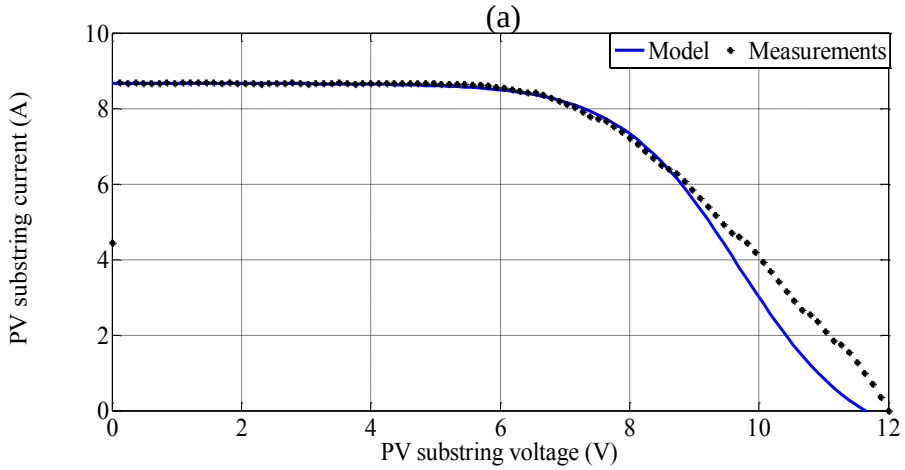

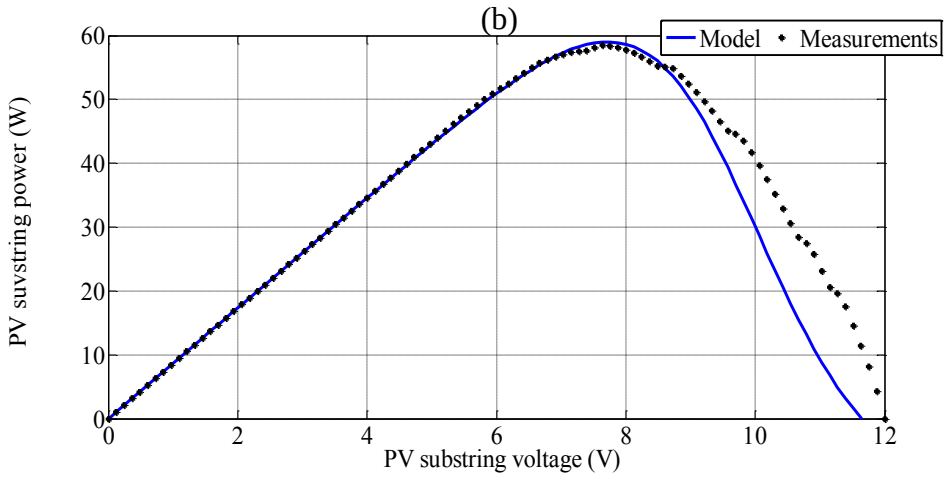

Figure 2. 13 Sunel Photovoltaic substring I-V (a) and P-V (b) curves at $G \approx 950\text{W}/m^2$ and $T_c \approx 40°\text{C}$

Table 2.3 NMBE and NRMSE evaluation for the TE500CR panel

Parameters	**NMBE**	**NRMSE**
P_{PV} (yield model)	3.77%	4.59%
I_{PV} (nonlinear model)	4.55%	6.89%

Table 2. 4 NMBE and NRMSE evaluation for the Sunel panel

Parameters	**NMBE**	**NRMSE**
P_{PV} (yield model)	2.26 %	3.45 %
I_{PV} (nonlinear model)	-2.19%	5.77%

Table 2.5 Temperature coefficients *a* for TE500CR and Sunel panels (Appendix C)

Parameters	**TE500CR**	**Sunel**
Manufacture	0.095%/K	0.039 %/K
Calculation	0.083 %/K	0.06 %/K

b. Battery Bank Model

The validation of the battery model was carried out by keeping the battery voltage constant (using the voltage regulator) and varying the load resistance. The results, presented in Figure 2.14, are compared to those obtained by the model detailed in Section 2.5.1.b, using data given by the manufacturer and the literature, shown in Table 2.6.

Table 2. 6 Numerical parameters for the lead– acid battery

Parameters	**Values**
C_p	210 A.h (Appendix C)
V_{bat}	12 V (Appendix C)
R_t	0.0126 Ω [65]
R_e	0.0168 Ω [65]
$R_s^{'}$	0.0168 Ω [65]
k_p	1.12 [40]

The *dod* values obtained by the experimental validation (directly obtained from the battery regulator) and the battery bank model are similar. This proves that the adopted model is efficient. Moreover, the relation between the *dod* and the battery current is clear: when the battery is in charge, I_{bat} is positive and the *dod* decreases. For example, using the measured results, starting from 50% of the battery capacity, the battery is charged for 10 min with a constant current equal to 4.5 A, and the *dod* decreases to 16%. When the battery is discharging with a constant current equal to 9.7 A for 10 min, the *dod* increases from 16% to 68%.

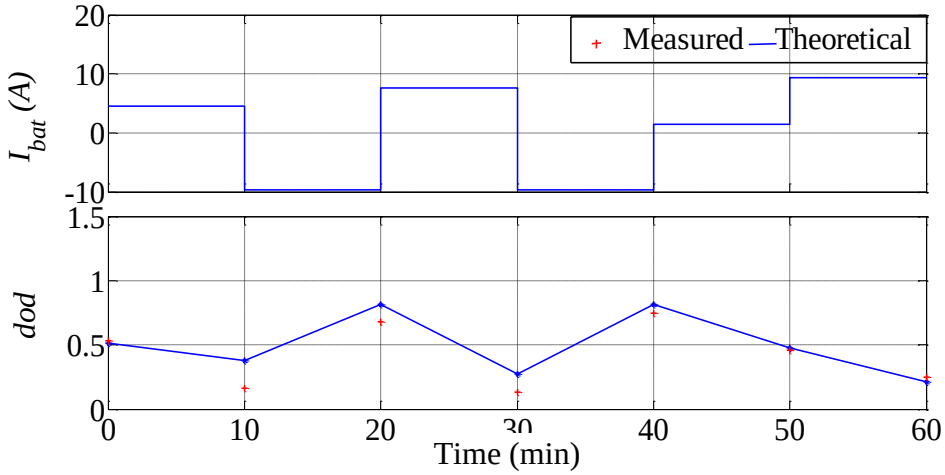

Figure 2. 14 Battery model validation

c. Inverter Model

The PWM signals for the control of the switches T_1, T_2 and T_3 are presented in Figure 2.15. The results of Figures 2.16 and 2.17 show that the inverter generates the voltage and current signals with an values $V_{eff} = 230V$ and $I_{seff} = 14.14A$, which corresponds to the nominal values for the induction machine used (Appendix D).

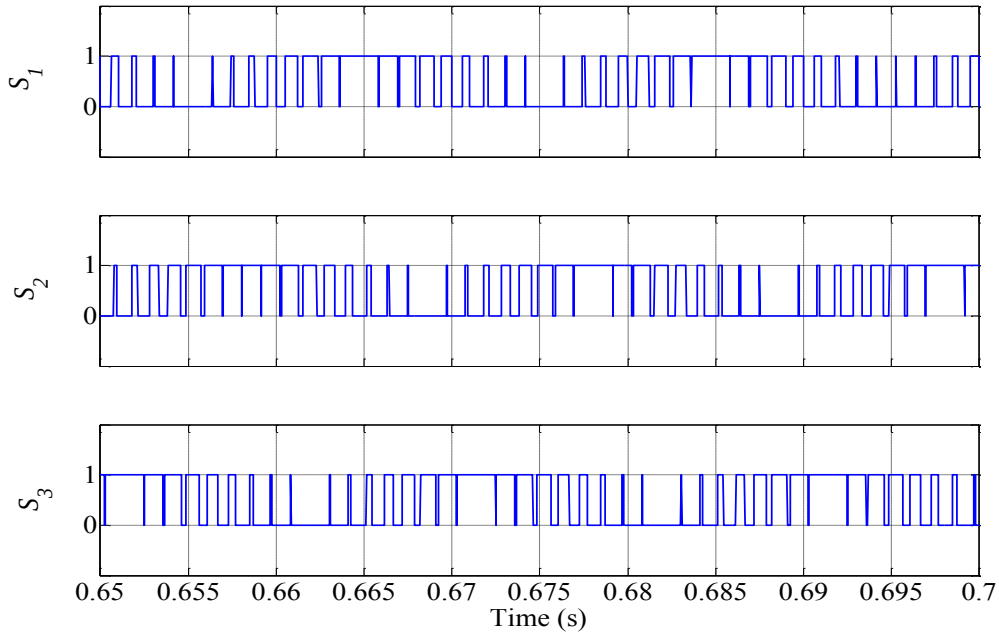

Figure 2. 15 PWM signals of the inverter

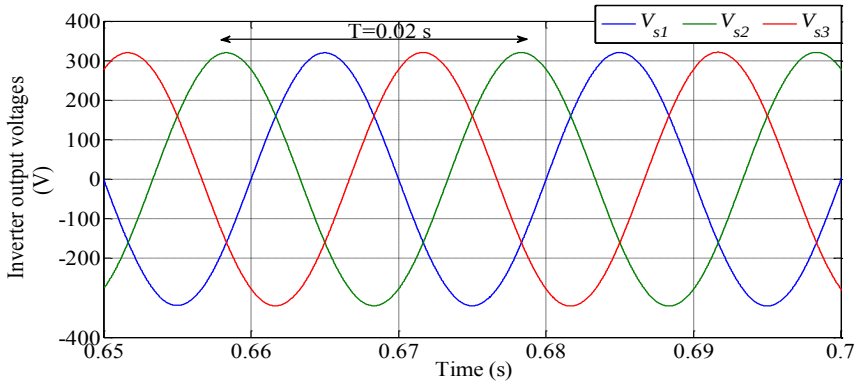

Figure 2. 16 Inverter output voltages

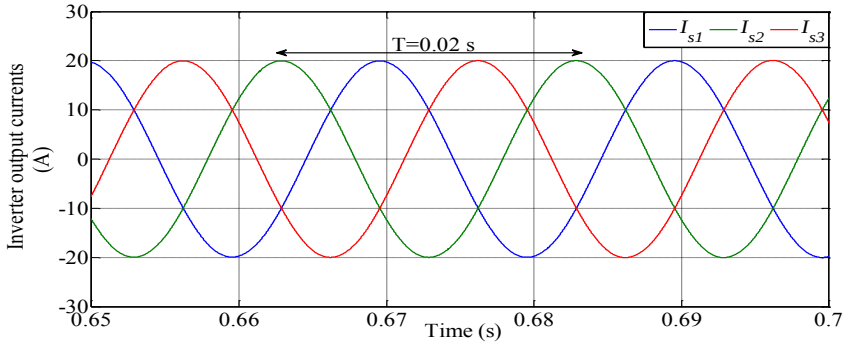

Figure 2. 17 Inverter output currents

d. Pump

The simulation results of the pump are presented in Figure 2.18.

Table 2. 7 IM parameters [67]

Parameters	**Values**
R_{ss}	5.72 Ω
R_{rr}	4.2 Ω
L_s	0.462 H
L_r	0.462 H
M	0.44 H
p	2
J	0.0049 kg.m²

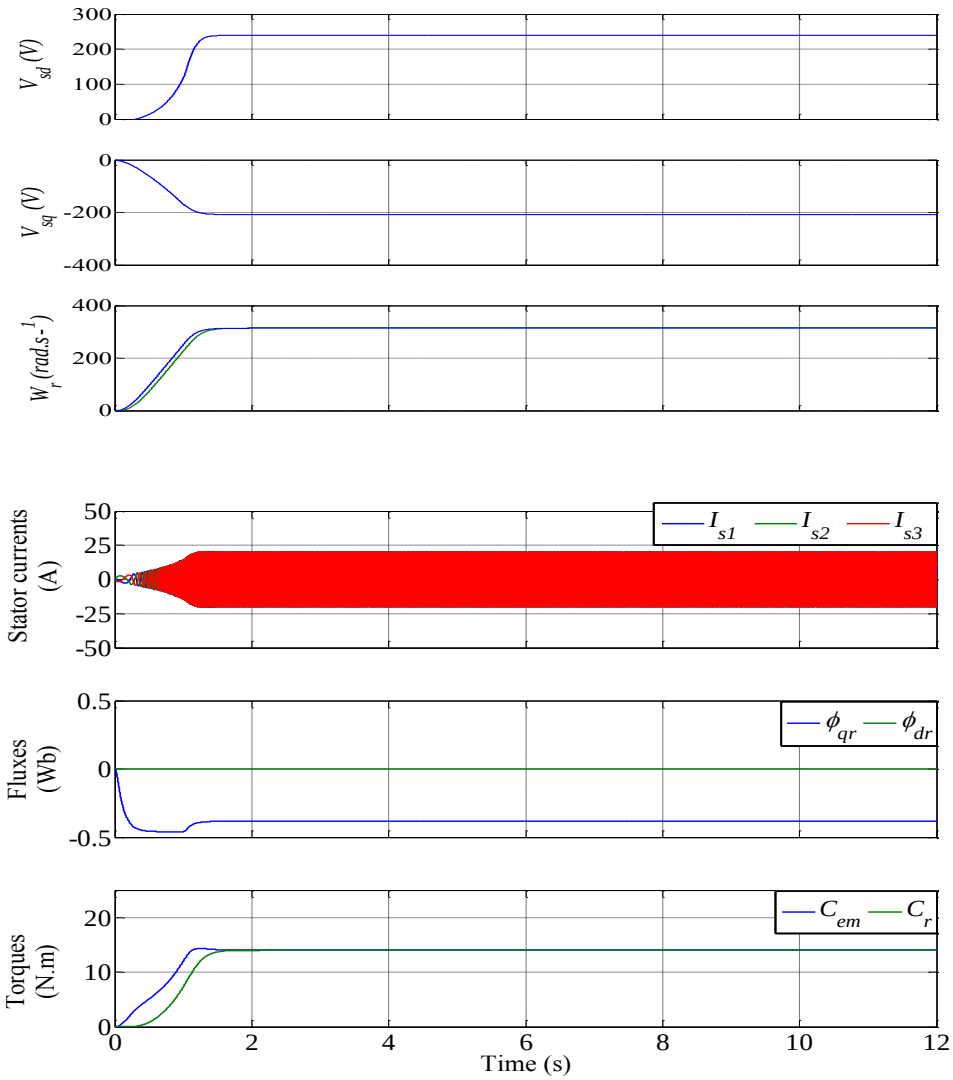

Figure 2. 18 IM simulation results using RFOC

2.6 System Components Sizing

In this section, we propose the algorithm used to size the installation components. The sizing results are validated using measured data of the target area and later using HOMER. Then, an economic comparison between the basic method and our proposed algorithm for sizing the components of a photovoltaic pumping installation is proposed.

2.6.1 Algorithm Proposal

A good sizing must fulfill that the installation provide the electrical demand of the load [70]. Hence, the algorithm's main objective is to ensure the load supply throughout the day, while protecting the battery against deep discharge or

excessive charge and guaranteeing the water volume needed for the irrigation. The scheme of the proposed approach is presented in Figure 2.19 [42]. The algorithm depends on:

- The water volume needed,
- the site characteristics,
- the panel characteristics,

Our algorithm aims to find the optimum panels surface S_{opt} and the batteries' number $n_{bat_{opt}}$ that guarantee the installation autonomy when supplying the pump. Hence, the idea consists in searching the optimal components sizes that ensure the balance between the charged and the extracted energies E_c and E_e, respectively. In fact, the battery bank supply the load when the panel does not generate the sufficient power, and is charged with the PV energy produced in excess (Figure 2.20). The energy balance can be expressed as follows:

$$E_c \simeq E_{AM} + E_{PM} \quad \textbf{(53)}$$

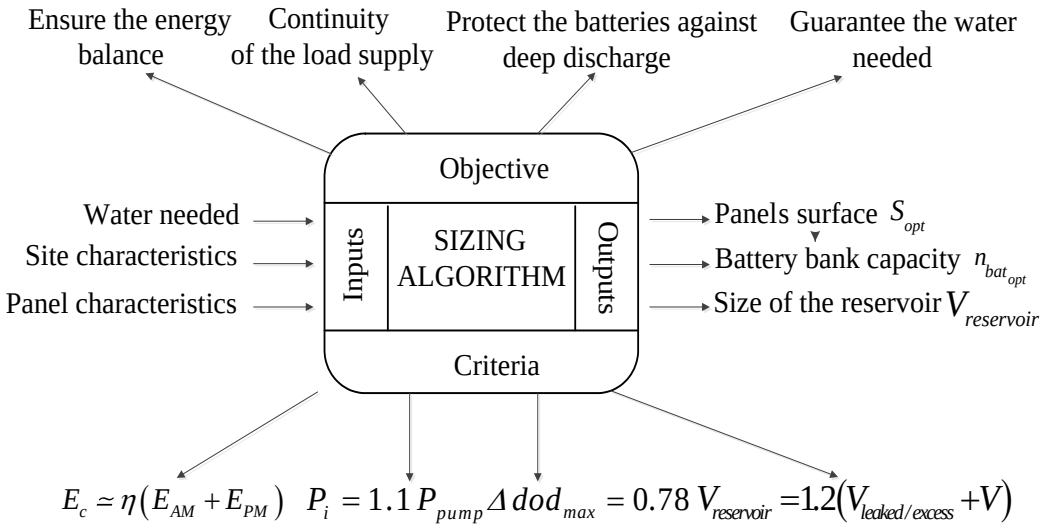

Figure 2.19 Planning of the proposed sizing algorithm

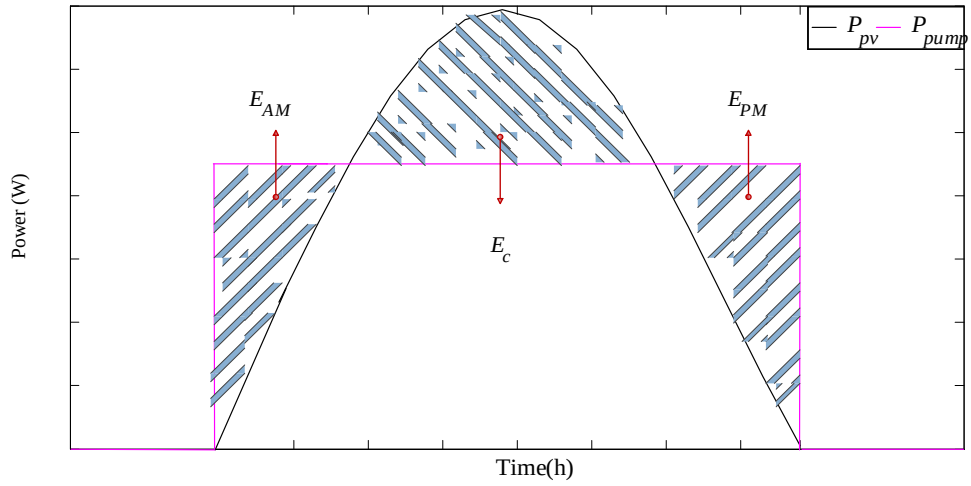

Figure 2.20 Energy balance principle

The sizing algorithm is performed using two sub algorithms during the crops' vegetative cycle (*March* to *July*): the first Algorithm 2.1 allows the size of the panel surface S_M and the number of batteries n_{bat_M} to be determined for each month *M*. Then, Algorithm 2.2 is performed to deduce the final system components' sizes. Algorithm 2.1 is detailed now in steps following the approach presented in Figure 2.21.

a) Algorithm 2.1: Determination of S_M *and* n_{bat_M}

Step 1 Estimation of the diffused and direct radiation using equations (13) and (19).

Step 2 Deduction of the solar radiation $H_t(t,d)$ in a tilted panel using (20).

Step 3 Estimation of the cell temperature $T_c(t)$ using (27).

Step 4 Deduction of the panel yield $\eta_{pv}(t)$ using (26) [53].

Step 5 Calculation of the crops' water needs *V*:

The determination of the water volume needed for tomato growth is essential to define the amount of water to be pumped. The water volume depends essentially on the crop growth stage and the evapotranspiration [71]. In the literature, many models have been used

to describe the evapotranspiration. For instance, [72] used the Penman Method, which depends essentially on the net radiation at the crop surface, the mean air temperature, and the wind speed. [73] presented some models to describe the evapotranspiration, such as the Thorenthwet method, which depends on the sunlight duration and the air temperature. The Blaney-Criddle method has also been used. This method includes the seasonal crop coefficient k_c, in addition to the sunlight duration and the air temperature, which provides better patterns of the needed water volume. For this reason, we use the Blaney-Criddle method in our study.

The daily water volume V_n, required by the crop is given by [71]:

$$V_n = k_c \, E_{To} \tag{54}$$

where:

k_c: the monthly crop growth coefficient,

E_{To}: the monthly reference evapotranspiration average, which depends on the ratio of the mean daily daytime hours for a given month to the total daytime hours in the year p and the mean monthly air temperature T for the corresponding month, is evaluated [73, 74]:

$$E_{To} = K \, p \left(0.46\,T + 8.13\right) \tag{55}$$

where K is the correction factor, expressed by [73]:

$$K = 0.03\,T + 0.24 \tag{56}$$

To obtain the necessary gross water, it is essential to estimate the irrigation losses. For this, an additional water quantity must be provided for the irrigation to compensate for those losses. Thus, the final recommended water volume is evaluated as follows [75]:

$$V = \left(k_c E_{To} - r_m\right)\left(1 + \frac{1 - l_f\left(1 - L_R\right)}{l_f\left(1 - L_R\right)}\right) \tag{57}$$

where:

r_m: the average monthly rain volume,

l_f : leaching efficiency coefficient as a function of the irrigation water applied [76],

L_R : the leaching fraction given by the humidity that remains in the soil, expressed by [77]:

$$L_R = \frac{EC_w}{5\,EC_e - EC_w} \quad \textbf{(58)}$$

EC_w : the electrical conductivity of the irrigation water (dS. m^{-1}),

EC_e : the crop salt tolerance (dS. m^{-1}).

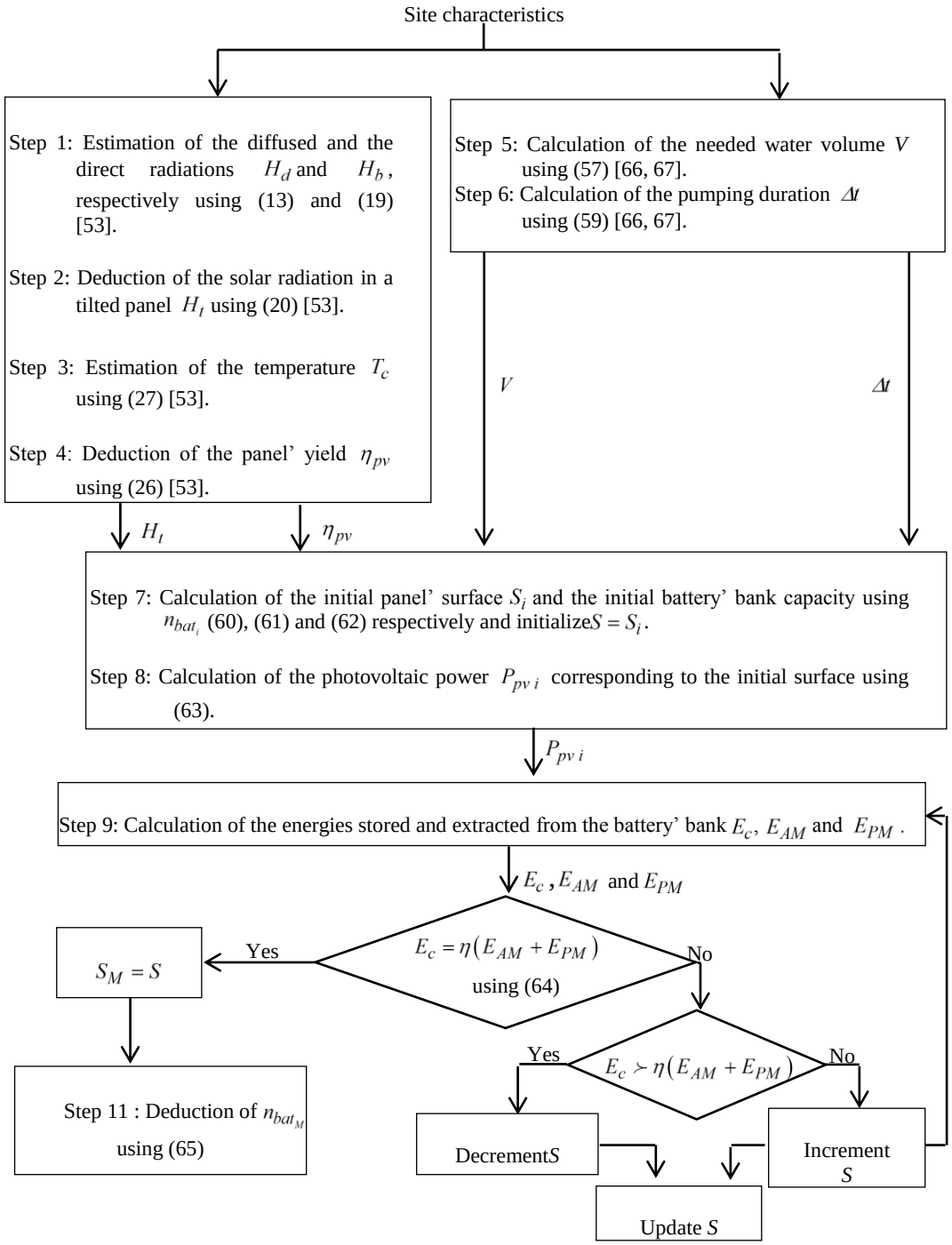

Figure 2.21 Sizing Algorithm 2.1 for each month *M*

Step 6 Calculation of the pumping duration Δt. In our application, the pump's flux is constant. Thus, Δt can be evaluated as follows:

$$\Delta t = \frac{P_{pump}}{Q} \tag{59}$$

Step 7 Calculation of the minimum panel surface S_i and the initial battery number n_{bat_i} using equations (60), (61) and (62) respectively, based on the irrigation frequency (Appendix B) [53]:

$$S_i = \frac{P_{pump}\ \Delta t}{W_{pv}\ \eta_{bat}{}^2\ \eta_l\ \eta_{pv}\ \eta_{reg}\ \eta_{inv}\ \eta_{opt\,ther}\ \eta_{matching}} \left(1 + \frac{d_{aut}}{d_{rech}}\right) \tag{60}$$

$$E_c = E_{tot}\ \Delta dod_{max} = E_d\ d_{aut} \tag{61}$$

Hence:

$$n_{bat_i} = \frac{E_d\ d_{aut}}{V_{bat}\ C_{bat} \Delta dod_{max}} \tag{62}$$

with:

P_{pump}: the pump power (W),

Δt: the water pumping duration (h),

d_{aut}: the days of autonomy,

d_{rech}: the days needed to recharge the battery,

W_{pv}: the average daily radiation (Wh/m^2 / day),

η_{bat}: the electrical efficiency of the battery bank,

η_l: the electrical efficiency of the installation that includes the ohmic wiring and mismatching wiring losses,

η_{pv}: the efficiency of each photovoltaic panel,

η_{reg}: the regulator performance,

η_{inv}: the inverter performance,

$\eta_{opt\,ther}$: the panel performance facing to optical and thermal effects (%),

$\eta_{matching}$: the panel matching performance (%),

E_d : the daily consumption (Wh),

V_{bat} : the battery voltage (V),

Δdod_{max} : the maximum dod variation (%),

C_{bat} : the nominal capacity for one battery (Ah).

Step 8 Calculation of P_{pvi} corresponding to the minimum panel surface S_i, using the following equation (63) [53]:

$$P_{pv\,i} = \eta_{pv}\,\eta_{otpther}\,\eta_{reg}\,\eta_{matching}\,S_i\,H_t \qquad \textbf{(63)}$$

where:

η_{pv} : the panels yield (%), (26),

$\eta_{opt\,ther}$: the panel performance facing to optical and thermal effects (%),

$\eta_{matching}$: the panel matching performance (%),

H_t : the solar radiation on a tilted panel (W/ m^2), (20),

S_i : the initial panel surface (m^2),

Step 9 Calculation of the energies expected to be stored and extracted from the battery each day by evaluating the area E_c and E_e, respectively, (Figure 2.20).

Step 10 If the discharged energy is higher than the charged energy, the algorithm increases the panel surface by the minimum increment of the PVP size commercially available: the algorithm looks for the best configuration to guarantee the balance between the demanded and the produced energies, by ensuring the equality between the charged E_c and discharged energies E_e in the battery bank (53).

The balance between the charged and the extracted energies E_c and E_e respectively, does not guarantee the system's autonomy, due to the fluctuation in the solar radiation and the energy losses in the installation components. Thus, to ensure the system's autonomy and

protect the battery against deep discharges, the algorithm is performed by adopting an efficiency coefficient η that allows the Δdod to be less than Δdod_{max} (η is equal to 1.28* η_{error} in our case, where η_{error} describes the error between the clear sky and measured solar energies). Thus, equation (53) becomes:

$$E_c \simeq \eta\left(E_{AM} + E_{PM}\right) \quad \textbf{(64)}$$

Moreover, to ensure the continuity of the load supply, the previous condition is performed with $P_i = 1.1 P_{pump}$.

Step 11 Deduction of n_{bat_M} [53]:

$$n_{bat_M} = \frac{E_c}{C_{bat}^{\ k_p}} \quad \textbf{(65)}$$

where:

E_c : the energy charged in the battery bank (Wh),

C_{bat} : the nominal capacity for one battery (Ah),

b) Algorithm 2.2: Deduction of S_{opt} and C_{opt}

Using Algorithm 2.2, presented in Figure 2.22, the final values of the panel surface S_{opt} and the capacities number $n_{bat_{opt}}$, are then deduced. S_{opt} corresponds to the maximum value of the panel surface obtained during the months. The optimum batteries number is the corresponding value for S_{opt}, since it is the most critical month.

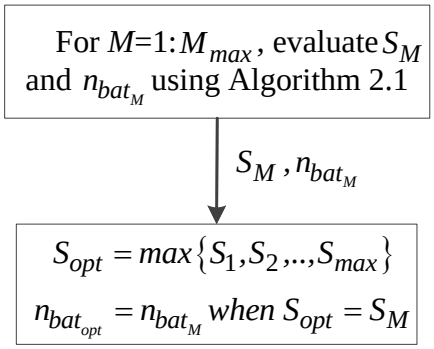

Figure 2. 22 Sizing Algorithm 2.2

2.6.2 Application to a Case Study

The sizing algorithm 2.2 is applied now to evaluate the components sizes of the studied installation. The proposed algorithm is tested during the months that correspond to the vegetative cycle of tomatoes (*March* to *July*), using data of the target area.

a. Sizing for the Case Study

Components parameters (Table 2.8), climatic and site characteristics data of the 10 ha land surface located in Medjez El Beb (Northern of Tunisia) have been used to calculate the components size.

Table 2.8 Components parameters

Parameters	**Values**
η_{bat}	90 % [40]
$\eta_{inverter}$	92 % (Appendix C)
η_{l}	95 % [40]
$\eta_{matching}$	80 % (Appendix C)
$\eta_{opt\,therm}$	90 % (Appendix (C)
η_{reg}	90 % [40]
η_{r}	10.58 % (Appendix C)

To evaluate the solar radiation on a tilted panel, the choice of the tilted angle has been chosen based on PVsyst analysis (Figures 2.23 and 2.24). In fact, considering the latitude angle as the tilted angle allows the transposition factor TF to be near to its optimum value (TF_{annual} = 96% for the annual and $TF_{monthly}$ = 90% for the sunny months).

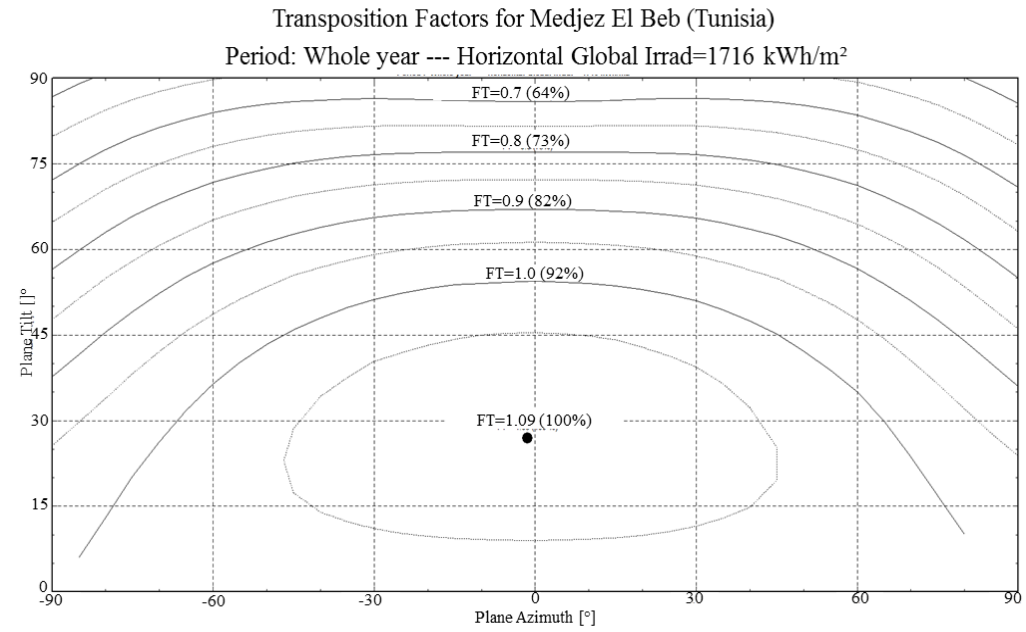

Figure 2. 23 Annual transposition factor for Medjez El Beb

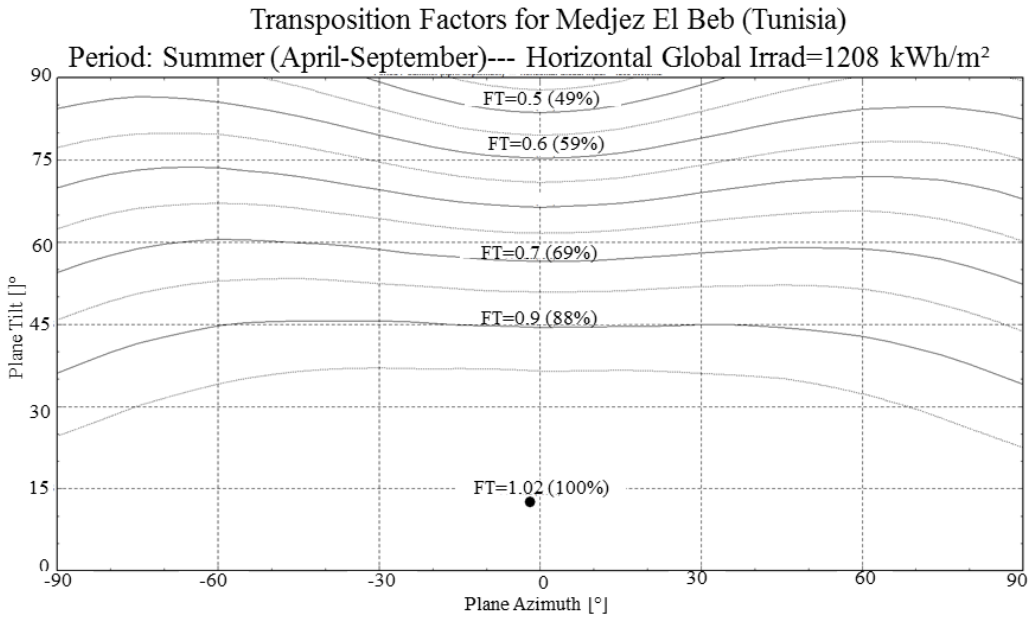

Figure 2. 24 Monthly transposition factor for Medjez El Beb

In our study, we will consider the TE500CR panel. The solar radiation G is presented in Figure 2.25, the ambient temperature T_a in Figure 2.26 and the average monthly rain volume r_m, the monthly reference evapotranspiration E_{To} and the monthly crop growth coefficient k_c in Figure 2.26.

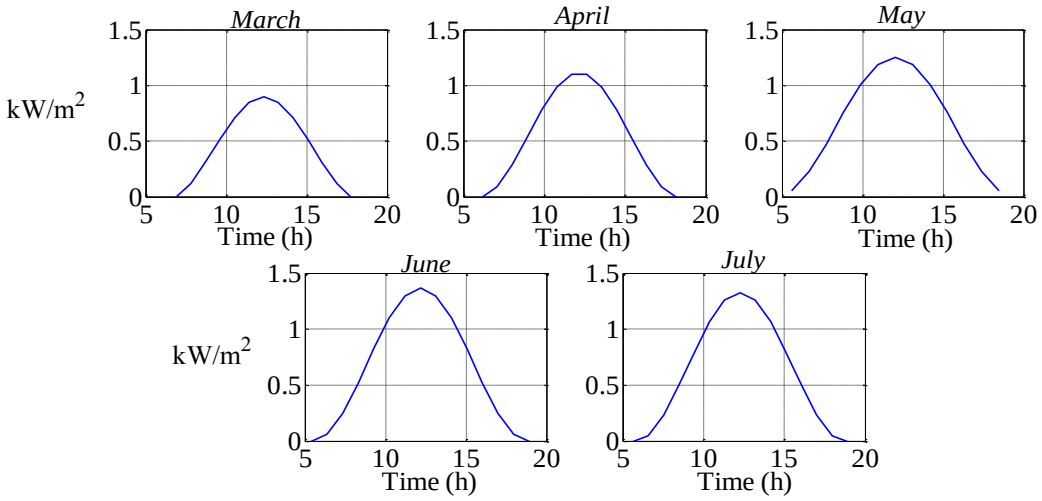

Figure 2.25 Solar radiation *G* for each month *M* at the target location

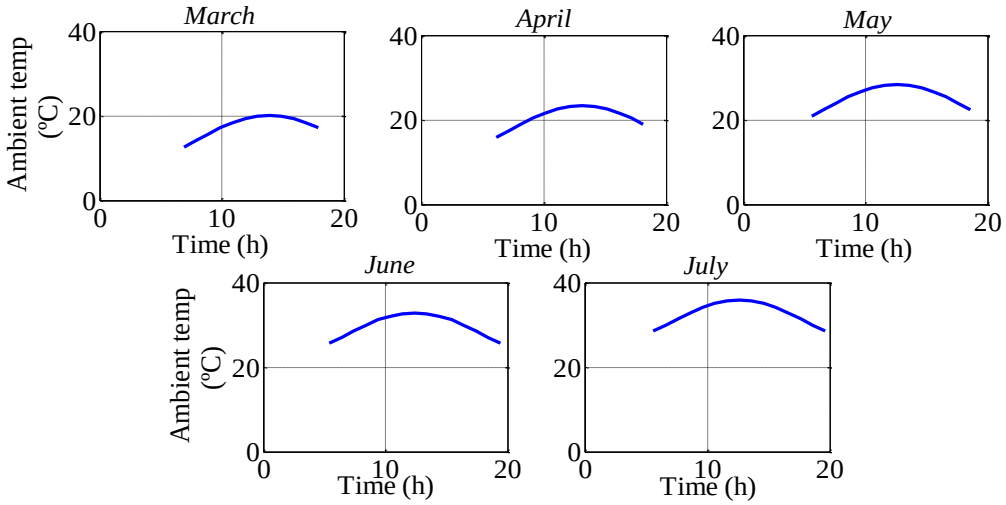

Figure 2.26 Ambient temperature T_a for each month *M* at the target location

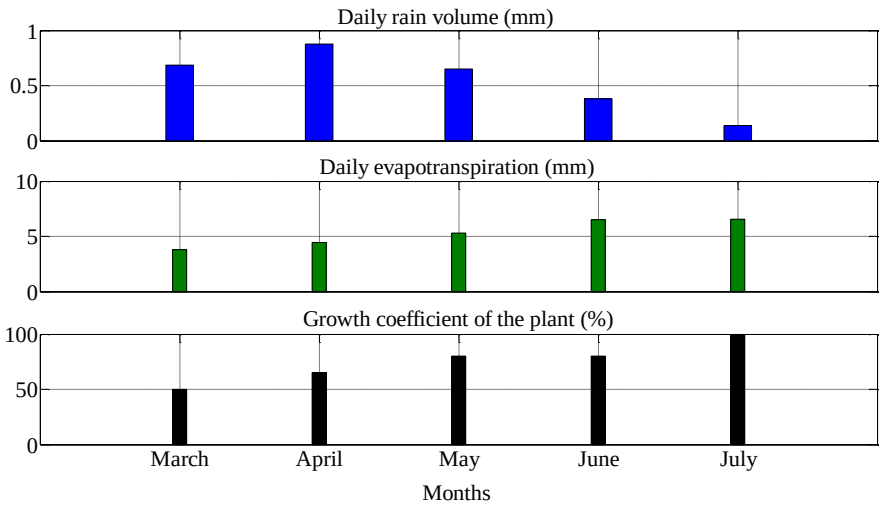

Figure 2. 27 Crops characteristics and daily rain estimation for each month *M*

The Algorithm 2.1 was first evaluated. That is, the solar radiation accumulated on a tilted panel is evaluated using (24). Then, the panel yield is calculated for each month using (26) (Table 2.9). In parallel, the water needed *V* is evaluated depending on the crops vegetative cycle and the site characteristics using (57), and thus, the pumping duration Δt is deduced using (59).

The initial values of S_i, and n_{bat_i}, summarized in Table 2.10, are used to test the condition (64). Indeed, if the charged energy is higher than the discharged energy, the panel surface is increased by the minimum panel available surface in the market (in our case, the increment is $0.5\,m^2$), and vice versa.

The maximum number of cloudy days per month n_{c_i} and the amount of clouds per day A_{c_i} are evaluated for each month *M* to deduce the days of autonomy. They are calculated using (66)–(67):

$$n_{c_i} = \frac{n_{M_i} \cdot \left(W_{pvc_i} - \bar{H}_{t_i}\right)}{(1 - DA_i) W_{pvc_i}} \tag{66}$$

$$A_{c_i} = \frac{W_{pvc_i} - \bar{H}_{t_i}}{W_{pvc_i}} \tag{67}$$

where:

n_{M_i} : the days number in the month *M*,

W_{pvc_i} : the solar energy for the month *M* using the clear sky model (Wh),

$\overline{H_{t_i}}$: the the solar energy for the month *M* using the clear database (Wh),

DA_i : the ratio between diffuse and global daily solar radiation.

Table 2.9 Climatic parameters, panel efficiency and irrigation parameters estimated for the case study

Months / *Results*	*March*	*April*	*May*	*June*	*July*
T_a (°C)	14	17.25	20	22	30
$\bar{H}$ (Wh)	4023.6	5512.3	5815.2	7392.2	7163.2
k_t (%)	54	51	54	61	64
W_{pv} (Wh) (24)	5908.6	7562.1	8030.9	9479.0	9136.7
η_{pv} (%) (26)	10.16	10.06	9.91	9.75	9.37
Water volume $m^3/10\,ha$ (57)	60.70	100.37	179.82	241.10	321.03
Pumping duration Δt (h) (59)	2.5	4.13	7.41	9.93	13.25

Table 2.10 Initial values of the panels surface and number of batteries

Months / *Results*	*March*			*April*			*May*
W_{pvc} (clear sky model) (Wh)	5760			7180			8120
Maximum number of cloudy days per month n_c (66)	9			7			9
Clouds rate per day A_c (%) (67)	30.15			23.23			28.38
Irrigation frequency f_i (Appendix B)	3	3	2	2	2	1	1
d_{aut}	1	1	1	1	1	1	1
d_{rech}	3	3	2	2	2	1	1

Initial panel surface (m^2) (60), (61)	61	61	68	89	89	107	203
Initial numbers of batteries n_{bat_i} (62)	4	4	4	5	5	5	10

Months / *Results*	*June*		*July*	
W_{pvc} (clear sky model) (Wh)	8500		8340	
Maximum number of cloudy days per month n_c (66)	3		4	
Clouds rate per day (%) A_c (67)	13.03		14.11	
Irrigation frequency f_i (Appendix B)	1	1	2	2
d_{aut}	1	1	1	1
d_{rech}	1	1	2	2
Initial panel surface (m^2) (60), (61)	234.5	337	168.5	168.5
Initial numbers of batteries n_{bat_i} (62)	14	18	18	18

Algorithm 2.1 results are summarized in Table 2.11 and evaluated in Figures 2.28 and 2.29. They show that the proposed strategy always ensures the needed water volume, respects the battery bank' depth of discharge limits and the energy balance. In fact, Figures 2.28 and 2.29 prove that the proposed algorithm guarantees the needed water volume for the crops irrigation, since the pump is supplied by the panels and the battery bank. This has been proved for all the months of the crops' vegetative cycle, using the daily clouds amount. Moreover, this algorithm ensures the energy balance for each month *M*: in Table 2.11, the efficiency coefficient η is around the fixed values throughout all the considered months. For this value, Δdod_{max} is guaranteed to be equal to 0.78.

For instance, in *July*, η is fixed to be equal to 1.46. The obtained value η_1 with the algorithm is equal to 1.47. Moreover, in *March*, the generated photovoltaic power during the morning is used to supply the pump together with the battery bank during the pumping duration. Then, the photovoltaic power generated is used to charge the battery bank for the rest of the day hours. The quotient between the cumulated and extracted energies is equal to 1.67, which is near to the value initially fixed in Algorithm 2.1 $(\eta = 1.7)$.Thus, the extracted energy (E_e) is almost equal to the accumulated energy (E_c).

For the energy balance, an error coefficient obtained by the evaluation of the daily clouds amount is used. Hence, in our study, we take into account the possibility of having cloudy days. For example, in *April* the amount of clouds per day is 23.23 %.

Figures 2.28 and 2.29 prove that the obtained panels surface and battery bank capacity obtained by Algorithm 2.1 satisfy the energy balance. In other terms, all the stored energy is consumed. This is possible thanks to the calculation of the number of batteries, which is done by considering the same Δdod_{max} value that can be reached, for all the months (Δdod_{max} = 0.78).

Hence, the obtained surface allows the load to be supplied during the requested pumping duration Δt, and also provides the energy E_c needed to charge the battery bank.

Table 2.11 Summary of the results of the calculation of the minimum panel surface and number of batteries needed each month *M*

Months / *Results*	*March*	*April*	*May*	*June*	*July*
η_{error}	1.30	1.23	1.28	1.13	1.14
$E_{AM} + E_{PM}$ (Wh/ day)	10991	14481	10239	12511	24046
E_c (Wh/ day)	18725	23035	16807	18033	35314
E_{pump} (Wh/ day)	11258	18615	33350	44716	59541

E_{PV} (Wh)	20371	29296	43378	55035	82802
$S_M\left(m^2\right)$	**37.5**	**41.5**	**54.5**	**61.5**	**101.5**
n_{bat_M} (65)	**4**	**5**	**4**	**5**	**8**
η (64)	***1.66***	***1.57***	***1.64***	***1.44***	***1.46***
$\eta_1 = \frac{E_c}{E_{AM} + E_{PM}}$ (64)	***1.7***	***1.59***	***1.64***	***1.44***	***1.47***

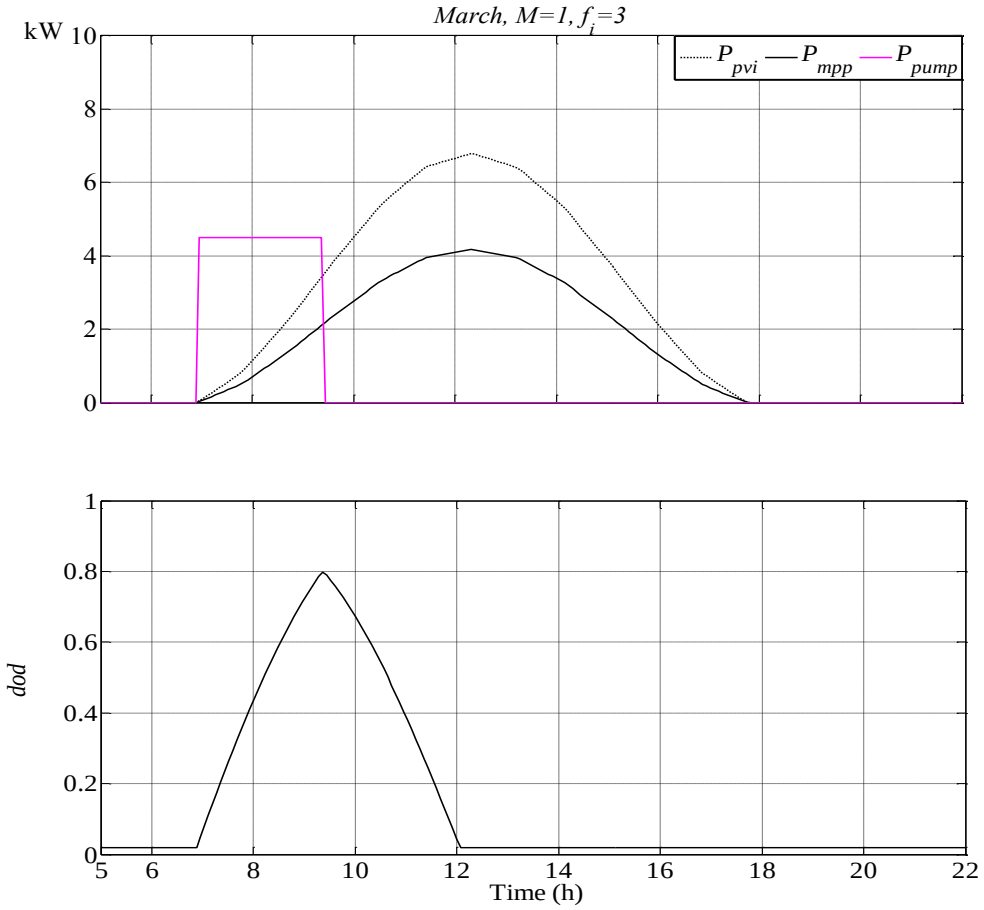

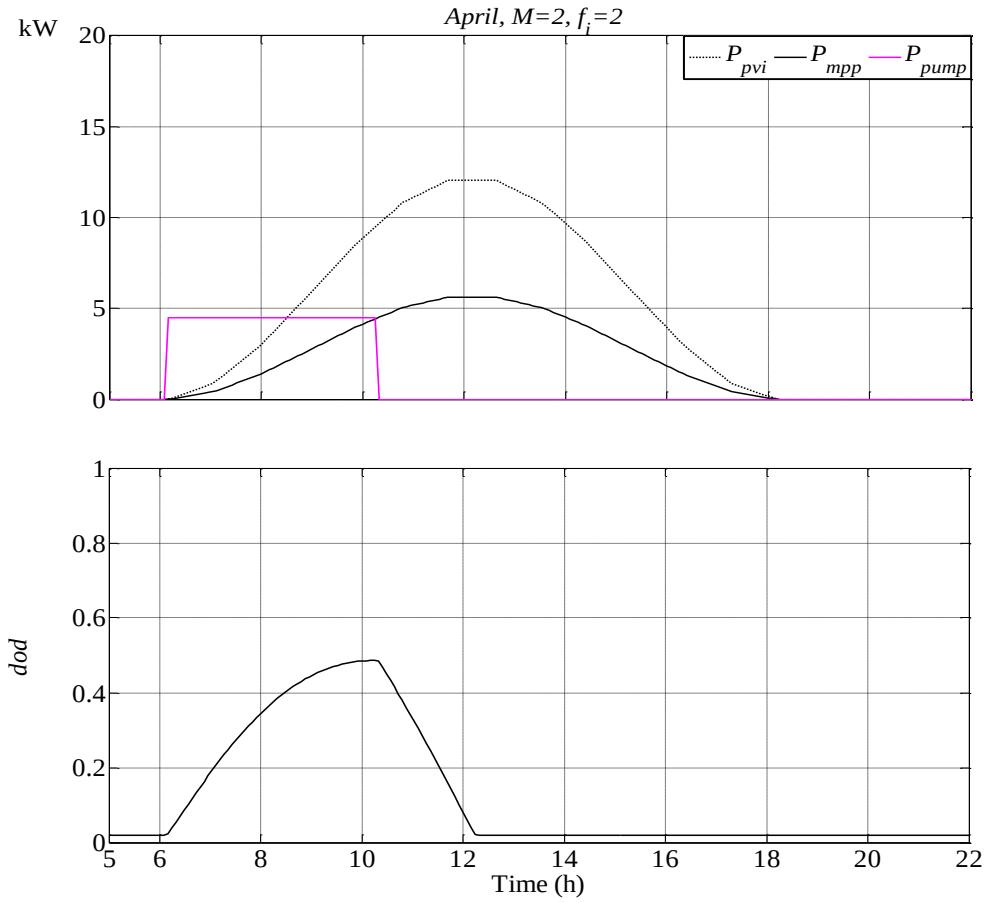
April, M=2, f_i=2
kW
P_{pvi} P_{mpp} P_{pump}
0
5
10
15
20
dod
0
0.2
0.4
0.6
0.8
1
5 6 8 10 12 14 16 18 20 22
Time (h)

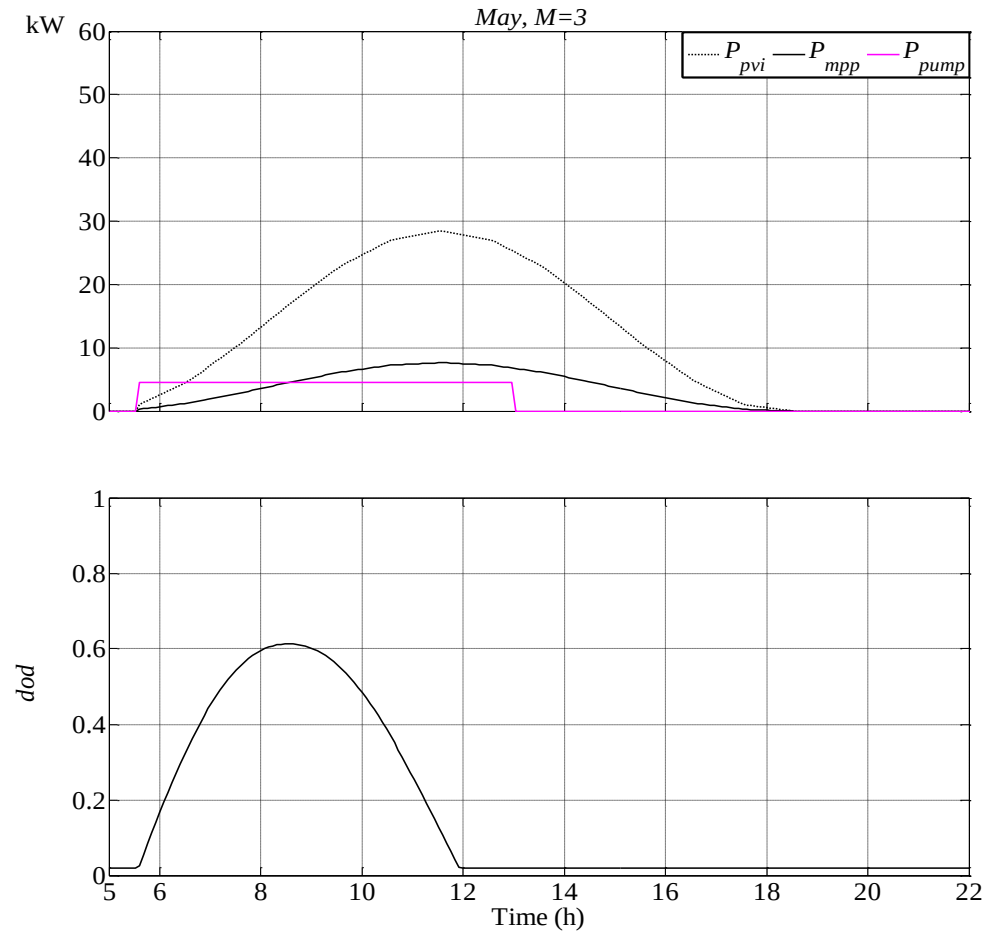
May, M=3
kW
P_{pvi} P_{mpp} P_{pump}
0
10
20
30
40
50
60
dod
0
0.2
0.4
0.6
0.8
1
5 6 8 10 12 14 16 18 20 22
Time (h)

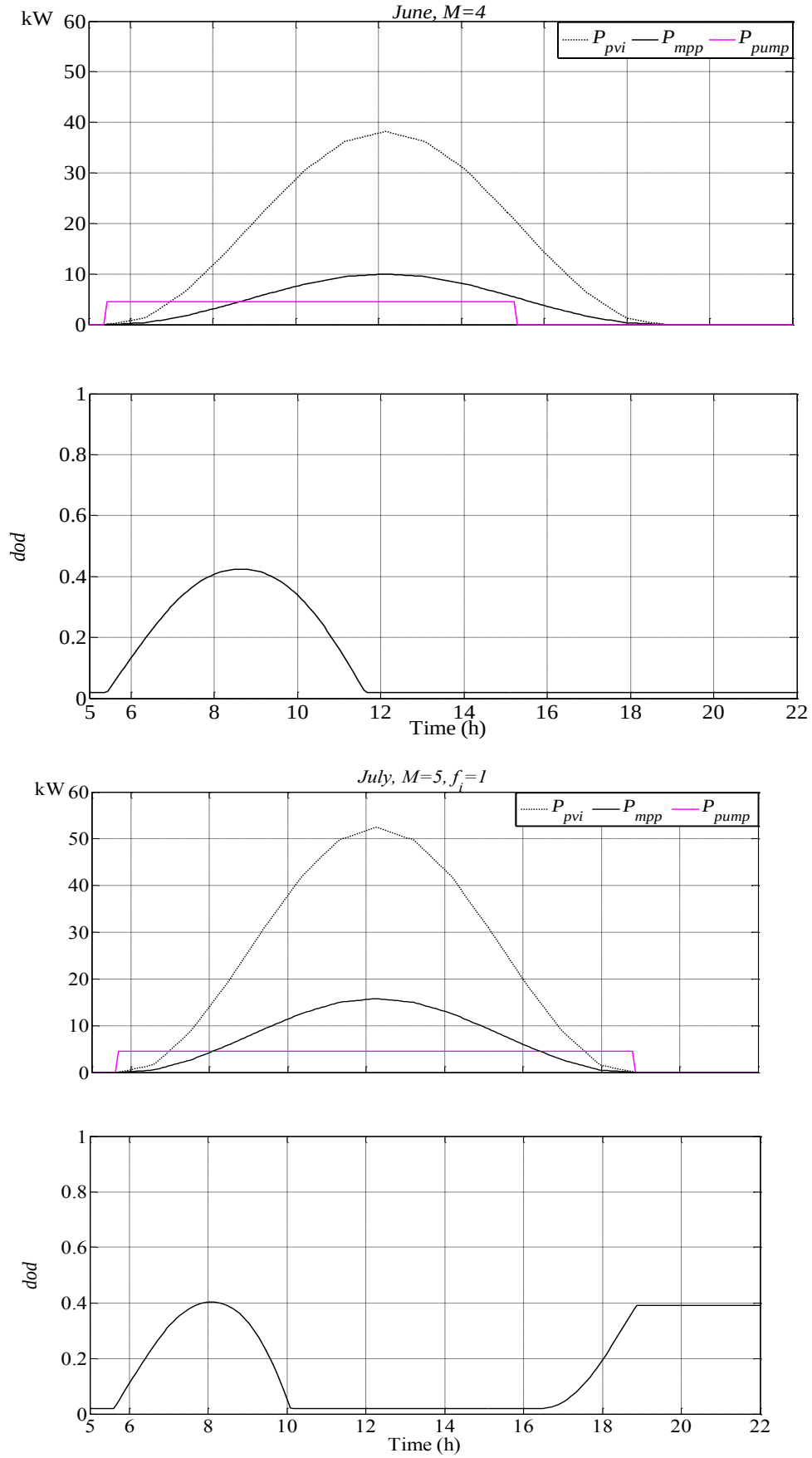

Figure 2. 28 Evaluation of Algorithm 2.1 for each month using mean climatic data values

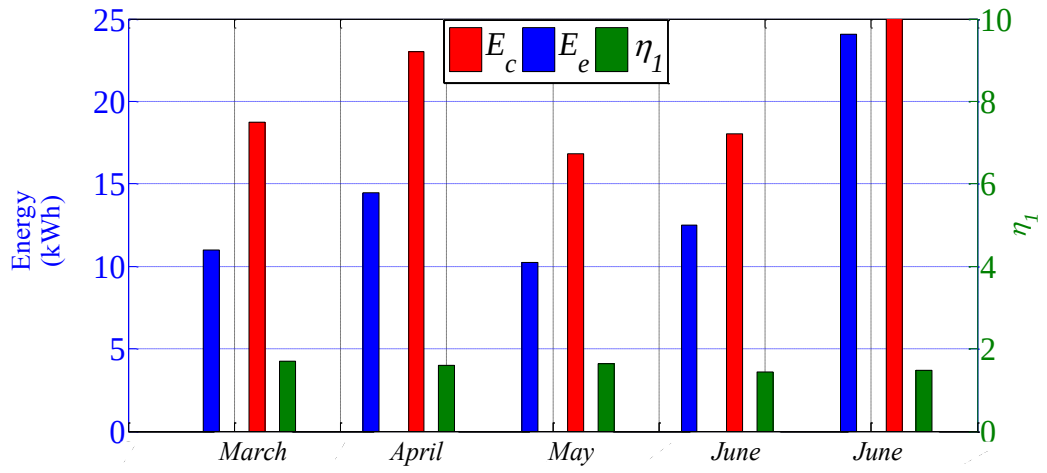

Figure 2.29 Summary of the daily energies using mean climatic data values for each month *M* using Algorithm 2.1

Using Algorithm 2.2, the final size of the panel surface and the batteries number are deduced. Hence, S_{opt} = 101.5 m^2, $n_{bat_{opt}}$ = 8 batteries (210 A.h/12 V). This result will be used, in the following subsection, to evaluate the sizing algorithm results using measured climatic data.

b. Validation Using Measured Climatic Data

To demonstrate the efficiency of the sizing algorithm, we use measured data of the solar radiation G and ambient temperature T_a of the target area, for the months of tomatoes' vegetative cycle (Figures 2.30- 2.31).

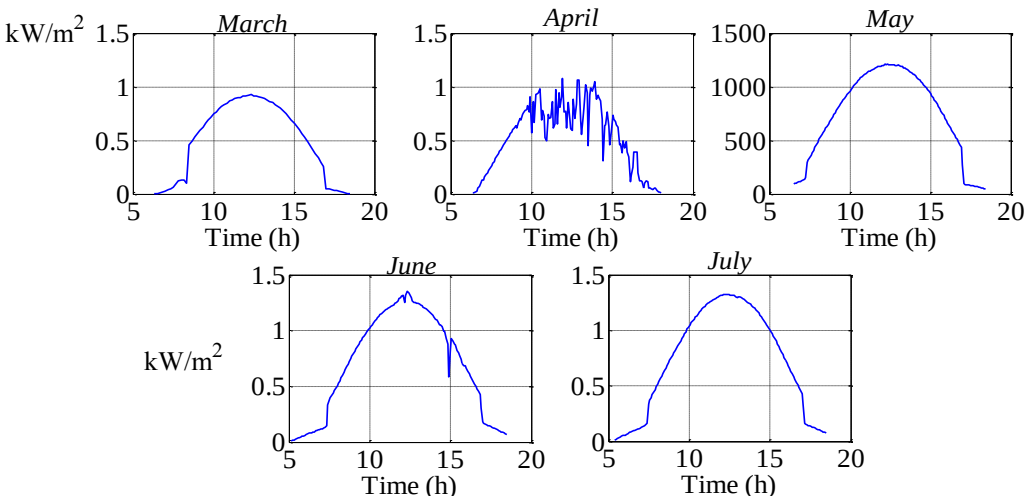

Figure 2.30 Measured solar radiation for each month *M*

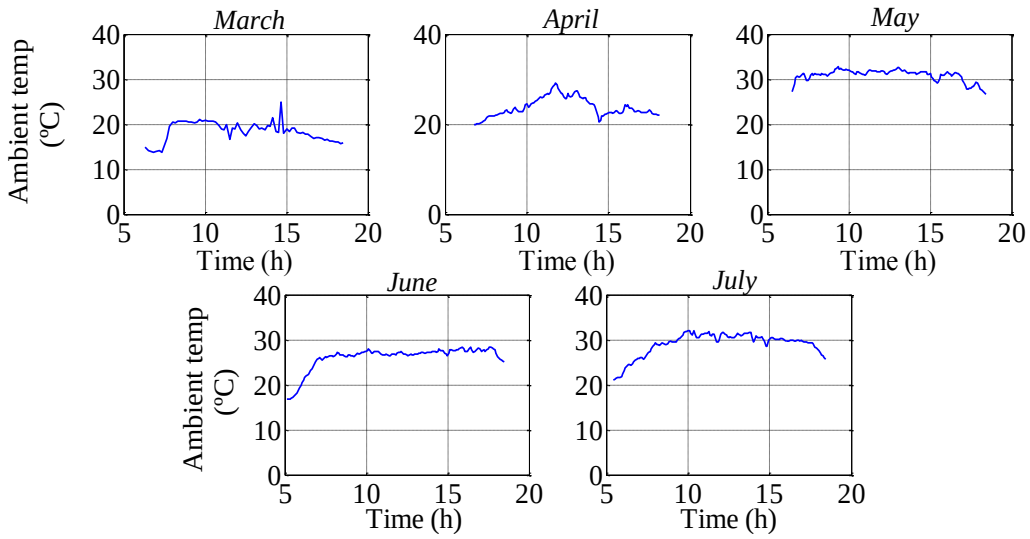

Figure 2.31 Measured ambient temperature for each month *M*

The charged and extracted energies E_c and E_e have been evaluated using Algorithm 2.1. The obtained values of η_{exp} for *July*, presented in Table 2.12, prove that the approach is validated with experimental data from G and T_a, since the values of η_{exp} is close to η and hence the pump is supplied during the pumping period (Figures 2.32 and 2.33). For the rest of the months, the charged energy E_c is higher than the energy in demand, since the components size that corresponds to *July* is used (the most critical month) [42].

Table 2.12 Energy balance evaluation using measured data

Months / *Results*	*March*	*April*	*May*	*June*	*July*
$E_{AM} + E_{PM}$ (Wh)	8121.6	4740.5	3109.4	8572.2	12855.0
E_c (Wh)	60394	49727	62763	56737	46269
$\eta_{exp} = \frac{E_c}{E_e}$ (64)	**7.43**	**10.48**	**20.18**	**6.61**	**3.59**

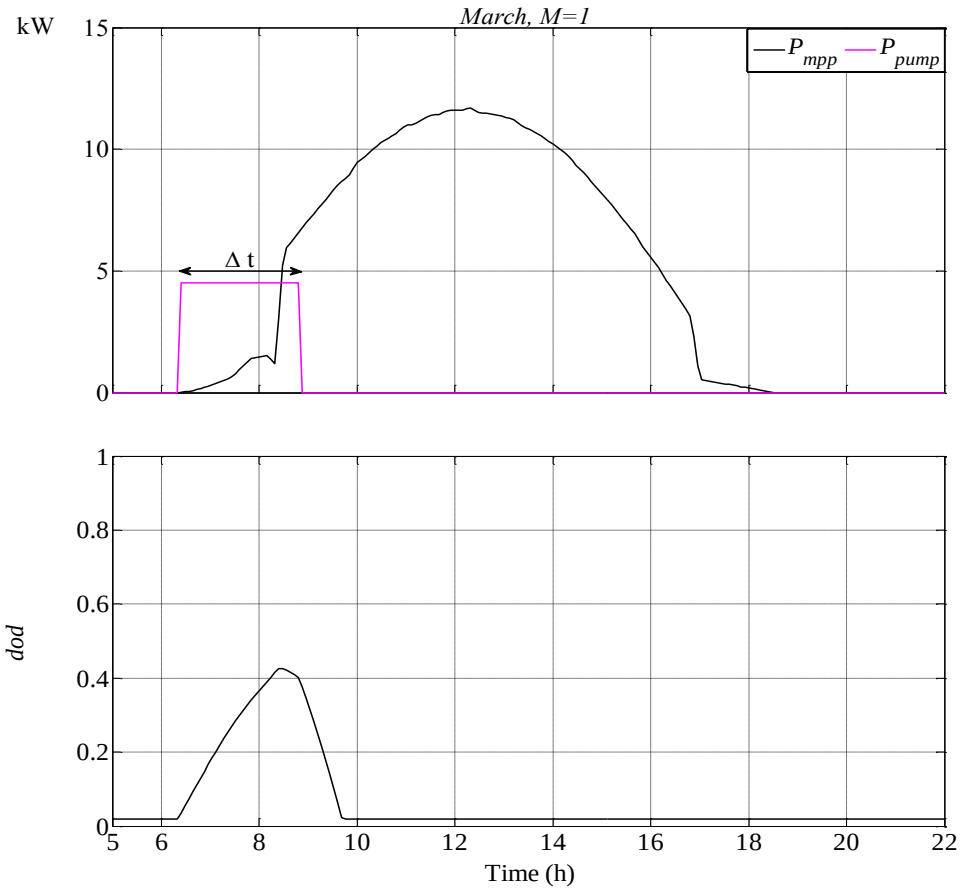
March, M=1
kW
15
10
5
0
Δ t
P mpp
P pump
1
0.8
0.6
0.4
0.2
0
dod
5 6 8 10 12 14 16 18 20 22
Time (h)

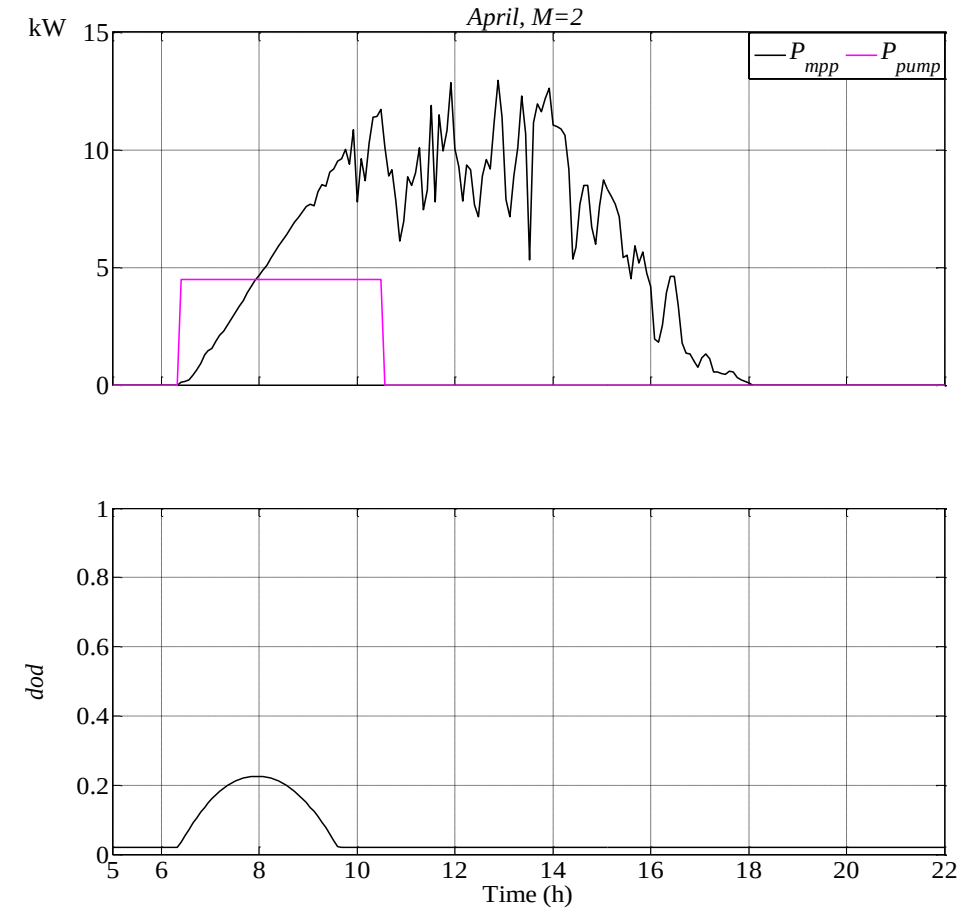
April, M=2
kW
15
10
5
0
P mpp
P pump
1
0.8
0.6
0.4
0.2
0
dod
5 6 8 10 12 14 16 18 20 22
Time (h)

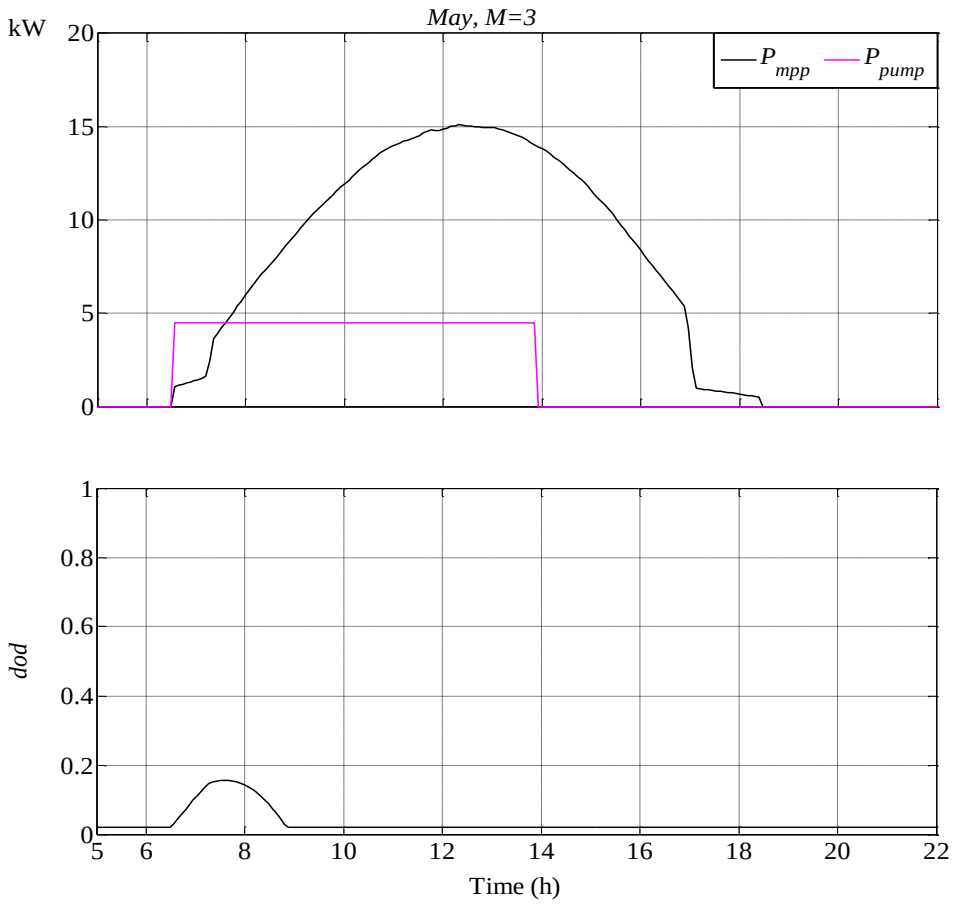
May, M=3
kW
20
15
10
5
0
P_{mpp}
P_{pump}
1
0.8
0.6
0.4
0.2
0
dod
5
6
8
10
12
14
16
18
20
22
Time (h)

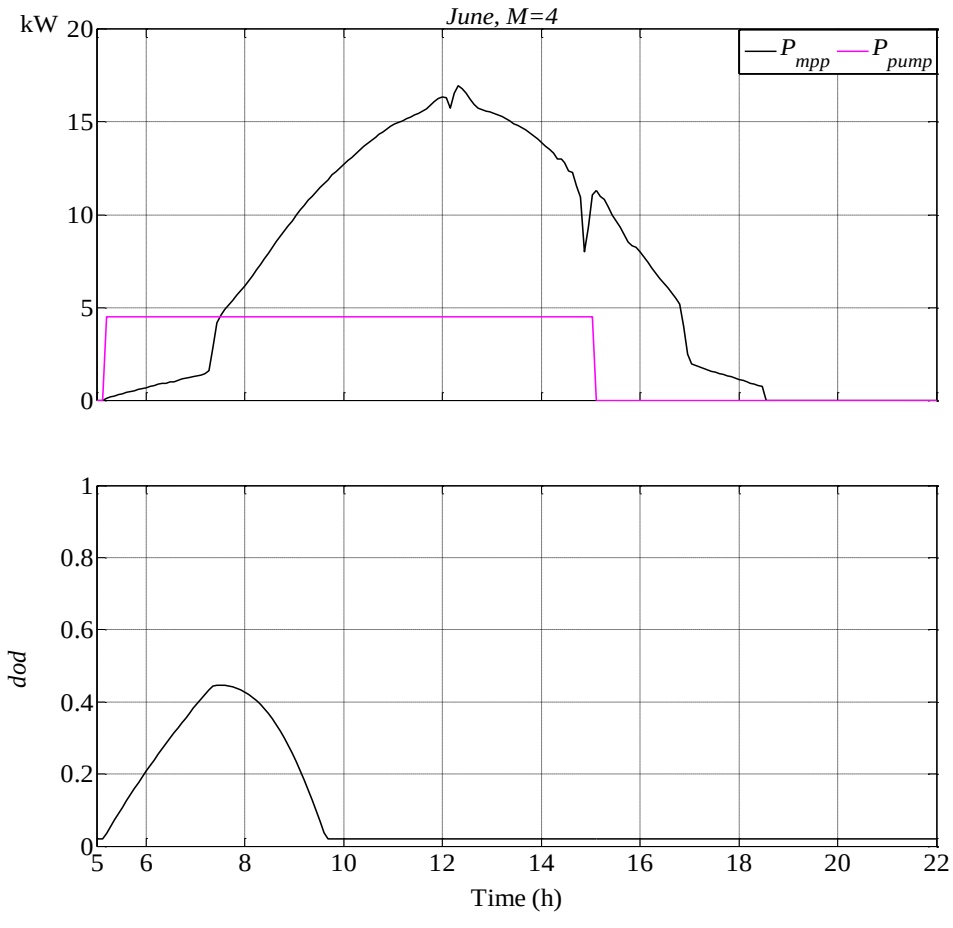
June, M=4
kW
20
15
10
5
0
P_{mpp}
P_{pump}
1
0.8
0.6
0.4
0.2
0
dod
5
6
8
10
12
14
16
18
20
22
Time (h)

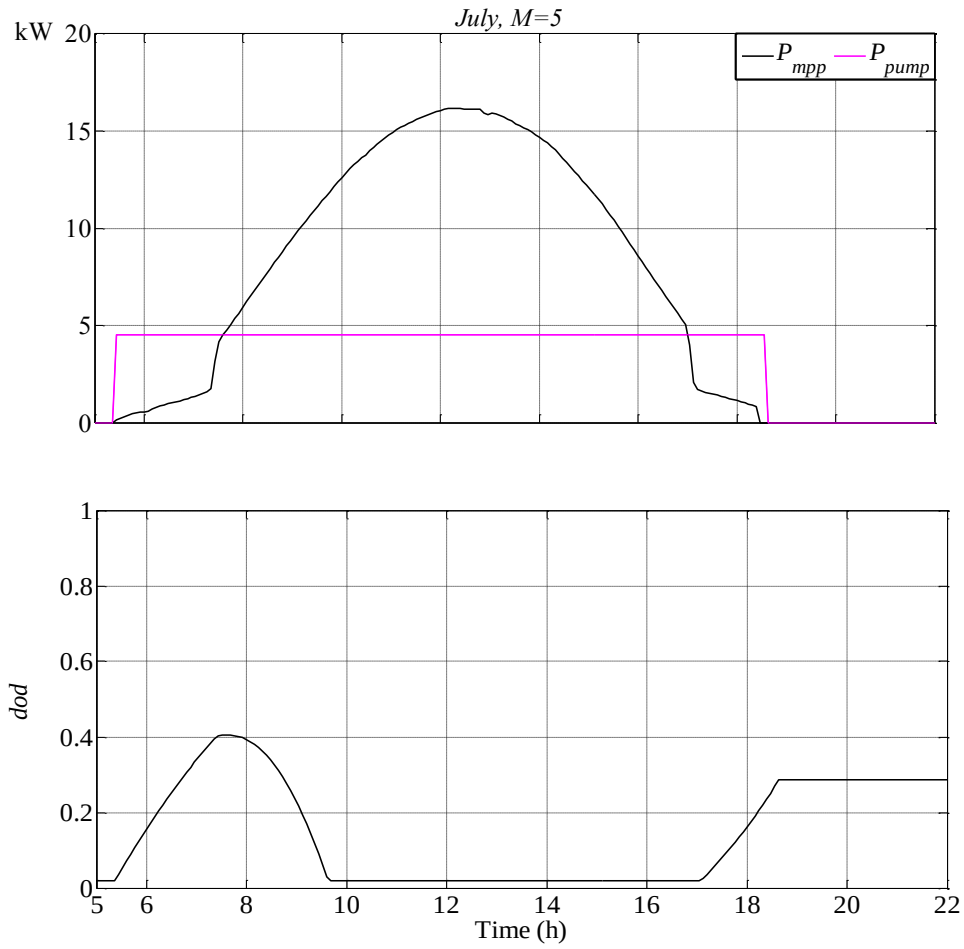

Figure 2. 32 Evaluation of the sizing algorithm using measured data for each month *M*

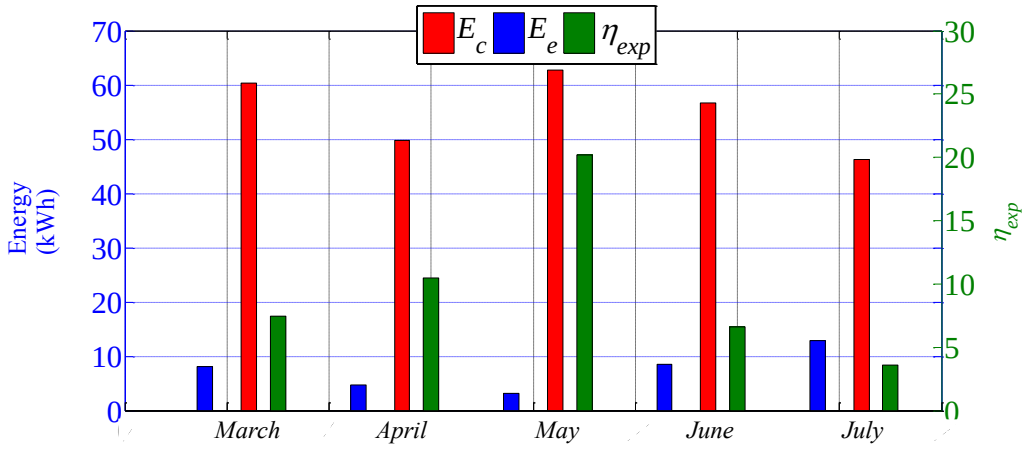

Figure 2. 33 Summary of the daily energies using data measured at the 15th of each month *M*

c. Validation Using HOMER

In order to test our approach, the installation sizes obtained by our algorithm are now compared with the components sizes obtained using HOMER. In fact, using Homer, the needed panels surface is 142 m^2, and the battery number is 14 batteries (210 A.h/ 12V). The simulation result, presented in Figure 2.34 and Figure 2.35 show that the panels size suggested by HOMER is higher than the surface really needed, obtained by our algorithm. This is because HOMER allows big importance to the day's autonomy. Hence, the installation components are oversized by HOMER.

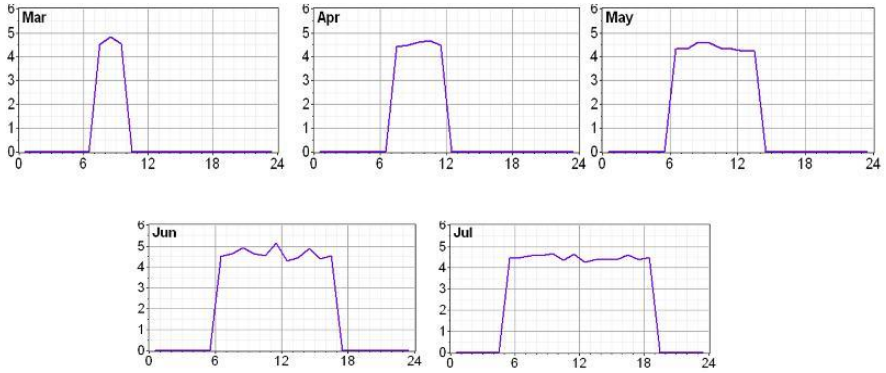

Figure 2.34 The inverter output power using HOMER

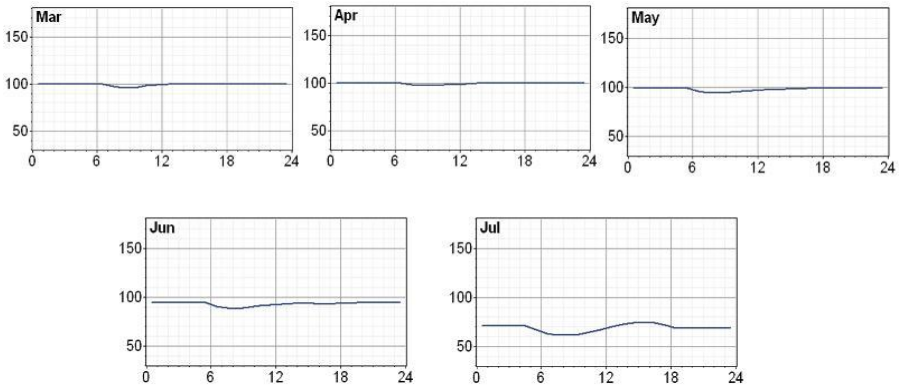

Figure 2. 35 The battery bank state of charge for one day in *July*

d. Validation Using PVsyst

The installation size has been also tested using PVsyst. The simulation show that the adopted size (S= 101.5 m^2 and n_{bat} =8 batteries/ 210 A.h/12V) gives good results (Figure 2.36). In fact, during the crops vegetative cycle, the solar

fraction (which is defined by the quotient of the available by the needed powers of the load), is equal to one, except in *June* and *July*, in which it is equal to 0.962 and 0.934, respectively. This leak of energy can be covered by considering an additional water volume in the reservoir, which will be studied in the next paragraph.

PVSYST V5.73		24/02/15

Stand Alone System: Simulation parameters

Project :	**STAND ALONE PUMPING SYSTEM**				
Geographical Site	**Medjez**			**Country**	**Tunisia**
Situation		Latitude	35.6°N	Longitude	9.6°E
Time defined as		Legal Time	Time zone UT+1	Altitude	5 m
		Albedo	0.20		
Meteo data :	Medjez, Synthetic Hourly data				
Simulation variant :	**New simulation variant_final_configuration_Imene**				
		Simulation date	24/02/15 12h12		

Simulation parameters

Collector Plane Orientation		Tilt	36°	Azimuth	0°

PV Array Characteristics

PV module	Si-poly	Model	**TE55-36P**		
		Manufacturer	Tenesol		
Number of PV modules		In series	10 modules	In parallel	23 strings
Total number of PV modules		Nb. modules	230	Unit Nom. Power	55 Wp
Array global power		Nominal (STC)	**12.65 kWp**	At operating cond.	11.33 kWp (50°C)
Array operating characteristics (50°C)		U mpp	161 V	I mpp	70 A
Total area		Module area	**102 m²**	Cell area	80.6 m²

PV Array loss factors

Thermal Loss factor		Uc (const)	20.0 W/m²K	Uv (wind)	0.0 W/m²K / m/s
=> Nominal Oper. Coll. Temp. (G=800 W/m², Tamb=20°C, Wind=1 m/s.)					NOCT 56 °C
Wiring Ohmic Loss		Global array res.	39 mOhm	Loss Fraction	1.5 % at STC
Module Quality Loss				Loss Fraction	2.3 %
Module Mismatch Losses				Loss Fraction	2.0 % at MPP
Incidence effect, ASHRAE parametrization		IAM =	1 - bo (1/cos i - 1)	bo Parameter	0.05

System Parameter		System type	**Stand Alone System**		
Battery		Model	**Open 12V / 210 Ah**		
		Manufacturer	Generic		
Battery Pack Characteristics		Voltage	168 V	Nominal Capacity	210 Ah
		Nb. of units	14 in series		
		Temperature	Fixed (20°C)		
Regulator		Model	Generic Default with MPPT converter		
		Technology	MPPT converter	Temp coeff.	-5.0 mV/°C/elem.
Converter	Maxi and EURO efficiencies		96.0/94.0 %		
Battery Management Thresholds		Charging	191.5/183.1 V	Discharging	164.6/176.4 V
	Back-Up Genset Command		165.5/180.6 V		
User's needs :		Ext. defined as file	load_a_1.txt		

Jan.	Feb.	Mar.	Apr.	May	June	July	Aug.	Sep.	Oct.	Nov.	Dec.	Year	
0.00	0.00	419	540	1116	1485	1953	0.00	0.00	0.00	0.00	0.00	5513	kWh

PVSYST V5.73		24/02/15

Stand Alone System: Main results

Project : **STAND ALONE PUMPING SYSTEM**

Simulation variant : **New simulation variant_final_configuration_Imene**

Main system parameters				
	System type	**Stand alone**		
PV Field Orientation	tilt	36°	azimuth	0°
PV Array	Nb. of modules	230	Pnom total	**12.65 kWp**
Battery	Model	Open 12V / 210 Ah	Technology	vented, plates
battery Pack	Nb. of units	14	Voltage / Capacity	**168 V / 210 Ah**
User's needs	Ext. defined as file	load_a_1.txt	global	5513 kWh/year

Main simulation results				
System Production	**Available Energy**	**19.69 MWh/year**	Specific prod.	1557 kWh/kWp/year
	Used Energy	5.33 MWh/year	Excess (unused)	8.80 MWh/year
	Performance Ratio PR	21.1 %	Solar Fraction SF	96.6 %
Loss of Load	Time Fraction	0.7 %	Missing Energy	0.18 MWh/year

Normalized productions (per installed kWp): Nominal power 12.65 kWp

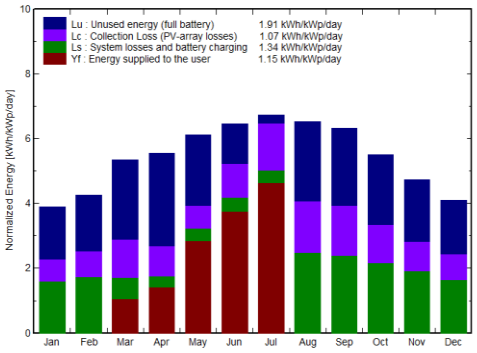

Performance Ratio PR and Solar Fraction SF

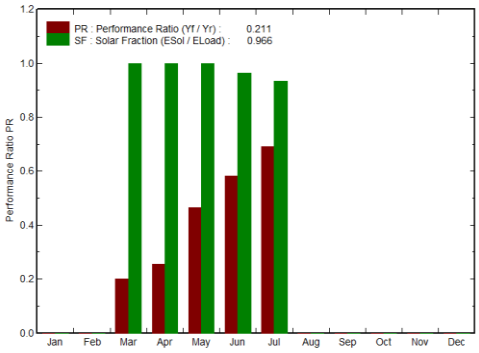

New simulation variant_final_configuration_Imene

Balances and main results

	GlobHor kWh/m²	GlobEff kWh/m²	E Avail MWh	EUnused MWh	E Miss MWh	E User MWh	E Load MWh	SolFrac
January	78.0	117.8	1.221	0.630	0.000	0.000	0.000	1.000
February	89.1	116.0	1.185	0.608	0.000	0.000	0.000	1.000
March	140.0	161.3	1.587	0.959	0.000	0.419	0.419	1.000
April	164.1	161.8	1.708	1.089	0.000	0.540	0.540	1.000
May	208.1	183.6	2.055	0.855	0.000	1.116	1.116	1.000
June	225.0	187.0	1.966	0.466	0.056	1.429	1.485	0.962
July	237.0	201.8	1.973	0.099	0.129	1.824	1.953	0.934
August	208.0	196.7	1.891	0.968	0.000	0.000	0.000	1.000
September	166.0	184.2	1.767	0.905	0.000	0.000	0.000	1.000
October	128.0	166.7	1.661	0.851	0.000	0.000	0.000	1.000
November	89.9	138.6	1.412	0.724	0.000	0.000	0.000	1.000
December	75.1	123.8	1.266	0.649	0.000	0.000	0.000	1.000
Year	1808.3	1939.5	19.692	8.801	0.185	5.328	5.513	0.966

Legends:

GlobHor	Horizontal global irradiation	E Miss	Missing energy
GlobEff	Effective Global, corr. for IAM and shadings	E User	Energy supplied to the user
E Avail	Available Solar Energy	E Load	Energy need of the user (Load)
EUnused	Unused energy (full battery) loss	SolFrac	Solar fraction (EUsed / ELoad)

PVSYST V5.73 | 24/02/15

Stand Alone System: Loss diagram

Project : **STAND ALONE PUMPING SYSTEM**

Simulation variant : **New simulation variant_final_configuration_lmene**

Main system parameters	System type	**Stand alone**			
PV Field Orientation	tilt	36°	azimuth	0°	
PV Array	Nb. of modules	230	Pnom total	**12.65 kWp**	
Battery	Model	Open 12V / 210 Ah	Technology	vented, plates	
battery Pack	Nb. of units	14	Voltage / Capacity	**168 V / 210 Ah**	
User's needs	Ext. defined as file	load_a_1.txt	global	5513 kWh/year	

Loss diagram over the whole year

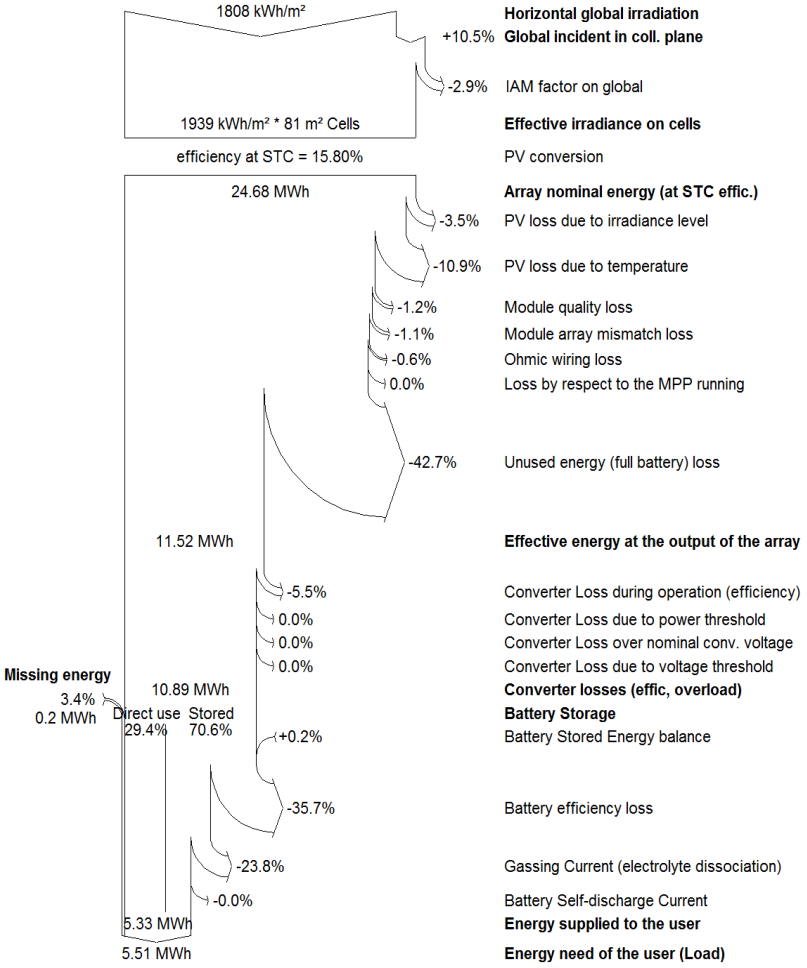

Figure 2. 36 PVsyst sizing simulation

e. Days of Autonomy

In the previous paragraph, the energetic installation balance has been demonstrated. In this paragraph, we aim to evaluate its autonomy. Hence, we now study the case when the cloudy days are consecutive (Table 2.13). The reservoir volume must ensure the installation autonomy. Thus, it must contain the possible leaking water volume in case of consecutive cloudy days and a battery bank discharged totally. Indeed, the water volume in excess or leak is evaluated using (68):

$$V_{leaked/excess} = V_{pumped} - \frac{n_c}{f_i} \cdot V \quad \textbf{(68)}$$

where:

V_{pumped} : the possible pumped water volume (m^3),

n_c : the number of cloudy days,

f_i : the irrigation frequency,

V: the water volume needed for irrigation for the month *M*.

Using Table 2.13 and Figure 2.37, the water volume in leak is maximum in *May* and *July* (1314.6 m^3 and 963.13 m^3, respectively). Hence, since these values are close, we choose the volume that corersponds *May*, to evaluate the reservoir volume. In this case, itis evaluated using (69):

$$V_{reservoir} = 1.2 \cdot \left(V_{leaked/excess} + V \right) \quad \textbf{(69)}$$

Finally, the reservoir volume choosed is 1800 m^3.

Table 2. 13 Cloudy days frequency and water volume needed for irrigation

Sizing	*March*	*April*	*May*	*June*	*July*
Water volume $m^3/10\,ha$ (57)	60.70	100.37	179.82	241.10	321.03

Daily pumped water (m^3)	274			281.6			291	321		321	
Maximum number of cloudy days per month n_c (66)	9			7			9	3		4	
Irrigation frequency f_i (Appendix B)	3	3	2	2	2	1	1	1	1	2	2
Excess/ leak water (m^3)	-7.82		-129.2		-119.52	-420.60	**-1314.6**	-417.68	**-963.13**		-321.06
Reservoir volume (m^3)							1793.3		1541.0		

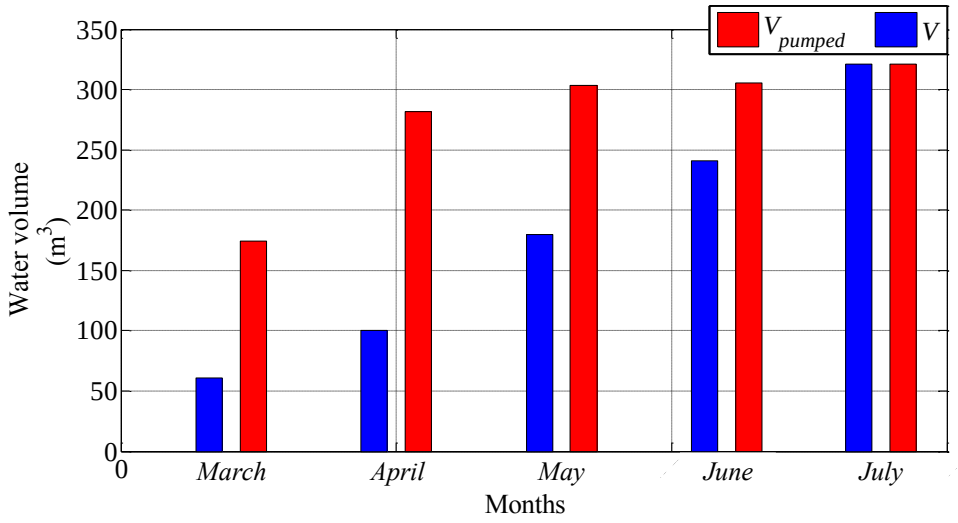

Figure 2. 37 Needed and possible pumped water volume averages during the tomato vegetative cycle in the case study

2.6.3 Economic Study for the Optimized Installation Size

To demonstrate the efficiency of our algorithm from an economic point of view, a brief economic comparison is now presented. For this, the installation' cost is

evaluated, using the components sizes obtained by the standard sizing evaluation and our algorithm [78]. The cost function is expressed by (70):

$$Cost = n_{pv}\left(C_{pv} + n_y\, M_{pv}\right) + n_{bat}\left(C_b + y_b\, C_b + \left(n_y - y_b - 1\right) M_b\right) + n_{chop}\, C_{chop}\left(y_{chop} + 1\right) + n_{chop}\, M_{chop}\left(n_y - y_{chop} - 1\right) + C_{inv}\left(y_{inv} + 1\right) + M_{inv}\left(n_y - y_{inv} - 1\right) \quad \textbf{(70)}$$

where:

n_{pv} : the number of photovoltaic modules,

n_{bat} : the batteries number.

The cost parameters are described in Table 2.14, together with the values selected in our application.

Table 2. 14 Cost parameters for the installation components [78]

Parameters	Name	Values
n_y (years)	the installation life time	20
C_{pv} (€/ module for n_y)	the photovoltaic module cost	265.81
M_{pv} (€/ module per year)	the photovoltaic module maintenance cost	2.66
C_b (€/ battery for n_y)	the battery cost	264
y_{bat}	the number of batteries replaced during n_y years	4
M_{bat} (€/ battery per year)	the maintenance cost for one battery	2.64
n_{chop}	the number of choppers	1
C_{chop} (€/chopper for n_y)	the chopper cost	200
y_{chop}	the number of chopper replaced during n_y years	0
M_{chop} (€/ chopper per year)	the maintenance cost for one chopper	2
C_{inv} (€/ inverter for n_y)	the cost of the inverter	1942
y_{inv}	the number of the inverter replaced	0

Parameters	Name	Values
	during n_y years	
M_{inv} (€/ inverter per year)	the maintenance cost for one inverter	19.42

The standard method for evaluating the size of the components consists in calculating the number of batteries $n_{bat_{std}}$ that allows the needed water to be pumped during the pumping time duration Δt using (71), to ensure the installation autonomy. Then, the panel surface S_{std} is deduced, such that it allows the load to be supplied and the battery bank to be charged, using (72) [53].

$$n_{bat_{std}} = \frac{P_{pump}\ \Delta t\ d_{aut}}{V_{bat}\ \Delta dod_{max}\ C_{bat}} \quad \textbf{(71)}$$

$$S_{std} = \frac{P_{pump}\ \Delta t}{W_{pv}\ \eta_{bat}{}^2\ \eta_l\ \eta_{pv}\ \eta_{reg}} \left(1 + \frac{d_{aut}}{d_{rech}}\right) \quad \textbf{(72)}$$

Following this, the values obtained in our case study for *July* are: $n_{bat_{std}} = 18$ batteris 210A.h/12V and $S_{std} = 337\ m^2$.

The installation costs results are sumerized in Table 2.15. The evaluation of the installation cost during 20 years proves that the proposed algorithm decreases significantly the installation cost, while ensuring the same energetic demand, as it has been previously prooved.

Table 2.15 Cost evaluation of the PV installation

Sizing	**Standard method**	**Proposed algorithm**
Cost (€)	134530	45805

2.7 Conclusion

This chapter described the components sizing of an autonomous photovoltaic installation for pumping water to irrigate a land planted with tomatoes. We have first presented the models used for the system sizing, and those that will be used in Chapter 3 for designing the management system. Models for the PV generator and the lead-acid battery were experimentally validated using meteorological data for the target area in the months corresponding to the vegetative cycle of the crop. The experimental validation of the components models proved the efficiency of these models, since the measured values follow the models results.

Then, a sizing algorithm is proposed to decide on the sizing of the installation elements. The algorithm has been tested for a 10 ha land surface in Medjez El Beb, Tunisia. The results show that the algorithm ensures the system's autonomy, the protection of the batteries against deep discharge and the needed water volume for crops irrigation by ensuring the pump supply during the needed pumping periode. The sizing algorithm was tested using measured values of the solar radiation and the ambient temperature. The obtained results show that the proposed approach gives good results when using measured values. This has been proved by validating the algorithm using HOMER. Then, a brief comparison of costs between the basic method for components sizing and our algorithm has been developed. This comparison proves that our algorithm allows the installation cost to be decreased, in addition to fulfilling the demand of water.

As a general conclusion, we have shown that our proposed algorithm is adequate for the determination of the optimum components' sizes for the photovoltaic irrigation installation. The results have been presented in [42] and [79].

Using the modeling and sizing results of this chapter, an online fuzzy management algorithm for the best energy distribution and satisfaction of the requirements of the pump will be described in the next chapter.

2.8 References

[1] Balghouthi, M; Chahbani, M. H; & Guizani, A. (2012). “Investigation of a solar cooling installation in Tunisia”. Applied Energy, 98, 138-148.

[2] Soussi, Meriem; Balghouthi, Moncef; & Guizani, Amenallah. (2013). “Energy performance analysis of a solar-cooled building in Tunisia: Passive strategies impact and improvement techniques”. Energy and Buildings, 67, 374-386.

[3] Bouadila, Salwa; Lazaar, Mariem; Skouri, Safa; Kooli, Sami; & Farhat, Abdelhamid. (2014). “Assessment of the greenhouse climate with a new packed-bed solar air heater at night, in Tunisia”. Renewable and Sustainable Energy Reviews, 35, 31-41.

[4] Young, Rachel. (2013). “Saving Water and Energy Together: Helping Utilities Build Better Programs”. American Council for an Energy-Efficient Economy, report number E13H.

[5] Ramos, Jorge. S; & Ramos, Helena. M. (2009). “Sustainable application of renewable sources in water pumping systems: Optimized energy system configuration”. Energy Policy, 37(2), 633-643.

[6] Demetrios, Papadopoulos. P; & Sotirios, Skretas. B. (2006). “A new approach for securing efficient operation of a water-pumping system fed by a PV generator”. In the proceedings of the Conference (ICEM).

[7] Hamidat, A; Benyoucef, Boumediene; & Hartani, Tarik. (2003). “Small-scale irrigation with photovoltaic water pumping system in Sahara regions”. Renewable Energy, 28(7), 1081-1096.

[8] Skretas, Sotirios. B; & Papadopoulos, Demetrios. P. (2008). “Systematic procedure for efficient design of electric water pumping systems fed by PV or/and WECS: Application using measured meteorological data for the city of Xanthi/Thrace, Greece”.Energy Conversion and Management, 49(4), 596-607.

[9] Anagreh, Y. (2001). “Steady state performance of series DC motor powered by wind driven self-excited induction generator”. Electrical Power Eng. Deot. Hijjawi faculty for Eng. Tech, Yarmouk University, Irbin Jordan.

[10] Velasco, M; Probst, O; & Acevedo, S. (2004). "Theory of wind-electric water pumping". Renewable energy, 29(6), 873-893.

[11] Muljadi, E; Nix, G; & Bialasiewicz, J. T. (2000). "Analysis of the dynamics of a wind-turbine water-pumping system". In the proceedings of the IEEE Conference on Power Engineering Society Summer Meeting (PESSM), 2506-2519.

[12] Díaz-González, Francisco; Sumper, Andreas; Gomis-Bellmunt, Oriol; & Villafáfila-Robles, Roberto. (2012). "A review of energy storage technologies for wind power applications". Renewable and Sustainable Energy Reviews, 16(4), 2154-2171.

[13] Bernstein, L; & Francois, L. E. (1973). "Comparison of drip, furrow and sprinkler irrigation". Soil Science, 115(1), 73-86.

[14] Shrivastava, P. K; Parikh, Madhusudan. M; Sawani, N. G; & Raman, S. (1994). "Effect of drip irrigation and mulching on tomato yield". Agricultural Water Management, 25(2), 179-184.

[15] Sweeeney, D.W; Graett, D.A; Bottcher. A.B; Lacario, S.J; & Camphll, K.L. (1987). "Tomato yield and nitrogen recover as influenced by irrigation method, nitrogen surlace and mulches". Hortic. Sci., 22, 27-29.

[16] Asiegbu, J. E. (1991). "Response of tomato and eggplant to mulching and nitrogen fertilization under tropical conditions". Scientia Horticulturae, 46(1), 33-41.

[17] Torantino, E; & Rubino, P. (1982). "Comparison of irrigation methods and irrigation regimes for processing tomato in Metapontum". Irrigation, 29, 17-26.

[18] Rana, Gianfranco; Katerji, Nader; Lazzara, Paola; & Ferrara, Rossana. Monica. (2012). "Operational determination of daily actual evapotranspiration of irrigated tomato crops under Mediterranean conditions by one-step and two-step models: Multiannual and local evaluations". Agricultural Water Management, 115, 285-296.

[19] Salas, Vicente; Olias, Emilio; Barrado, Alberto; & Lazaro, A. (2006). "Review of the maximum power point tracking algorithms for stand-alone photovoltaic systems".Solar energy materials and solar cells, 90(11), 1555-1578.

[20] Kaldellis, J. K; Zafirakis, D; & Kondili, E. (2010). "Optimum sizing of photovoltaic-energy storage systems for autonomous small islands".International Journal of Electrical Power & Energy Systems, 32(1), 24-36.

[21] Sidrach-de-Cardona, M; & Mora López, Llanos. (1998). "A simple model for sizing stand-alone photovoltaic systems".Solar Energy Materials and Solar Cells, 55(3), 199-214.

[22] Khatib, Tamer; Mohamed, Zah.A; & Sopian, K. (2013). "A review of photovoltaic systems size optimization techniques". Renewable and Sustainable Energy Reviews, 22, 454-465.

[23] Jakhrani, Abdul Qayoom; Othman, Al-Khalid; Rigit, Andrew; Ragai. Henry; Samo, Saleem. Raza; & Kamboh, Shakeel. Ahmed. (2012). "A novel analytical model for optimal sizing of standalone photovoltaic systems". Energy, 46(1), 675-682.

[24] Acakpovi, Amevi; Xavier, Fifatin. Francois; & Awuah-Baffour, Robert. (2012). "Analytical method of sizing photovoltaic water pumping system". In the proceedings of the 4th IEEE International Conference on Adaptive Science & Technology, 65-69.

[25] Shrestha, G. B; & Goel, L. (1998). "A study on optimal sizing of stand-alone photovoltaic stations". IEEE Transactions on Energy Conversion, 13(4), 373-378.

[26] Barra, Luciano; Catalanotti, Sergio; Fontana, F; & Lavorante, F. (1984). "An analytical method to determine the optimal size of a photovoltaic plant". Solar Energy, 33(6), 509-514.

[27] Groumpos, P. P; & Papageorgiou, G. (1987). "An optimal sizing method for stand-alone photovoltaic power systems". Solar Energy, 38(5), 341-351.

[28] Mellit, A; Benghanem, M; Hadj Arab, A; & Guessoum, A. (2003). "Modelling of sizing the photovoltaic system parameters using artificial neural network". In the proceedings of the IEEE Conference on Control Applications, 353-357.

[29] Yang, Hongxing; Zhou, Wei; Lu, Lin; & Fang, Zhaohong. (2008). "Optimal sizing method for stand-alone hybrid solar–wind system with LPSP technology by using genetic algorithm". Solar Energy, 82(4), 354-367.

[30] Khatib, Tamer; Mohamed, Azah; Sopian, K; & Mahmoud, M. (2012). "A new approach for optimal sizing of standalone photovoltaic systems". International Journal of Photo Energy, 2012.

[31] Klein, S. A; & Beckman, W. A. (1987). "Loss-of-load probabilities for stand-alone photovoltaic systems". Solar Energy, 39(6), 499-512.

[32] Abouzahr, I; & Ramakumar, R. (1991). "Loss of power supply probability of stand-alone photovoltaic systems: a closed form solution approach". IEEE Transactions on Energy Conversion, 6(1), 1-11.

[33] Maghraby, H. A. M; Shwehdi, M. H; & Al-Bassam, G. K. (2002). "Probabilistic assessment of photovoltaic (PV) generation systems". IEEE Transactions on Power Systems, 17(1), 205-208.

[34] Mellit, A; Benghanem, M; & Kalogirou, S. A. (2007). "Modeling and simulation of a stand-alone photovoltaic system using an adaptive artificial neural network: Proposition for a new sizing procedure". Renewable Energy, 32(2), 285-313.

[35] https://users.homerenergy.com/downloads/

[36] http://lorentz1.software.informer.com/

[37] http://www.pvsyst.com/fr/download

[38] http://sourceforge.net/projects/rapsim/files/latest/download

[39] http://www.retscreen.net/fr/home.php

[40] Ben Ammar, Mohsen. (2011). "Contribution à l'optimisation de la gestion des systèmes multi-sources d'énergies renouvelables". Thesis presented at the National School of Engineering of Sfax, Tunisia.

[41] Bernal-Agustín, Jose. L; & Dufo-López, Rodolfo. (2009). ''Simulation and optimization of stand-alone hybrid renewable energy systems''. Renewable and Sustainable Energy Reviews, 13(8), 2111-2118.

[42] Yahyaoui, Imene; Chaabene, Maher; & Tadeo, Fernando. (2013). "An algorithm for sizing photovoltaic pumping systems for tomato irrigation". In the proceedings of the IEEE Conference on Renewable Energy Research and Applications (ICRERA), 1089-1095.

[43] Khatib, Tamer; Mohamed, Azah;& Sopian, Kamaruzzman Bin. (2012). "A review of solar energy modeling techniques''.Renewable and Sustainable Energy Reviews, 16(5), 2864-2869.

[44] Posadillo, R; & López Luque, R. (2009). "Hourly distributions of the diffuse fraction of global solar irradiation in Córdoba (Spain)". Energy Conversion and Management, 50(2), 223-231.

[45] El-Sebaii, A. A; Al-Hazmi, F. S; Al-Ghamdi, A. A; & Yaghmour, S. J. (2010). "Global, direct and diffuse solar radiation on horizontal and tilted surfaces in Jeddah, Saudi Arabia". Applied Energy, 87(2), 568-576.

[46] Moghadam, Hamid; Tabrizi, Farshad. Farshchi; & Sharak, Ashkan. Zolfaghari. (2011). "Optimization of solar flat collector inclination". Desalination, 265(1), 107-111.

[47] Arunkumar, T; Jayaprakash, R; Denkenberger, D; Ahsan, Amimul; Okundamiya, M. Sanjay; Tanaka, Hiroshi; & Aybar, H. Ş. (2012). "An experimental study on a hemispherical solar still". Desalination, 286, 342-348.

[48] Şen, Zekai. (2008). "Solar energy fundamentals and modeling techniques: atmosphere, environment, climate change and renewable energy". (Vol. 276). Springer, ISBN 978-1-84800-133-6.

[49] Clean Energy Decision Support Centre, "Phovoltaic project analysis, Chapter", Catalogue no: M39-99/2003E, RETScreen International 2001-2004, ISBN 0-662-35672-1.

[50] Orgill, J. F; & Hollands, K. G. T. (1977). "Correlation equation for hourly diffuse radiation on a horizontal surface". Solar Energy, 19(4), 357-359.

[51] Erbs, D. G; Klein, S. A; & Duffie, J. A. (1982). "Estimation of the diffuse radiation fraction for hourly, daily and monthly-average global radiation". Solar Energy, 28(4), 293-302.

[52] Collares-Pereira, Manuel; & Rabl, Ari. (1979). "The average distribution of solar radiation-correlations between diffuse and hemispherical and between daily and hourly insolation values". Solar Energy, 22(2), 155-164.

[53] Chaabene, Maher. (2009). "Gestion énergétique des systèmes photovoltaïques", master course at the National School of Engineering of Sfax, Tunisia.

[54] Duffie, John. A; & Beckman, William. A. (2013). "Solar engineering of thermal processes". John Wiley & Sons, ISBN 978-1-118-43348-5.

[55] Kenny, R. P; Friesen, G; Chianese, D; Bernasconi, A; & Dunlop, E. D. (2003). "Energy rating of PV modules: comparison of methods and

approach". In the proceedings of the 3rd IEEE World Conference on Photovoltaic Energy Conversion, 2015-2018.

[56] Xiao, W; Dunford, W. G; & Capel, A. (2004, June). "A novel modeling method for photovoltaic cells". In the proceedings of the 35th IEEE Annual Conference on Power Electronics Specialists, 1950-1956.

[57] Adamo, Francesco; Attivissimo, Filippo; Di Nisio, Attilio; & Spadavecchia, Maurizio. (2011). "Characterization and testing of a tool for photovoltaic panel modeling". IEEE Transactions on Instrumentation and Measurement, 60(5), 1613-1622.

[58] González-Longatt, Francisco. M. (2005). "Model of photovoltaic module in Matlab". In the proceedings of the second Iberoamerican Conference of Electrical, Electronics and Computation Students, 1-5.

[59] Chenni, R; Makhlouf, M; Kerbache, T; & Bouzid, A. (2007). "A detailed modeling method for photovoltaic cells". Energy, 32(9), 1724-1730.

[60] De Blas, M. A; Torres, J. L; Prieto, E; & Garcıa, Antonio. M. Mora. (2002). "Selecting a suitable model for characterizing photovoltaic devices". Renewable Energy, 25(3), 371-380.

[61] Zhang, C. P; Sharkh, S. M; Li, X; Walsh, F. C; Zhang, C. N; & Jiang, J. C. (2011). "The performance of a soluble lead-acid flow battery and its comparison to a static lead-acid battery". Energy Conversion and Management, 52(12), 3391-3398.

[62] Collins, John; Kear, Gareth; Li, Xiaohong; Low, John C. T; Pletcher, Derek; Tangirala, Ravichandra; Stratton-Campbell, Duncan; Walsh, Frank C; & Caiping. (2010). "A novel flow battery: A lead acid battery based on an electrolyte with soluble lead (II) Part VIII. The cycling of a 10cm× 10cm flow cell". Journal of Power Sources, 195(6), 1731-1738.

[63] Fendri, Dalia; & Chaabene, Maher. (2012). "Dynamic model to follow the state of charge of a lead-acid battery connected to photovoltaic panel". Energy Conversion and Management, 64, 587-593.

[64] Ben Salah, Chokri; & Ouali, Mohamed. (2012). "Energy management of a hybrid photovoltaic system". International Journal of Energy Research, 36(1), 130-138.

[65] Guasch, D; & Silvestre, S. (2003). "Dynamic battery model for photovoltaic applications". Progress in Photovoltaics: Research and Applications, 11(3), 193-206.

[66] Sallem, Souhir; Chaabene, Maher; & Kamoun, Mohammed. Ben. Ali. (2009). "Energy management algorithm for an optimum control of a photovoltaic water pumping system". Applied Energy, 86(12), 2671-2680.

[67] Sallem, Souhir. (2009). "Contribution à l'integration d'une machine doublement alimentée dans des systems autonomies". Thesis presented at the National School of Engineering of Sfax, Tunisia.

[68] Al Ibrahim, Aabdulrahman. Mohammed. (1997). "Optimum Selection of Direct-Coupled Photovoltaic Pumping System in Solar Domestic Hot Water Systems". Thesis presented at the University Of Wisconsin- Madiso USA.

[69] Roger, J. A; Perez, A; Campana, D Castiel, A; & Dupuy, C. H. S. (1978). "Calculations and in situ experimental data on a water pumping system directly connected to a 1/2 Kw photovoltaic convertors array". In the proceedings of the Photovoltaic Solar Energy Conference, 1211-1220.

[70] Wrixon, G. T; & McCarthy, S. (1988). "Optimization and analysis of photovoltaic systems using a computer model". In the proceedings of the IEEE Conference on Photovoltaic Specialists, 1293-1297.

[71] Rana, G; Katerji, N; Lazzara, P; & Ferrara, R. M. (2012). "Operational determination of daily actual evapotranspiration of irrigated tomato crops under Mediterranean conditions by one-step and two-step models: Multiannual and local evaluations". Agricultural Water Management, 115, 285-296.

[72] Gong, Lebing; Xu, Chong-yu; Chen, Deliang D; Halldin, Sven; & Chen, Yongqin. David. (2006). "Sensitivity of the Penman–Monteith reference evapotranspiration to key climatic variables in the Changjiang (Yangtze River) basin". Journal of Hydrology, 329(3), 620-629.

[73] Obid, Kareem. R; Khaleel, Basim; & Nife, Kadhim. "The Comparison between different methods for estimating consumptive use of water in Iraq". (2013). Journal of Babylon University/ Engineering Sciences, (21) 27-36.

[74] Kashyap, P. S; & Panda, R. K. (2001). "Evaluation of evapotranspiration estimation methods and development of crop-coefficients for potato crop in a sub-humid region". Agricultural Water Management, 50(1), 9-25.

[75] Beltrán, Julián. Martinez. (1999). "Irrigation with saline water: benefits and environmental impact". Agricultural Water Management, 40(2), 183-194.

[76] Van Hoorn, J. W. (1981). "Salt movement, leaching efficiency, and leaching requirement". Agricultural Water Management, 4(4), 409-428.

[77] Letey, J; Hoffman, G. J; Hopmans, J. W; Grattan, S. R; Suarez, D; Corwin, D. L; Oster, J.D; Wu, L; & Amrhein, C. (2011). "Evaluation of soil salinity leaching requirement guidelines". Agricultural Water Management, 98(4), 502-506.

[78] Eftichios, Koutroulis; Dionissia Kolokotsa; Antonis Potirakis; & Kostas Kalaitzakis. (2006). "Methodology for optimal sizing of stand-alone photovoltaic/wind-generator systems using genetic algorithms".Solar Energy, 80(9), 1072-1088.

[79] Yahyaoui, Imene**;** Ammous, Mahmoud; & Tadeo, Fernando. (2015). "Algorithm for optimum sizing of a photovoltaic water pumping system". International Journal of Computer Applications (IJCA), (accepted).

Chapter 3: Energy Management of the Photovoltaic Irrigation Installation

Contents

3.1 Motivation

As it has been seen in the previous chapter, photovoltaic panels generate energy intermittently, due to the frequent changes in the solar radiation [1-3] (see Chapter 2, Section 2.5). Moreover, the energy generation depends on the climatic parameters (namely the solar radiation), the site and the panel characteristics [4-6]. In general, photovoltaic energy is abundant during the warm season, characterized by an important sunlight, and it is low during the cold season, characterized by rapid changes in the solar radiation. Hence, owing to the variability of the photovoltaic energy generated, the use of an energy management strategy is important, especially for autonomous installations, for which a precise balance between the photovoltaic power generated and the power required by the load is required [7-10].

In this context, in this chapter we focus on the energy management of our off-grid photovoltaic installation presented in Chapter 2, Section 2.3, destined to supply the water pump for irrigation. In fact, as the system is off-grid, the installation must always provide the energy needed by the load. Thus, in case of insufficient generated energy, a battery bank is used to provide the missing energy (Figure 3.1). The main objective of the management approach, developed in this chapter, is to decide the connection of the system components that ensures supplying the load and pumping the water volume needed, taking into account the safe operation of the battery bank. Hence, a careful planning of the load connections to the photovoltaic generator and/ or to the battery bank is required. Based on optimization tools, the proposed strategy guarantees a maximum use of the energy generated by the photovoltaic panel.

Thus, this chapter establishes a management strategy for a photovoltaic installation destined to water pumping for irrigation of a land planted with tomatoes [11]. Section 3.2 reviews some methods used in the literature for the energy management of renewable irrigation installations. Then, Section 3.3 presents the problem formulation. Our approach, based on fuzzy logic, is presented in Section 3.4. The energy management algorithm is tested on a case study in Section 3.5 and validated experimentally in Section 3.6. Finally, Section 3.7 presents the chapter' conclusion.

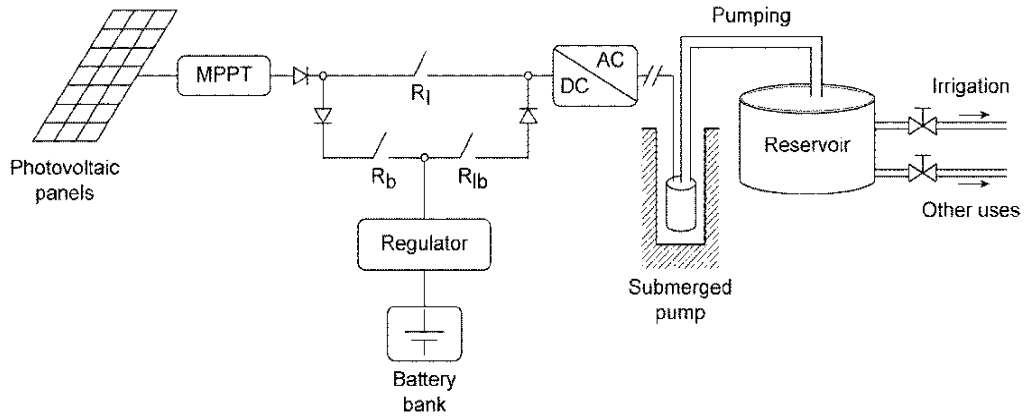

Figure 3. 1 Scheme of the off-grid photovoltaic irrigation system

3.2 Review of Renewable Energy Management in Irrigation

As it has been mentioned, the energy management is important in off-grid applications, especially for installations for which autonomy is required, independently of the climatic conditions. Hence, the choice of the adequate management method is relevant in optimizing the energy exploitation. Some of these methods are discussed now:

3.2.1 Review of Energy Management Methods

In the literature, several management methods have been studied for photovoltaic water pumping installations. In fact, some works have focused in pumping water over the sun [12-15]. These installations directly use all the PV energy generated for pumping water, so they are simple, but water is only pumped when there is enough solar radiation. To solve this, PV installations equipped with batteries have been used: the regulation of the battery bank voltage has been used to disconnect or connect loads to both photovoltaic panels and batteries, and thus charging or discharging the batteries [16]. This method allows regulating the battery bank voltage. However, the battery bank is always operating, which causes reducing the battery bank' life time. In addition, intelligent tools have been used for the energy management. For instance, Artificial Neural Networks (ANN) have been developed for the optimum operation of water pumping installations [17]. Moreover, [18] and [19] have respectively proven the efficiency of Genetic Algorithms and Non-Linear Programming, in the energy

management of photovoltaic irrigation installations. Despite the efficiency of these methods, the necessity of an update for the data base remains the main drawback of the ANN [20-21]. The main disadvantage of the GA is its long counting time and the lack of guarantee that a global optimal solution can always be found [22-23]. For this, fuzzy logic has been extensively used in this kind of purpose [24- 33]. This approach is selected here, and reviewed now in detail.

3.2.2 Fuzzy Logic for Energy Management

Fuzzy logic has already proven its efficiency in ensuring an adequate energy management of photovoltaic plants [24]. In fact, in autonomous photovoltaic installations, this tool has been used for optimizing the energy use, guaranteeing the plant autonomy and protecting the batteries against deep discharge and excessive charge, while supplying non-controllable loads [25]. Moreover, it has been used in renewable installations that supply controllable loads [24, 26] and constant critical and time-varying non-critical loads [27]. Researchers have also used it in simpler applications in agriculture. For instance, fuzzy logic has been used to decide crop irrigation time and nutrient injection, knowing the solar radiation and the crop canopy temperature [28]. Moreover, the efficiency of this tool has been proven in controlling the internal climatic variables in greenhouses and batteries charging/discharging [29], and increasing the pumped water volume in water pumping installations, using Fuzzy Management Algorithms (FMA) [8, 9].

The efficiency of this control method in various applications is given by its ease of use. In fact, it is complicated in many installations to give exact rules for energy management [8, 24]. Thus, fuzzy logic is considered a good method for solving this problem, since it gives a simple method to decide control actions, using linguistic rules [9, 30]. Moreover, based on the knowledge base, the fuzzy rules are written in a simple manner that describes directly the control decisions. Mamdani-type fuzzy logic is used here within the management algorithm, as it is simple to learn for operators with little technical training [31] and can be implemented using standard components, such as Programmable Industrial Controllers [32]. For these reasons, in our application, we choose to use a Fuzzy

energy management approach for our photovoltaic installation for irrigation [11, 33].

3.3 Problem Formulation

The proposed energy management strategy aims to optimize, at each sample time, the electrical energy produced from a PV installation composed of a PV generator and a battery bank, which supply a water pump (Figure 3.1). More precisely, our goal is to develop a management algorithm that maximizes the use of photovoltaic power generated, minimizes the battery use and guarantees the water volume needed for irrigation, by controlling the switching of the relays R_b, R_l and R_{lb} that link the installation' components.

The decision on these switching is carried by a Management Algorithm, based on the estimations of the photovoltaic power generated $\tilde{P}_{pv}$, the power demanded by the pump $\left(\tilde{P}_{pump}\right)$, the battery bank'depth of discharge (dod) and the water volume in the reservoir L. $\tilde{P}_{pv}$ is estimated using the measured values of the solar radiation G and the ambient temperature T_a. $\tilde{P}_{pump}$ and dod are estimated using the measured currents I_{pump} and I_{bat} respectively (see Chapter 2, Section 2.6). The level L is measured directly using a pressure sensor (see Appendix F).

The proposed energy management is performed via two main steps: the first step consists in the acquisition of the currents I_{pv} and I_{bat}, and the acquisition or the prediction of the climate-related site parameters; this allows the power produced by the photovoltaic panels $\tilde{P}_{pv}$ and the dod to be predicted. In the second step, using the Fuzzy logic, an algorithm deduces the instants and duration when the load is connected to the power sources (Figure 3.2).

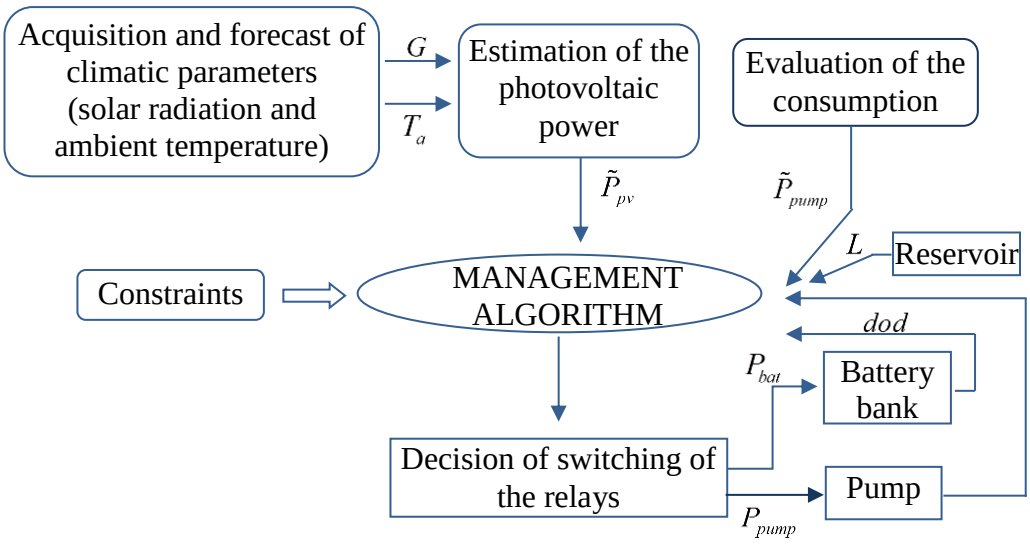

Figure 3. 2 Energy management strategy

3.4 Proposed Energy Management Algorithm

As it has been mentioned in Section 3.1, our aim is to develop an algorithm for the efficient energy management of the autonomous photovoltaic irrigation installation, composed of photovoltaic panels coupled to a lead-acid battery bank, to ensure the energy availability, even if the irradiation is low (Figure 3.1). Based on some previous proposals [8, 11], a general fuzzy management algorithm (FMA) is proposed here.

3.4.1 Energy Management Strategy

We aim to establish a management algorithm that ensures the water volume needed for the crops irrigation, through the control of the relays that link the installation components. Hence, a fuzzy management algorithm is proposed here to decide the connection time of the system components, using only a knowledge base of the system [9] (Section 3.2). The components connection times are decided by means of Fuzzy rules, which are based on the estimated photovoltaic power and the water volume in the reservoir, while taking into account the constraints related to the battery bank safe operation.

In normal cases, the photovoltaic panels are used to supply the pump and charge the battery bank. To minimize the battery use, the water pumping is performed during the daylight. This ensures a depth of discharge (dod) between two fixed values dod_{min} and dod_{max} for a continuous pump operation (that stops when the tank is full or the battery discharged).

The management algorithm decides the switching times of the three relays R_b R_l and R_{lb}, that connect the photovoltaic system components (Figure 3.1). Hence, it is necessary to establish some criteria that define the algorithm. These criteria are related to (Figure 3.3):

i. The photovoltaic energy generated P_{pv}.
ii. The battery bank depth of discharge dod.
iii. The water volume in the reservoir L.

The management criteria are then defined as follows:

a) Maintain a high water level in the reservoir, to guarantee the water volume needed for the crop irrigation.
b) When the reservoir contains enough water, store the excess of photovoltaic energy in the battery bank.
c) Ensure a depth of discharge dod less than dod_{max}, to protect the batteries against the deep discharge, and higher than dod_{min}, to protect them from the excessive charge.
d) Ensure a margin of 10% of the photovoltaic power: the pump can be connected to the panel only if the measured photovoltaic power P_{pv} is 10% higher than the required power by the pump P_{pump}, to guarantee a continuous power supply for the pump.

These criteria are established to meet fixed objectives (Figure 3.3):

O1) Provide the required irrigation when needed, by storing water in the reservoir.
O2) Minimize the use of the battery bank.

O3) Protect the batteries against the excessive charge and discharge, by disconnecting them, respectively, from PVs and the pump when they are not used.

O4) Ensure a continuous power supply, especially during weather changes:

During the day, the instantaneous power P_{pump} verifies that:

$$P_{pump} = P_{pv} + \bar{P}_{Bat} \quad \textbf{(73)}$$

and the current absorbed by the load I_{pump} is just:

$$I_{pump} = I_{pv} + \bar{I}_{Bat} \quad \textbf{(74)}$$

According to the fourth criterion, the panel supplies the load without the battery bank it provides 110 % of the demand. This criterion ensures a continuous power supply of the pump. Thus:

$$I_{pv} \geq 1.1\, I_{pump} \quad \textbf{(75)}$$

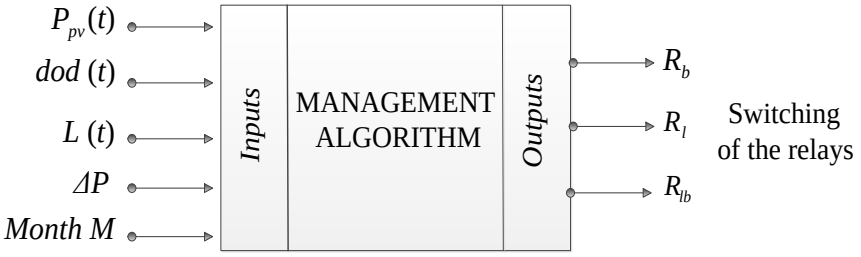

Figure 3. 3 Structure of the proposed energy management algorithm

As it has been mentioned, in order to derive an Energy Management Algorithm that can be easily implemented, tuned, maintained by persons with low technical training, and adapted to different installations and irrigation facilities, the management algorithm is implemented using Fuzzy logic.

The proposed algorithm needs preliminary treatment of some data that will be provided later to the fuzzy algorithm: the expected photovoltaic power (using the model given by [34]), the *dod* [8, 9] and the stored water in the reservoir. In fact, during the night, in case of lack of water volume in the reservoir, due to an unexpected water extraction or in case of pumping insufficient water volume during the day, the missing water volume is recovered using the battery bank, if it is charged.

For this, the length of time Δt_{bat} for which the battery is capable to supply the pump without exceeding dod_{max}, is evaluated using (57) [8, 9]:

$$\Delta t_{bat} = \left(dod_{max} - dod\left(t\right) \right) \frac{C_p}{I_{bat}^{k_p}} \quad \textbf{(76)}$$

where:

dod_{max}: the maximum allowed value for the dod,

C_p: the Peukert capacity (A.h),

I_{bat}: the battery current (A),

k_p: the Peukert constant.

After estimating these inputs, the Fuzzy tool generates the decisions, following the management algorithm that is now explained.

3.4.2 Relays Switching Modes

To achieve our objectives O1-O4 explained in Section 3.4, six operating modes are defined for the switching of the three relays R_b, R_l and R_{lb}:

1/ At night, in normal conditions, the volume in the reservoir is full, so all the relays would be *off* (*mode 1*). This mode would be maintained during the irrigation period, when the tank volume decreases.

2/ During the early hours of the morning, *mode 2* is possible, since the battery bank and the photovoltaic panels supply the pump. In this case, the relays R_l and R_{lb} would be *on*.

3/ The third mode (*mode 3*) consists in pumping water and charging the battery bank with the energy in excess. In this case, the relays R_l and R_b would be *on* and the relay R_{lb} would be *off*.

4/ When the reservoir is full, the photovoltaic energy generated is fully used to charge the battery bank when the batteries are discharged. This corresponds to *mode 4*, for which the relay R_b would be *on*.

5/ The relay R_l is switched *on* during the fifth mode (*mode 5*), to allow the pump to be supplied when the panels produce a sufficient power to the pump, with an excess margin of 10%.

6/ During the sixth mode (*mode 6*), only the relay R_{lb} would be switched *on*. This mode is possible during the night when the water volume in the reservoir is less than the volume needed to irrigate the crops.

3.4.3 Fuzzy Energy Management Algorithm

The energy management algorithm is based on four steps: the extraction of the knowledge base, the fuzzification, the inference diagram and the defuzzification [26, 35]. These four steps are presented now in detail in our proposal (following the structure presented in Figure 3.4).

a. Knowledge Base

The knowledge base is generated on the basis of the specifications:

i. Photovoltaic Power $\tilde{P}_{pv}$

The photovoltaic power $\tilde{P}_{pv}$ generated is periodically estimated and then partitioned in three fuzzy sets that cover the interval $X = \left[0, P_{pv\ max}\right]$ at *low*, *medium* and *high* power generation levels, respectively:

$$\forall x \in \mathcal{X}, \mu_L(x) + \mu_M(x) + \mu_H(x) = 1 \quad \textbf{(77)}$$

where $\mu_L(x)$, $\mu_M(x)$ and $\mu_H(x)$ are, respectively, the *low*, *medium* and *high* membership functions at the measured power level x.

ii. Battery *dod*

It is composed of three fuzzy sets that cover the interval $D = \left[0, dod_{max}\right]$ at *low*, *medium* and *high* production levels, respectively, and verify:

$$\forall d \in \mathcal{D}, \mu_{dL}(d) + \mu_{dM}(d) + \mu_{dH}(d) = 1 \quad \textbf{(78)}$$

where $\mu_{dL}(d), \mu_{dM}(d)$ and $\mu_{dH}(d)$ are, respectively, the *low*, *medium* and *high* membership functions of the estimated *dod* d.

iii. Stored Water Volume v

The third partition is composed of three fuzzy sets in the interval $V = [0, V_{max}]$ which verify:

$$\forall v \in \mathcal{V}, \mu_{vL}(v) + \mu_{vM}(v) + \mu_{vH}(v) = 1 \quad \textbf{(79)}$$

where $\mu_{vL}(v)$, $\mu_{vM}(v)$ and $\mu_{vH}(v)$ are, respectively, the membership functions of v.

As the definition of *low*, *medium* and *high* depends on the use of the auxiliary sets, we define the following fuzzy variables:

❖ Months M

This partition is composed of as many fuzzy sets as months, given by the set $\mathcal{M} = \{m_1, m_2, ..., m_t\}$ and verify:

$$\forall m \in \mathcal{M}, \mu_{m_1}(m) + \mu_{m_2}(m) + ... + \mu_{m_t}(m) = 1 \quad \textbf{(80)}$$

where $\mu_{m_i}(m)$ are the membership functions corresponding to the month m.

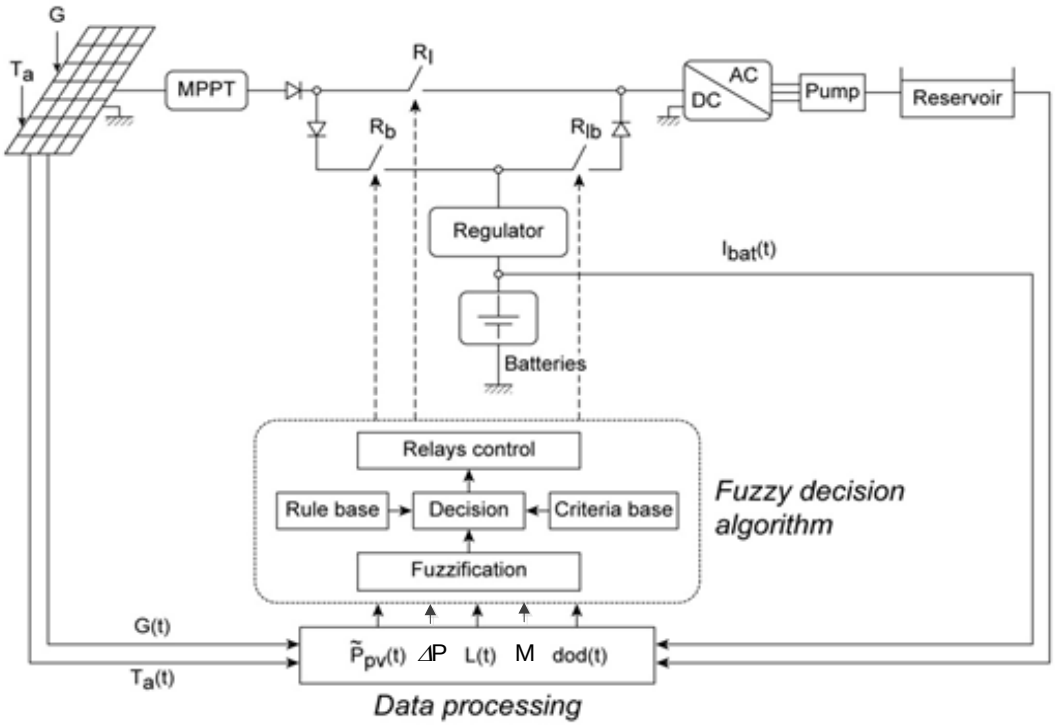

Figure 3. 4 Proposed structure for the implementation of the management system

❖ Water Level L

This partition is composed of as many fuzzy sets as months, denoted by the set $\mathcal{L}=(l_1,l_2,...,l_t)$. The interval of the possible water level $L=[0,L_{max}]$ is covered by these fuzzy sets and verify:

$$\forall l \in \mathcal{L} \mu_{l_1}(l)+\mu_{l_2}(l)+...+\mu_{l_t}(l)=1 \quad \textbf{(81)}$$

where $\mu_{l_i}(l)$ is the membership function corresponding to l_i evaluated at l.

iv. Power difference ΔP

This partition is composed of two fuzzy sets $\mathcal{F}=(f_1,f_2)$ and verify:

$$\forall f \in \mathcal{F}, \mu_{f_1}(f)+\mu_{f_2}(f)=1 \quad \textbf{(82)}$$

where $\mu_{f_e}(f)$ is the membership function corresponding to f_e evaluated at f.

v. Relays R_l, R_b, R_{lb}

To decide the switching of the relays R_l, R_b, R_{lb}, depending on the fuzzy variables x, d and *v*, two fuzzy sets are planned $O=\{on,off\}$. They cover the domain $\mathcal{O}=[0,1]$ and verify $\forall o \in \mathcal{O}$:

$$\begin{cases} \mu_{off\,\eta}(o)+\mu_{on\,\eta}(o)=1 \\ \mu_{off\,\eta_b}(o)+\mu_{on\,\eta_b}(o)=1 \\ \mu_{off\,\eta_{lb}}(o)+\mu_{on\,\eta_{lb}}(o)=1 \end{cases} \quad \textbf{(83)}$$

where the switching controls given to relays are provided by the membership functions corresponding to r_l, r_b, r_{lb}, respectively, evaluated at o.

Based on this structure, the fuzzy rules of therelays' switching times are classified according to three sets of dod (Figure 3.5):

- $dod \in [0 \;\; d_{dL_{max}}]$: the pump is supplied by the panels and/ or the battery bank,
- $dod \in [d_{dL_{min}} \;\; d_{dM_{max}}]$: supplying the pump is preferred to charging the battery bank,

- $dod \in \left[d_{dM_{min}} \quad d_{dH_{max}} \right]$: charging the battery bank is preferred to supplying the pump since the panels produce insufficient power to the pump and the battery bank is discharged.

b. Fuzzification

i. Photovoltaic Power $\tilde{P}_{pv}$

The membership functions of $\mu_L(x_{0i}), \mu_M(x_{0i}), \mu_H(x_{0i})$ corresponding to $\tilde{P}_{pv}$ are expressed as follows (Figure 3.5):

$$\mu_L(x_{0i}) = \begin{cases} 1 & if \quad 0 < x < x_{L_{min}} \\ \dfrac{x_{0i} - x}{\varepsilon_{x_{0i}}} & if \quad x_{L_{min}} < x < x_{L_{max}} \\ 0 & otherwise \end{cases} \tag{84}$$

$$\mu_M(x_{0i}) = \begin{cases} \dfrac{x - x_{0i}}{\varepsilon_{x_{0i}}} & if \quad x_{M_{min1}} < x < x_{M_{min2}} \\ 1 & if \quad x_{M_{min2}} < x < x_{M_{max1}} \\ \dfrac{x_{0i} - x}{\varepsilon_{x_{0i}}} & if \quad x_{M_{max1}} < x < x_{M_{max2}} \\ 0 & otherwise \end{cases} \tag{85}$$

$$\mu_H(x_{0i}) = \begin{cases} 1 & if \quad x > x_{H_{max}} \\ \dfrac{x - x_{0i}}{\varepsilon_{x_{0i}}} & if \quad x_{H_{min}} < x < x_{H_{max}} \\ 0 & otherwise \end{cases} \tag{86}$$

ii. Battery Depth of Discharge *dod*

The membership functions of $\mu_{dL}(d_{0k}), \mu_{dM}(d_{0k}), \mu_{dH}(d_{0k})$ corresponding to *dod* are expressed as follows (Figure 3.5):

$$\mu_{dL}(d_{0k}) = \begin{cases} 1 & if \quad 0 < d < d_{dL_{min}} \\ \dfrac{d_{0k} - d}{\varepsilon_{d_{0k}}} & if \quad d_{dL_{min}} < d < d_{dL_{max}} \\ 0 & otherwise \end{cases} \tag{87}$$

$$\mu_{dM}(d_{0k}) = \begin{cases} \dfrac{d - d_{0k}}{\varepsilon_{d_{0k}}} & if \quad d_{dM_{min1}} < d < d_{dM_{min2}} \\ 1 & if \quad d_{dM_{min2}} < d < d_{dM_{max1}} \\ \dfrac{d_{0k} - d}{\varepsilon_{d_{0k}}} & if \quad d_{dM_{max1}} < d < d_{dM_{max2}} \\ 0 & otherwise \end{cases} \tag{88}$$

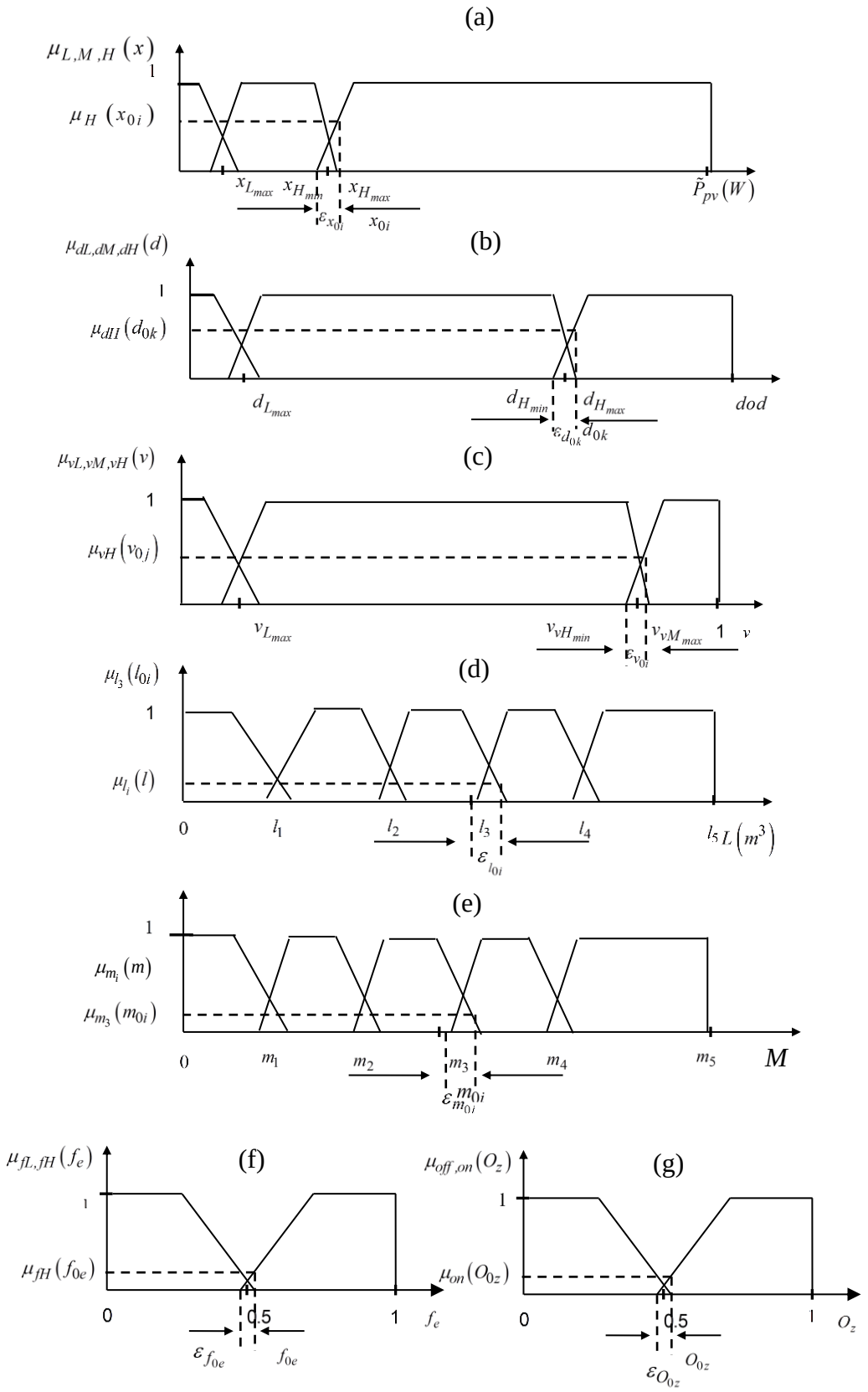

Figure 3. 5 Membership functions corresponding to: (a) photovoltaic power $\tilde{P}_{pv}$, (b) battery dod, (c) fuzzified water volume v, (d) water volume L, (e) months M, (f) Power difference ΔP and (g) control signals of each relay O_z

$$\mu_{dH}\left(d_{0k}\right)=\begin{cases}1 & if \quad d>d_{dH_{max}}\\ \dfrac{d-d_{0k}}{\varepsilon_{d_{0k}}} & if \quad d_{dH_{min}}<d<d_{dH_{max}}\\ 0 & otherwise\end{cases} \tag{89}$$

iii. Water Volume v

The membership functions of $\mu_{vL}\left(v_{0j}\right),\mu_{vM}\left(v_{0j}\right),\mu_{vH}\left(v_{0j}\right)$ corresponding to the water volume v are expressed as follows (Figure 3.5):

$$\mu_{vL}\left(v_{0j}\right)=\begin{cases}1 & if \quad 0<v<v_{vL_{min}}\\ \dfrac{v_{0j}-v}{\varepsilon_{v_{0j}}} & if \quad v_{vL_{min}}<v<v_{vL_{max}}\\ 0 & otherwise\end{cases} \tag{90}$$

$$\mu_{vM}\left(v_{0j}\right)=\begin{cases}\dfrac{v-v_{0j}}{\varepsilon_{v_{0j}}} & if \quad v_{vM_{min1}}<v<v_{vM_{min2}}\\ 1 & if \quad v_{vM_{min2}}<v<v_{vM_{max1}}\\ \dfrac{v_{0j}-v}{\varepsilon_{v_{0j}}} & if \quad v_{vM_{max1}}<v<v_{vM_{max2}}\\ 0 & otherwise\end{cases} \tag{91}$$

$$\mu_{vH}\left(v_{0j}\right)=\begin{cases}1 & if \quad v>v_{vH_{max}}\\ \dfrac{v-v_{0j}}{\varepsilon_{v_{0j}}} & if \quad v_{vH_{min}}<v<v_{vH_{max}}\\ 0 & otherwise\end{cases} \tag{92}$$

iv. Power difference ΔP

The membership functions of $\mu_{fL}\left(f_{0e}\right),\mu_{fH}\left(f_{0e}\right)$ corresponding to ΔP are expressed as follows:

$$\mu_{fL}\left(f_{0e}\right)=\begin{cases}1 & if \quad 0<f<f_{fL_{min}}\\ \dfrac{f_{0e}-f}{\varepsilon_{f_{0e}}} & if \quad f_{fL_{min}}<f<f_{fL_{max}}\\ 0 & otherwise\end{cases} \tag{93}$$

$$\mu_{fH}\left(f_{0e}\right)=\begin{cases}1 & if \quad f>f_{fH_{max}}\\ \dfrac{f-f_{0e}}{\varepsilon_{f_{0e}}} & if \quad f_{fH_{min}}<f<f_{fH_{max}}\\ 0 & otherwise\end{cases} \tag{94}$$

v. Switching Control of the Relays R_l, R_b, R_{lb}

The relays' membership functions $\mu_{off\ r_l, r_b, r_{lb}}(o_{0z}), \mu_{on\ r_l, r_b, r_{lb}}(o_{0z})$ corresponding to the relays R_l, R_b and R_{lb} are expressed as follows (Figure 3.5):

$$\mu_{off\ r_l, r_b, r_{lb}}(o_{0z}) = \begin{cases} 1 & if \quad 0 < o < o_{off_{min}} \\ \dfrac{o_{0z} - o}{\varepsilon_{o_{0z}}} & if \quad o_{off_{min}} < o < o_{off_{max}} \\ 0 & otherwise \end{cases} \tag{95}$$

$$\mu_{on\ r_l, r_b, r_{lb}}(o_{0z}) = \begin{cases} 1 & if \quad o > o_{on_{max}} \\ \dfrac{o - o_{0z}}{\varepsilon_{o_{0z}}} & if \quad o_{on_{min}} < o < o_{on_{max}} \\ 0 & otherwise \end{cases} \tag{96}$$

c. Inference Diagram

Based on the fuzzified inputs ($\tilde{P}_{pv}$, *dod* and *v*), the fuzzy rules used for the inference diagram decide the relays switching. During the day, the relays switching decisions are given in Table 3.1. At night, if there is no water extraction or the pumped water volume during the day is sufficient for the irrigation, all the relays would be *off*; otherwise, if the battery bank is charged, the relay R_{lb} would be *on*, to pump the missing water volume needed for irrigation.

The numerical value of the signals' control $r_{0l,b,lb}$ for the three relays is obtained from:

$$r_{0l,b,lb} = \frac{\int_0^1 r_{on}\, \mu_{r_{l\,on}}\, dr_{on}}{\int_0^1 \mu_{r_{l\,on}}\, dr_{on}} \tag{97}$$

Table 3.1 Fuzzification of the knowledge base

- *dod* is *dL*

v \ P_{pv}	*L*	*M*	*H*
vL	r_{lb} *is on* r_l *is on* r_b *is off*	r_{lb} *is on* r_l *is on* r_b *is off*	r_{lb} *is off* r_l *is on* r_b *is on*
vM	r_{lb} *is on* r_l *is on* r_b *is off*	r_{lb} *is on* r_l *is on* r_b *is off*	r_{lb} *is off* r_l *is on* r_b *is on*
vH	r_{lb} *is off* r_l *is off* r_b *is off*	r_{lb} *is off* r_l *is off* r_b *is off*	r_{lb} *is off* r_l *is off* r_b *is off*

- *dod* is *dM*

v \ P_{pv}	*L*	*M*	*H*
vL	r_{lb} *is on* r_l *is on* r_b *is off*	r_{lb} *is on* r_l *is on* r_b *is off*	r_{lb} *is off* r_l *is on* r_b *is on*
vM	r_{lb} *is on* r_l *is on* r_b *is off*	r_{lb} *is on* r_l *is on* r_b *is off*	r_{lb} *is off* r_l *is on* r_b *is on*
vH	r_{lb} *is off* r_l *is off* r_b *is on*	r_{lb} *is off* r_l *is off* r_b *is on*	r_{lb} *is off* r_l *is off* r_b *is on*

- *dod* is *dH*

v \ P_{pv}	*L*	*M*	*H*
vL	r_{lb} *is off* r_l *is off* r_b *is on*	r_{lb} *is off* r_l *is off* r_b *is on*	r_{lb} *is off* r_l *is on* r_b *is on*
vM	r_{lb} *is off* r_l *is off* r_b *is on*	r_{lb} *is off* r_l *is off* r_b *is on*	r_{lb} *is off* r_l *is on* r_b *is on*
vH	r_{lb} *is off* r_l *is off* r_b *is on*	r_{lb} *is off* r_l *is off* r_b *is on*	r_{lb} *is off* r_l *is off* r_b *is on*

d. Defuzzification

The control of the three relays is deduced as follows (Figure 3.5):

$$If \quad r_{l,b,lb} \leq 0.5 \; then \quad R_{l,b,lb} \quad is \quad off \qquad \textbf{(98)}$$

$$If \quad r_{l,b,lb} > 0.5 \quad then \quad R_{l,b,lb} \quad is \quad on \tag{99}$$

3.5 Application to a Case Study

In order to test the efficiency of the proposed algorithm, we validated our approach using data of our target application: a land planted with tomatoes, located in Medjez El Beb, presented previously in Chapter 1, Section 1.1. This application is prompted by the fact that tomatoes must be irrigated regularly, especially during flowering and fruit formation [36]: the vegetative cycle in the target area is given from *March* to *July*.

The irrigation is gravity-based: $200\,m^3/h$ just before sunrise, to irrigate a 10 ha field by a low-pressure gravity-driven drip system. For this, a 4.5 kW pump submerged in an 80 meter wall, and a 1800 m^3 reservoir are available. First, the PV and batteries were sized using the algorithm presented in Chapter 2, Section 2.6 [37]: A 10.74 kW PV system ($101.5\,m^2$ panel surface equipped with a Maximum Power Point Tracker) and a battery bank composed of 8 batteries (210 Ah/12V) with regulator have been selected. Using the algorithm presented in Section 3.4, we shall now describe the energy management (Figure3.4) in detail.

3.5.1 Algorithm Parameterization

a. Photovoltaic Power P_{pv}

The panels non-linear model, detailed in Chapter 2, Section 2.5, is used here to evaluate the photovoltaic power P_{pv} [34]. Then, P_{pv} is classified as follows:

a) If $P_{pv} \in [0 \;\; 10\,W]$, then P_{pv} is considered *low*.

b) If $P_{pv} \in [10\,W \;\; 4500\,W]$, then P_{pv} is considered *medium*.

c) If $P_{pv} \in [4500\,W \;\; 10740\,W]$, then P_{pv} is considered *high*.

b. Battery Depth of Discharge dod

The battery non-linear model [8, 9, 38], detailed in Chapter 2, Section 2.5, is used here to evaluate the *dod* , which is classified as follows:

i) If $dod \in [0\ \ 0.02]$, then *dod* is considered *low*.
ii) If $dod \in [0.02\ \ 0.8]$, then *dod* is considered *medium*.
iii) If $dod \in [0.8\ \ 1]$, then *dod* is considered *high*.

c. Stored Water Volume v

Using the water need model [28, 36] (Chapter 2, Section 2.6), the water volume *V* corresponding to each month of tomatoes vegetative cycle at the target location is:

1) The mean water volume of *March* (m_1) is $l_1 = 60\ m^3/day$.
2) The mean water volume of *April* (m_2) is $l_2 = 100\ m^3/day$.
3) The mean water volume of *May* (m_3) is $l_3 = 179\ m^3/day$.
4) The mean water volume of *June* (m_4) is $l_4 = 241\ m^3/day$.
5) The mean water volume of *July* (m_5) is $l_5 = 321\ m^3/day$.

The fuzzification of the water volume depends on the month and is described in Table 3.2.

Table 3.2 Water fuzzification corresponding to each month *M*

Month M / *L*	m_1	m_2	m_3	m_4	m_5
l_1	*low*	*low*	*low*	*low*	*low*
l_2	*high*	*medium*	*low*	*low*	*low*
l_3	*high*	*high*	*medium*	*low*	*low*
l_4	*high*	*high*	*high*	*medium*	*low*
l_5	*high*	*high*	*high*	*high*	*medium*

3.5.2 Results and Discussions

The management algorithm was implemented using the models presented in [11, 33]. Simulations were carried out using data (solar irradiation, ambient temperature, rainfall, etc.) from the target location (Medjez El Beb) for the irrigation season from *March* to *July*. Obtained results (Figures 3.6-3.11) prove that the algorithm fulfills the objectives: relays switching ensures the system's autonomy. The water demand is fulfilled and the battery and load are correctly disconnected when not used.

For example, we study here the case when in *March* $f_i = 3$. In fact, on *March* 13^{th} (Figure 3.6), the pump is supplied by the panel and/ or the battery, following the algorithm constraints and goals. Indeed, at night, the tank contains the water needed by the crops (60 m^3). So the irrigation step is finished one hour before sunrise to allow a better absorption of the water by the crops [39]. Thus, during irrigation (Δ_{irg}), the water volume decreases, following the constant irrigation flow rate (200 m^3/h). At 8:45 a.m, the tank is empty and the battery is charged. Hence, the system uses both energies from the panel and the battery to pump water. At 4 p.m., the tank is full. Hence, the available photovoltaic energy is used to charge the battery since the battery is not full charged, so only R_b is switched *on*. During all of these modes, the *dod* is always maintained between the prefixed values (0.02 and 0.8), which guarantees the battery's safety.

Then, in *March*, 14^{th}, the energy generated is used to full the reservoir with water, since there is no irrigation. In *March*, 15^{th}, the PV enegy is not used since the reservoir and the battery bank are full.

In *March*,16^{th} (Figure 3.6), from the starting defect time t_{sd} = 3:50 a.m. until the end defect time t_{ed} = 5:00 a.m., an additional water extraction is applied with a flow rate= 150 m^3/h. Thus, the developed algorithm allows the relay R_{lb} to be switched *on*, which orders the battery bank to supply the pump, so as to compensate the loss in water volume until 5 a. m, while the *dod* is less than 0.8. In this case, the pumping is performed to have the water needed for the plants irrigation in *March*, since the reservoir can be fulled in the next day, using also the panels. This strategy allows having the reservoir full and minimizing the battery bank use.

In case the battery is discharged (at the beginning of a day of *April*, 13^{th}, Figure 3.7), the initial *dod* is equal to 0.8, which corresponds to the maximum permitted value for *dod*. Hence, the water pumping is not permitted and the photovoltaic energy is used to charge the battery until having an excess of generated photovoltaic energy at t_{on} =8:20 a.m.

At the end of *May* 13^{th} (Figure 3.8), the pumped water volume is equal to 227 m^3, which is higher than the needed water volume for this month (179 m^3). For this reason, the pumping process is stopped at sunset time t_{ss}, to save electric energy. This proves the algorithm efficiency in guaranteeing the coherence between saving water and electric energy.

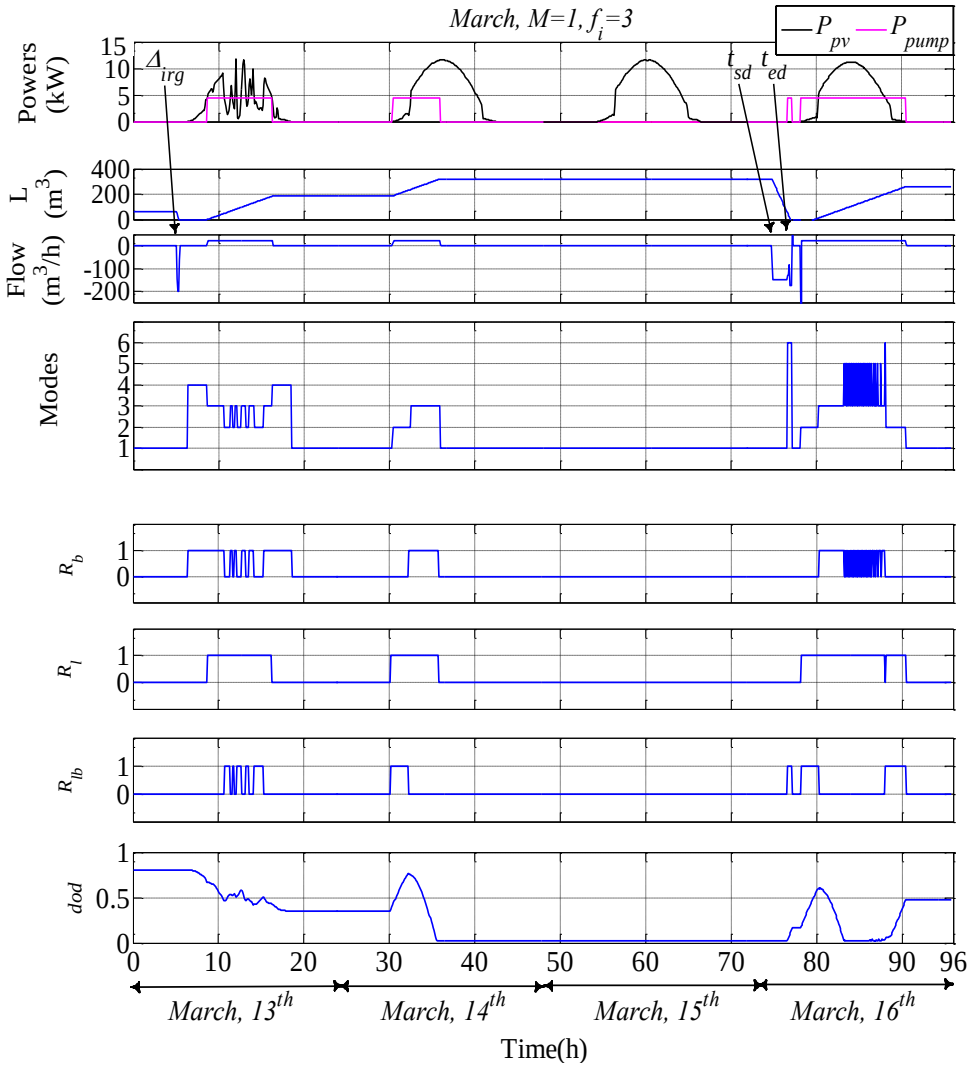

Figure 3. 6 Algorithm response in the case study for four days in *March* (f_i = 3)

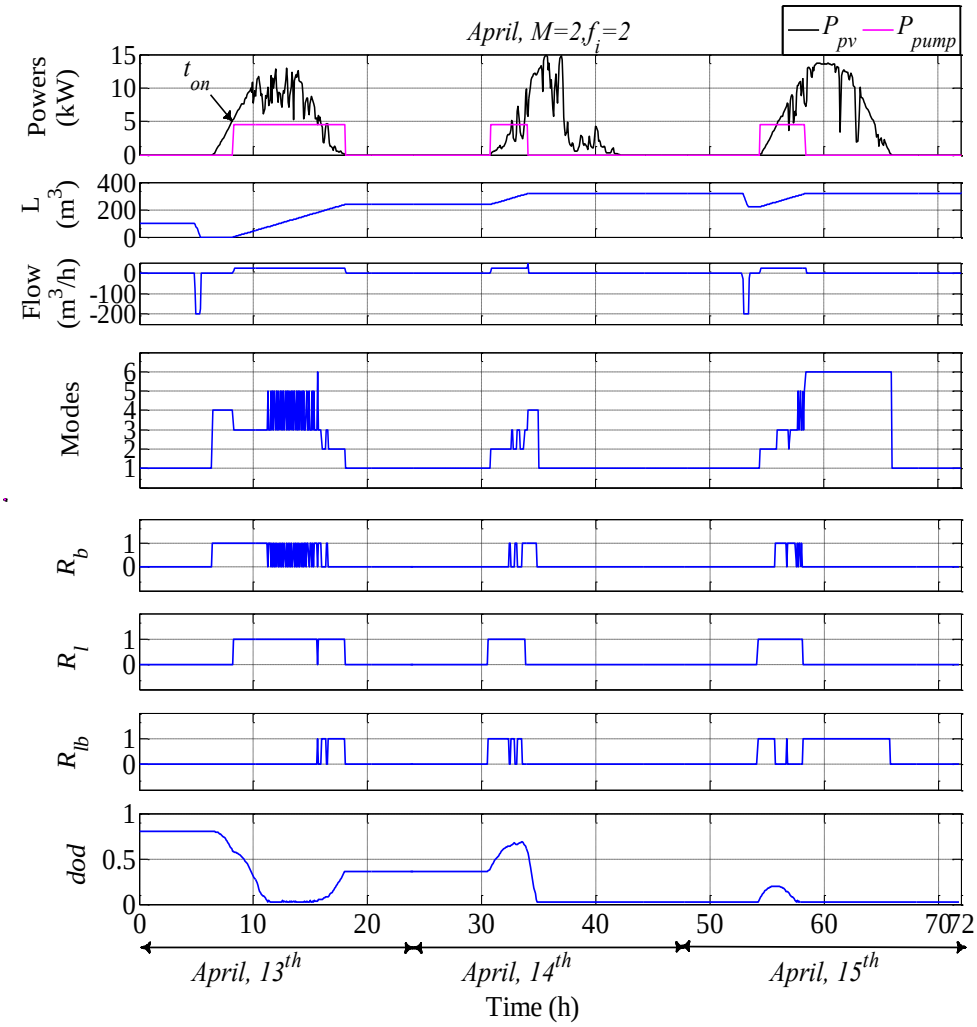

Figure 3. 7 Algorithm response in the case study for three days in *April* (f_i = 2)

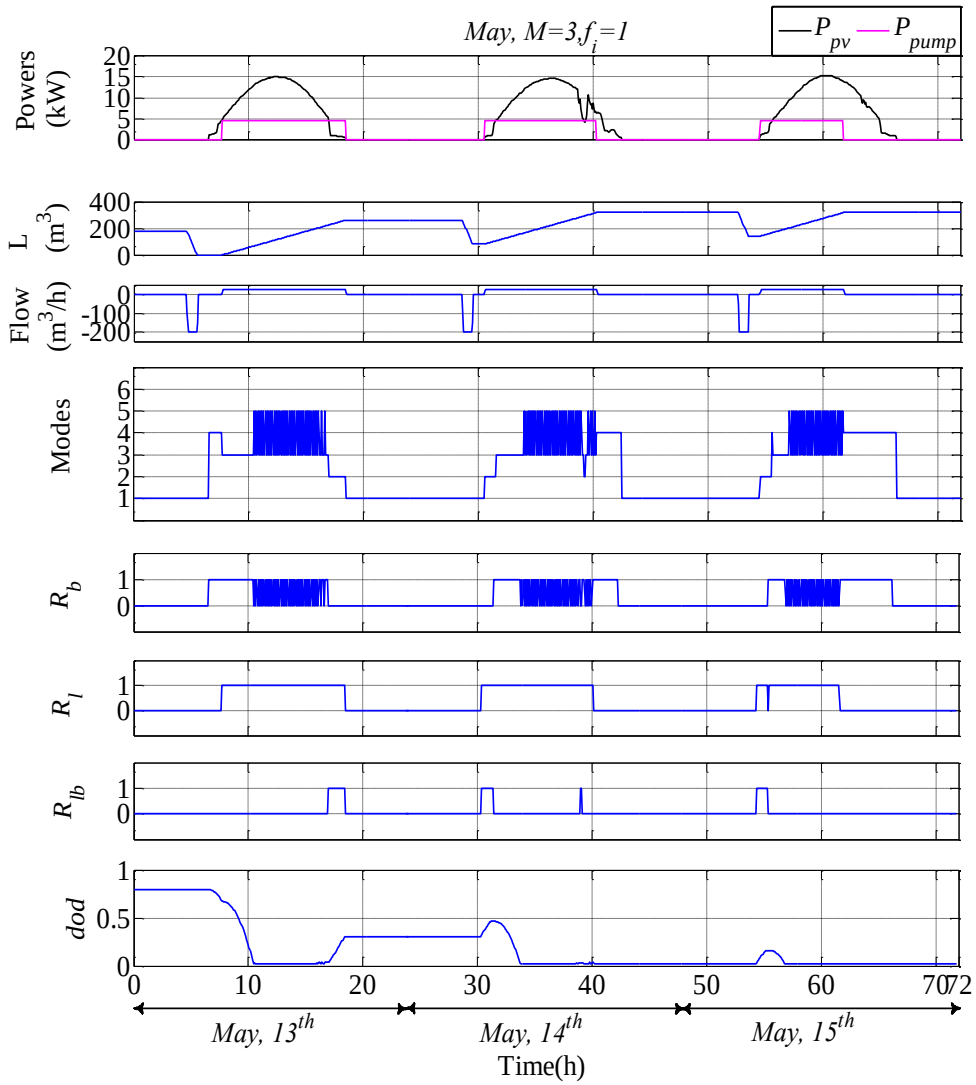

Figure 3. 8 Algorithm response in the case study for three days in *May* (f_i = 1)

To clarify the internal working of the algorithm, the control defuzzification signals of relays are presented for specific days of *June* and *July*, selected as there were rapid changes in the photovoltaic power, for example at t_{c_1}, t_{c_2}, t_{c_3} and t_{c_4} (Figure 3.9 and Figure 3.10). It can be seen that the control signals ensure relays complementary switching (relays R_b and R_{lb}) since each relay is considered *on* when the membership degree for the relay control signal is higher than 0.5 otherwise it is *off*, enabling then a continuous power supply for the pump and the system autonomy. This is detailed in Figure 3.11 where the FMA ensures pumping the water volume expected for *July* and the *dod* to be less than 0.8.

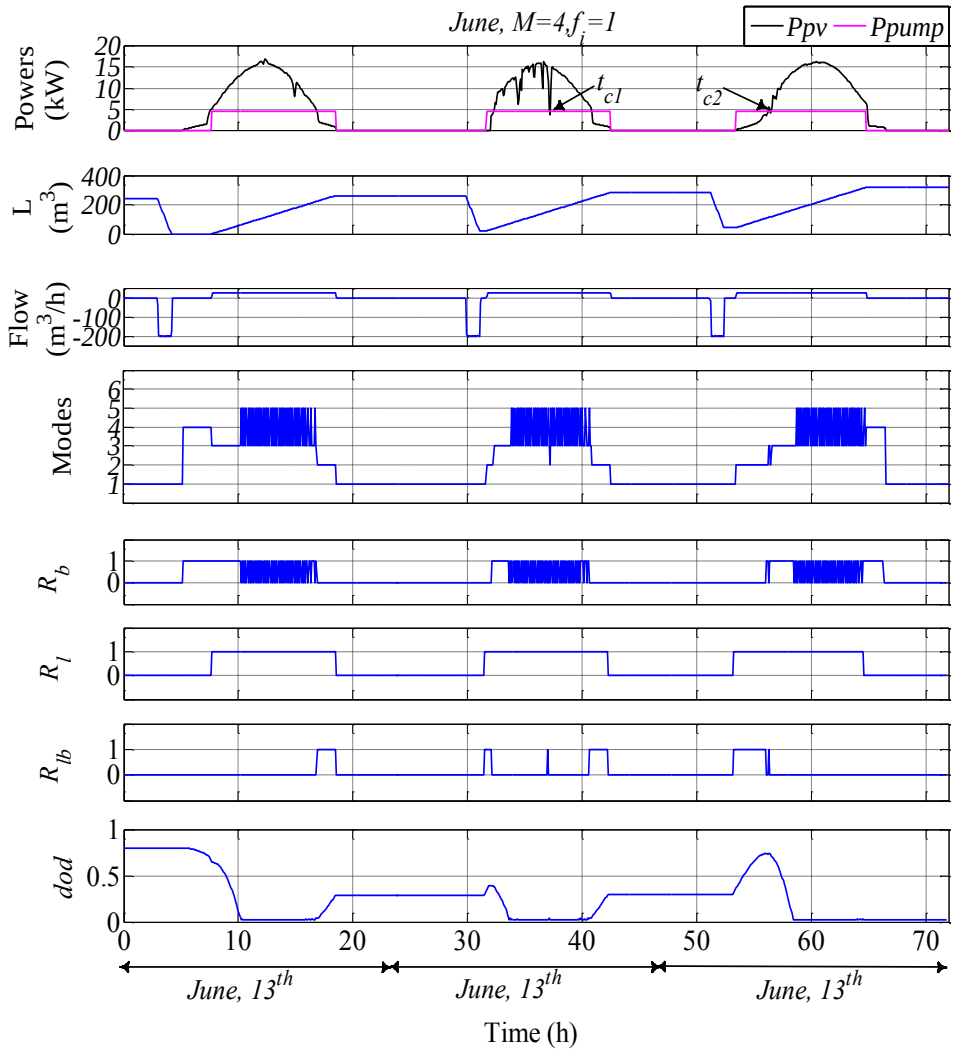

Figure 3. 9 Algorithm response in the case study for three days in *June* ($f_i = 1$)

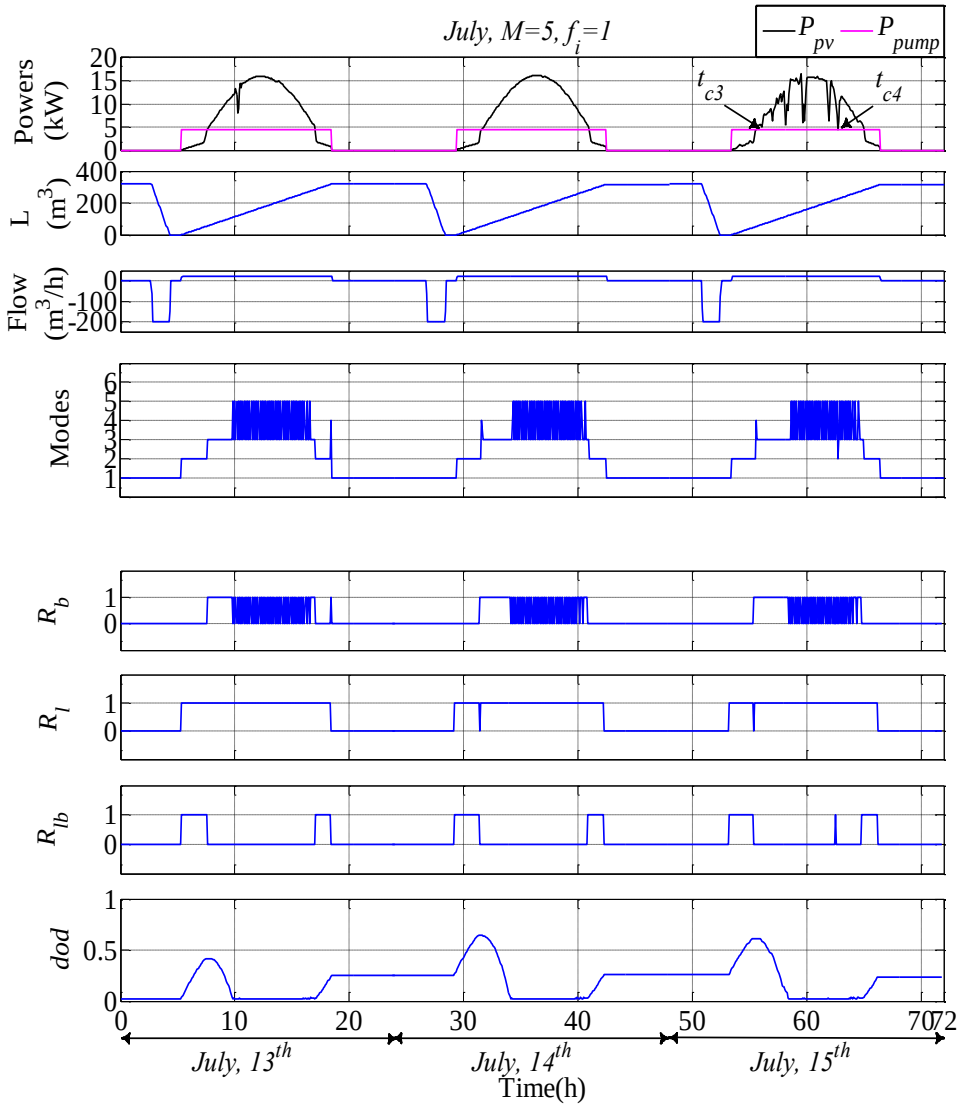

Figure 3. 10 Algorithm response in the case study for three days in *July*

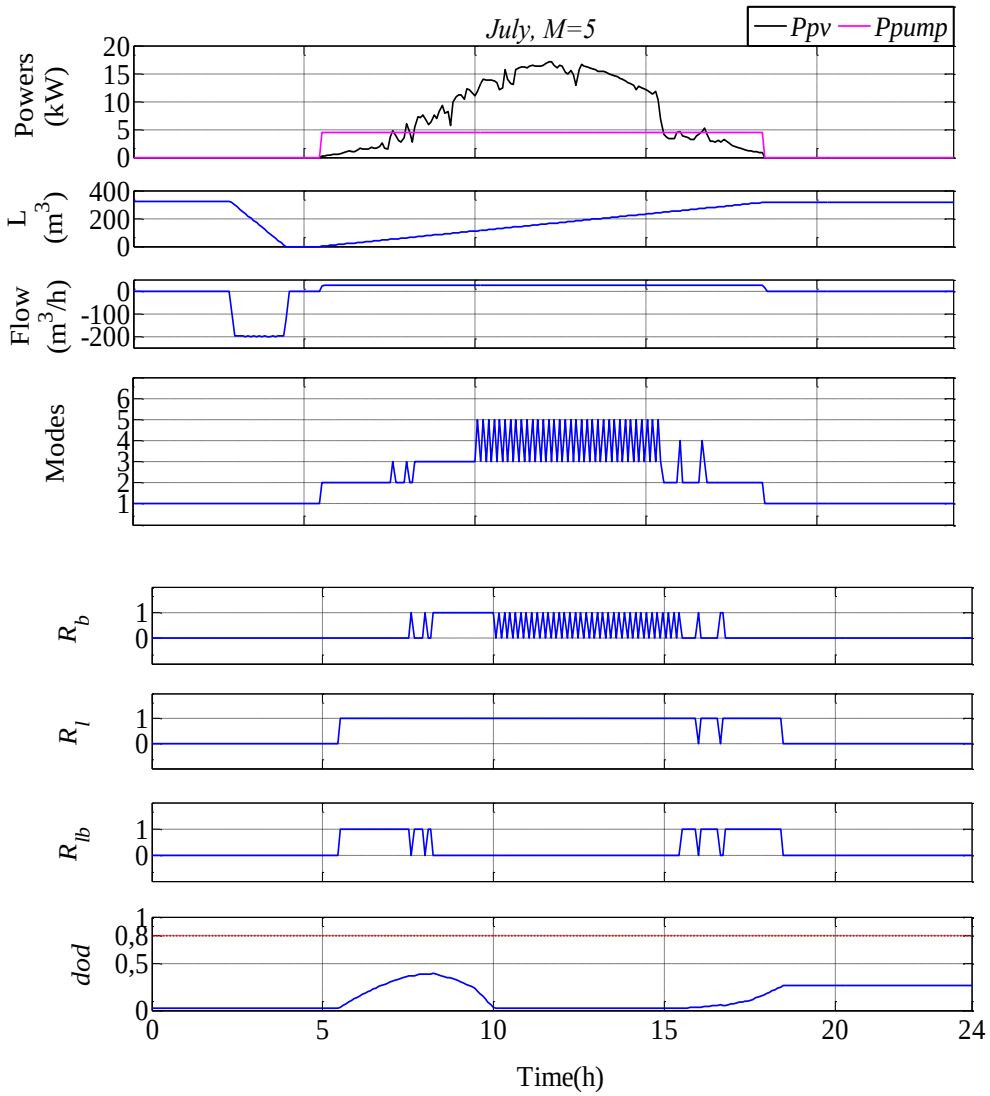

Figure 3. 11 Defuzzification of the control signals for a specific day of *July*

The proposed algorithm is evaluated from *March* to *July* as this is the growing season for tomatoes in the target location. It is clear that it ensures pumping more water volume than needed, especially during *March* and *April* (Figures 3.12). Moreover, the use average of the panel and the battery bank in supplying the pump demonstrate the minimization of the battery bank use: the battery bank maximum contribution in supplying the pump represents 26% of the panels contribution (Figure 3.13). This proves the algorithm's efficiency in keeping the battery bank charged and minimizing its use.

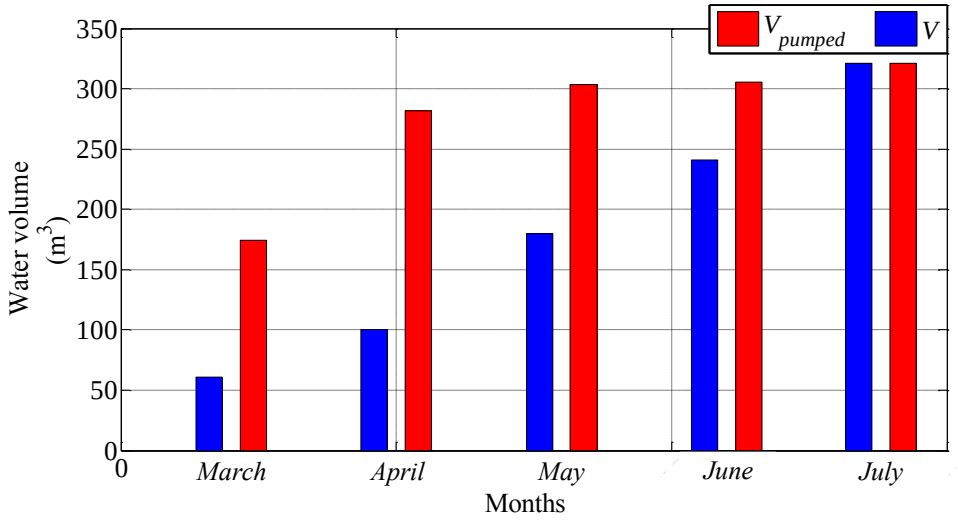

Figure 3. 12 Needed and possible pumped water volume averages during the tomato vegetative cycle in the case study

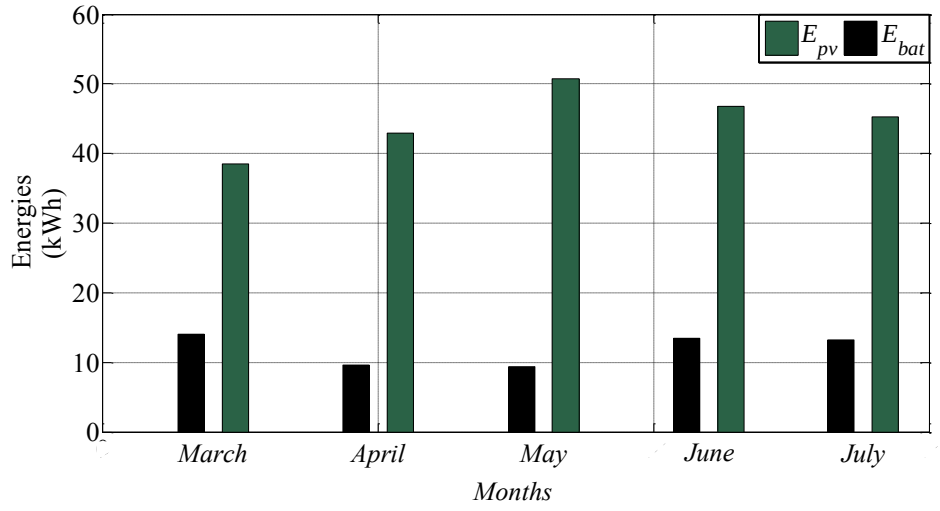

Figure 3. 13 Use average of PV and batteries to supply the pump for the case study

3.6 Experimental Validation

In this section, we validate the management algorithm proposed in Section 3.4. For this, an installation was designed and installed in the laboratory of Automatic Control of the School of Industrial Engineering, University of Valladolid. The plant is composed of a Programmable Power Supply (PPS) (Appendix G), which generates the PV power, a lead-acid battery 12A.h/12V, an inverter (Appendix H), a pump, two reservoirs, sensors of pressure and current (Appendix F) and an acquisition card (Appendix I), installed in a computer, as it is shown in Figure 3. 14.

3.6.1 Installation Description

The installation allows the photovoltaic power to be generated, sensors data to be acquired and recorded in the computer, and the relays control signals to be generated by the control algorithm presented in Section 3.4. These functions are described now (Figure 3.14).

- *Photovoltaic power generation:*

  This step is ensured via the programmable power supply which, in our plant, substitutes the photovoltaic panels and the chopper (that tracks the MPP), in order to make the results reproducible, making possible to evaluate the control algorithm in different situations. In fact, the supply signal is first programmed using the own PPS software, and then it is transmitted to the computer via an USB connection.

- *Data acquisition:*

  The real time signals acquisition is performed using the analogical inputs of the PCI-DAS card (Appendix I), installed in the computer. This card acquires the analogic signals that corresponds to the water level in the tank $L(t)$, received from the pressure sensor, and the battery current $I_{bat}(t)$ signal, received from the current sensor. These signals are the inputs which are then used to the generation of the relays control signals, using the algorithm proposed in Section 3.4.

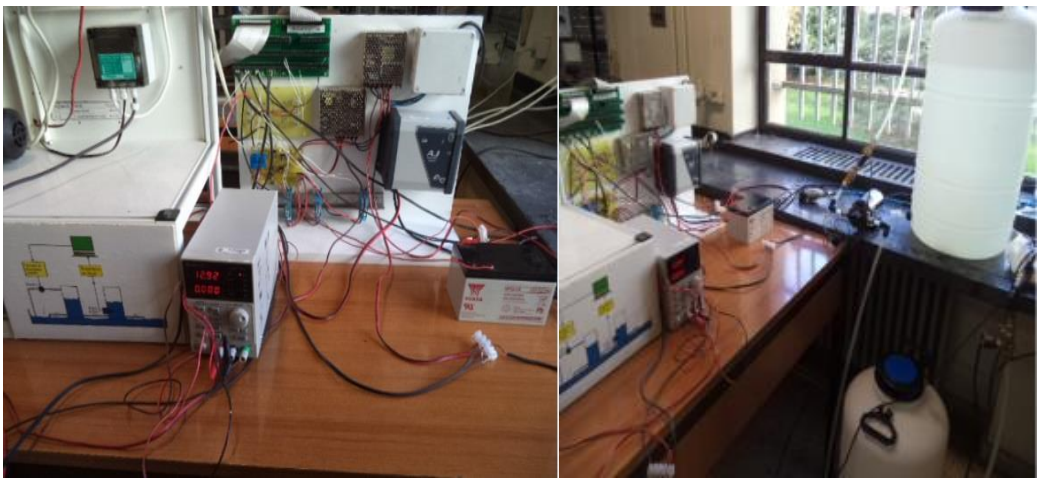

Figure 3. 14 Laboratory system developped for the energy management validation

- *Generation of the relays control signals:*

  The acquired sensors signals are used by the algorithm developped in Section 3.4, and implemented in Matlab, in order to generate the control signals for the relays R_l, R_b and R_{lb} via the outputs of the PCI-DAS card (this card is described in Appendix I).

3.6.2 Cases Study Validation

In this section, we validate some cases study proposed in Section 3.5 (Figures 3.15- 3.19). The management algorithm proposed is tested for typical days for each month during the crop vegetative cycle. This allows validating the possible operating modes discussed in 3.4.2. Figures 3.15 show that in *March*, when the panel generates power less than de demanded by the pump and the reservoir is not full, the relay R_{lb} is switched on to connect the battery bank to the pump. This corresponds to *mode 2*. *Modes 4* is possible when the relays R_l and R_b are switched *on* (Figure 3.16).

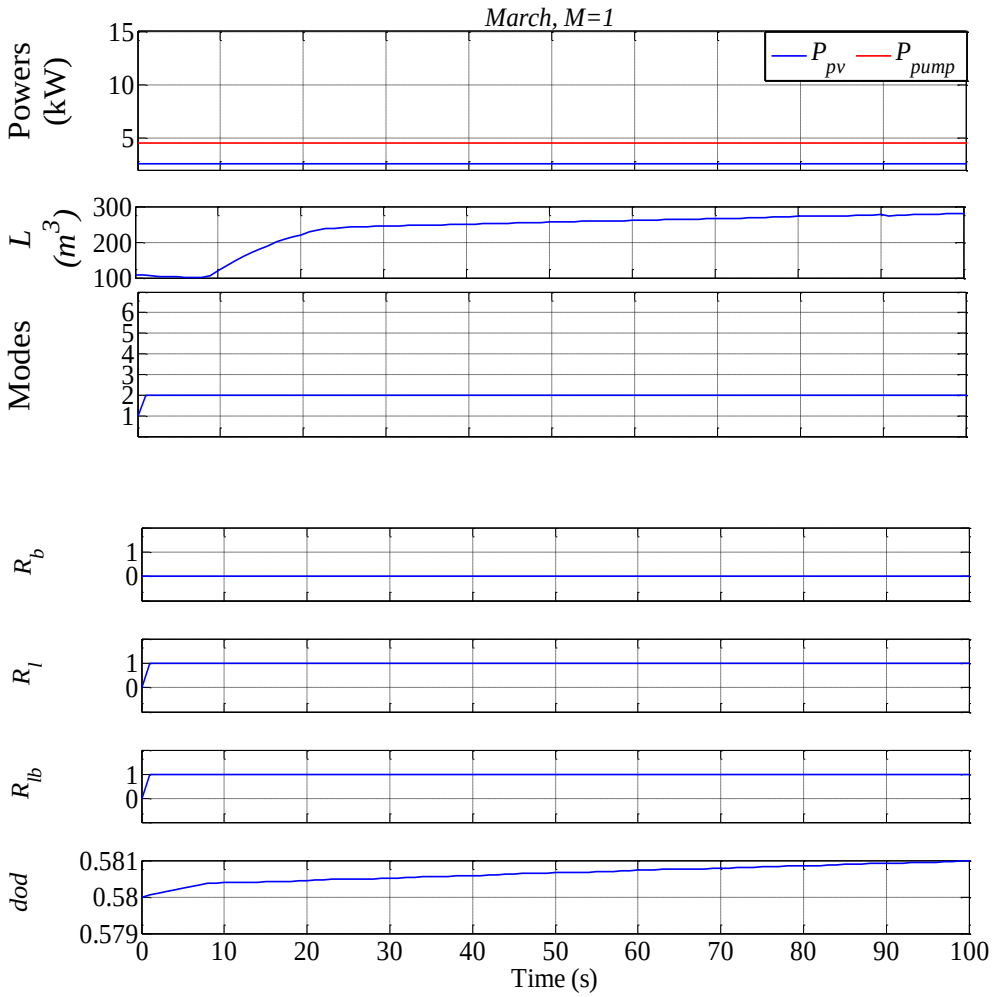

Figure 3. 15 Energy management algorithm response in *March*

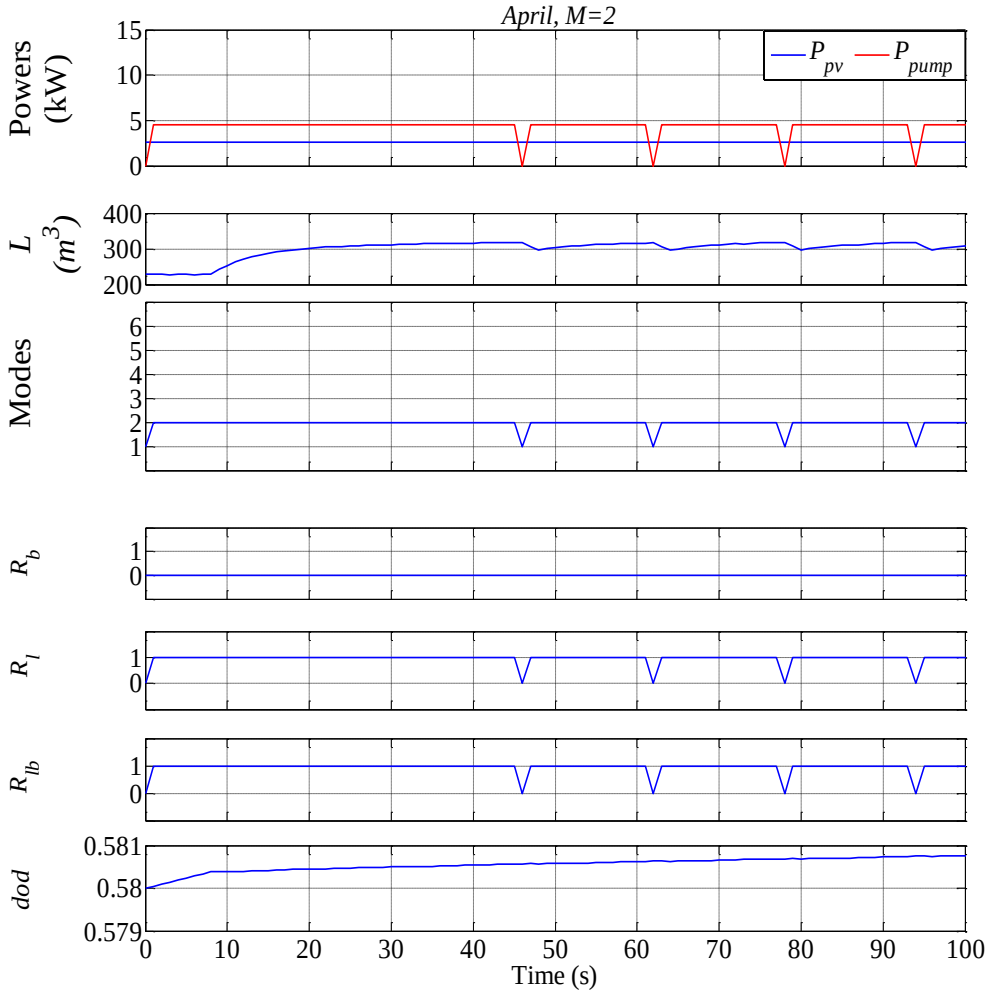

Figure 3. 16 Energy management algorithm response in *April*

In *May*, when the panel produces power in excess, this energy is used to supply the pump and charge the battery bank. This corresponds to *mode 3*, in which, the relays R_l and R_b are switched on (Figure 3.17).

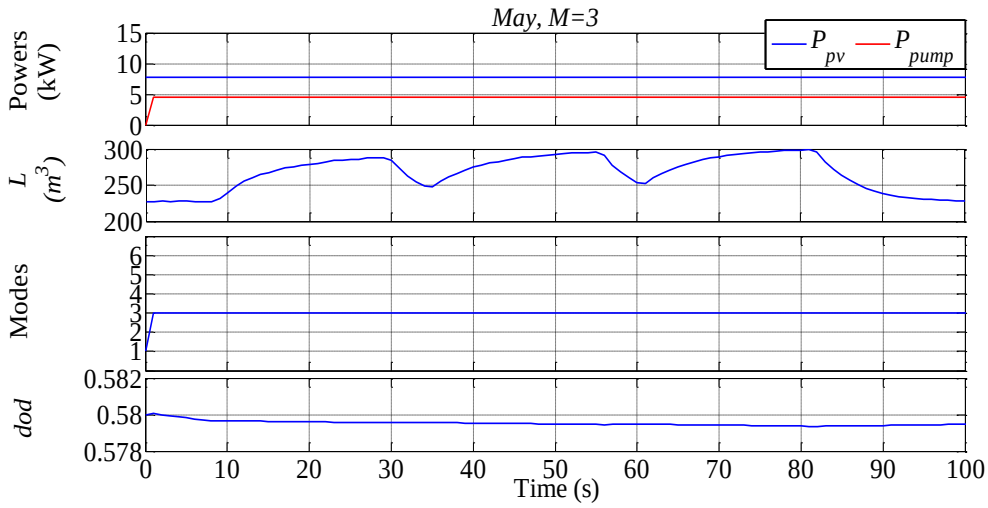

Figure 3. 17 Energy management algorithm response in *May*

When the battery is discharged and the energy produced by the panel is not sufficient for the pump supply, the photovoltaic power is used to charge the battery bank. Hence, only the relay R_b is switched on, corresponding to *mode 4* (see Figures 3.18 and 3.19).

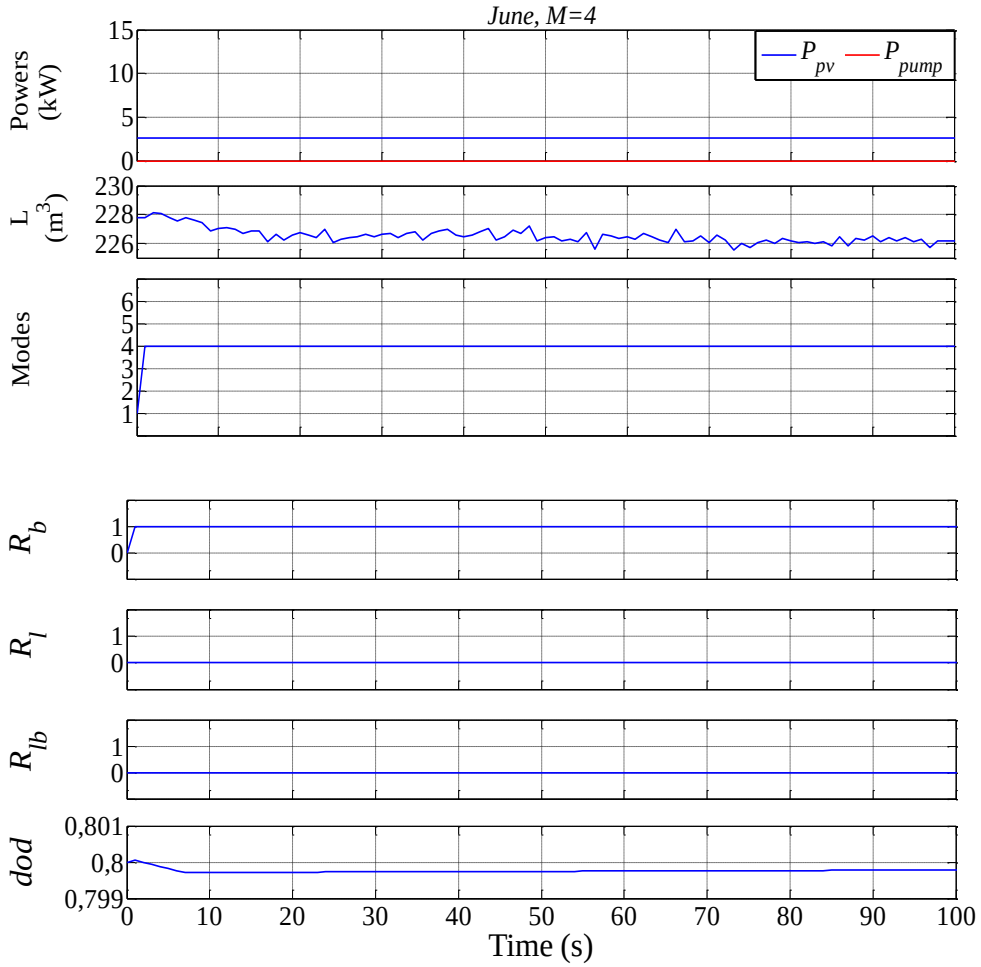

Figure 3. 18 Energy management algorithm response in *June*

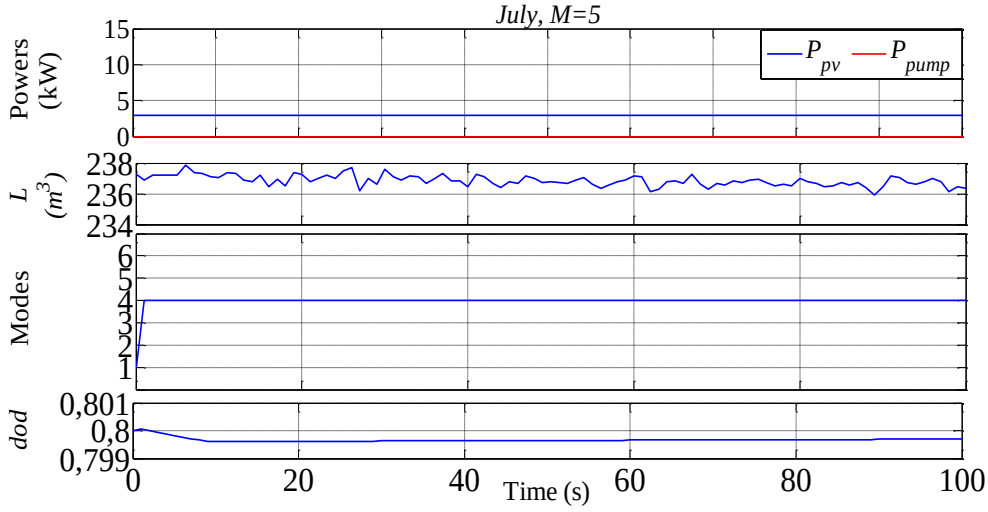

Figure 3. 19 Energy management algorithm response in *July*

3.7 Conclusion

A fuzzy management algorithm for the operation of a photovoltaic irrigation system composed of photovoltaic panels, a lead-acid battery bank and a submerged pump, has been presented and evaluated. The algorithm makes decisions on the interconnection time of the photovoltaic panel, the battery bank and the pump, depending on the photovoltaic power generated, the battery depth of discharge and the stored water amount.

The control algorithm aims to ensure a continuous pump supply and the battery bank protection against deep discharge and excessive charge. The algorithm effectiveness has been tested on a specific case study, during the vegetative cycle of tomatoes (from *March* to *July*). Using data from the target location, system simulation shows that the algorithm guarantees the system autonomy and the battery safety. It must be pointed out that the proposed algorithm is general, in the sense that it can be used for PV irrigation of systems of different sizes, by providing the monthly water demands.

The work was tested in a 1:150 pilot system, with photovoltaic energy produced by a controllable power supply, in order to compare different energy management strategies in similar situations. Moreover, meteorological predictions were included in the algorithm.

As a general conclusion, we have shown that fuzzy algorithms are very adequate for energy management systems, and that simple energy management systems can improve the operation of off-grid PV systems. The results have been presented in [11], [33] and [40].

Currently, further work is being carried out to adapt the algorithm in a photo thermic installation destined to water desalination.

3.8 References

[1]Girish, Kumar. Singh. (2013). “Solar power generation by PV (photovoltaic) technology: a review”. Energy, 53, 1-13.

[2]Abdeen, Mustafa. Omer. (2008). “Energy, environment and sustainable development”. Renewable and Sustainable Energy Reviews, 12(9), 2265–2300.

[3]Jung, Jee. Hoon; &Sheehab, Ahmed. (2012). “Real-time simulation model development of single crystalline photovoltaic panels using fast computation methods”. Solar Energy, 86(6), 1826-1837.

[4]Etienne, Saloux; Alberto, Teyssedou; & Mikhail, Sorin. (2011). “Explicit model of photovoltaic panels to determine voltagesand currents at the maximum power point”. Solar Energy, 85(5), 713–722.

[5]Lo Brano, Valerio; Orioli, Aldo; Giuseppina, Ciulla;& Di Gangi, Alessandra. (2010). “An improved five-parameter model for photovoltaic modules”. Solar Energy Materials and Solar Cells, 94(8), 1358–1370.

[6]Celik, Ali. Naci; & Acikgoz, Nasır. (2007) “Modelling and experimental verification of the operating current of mono-crystalline photovoltaic modules using four- and five-parameter models”. Applied Energy, 84(1), 1–15.

[7]Semaoui, Smail; Hadj Arab, Amar; Seddik Bacha;&Azoui, Boubekeur. (2013). “The new strategy of energy management for a photovoltaic system without extra intended for remote-housing”. Solar Energy, 94, 71–85.

[8]Sallem, Souhir; Chaabene, Maher; & Kamoun, Mohammed. Ben Ali. (2009). “Energy management algorithm for an optimum control of a photovoltaic water pumping system”. Applied Energy, 86(12), 2671–2680.

[9]Sallem, Souhir; Chaabene, Maher; & Kamoun, Mohammed. Ben Ali. (2009). “Optimum energy management of a photovoltaic water pumping system”. Energy Conversion and Management, 50(11), 2728–2731.

[10] Gergaud, Olivier. (2002). ‘‘Modélisation énergétique et optimisation économique d’un système éolien et photovoltaïque couplé au réseau et associé à un accumulateur”. Thesis of the Normal School of Cachan, France.

[11] Yahyaoui, Imene; Chaabene, Maher; & Tadeo, Fernando. (2014b). “Energy management for photovoltaic irrigation with a battery bank”. International Journal of Energy Optimization and Engineering, accepted August 4^{th} , 2014.

[12] Betka, Achour; & Attali, A. (2010). “Optimization of a photovoltaic pumping system based on the optimal control theory”. Solar Energy, 84(7), 1273-1283.

[13] Arrouf, Mohamed;& Ghabrour, S. (2007). “Modelling and simulation of a pumping system fed by photovoltaic generator within the Matlab/Simulink programming environment”. Desalination, 209(1), 23-30.

[14] Ghoneim, A. A. (2006). “Design optimization of photovoltaic powered water pumping systems”. Energy Conversion and Management, 47(11), 1449-1463.

[15] Belgacem, Ben Ghanem. (2012). “Performance of submersible PV water pumping systems in Tunisia”. Energy for Sustainable Development, 16(4), 415-420.

[16] Messikh, L; Chikhi, S; Chikhi, F; & Chergui, T. (2008). ‘‘Mise au point d’un régulateur de charge/décharge de batterie avec seuils adaptatifs de tension pour les applications photovoltaïques’’. Revue des Energies Renouvelables, 11(2), 281-290.

[17] Kalogirou, S. A. (2001). “Artificial neural networks in renewable energy systems applications: a review”. Renewable and sustainable energy reviews, 5(4), 373-401.

[18] Al-Alawi, Ali; M Al-Alawi, Saleh; & M Islam, Sayed. (2007). “Predictive control of an integrated PV-diesel water and power supply system using an artificial neural network”. Renewable Energy, 32(8), 1426-1439.

[19] Moradi-Jalal, Mahdi; Marino, Miguel. A; & Afshar, Abbas. (2003). "Optimal design and operation of irrigation pumping stations". Journal of Irrigation and Drainage Engineering, 129(3), 149-154.

[20] Liu, X; Fang, X; Qin, Z; Ye, C;& Xie, M. (2011). ''A short-term forecasting algorithm for network traffic based on chaos theory and SVM''. Journal of network and systems management, 19(4), 427-447.

[21] Hemanth, De Jude; Vijila, C. Kezi. Selva; & Anitha, J. (2010). "Application of neuro-fuzzy model for mr brain tumor image classification". Biomedical Soft Computing and Human Sciences, 16(1), 95-102.

[22] Lee, Jia. Chu; Lin, Whei. Min; Liao, Gwo. Ching;& Tsao, Ta. Peng. (2011). "Quantum genetic algorithm for dynamic economic dispatch with valve-point effects and including wind power system". International Journal of Electrical Power & Energy Systems, 33(2), 189-197.

[23] Moradi, Mohammad. Hasan; & Abedini, Mohammad. (2012). "A combination of genetic algorithm and particle swarm optimization for optimal DG location and sizing in distribution systems". International Journal of Electrical Power & Energy Systems, 34(1), 66-74.

[24] Ben Salah, Chokri; Chaabene, Maher; & Ben Ammar, Mohsen. (2008). "Multi-criteria fuzzy algorithm for energy management of a domestic photovoltaic panel". Renewable Energy, 33(5), 993–1001.

[25] Yahyaoui, Imene; Sallem, Souhir; Kamoun, Mohammed. Ben Ali; & Tadeo, Fernando. (2014). "A proposal for management of off-grid photovoltaic systems with non-controllable loads using fuzzy logic". Energy Conversion and Management, 78, 835-842.

[26] Berrazouane, Sofiane; & Mohammedi, Kamal. (2014). "Parameter optimization via cuckoo optimization algorithm of fuzzy controller for energy management of a hybrid power system". Energy Conversion and Management, 78, 652–660.

[27] Welch, Richard. L; & Venayagamoorthy, Ganesh. Kumar. (2010). "Energy dispatch fuzzy controller for a grid-independent photovoltaic system". Energy Conversion and Management, 51(5), 928–937.

[28] Hahn, Federico. (2011). "Fuzzy controller decreases tomato cracking in greenhouses". Computers and Electronics in Agriculture, 77(1), 21-27.

[29] Cheikh, M. A; Aïssa, B. H; Malek, A; & Becherif, Mohamed. (2010). "Mise au point d'une régulation floue pour serre agricole à énergie solaire''. Revue des Energies Renouvelables, 13(3), 421-443.

[30] Kahraman, Cengiz; Kaya, Ihsan; & Cebi, Selcuk. (2009). "A comparative analysis for multiattribute selection among renewable energy alternatives using fuzzy axiomatic design and fuzzy analytic hierarchy process". Energy, 34(10), 1603-1616.

[31] Bouchon-Meunier, B; Foulloy, L; & Ramdani, M. (1994). ''La logique floue''. (Vol. 2702). Presses universitaires de France.

[32] Saad, N; & Arrofiq, M. (2012). ''A PLC-based modified-fuzzy controller for PWM-driven induction motor drive with constant V/Hz ratio control''. Robotics and Computer-Integrated Manufacturing, 28(2), 95-112.

[33] Yahyaoui, Imene; Chaabene, Maher; & Tadeo, Fernando. (2014b). "A fuzzy based energy management for a photovoltaic pumping plant for tomatoes irrigation". In the proceedings of the IEEE International Renewable Energy Congress (IREC), 122-127.

[34] Campana, Pietro. Elia; Li, Hailong; & Yan, Jinyue. (2013). "Dynamic modelling of a PV pumping system with special consideration on water demand". Applied Energy, 112, 635–645.

[35] Beccali, M; Cellura, M;& Ardente, D. (1998). "Decision making in energy planning: the ELECTRE multicriteria analysis approach compared to a fuzzy-sets methodology". Energy Conversion and Management, 39(16), 1869-1881.

[36] Shankara, Naika; De Jeude, Joep Van Lidt; De Goffau, Marja; Hilmi, Martin; & Van Dam, Barbara. (2005). "Production, processing and marketing. Agromisa Foundation and CTA".

[37] Yahyaoui, Imene; Chaabene, Maher;& Tadeo, Fernando.(2013). "An algorithm for sizing photovoltaic pumping systems for tomatoes irrigation". In the proceedings of the IEEE International Conference on Renewable Energy Research and Applications (ICRERA), 1089-1095.

[38] Serna, Álvaro; &Tadeo, Fernando. (2014). "Offshore hydrogen production from wave energy". International Journal of Hydrogen Energy, 39(3), 1549–1557.

[39] Saleh, Mohammed. Ismail; Ozawa, Kiyoshi; & Khondaker, Nur. A. (2007). "Effect of irrigation frequency and timing on tomato yield, soil water dynamics and water use efficiency under drip irrigation". In the proceedings of the eleventh International Water technology Conference (IWTC), 15-18.

[40] Yahyaoui, Imene; Chaabene, Maher; & Tadeo, Fernando. (2015). "Fuzzy Energy Management for Photovoltaic Water Pumping System". International Journal of Computer Applications (IJCA), 110(9), 29-36.

Chapter 4: Conclusions and Future Work

Contents

4.1 Conclusions

This thesis has presented several contributions on the sizing and control of autonomous photovoltaic irrigation installations. More precisely, an algorithm for the optimum sizing of the components and a fuzzy control algorithm for optimal energy management have been proposed:

1) We have developed an algorithm for the optimal sizing of an autonomous photovoltaic irrigation installation composed of photovoltaic panels, a battery bank, an inverter, a water pump and a reservoir. The algorithm proposal allows the pumping of the water volume needed for irrigation. Moreover, by specifying some criteria related to the use of the battery bank, the sizing algorithm enhances the battery bank's life time.

   The algorithm has been validated focusing on a specific problem (tomato irrigation in a region in the north of Tunisia) and using climatic data from the target area during the vegetative cycle. The algorithm has been presented in the publications [D] and [E].

2) In addition, we have established a fuzzy control algorithm for the energy management of the photovoltaic installation. The algorithm ensures the system's autonomy and the pumping of the water volume needed to irrigate the tomatoes. Moreover, it guarantees that the charge in the battery bank is maintained between two fixed values, to protect it from excessive charges and discharges. The main idea of the algorithm is based on measuring the photovoltaic current, the water level in the reservoir, the well water flow and the battery bank depth of discharge (estimated from the battery bank current), to deduce the switching of the relays that link the components.

   The control algorithm's efficiency has been validated experimentally in a small-scale water pumping plant installed in the laboratory. The results are promising, also making it possible to manage some critical cases, such as the control of a water leak in the reservoir.

   A preliminary algorithm was first proposed in [F] and later published in detail in [A], for a generic non-controllable load. Then, the management algorithm for irrigation was presented in [G]. The definitive version is detailed in [B] and validation is presented in [C].

4.2 Publications Arising from the Thesis

The work developed in this thesis has been presented in several journal articles and conferences, which are cited now.

❖ *Articles in journals*:

[A] **Yahyaoui, Imene**; Sallem, Souhir; Kamoun, Mohammed. Ben Ali; & Tadeo, Fernando. (2014). "A proposal for management of off-grid photovoltaic systems with non-controllable loads using fuzzy logic". Energy Conversion and Management, 78, 835-842. *IF: 3.59*. doi: 10.1016/j.enconman.2013.07.091.

[B] **Yahyaoui, Imene**; Chaabene, Maher; & Tadeo, Fernando. (2015). "Energy management for photovoltaic irrigation with a battery bank". International Journal of Energy Optimization and Engineering, accepted (August, 4th, 2014). IF: 0.

[C] **Yahyaoui**, **Imene**; Chaabene, Maher; &Tadeo, Fernando. (2015). "Fuzzy energy management for photovoltaic water pumping system". International Journal of Computer Applications (IJCA), 110, 29-36. *IF: 0.715*. doi : 10.5120/19346-1049.

[D] **Yahyaoui**, **Imene;** Ammous, Mahmoud; & Tadeo, Fernando. (2015). "Algorithm for optimum sizing of a photovoltaic water pumping system".International Journal of Computer Applications (IJCA). *IF: 0.715*.

❖ *Papers in conferences:*

[E] **Yahyaoui**, **Imene**; Chaabene, Maher; & Tadeo, Fernando. (2013). "An algorithm for sizing photovoltaic pumping systems for tomato irrigation". In the proceedingsof the IEEE International Conference on Renewable Energy Research and Applications (ICRERA), 1089-1095.

[F] **Yahyaoui, Imene**; Sallem, Souhir; Kamoun, Mohammed. Ben Ali; & Tadeo, Fernando. (2012). "Fuzzy energy management of off-grid PV/battery system". In the proceedings of the International Renewable Energy Conference (IREC), 779-786.

[G] **Yahyaoui**, **Imene**; Chaabene, Maher; & Tadeo, Fernando. (2014). "A fuzzy based energy management for a photovoltaic pumping plant for tomato irrigation". In the proceedings of the IEEE International Renewable Energy .

Conference (IREC), 122-127

[H] **Yahyaoui**, **Imene**; Jeddi, Nafaa; Charfi Sana; Chaabene, Maher; & Tadeo, Fernando. (2015). "MPPT techniques for a photovoltaic pumping system". In the proceedings of the IEEE International Renewable Energy Conference (IREC), (accepted).

[I] **Yahyaoui, Imene;** Chaabene, Maher; & Tadeo, Fernando. (2014). "Genetic algorithm based energy management of an off-grid PV/Battery system". In the proceedings of the Simposio de Inginieria de Control (CEA), 96 -99.

[J] **Yahyaoui**, **Imene**; Sallem, Souhir; Chaabene, Maher; & Tadeo, Fernando. (2012). "Vector control of an induction motor for photovoltaic pumping". In proceedings of the International Renewable Energy Conference (IREC), 877-883.

❖ *Others publications:*

[K] **Yahyaoui, Imene**; Ouachani, Ilyes; Ammous, Mahmoud; Chaabene, Maher; &Tadeo, Fernando. (2015). "Energy management for a photovoltaic- wind system with non-controllable load". In the proceedings of the IEEE International Renewable Energy Conference (IREC), (accepted).

[L] Ammous, Mahmoud; **Yahyaoui, Imene**; Chaabene, Maher; & Harb, Ahmad. (2015). "On fuzzy logic control of PV/T based reverse osmosis desalination plant". In the proceedings of the IEEE International Renewable Energy Conference (IREC), (accepted).

[M] Charfi, Sana; **Yahyaoui, Imene**; Ammous, Mahmoud; & Chaabene, Maher. ''Characterization of an off- grid hybrid system: modelling and simulation''. In the proceedings of the IEEE International Renewable Energy Conference (IREC), (accepted).

4.3 Future Work

The work developed during this thesis may be continued in different ways:

1. The sizing algorithm developed may easily be applied to other agricultural applications.

2. The energy management algorithm, established for the PV installation, may be extended to wind energy. Hence, the algorithm opens the door for other applications that integrate sizing, control and optimal operation of the plant. In particular, the installation can be used during the whole year for a continuation of outdoor and greenhouse agriculture [K], as is often done in practice, or for reverse osmosis desalination plants [L].
3. An economic study for using the PV energy for our application should be established, to justify the use of renewable energies for these applications, especially PV energy in sunny areas. For this, a preliminary water pumping installation that contains a diesel engine has been developed [M].
4. The energy management could benefit from improved sensors during pumping, low level controllers of the induction machines and better estimations of the battery bank depth of discharge (by taking into account its internal temperature effect).

Appendix A: Extended Abstract in Spanish

A.1 Índice de Contenidos

A.2 Resumen

En las últimas décadas, la energía fotovoltaica se ha convertido en una fuente eficaz de energía para la producción de la electricidad, que se utilizará en sitios aislados o será inyecta en la red. En zonas aisladas, las instalaciones fotovoltaicas se han utilizado para el bombeo de agua para la agricultura o para fines humanos, debido su facilidad de instalar y su bajo coste de mantenimiento después de la instalación. Sin embargo, la variabilidad inherente exige elegir cuidadosamente el tamaño de la instalación y proporcionar un algoritmo de gestión de la energía.

Por lo tanto, esta tesis se centra en el cálculo del tamaño y la gestión energética de una instalación fotovoltaica autónoma destinada al bombeo de agua para irrigación en un lugar aislado. Normalmente, este tipo de instalaciones se utiliza ampliamente en las regiones áridas y semi-áridas como el Magreb y el Sur de Europa, donde existe una importante disponibilidad de radiación solar. Se requiere el funcionamiento correcto de estas plantas para satisfacer la demanda de agua, optimizar el uso de la energía fotovoltaica y para extender el tiempo de vida de los componentes. Estos objetivos se pueden asegurarse por un buen dimensionamiento de los componentes y una gestión óptima de la energía, que representan las dos partes principales de la tesis.

De hecho, la primera parte de esta tesis se trata del dimensionamiento de los componentes de la instalación de riego fotovoltaico, es decir, los paneles fotovoltaicos y el banco de baterías. Por lo tanto, un algoritmo para el dimensionamiento óptimo de los componentes de la instalación se ha establecido, con base en las necesidades de agua de los cultivos, las características climáticas del sitio y las restricciones de los componentes. Para esto, fue necesario seleccionar algunos modelos de los componentes de la instalación, que han sido validados experimentalmente. Además, se han estudiado algunas técnicas relacionadas con la extracción máxima de energía fotovoltaica. Entonces, el algoritmo de dimensionamiento ha sido validado con datos medidos de la zona objetivo (Medjez El Beb, al norte de Túnez).

La segunda parte de la tesis se trata de la gestión energética de la instalación de riego fotovoltaico. Por lo tanto, un algoritmo basado en la lógica borrosa se ha establecido, a fin de gestionar la energía generada por los paneles y se almacena en el banco de baterías. Por su facilitad de implementarla, la lógica borrosa fue utilizada por el algoritmo de gestión energética, además que depende solamente del conocimiento del usuario. El algoritmo es función de la potencia fotovoltaica generada, la profundidad de la batería de descarga, el nivel del agua en el depósito y el flujo de agua. La decisión de la conexión y desconexión de los componentes de la instalación se deducen usando las reglas borrosas. La eficiencia del algoritmo ha sido evaluada en primer lugar por simulación. Después, se fue valida en una planta instalada en el laboratorio.

Por lo tanto, esta tesis ha contribuido en el cálculo del dimensionamiento óptimo de los componentes y la gestión energética de la instalación de riego fotovoltaico, utilizando algoritmos genéricos.

A.3 Objetivos de la Tesis

La tesis trata la modelización, el dimensionamiento y la gestión energética de una instalación fotovoltaica autónoma destinada al bombeo de agua para regar una tierra plantada de tomates. El primer tema consiste en elaborar un algoritmo de dimensionamiento que da los tamaños óptimos de los componentes del sistema que son la superficie de los paneles fotovoltaicos y la capacidad del banco de baterías. Para ello, fue necesario desarrollar y validar los modelos de los componentes del sistema. Estos modelos se utilizan para validar el algoritmo de dimensionamiento, a partir de datos meteorológicos de la zona estudiada en los meses correspondientes al ciclo vegetativo de los cultivos.

El segundo objetivo de la tesis es establecer un algoritmo óptimo para la gestión energética de la instalación fotovoltaica, basado en la lógica borrosa. La idea consiste en la adecuación de la energía demandada por la bomba con la energía disponible en el panel y / o el banco de baterías, con el fin de cumplir con los requisitos energéticos de la carga y las necesidades de agua de los cultivos.

Esto está garantizado usando datos climáticos medidos y predichos como la radiación solar y la temperatura ambiente. El propósito algoritmo es también de decidir entre el ahorro de energía en la batería o el agua en el tanque, dependiendo del mes y el estado de crecimiento de los cultivos.

A.4 Contribuciones de la Tesis

La tesis presenta varias aportaciones sobre el cálculo del tamaño y el funcionamiento óptimo de la instalación de riego fotovoltaico, de la siguiente manera:

1. El desarrollo de un algoritmo de dimensionamiento óptimo de los componentes de la instalación fotovoltaica, que cumplan los requisitos de riego durante el ciclo vegetativo de los tomates, y el aumento del tiempo de duración de la batería. El algoritmo se valida usando mediciones de la zona estudiada (Capítulo 2).
2. La elaboración de un algoritmo basado en la lógica borrosa para el funcionamiento óptimo de la instalación de riego fotovoltaico e equilibrar el consumo de energía con la energía producida (Capítulo 3). La idea clave es manipular la energía generada por los paneles y las baterías para cumplir con la demanda de agua y la operación segura del banco de baterías. Eso es posible con el uso de las predicciones de las variables climáticas para la generación de energía fotovoltaica y las necesidades de riego. El algoritmo ha sido validado en una planta realista en el laboratorio.

A.5 Organización de la Tesis

La tesis está organizada de la siguiente manera:

Capítulo 1 Este capítulo presenta el contenido de la tesis. La Sección 1.1 describe la motivación de la tesis. La Sección 1.2 detalla la situación de la energía renovable en el mundo. Los objetivos, las principales contribuciones y la organización de la tesis se presentan también.

Capítulo 2 Este capítulo trata el dimensionamiento de la instalación fotovoltaica de bombeo de agua. En primer lugar, la Sección 2.2 está dedicada a las tecnologías de energías renovables utilizadas para instalaciones de bombeo. La

Sección 2.3 describe los componentes de la instalación. El problema del dimensionamiento, seguido por el modelado de los elementos del sistema y su validación están detallado en las Secciónes 2.4 y 2.5, respectivamente.

El dimensionamiento de los componentes de la instalación fotovoltaica está detallado en la Sección 2.6. La eficiencia del algoritmo está comprobada utilizando los datos climáticos medidos de la zona estudiada.

Capítulo 3 : Este capítulo se centra en la gestión de la energía de la instalación de riego fotovoltaico. La Sección 3.2 presenra un estado de arte de la gestión energética en Riego. La Sección 3.3 detalla la formulación del problema. La propuesta del algoritmo se explica en la sección 3.3. Los resultados del algoritmo se presentan en la Sección 3.5 y la validación experimental de los de los casos de estudios se ilustran en la Sección 3.6.

Capítulo 4 : En este capítulo se resumen las conclusiones, las publicaciones derivadas de la tesis y los trabajos futuros.

Apéndice A: En este apéndice es un resumen extendido en español de la tesis, que resume los objetivos, las contribuciones, la organización, las conclusiones y los trabajos futuros de la tesis.

Apéndice B: El riego de las Tomates está detalaldo en este apéndice.

Apéndice C: Este apéndice están resumidos las características de los panels y las beterias.

Apéndice D: Este apéndiceresume el modelado y el controlo de la maquinaasíncrona.

Apéndice E: Los métodos del MPPT yel diseño y el control del conversor está descrito en este apéndice.

Apéndice F: Los sensores de presión y flujo están descritos en el Apéndice F.

Apéndice G: La fuente de potencia programable está descrita en el Apéndice G.

Apéndice H: El inversorestádescrito en este apéndice.

Apéndice I: La tarjeta de adquisición está descrita en este apéndice.

Apéndice J: Este apéndice resume las listas de figuras, tablas, símbolos, acrónimos y paginas web.

A.6 Conclusiones

Esta tesis ha presentado varias contribuciones sobre el dimensionamiento y control de una instalación de riego fotovoltaico autónomo. Más precisamente, se ha propuesto un algoritmo para el dimensionamiento óptimo de la instalación componentes y un algoritmo de control difuso para la gestión óptima de la energía:

1. Hemos desarrollado un algoritmo para el dimensionamiento óptimo de una instalación fotovoltaica autónoma con destino a riego. Este algoritmo permite bombear el volumen de agua requerido y necesario para la irrigación de cultivos. Por otra parte, mediante la especificación de algunos criterios relacionados con la profundidad de descarga del banco de baterías, el algoritmo de dimensionamiento asegura un mejor tiempo de vida útil del banco de baterías. Centrándose en un problema específico (tomates riego en una región en el norte de Túnez), el algoritmo ha sido validado, utilizando datos climáticos de la zona estudiada, durante el ciclo vegetativo. El algoritmo ha sido presentado en [E].
2. Además, hemos establecido un algoritmo de control borroso para la gestión de la energía fotovoltaica. El algoritmo asegura la autonomía del sistema y el volumen de bombeo de agua necesaria para el riego de los tomates. Además, se garantiza una profundidad de descarga del banco de baterías mantenida entre dos valores fijos, para protegerlo del exceso de carga y descarga. La idea es sencilla: mediante la medición de la corriente fotovoltaica, el nivel del agua en el depósito, y el flujo de agua de pozo y la profundidad banco de baterías de descarga (estimada a partir de la corriente de banco de baterías), para deducir la conmutación de los relés que enlazan los componentes de la instalación fotovoltaica.

   La eficiencia del algoritmo ha sido validada experimentalmente en una planta de bombeo de agua a pequeña escala instalado en el laboratorio. Los resultados son prometedores en el sentido de que también somos capaces de gestionar algunos casos críticos, en los que tenemos una fuga de volumen de

agua en el depósito, sin dejar de cumplir la demanda de agua.Un algoritmo preliminar fue propuesto por primera vez en [D] y [A], para una carga no controlable genérica. Entonces, el algoritmo de gestión de aplicaciones de riego se presenta en [F]. La versión definitiva es detallada y validada, respectivamente, en [B] y [I].

A.7 Publicaciones Derivadas de la Tesis

El trabajo desarrollado en esta tesis se ha presentado en varios artículos y conferencias de revistas, que se citan ahora.

- *Articulos en Revistas*:

[A] **Yahyaoui, Imene**; Sallem, Souhir; Kamoun, Mohammed. Ben Ali; & Tadeo, Fernando.(2014). "A proposal for management of off-grid photovoltaic systems with non-controllable loads using fuzzy logic". Energy Conversion and Management, 78, 835-842. *IF: 3.59*. doi: 10.1016/j.enconman. 2013.07.091.

[B] **Yahyaoui, Imene**; Chaabene, Maher; & Tadeo, Fernando.(2015). "Energy management for photovoltaic irrigation with a battery bank".International Journal of Energy Optimization and Engineering, accepted (August, 4th, 2014). *IF: 0*.

[C] **Yahyaoui**, **Imene**; Chaabene, Maher; &Tadeo, Fernando. (2015). "Fuzzy energy management for photovoltaic water pumping system". International Journal of Computer Applications (IJCA), 110, 29-36. *IF: 0.715*. 10.5120/19346-1049.

[D] **Yahyaoui**, **Imene;** Ammous, Mahmoud; & Tadeo, Fernando. (2015). "Algorithm for optimum sizing of a photovoltaic water pumping system".International Journal of Computer Applications (IJCA). *IF: 0.715*.

- *Papeles en Congresos:*

[E] **Yahyaoui**, **Imene**; Chaabene, Maher; & Tadeo, Fernando. (2013). "An algorithm for sizing photovoltaic pumping systems for tomato irrigation". In the proceedings of the IEEE International Conference on Renewable Energy Research and Applications (ICRERA), 1089-1095.

[F] **Yahyaoui, Imene**; Sallem, Souhir; Kamoun, Mohammed. Ben Ali; & Tadeo, Fernando. (2012). "Fuzzy energy management of off-grid PV/battery

system". In the proceedings of the International Renewable Energy Conference (IREC), 779-786.

[G] **Yahyaoui**, **Imene**; Chaabene, Maher; & Tadeo, Fernando. (2014). "A fuzzy based energy management for a photovoltaic pumping plant for tomato irrigation". In the proceedings of the IEEE International Renewable Energy Conference (IREC), 122-127.

[H] **Yahyaoui**, **Imene**; Jeddi, Nafaa; Charfi Sana; Chaabene, Maher; & Tadeo, Fernando. (2015). "MPPT techniques for a photovoltaic pumping system". In the proceedings of the IEEE International Renewable Energy Conference (IREC), (accepted).

[I] **Yahyaoui, Imene;** Chaabene, Maher; & Tadeo, Fernando. (2014). "Genetic algorithm based energy management of an off-grid PV/Battery system". Inthe proceedings of the Simposio de Inginieria de Control (CEA), 96 -99.

[J] **Yahyaoui**, **Imene**; Sallem, Souhir; Chaabene, Maher; & Tadeo, Fernando. (2012). "Vector control of an induction motor for photovoltaic pumping".In proceedings of the International Renewable Energy Conference (IREC), 877-883.

❖ *Otras Publicaciones:*

[K] **Yahyaoui, Imene**; Ouachani, Ilyes; Ammous, Mahmoud; Chaabene, Maher; &Tadeo, Fernando. (2015). "Energy management for a photovoltaic- wind system with non-controllable load". In the proceedings of the IEEE International Renewable Energy Conference (IREC), (accepted).

[L] Ammous, Mahmoud; **Yahyaoui, Imene**; Chaabene, Maher; & Harb, Ahmad. (2015). "On fuzzy logic control of PV/T based reverse osmosis desalination plant". In the proceedings of the IEEE International Renewable Energy Conference (IREC), (accepted).

[M] Charfi, Sana; **Yahyaoui, Imene**; Ammous, Mahmoud; & Chaabene, Maher. ''Characterization of an off- grid hybrid system: modelling and simulation''. In the proceedings of the IEEE International Renewable Energy Conference (IREC), (accepted).

A.8 Trabajos Futuros

El trabajo desarrollado durante esta tesis se puede continuar en diferentes formas:

1. El algoritmo del dimensionamiento desarrollado se puede generalizar para otras aplicaciones.
2. El algoritmo de gestión de la energíadela instalación fotovoltaica puede extenderse a la energía eólica o instalaciones de osmosis inversa: se puede aplicarlo para otras aplicaciones, integrando el dimensionamiento y el control de la planta (los invernaderos) [K] y [L].
3. Un estudio económico para el uso de la energía fotovoltaica se debe establecer, para justificar el uso de las energías renovables para estas aplicaciones. Por eso, hemos empezado al modelado de una instalación de riego con motor diésel [M].
4. El algoritmo de gestión debe beneficiarse de la mejora en el control avanzado de las máquinas asíncronas y una mejor estimación de la profundidad banco de baterías de descarga (teniendo en cuenta su efecto temperatura interna).

Appendix B: Tomatoes Irrigation

B.1 Climatic Study

Tomato is not resistant to drought. Hence, its yield decreases considerably after short periods of water deficiency. The regularity in watering the plants is important, especially during flowering and fruit formation [B1]. The needed water amount depends on the type of the soil and on the weather (amount of rain, humidity and temperature) [B1]. In Tunisia, generally farmers use furrow or drip irrigation, which is a common method for irrigating tomatoes thanks to its economic advantages in saving water and increasing the yield production [B2]. Farmers adopt this technique for greenhouses and for outdoor cultivation for which, the frequency of tomatoes irrigation depends on the growing stage of the plant and the rainfall. In this sense, [B3] established a guideline for the irrigation frequency and duration, to adjust correctly the irrigation pattern to the actual weather and the water limiting conditions in Tunisia. This study allows:

- Adjusting the irrigation frequency to the actual weather conditions throughout the growing season.
- Selecting the irrigation duration as a function of the irrigation installation characteristics.

The irrigation calendars establishment requires a good knowledge of the meteorological parameters of the target region. Among them, the reference crop evapotranspiration (ETo) and the rainfall levels, which can be expected for a given 10-days period [B3]. The reference crop evapotranspiration is derived from a 10-day climatic data of the region [B4]. Since the irrigation objective chart is to adjust the irrigation calendar to the actual weather conditions, several irrigation calendars are developed, using various probability levels for rainfall and ETo. Hence, four weather conditions can be distinguished [B3]:

❖ Hot weather conditions without any rainfall (20% ETo and no rain),
❖ Dry (40% ETo and 80% rain),
❖ Normal (mean ETo and rain),
❖ Humid (60% ETo and 20% rain).

B.2 Soil Data

Medjez El Beb 'soil type is a clay-loam, which is characterized by a water volume content at field capacity and wilting point (which is the water level below the plant is shriveled) equal to, respectively, 42 and 26%. The corresponding total available soil water (TAW) is 160 mm (water)/ m (soil depth). The infiltration rate is 100 mm/day.

B.3 Crop Data

Tomatoes harvested in Tunisia during the summer period are sown in nursery plants during *February*. In *March*, the seedlings are transplanted in the fields. Eight to ten weeks after sowing, flowering occurs in the middle of *May*. At the end of this month and at the beginning of June, fruits ripening occur. In *July*, the fruits are ready to be harvested.

B.4 Irrigation Intervals

The net irrigation requirement is obtained by subtracting from the crop water requirement (ETo) the expected rainfall volume. Hence, the irrigation interval can be derived from the calculated irrigation requirement by means of soil characteristics. Generally, the irrigation will be frequent during peak periods when the crop water demand is high and rainfall small. Thus, the irrigationis less frequent at when ETo is small or rainfall is frequent.

The chart presents guidelines to:

- Adjust the irrigation interval to the varying climatic conditions during the growing season,
- Select the irrigation duration as a function of type, layout and efficiency of the drip system.

The guidelines are based on information concerning the actual weather conditions, local and technical aspects of the irrigation system and the crop response to water. The combination of all this information results in an irrigation calendar that is specific for a given farm and adjustable to the actual weather conditions.

Some guidelines were proposed to adjust the irrigation frequency to the actual weather conditions throughout the growing season (Tables B.1 and B.2). Since little or no rainfall is expected during the summer period, the farmer is advised to irrigate daily in June. During the ripening stage (*July*), the crop is less sensitive to water stress and the irrigation interval may be increased to two days. At the middle of *April*, during the crop development stage, the irrigation interval depends on the actual weather conditions: when it is hot and it does not rain or it is rather dry, it is recommended to irrigate every two days. Under normal rainfall conditions, the irrigation interval might be increased to three days. In practice, as *April* is wet and the rains are well distributed, no irrigation is required during most of the month since rainfall provides the crop water requirements.

Table B. 1 Irrigation chart for drip irrigated tomatoes in the region of Tunis

Irrigation interval in days

Month		March			April			May			June			July		
Decade		1*	2	3	1	2	3	1	2	3	1	2	3	1	2	3
meteo conditions	Hot+Dry	3 days		2 days			1 day								2 days	
	Dry	4 days		3 days		2 days		1 day							2 days	
	Normal				3 days		2 days			1 day					2 days	
	Wet						3	2 days			1 day				2 days	
Growth period		Establishment			Vegetative			Flowering			Yield formation			Ripening		
Sensibility to water stress		Sensible (a)			Moderate (b)			Very sensible (a,c)			Sensible (a)			Moderate		

* Initial soil wetness: Optimal soil water conditions (rainfall or pre-irrigation)

a - the crop is most sensitive to water deficit during and immediately after transplanting and during flowering and yield formation.

b - moderate water deficit during the vegetative period enhances root growth.

c - water deficit during the flowering period causes flower drop.

Table B. 2 Irrigation duration

Discharge per unit surface (litre/hour.m2)	Irrigation efficiency	
	Good (90%)	Medium (70%)
2	3 h 30 min	4 h 15 min
3	2 h 15 min	3 h 00 min
4	1 h 45 min	2 h 15 min
5	1 h 30 min	1 h 45 min
6	1 h 15 min	1 h 30 min
7	1 h 00 min	1 h 15 min
8	1 h 00 min	1 h 00 min
9	0 h 45 min	1 h 00 min
10	0 h 45 min	1 h 00 min

Given the type of the installation, the distance between emitters on the lateral, the lateral spacing and the emitter discharge, the discharge per unit area can easily be calculated (Figure B.1). Consequently, using this method, the total crops consumption of water for every 10 days can be calculated.

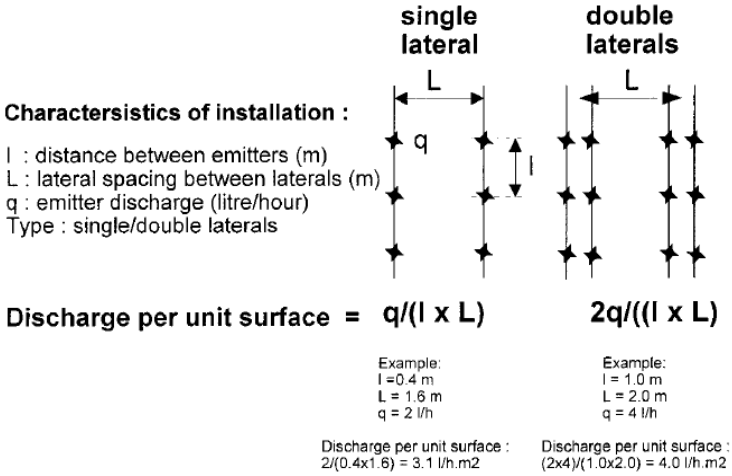

Figure B. 1 Calculation of the discharge per unit surface (l/ $h^{-1}.m^{-2}$)

B.5 References

[B1] Shankara Naika; Joep van Lidt de Jeude; Marja de Goffau; Martin Hilmi; & Barbara van Dam. (2005). “Cultivation of tomato”. Agromisa Foundation, Wageningen.

[B2] Saleh.M, Ismail; Kiyoshi, Ozawa;& Nur. A, Khondaker. (2007). “Effect of irrigation frequency and timing on tomato yield, soil water dynamics and water use efficiency under drip irrigation”. In the Proceedings of the Eleventh International Water Technology Conference, 15-18.

[B3] Raes.D; Sahli, A; Van. Looij, J; Ben Mechlia, & N; Persoons, E. (2000). “Chart for guiding irrigation in real time”. Irrigation and drainage Systems, 14, 343-352.

[B4] Allen, R. G; Pruitt, W. O; Wright, J. L; Howell, T. A; Ventura, F; Snyder, R; ... & Elliott, R. (2006). “A recommendation on standardized surface resistance for hourly calculation of reference ET by the FAO56 Penman-Monteith method”. Agricultural Water Management, 81(1), 1-22.

Appendix C: Panels and Batteries Characteristics

C.1 Panels Characteristics

C.1.1 TE500CR Panel

PLAN MY POWER

TE500CR+ – Solar panel

Photovoltaic module

55- 60 Watts Peak 12 Volts, Multicristaline , Glass/ Tedlar

156 x 78 mm cellssize

The TE 500 CR+ series modules use multicristaline technology. Our high efficiency solar cells are individually characterized and electronically matched in prior to interconnection. Encapsulation beneath high transmission tempered glass is accomplished using an advanced, UV resistant thermal setting plastic. The encapsulant, ethylene vinyl acetate, cushions the solar cells within the laminate and ensures the operating characteristics of the solar cells under virtually any climatic conditions. The rear surface of the module is completely sealed from moisture and mechanical damage by a continuous high strength polymer sheet. The glass/Tedlar construction of the module minimizes weight while providing a durable, protective environment for the solar cells. In addition, the aluminium frame for this module is designed for easy and rapid installation.

Applications

- Telecommunication
- Cathodic protection
- Water pumping
- Signalling
- Rural electrification
- Private residences

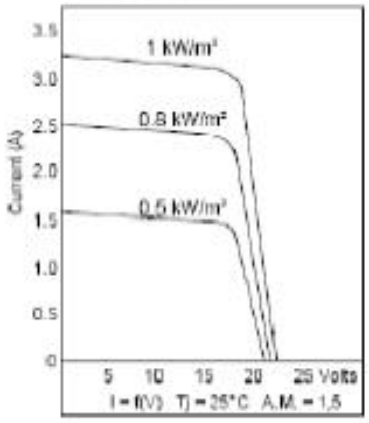

TE500CR+ Data sheet

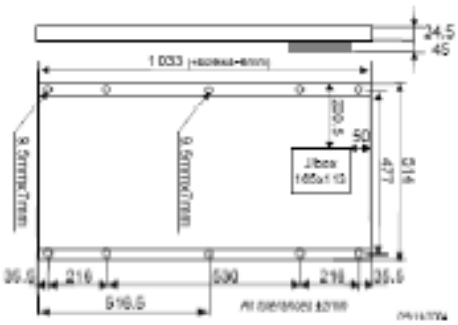

		TE 500 CR+			
Module Code TE: 9560		**650A3**	**650A2**	**650A1**	**650A0**
Encapsulation		Glass / Tedlar			
Size of cells	mm	156 x 78			
Number of cells	pcs	36 / 3 x 12			
Typical power 1)	Wp	50	55	60	65
Nominal voltage battery	V	12			
Voltage at typical power	V	17,00	17,50	17,80	18,00
Current at typical power	A	2,90	3,10	3,30	3,60
Open circuit voltage	V	21,40	21,70	22,00	22,30
Short circuit current	A	3,10	3,50	3,70	3,90
Connection		Junction box			
Maximum Syst. Oper. Voltage	V	600			
Diodes		2 by-pass (in option)			
Weight (net)	kg	7,00			
Using + Storage Temp.	°C	- 40 / + 85			
Relative humidity		0 up to 100%			
Warranty	Year	25*			

(*) 10 Years for maritime and tropical applications
(above specifications @ STC: Insol. 1.000W/m², AM 1.5 , Cell T 25°C)
1) Wp (Watt peak) = Peak power
(Tolerance = ± 10%)
Standards : Module certified to IEC 61215

C.1.2 Sunel Panel

a. Panel Datasheet

Parametri Meccanici		
dimensioni (incluso telaio)	1661 x 997 x 41	mm
peso	23 +/- 1	kg
carico statico lato posteriore (prova 1 ora)	2400	N/m^2
carico statico lato anteriore (prova 1 ora)	2400	N/m^2
Componenti		
vetro	vetro solare temperato spessore 4 mm	
celle	60 celle silicio monocristallino da 6" (156 mm)	
telaio	modello standard 3-S in alluminio	
Certificati, Classe di sicurezza e garanzie		
omologazione IEC 61215 ed. 2	Certificato TUV ID: 60026511	
omologazione IEC 61730 (Classe II)	Certificato TUV ID: 60026512	
grado di protezione IP	65	
garanzia di prodotto (contro difetti di materiali e/o produzione)	Tipo Standard: 3 anni Tipo Plus: 5 anni	
garanzia di prestazione (potenza erogata, Tipo Standard e Plus)	90% della pruzione nominale fino a 10 anni 80% della produzione nominale fino a 25 anni	

Dati elettrici in Condizioni di Prova Standard (STC)[1]				
		Tipo Standard	Tipo Plus	
potenza nominale @ STC[1]	P_{MAX}	245	245	W
tensione @ punto di massima potenza	V_{MPP}	30,4	30,4	V
corrente @ punto di massima potenza	I_{MPP}	8,1	8,1	A
tensione a circuito aperto	V_{OC}	36,7	36,7	V
corrente di corto circuito	I_{SC}	8,6	8,6	A
tolleranza sulla potenza erogata		+3 / -3	+3 / -0	%
coefficiente di temperatura di V_{oc}	β_2	-0,36	-0,36	1/K
coefficiente di temperatura di I_{sc}	α_2	0,039	0,039	1/K
1) Radiazione = 1000 W/m^2, temperatura modulo = 25 °C, distribuzione spettrale con indice di massa d'aria (air-mass "AM") = 1,5				
Parametri elettrici generali				
massima tensione di sistema	V_{OC} @ STC	1000		V
massima corrente inversa	I_R	17		A

b. Installation Description

The PV modules are installed on the roof of the IDRILab building where there is the power system laboratory. Figure C.1 shows two examples of monitored

PV systems; specifically the modules can be monitored separately (Fig. 2, on the left) or connected in series to form a string.

Figure C. 1 PV module installed on the roof of IDRILab building: single PV modules (left), PV string (right).

For sake of flexibility and in the perspective of new researches in the PV field (e.g. PV/-photovoltaic thermal systems, BIPV– Building Integrated Photovoltaics), the layout of the electrical installations has been organized in three nodes (Figure C.2)

1) Switchboard on the roof (Figure C.3): it contains the switches and terminal which owns both the power that the sensor part of the photovoltaic modules. This framework is positioned in proximity of the modules to facilitate the connections and is also equipped with a compartment for accommodating future electronic devices for special needs.
2) Switchboard in the lab (Figure C. 4): it is placed in the laboratory in the vicinity of the measuring equipment to facilitate connections with the same equipment as well as their power. The electrical panel is also equipped with power supplies for powering the sensors of temperature and radiation.
3) Rack in the lab (Figure C.5): it contains the acquisition cards and the electronic loads.

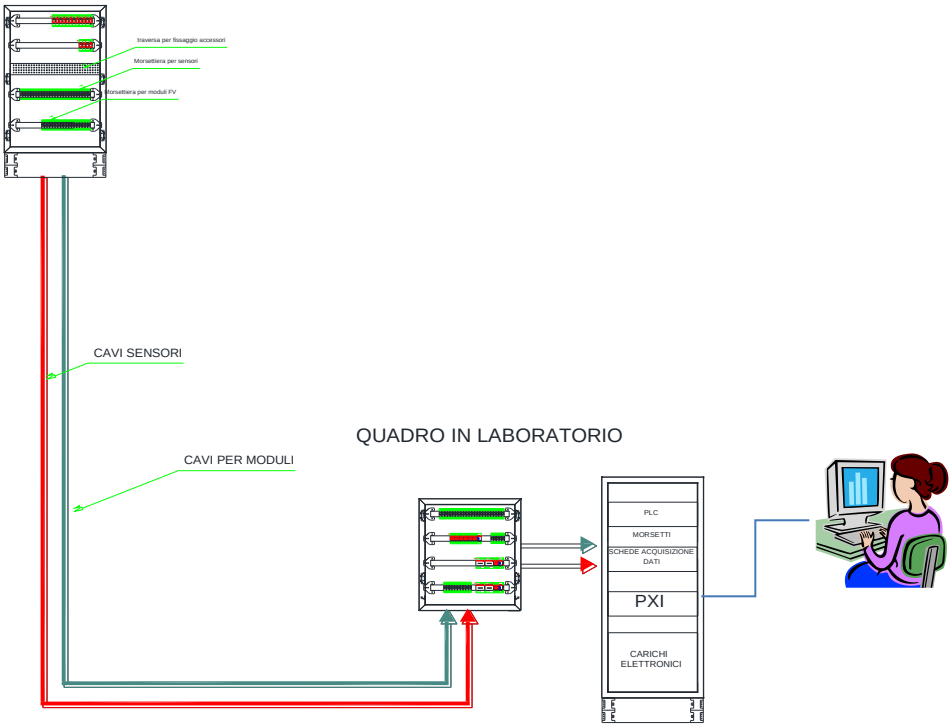

Figure C. 2 Layout of the electric distribution

Figure C. 3 Switchboard installed on the roof of the power system lab

Figure C. 4 Electric switchboard in the power system lab

Figure C. 5 Rack that lodges appliances, terminals and wiring

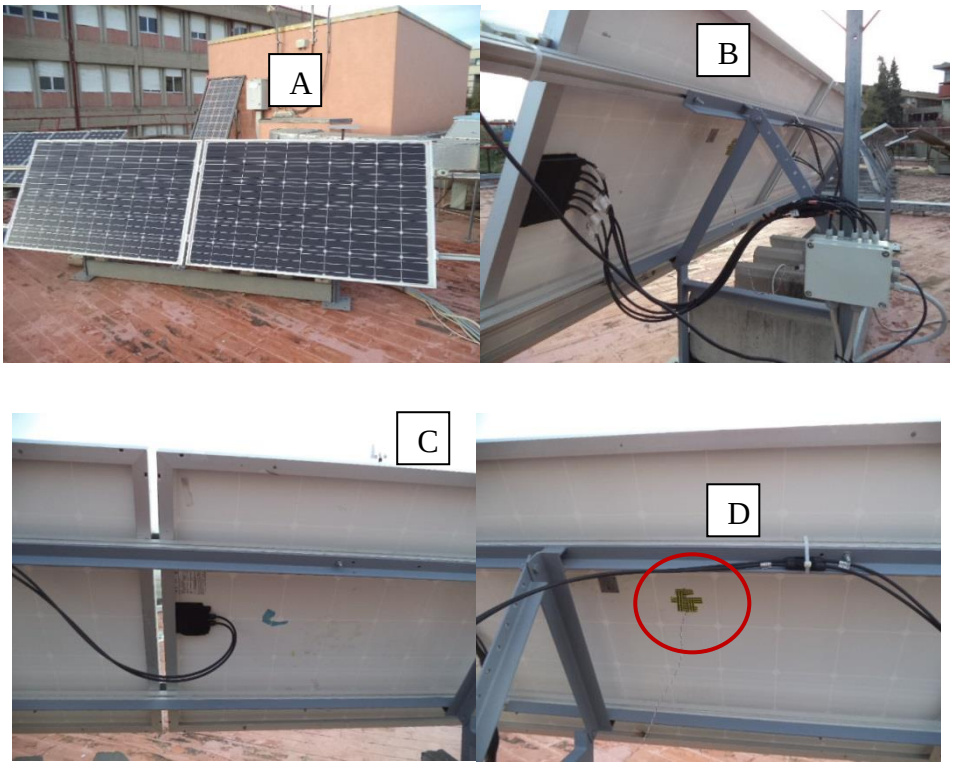

Figure C. 6 Multi-terminal PV module experimental set-up: A) front view of the two PV modules; B) string box of multi terminal PV module; C) string box of the conventional PV module; D) temperature sensor

c. Panel Yield at STC

The panel yield η_r at STC is calculated as follows:

$$\eta_r = \frac{P_{pv\,STC}}{G_{STC} * S_{module}} \qquad \textbf{(C. 1)}$$

Using (B.1), the panel yield for the TE500 CR is 10.58% and for the Sunel panel is 14.79%.

C.2 Batteries Characteristics

SPECIFICATIONS TECHNIQUES
BATTERIE SPECIALE POUR
APPLICATION PHOTOVOLTAIQUE

Marque		ASSAD
Type		SLT210
Tension Nominale		12 V
Courant Nominal		10 A
Capacité à 25°c	en 10h en 20h en 100h	160 AH 180 AH 210 AH
Plaque positive	Type Epaisseur Nombre de Tubes par plaque Nombre de plaques par Elément	Tubulaire 9,5 mm 15 06
Plaque négative	Type Epaisseur Nombre de plaques par élément	Plane 3,10 et 4,10 mm 02 et 05 respectivement
Endurance en cycle	à 80% de décharge à 50% de décharge à 20% de décharge	1200 2100 5000
Courbe de cyclage en fonction de la profondeur de décharge		Voir courbe ci-joint
Nature de la Batterie		Monobloc
Densité de l'électrolyte		1,26 g/cm^3
Température idéale de fonctionnement		25°C
Température de service		-18°C à +50°C
Décharge profonde recommandée		80%
Tension de décharge profonde		10,5 Volts
Tension max. de charge		14,0 Volts
Intervalle d'entretien		1 an dans les conditions optimales
Auto décharge (à 25° C)		0,03% par jour
Bac		Transparent
Electrolyte		Acide sulfurique dilué
Type de séparateur		Caoutchouc avec laine de verre
Pureté du plomb (Matière Active)		99,99%
Taux d'antimoine		1,7% Sb pour les plaques positives 1,7% Sb pour les plaques négatives
Quantité d'électrolyte (Dans l'alliage des grilles)		13,5 litres
Poignée		Corde robuste et résistante à l'acide
Dimensions extérieures en mm (L x l x H)		518 x 279 x 235
Poids de batterie humide avec Electrolyte		57 kg
Bornes		Vis et écrou
Garantie		4 ans (2 ans de garantie Totales + 2 ans dégressifs

FICHE D'ESSAI
BATTERIE SOLAIRE
TYPE SLT210

* Régime : 20 heures (C20)
* Plaque positives tubulaire : Type TH25
* Plaque négatives planes : Type R38 CL
* Densité de l'électrolyte 1,260 g/cm^3

Référence Batterie	Capacité en 10 heures	Capacité en 20 heures	Capacité en 100 heures
SLT210	160 AH	180 AH	210 AH

TESTS DE PERFORMANCE DE LA BATTERIE SLT210

- Type : SLT210 – 180AH / 20H
- Nombre de plaques positives par cellule : 6
- Nombre de plaques négatives par cellule : 7
- Densité de l'électrolyte : 1,260g / cm^3 à 25°C
- Tension d'arrêt : 10,5 Volts

	Capacité AH	Courant de décharge
C 5	140	36 A
C 10	160	18 A
C 20	180	09 A
C 100	210	1,8 A

C.3 Installations Performance

These values are obtained from PVsyst.

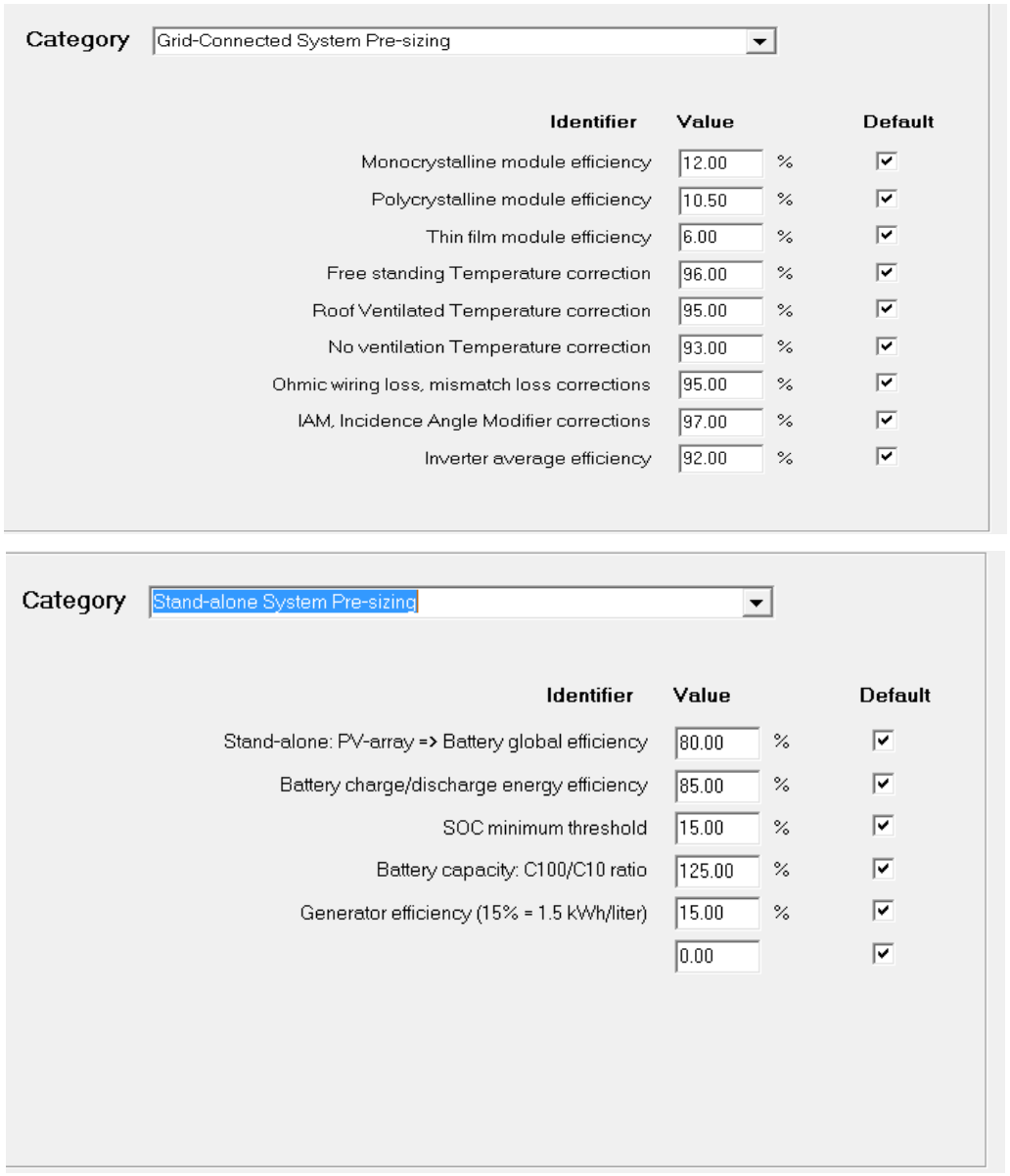

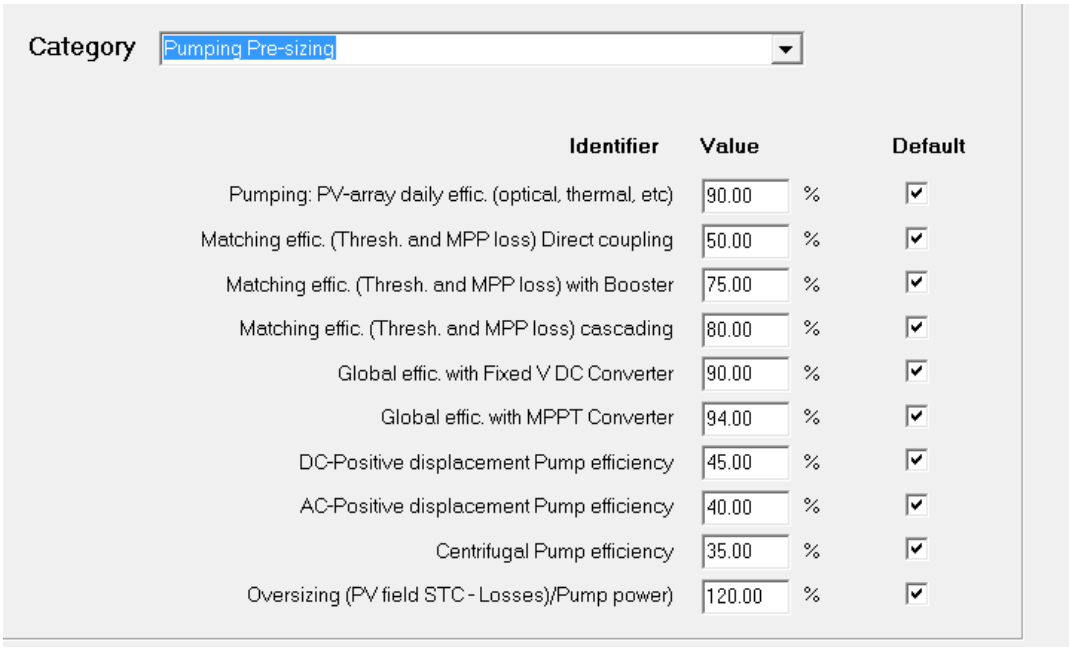
Category
Pumping Pre-sizing
Identifier
Value
Default
Pumping: PV-array daily effic. (optical, thermal, etc) 90.00 %
Matching effic. (Thresh. and MPP loss) Direct coupling 50.00 %
Matching effic. (Thresh. and MPP loss) with Booster 75.00 %
Matching effic. (Thresh. and MPP loss) cascading 80.00 %
Global effic. with Fixed V DC Converter 90.00 %
Global effic. with MPPT Converter 94.00 %
DC-Positive displacement Pump efficiency 45.00 %
AC-Positive displacement Pump efficiency 40.00 %
Centrifugal Pump efficiency 35.00 %
Oversizing (PV field STC - Losses)/Pump power) 120.00 %

Appendix D: The Induction Machine: Modelling and Control

D.1 Space Vector Notion

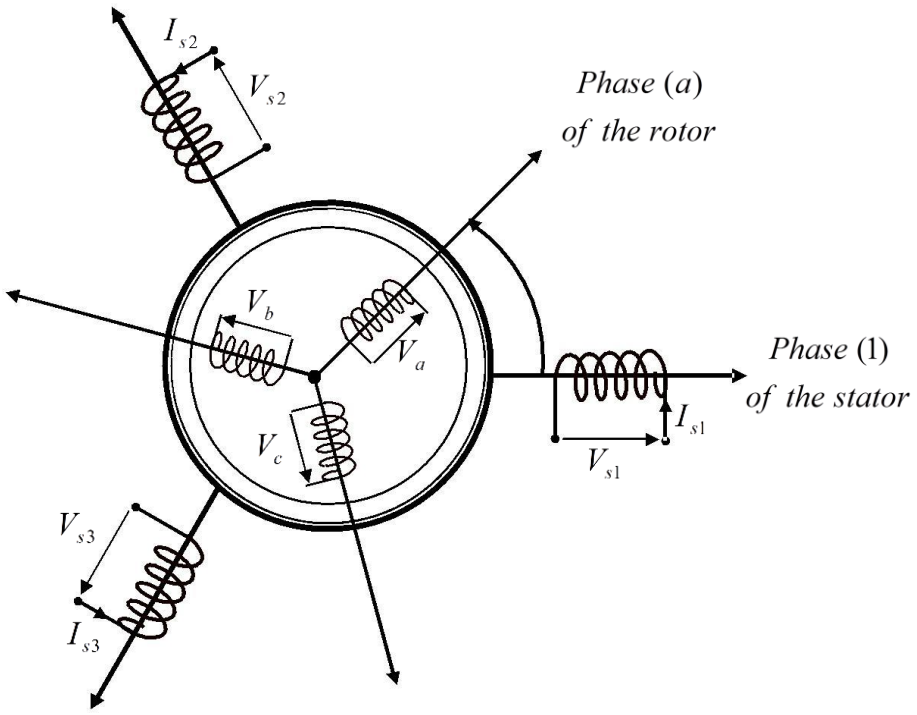

Figure D. 1 Schematic representation of the IM

The space vactor $\bar{x}$ is defined by:

$$\bar{x} = \frac{2}{3}\left(x_1 + ax_2 + a^2 x_3\right)$$

where:

$$a = e^{j\frac{2\pi}{3}}$$

and:

$$\begin{cases} x_1 = X_1 \cos\left(wt + \varphi_1\right) \\ x_2 = X_2 \cos\left(wt + \varphi_2\right) \\ x_3 = X_3 \cos\left(wt + \varphi_3\right) \end{cases} \quad \textbf{(D.1)}$$

D.2 Refrence Change

In the refrence $\left(\vec{Ox}, \vec{Oy}\right)$, the variable $\overline{\mathrm{X}}$ can be expressed by $\overline{X}_n$, where:

$\overline{X}_n = Xe^{-j\beta}$ and $\frac{d\beta}{dt} = w_s$.

This change allows the stator and rotor variable to be constant in the permanent state using a refe stator reference in the stator field (Figure D.2).

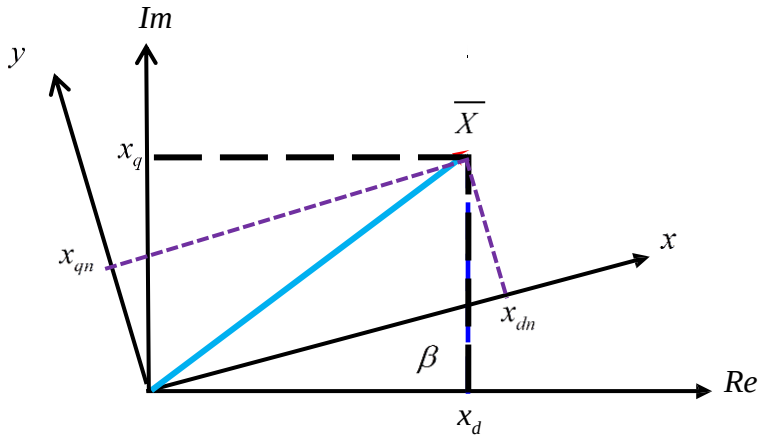

Figure D. 2 Representation of the used reference frame

D.3 Equations of the IM using the Space Vectors

Using the vector transformation for the voltage currents and fluxes vectors in the stator and the rotor, we obtain [D1]:

$$\begin{cases} \overline{V_s} = \frac{2}{3}\left(V_{s1} + aV_{s2} + a^2V_{s3}\right) \\ \overline{I_s} = \frac{2}{3}\left(I_{s1} + aI_{s2} + a^2I_{s3}\right) \\ \overline{\psi_s} = \frac{2}{3}\left(\psi_{s1} + a\psi_{s2} + a^2\psi_{s3}\right) \\ \overline{V_r} = \frac{2}{3}\left(V_a + aV_b + a^2V_c\right) \\ \overline{I_r} = \frac{2}{3}\left(I_a + aI_b + a^2I_c\right) \\ \overline{\psi_r} = \frac{2}{3}\left(\psi_a + a\psi_b + a^2\psi_c\right) \end{cases} \quad \textbf{(D.2)}$$

The electric and magnetic equations that describe the IM operation can be expressed by [D1]:

$$\begin{cases} \overline{V_s} = R_{ss}I_s + \frac{d}{dt}\psi_s \\ \overline{V_r} = R_rI_r + \frac{d}{dt}\psi_r \end{cases} \quad \textbf{(D.3)}$$

and:

$$\begin{cases} \overline{\psi_s} = L_s\overline{I_s} + me^{j\theta}\overline{I_r} \\ \overline{\psi_r} = L_r\overline{I_r} + me^{j\theta}\overline{I_s} \end{cases} \quad \textbf{(D.4)}$$

The electromagnetic torque C_{em} is expressed by [D1]:

$$C_{em} = \frac{3}{2} m\, Im\left(\overline{I_s} \left(\overline{I_r} e^{j\theta} \right)^* \right) \quad \textbf{(D.5)}$$

The mechanic equation is expressed by [D1]:

$$\frac{d}{dt} w_m = \frac{d^2}{dt^2} \theta = \frac{1}{J} p\left(C_{em} - C_r \right) \quad \textbf{(D.6)}$$

D.4 State Equations

Using equations (D.4, D.5 and D.6) and using the refrence field related to the stator, the rotor variables are [D2]: $I_r^{'} = I_r e^{j\theta}, \overline{\psi_r}^{'} = \overline{\psi_r} e^{j\theta}$ *and* $V_r^{'} = V_r e^{j\theta}$

The electric equations for the stator and rotor circuits can be expressed by (D.7) [D2]:

$$\begin{cases} \overline{V_s} = R_{ss} \overline{I_s} + \dfrac{d}{dt} \overline{\psi_s} \\ \overline{V_r}^{'} = R_r \overline{I_r}^{'} + \dfrac{d}{dt} \overline{\psi_r}^{'} - j w_r \overline{\psi_r}^{'} \end{cases} \quad \textbf{(D.7)}$$

The magnetic equations following the stator reference is expressed by [D2]:

$$\begin{cases} \overline{\psi_s} = l_s \overline{I_s} + M \overline{I_r}^{'} \\ \overline{\psi_r}^{'} = l_r \overline{I_r}^{'} + M \overline{I_s} \end{cases} \quad \textbf{(D.8)}$$

The mechanic equation becomes [D2]:

$$J \frac{d^2\theta}{dt} = J \frac{dw_m}{dt} = C_{em} - C_r = \frac{3}{2} m\, Im\left(\overline{I_s} \left(\overline{I_r}^{'} \right)^* \right) - C_m \quad \textbf{(D.9)}$$

To obtain the state equations of the IM, the fluxes have been choosen as state variables. Then, the changing the complex differential system obtained to differential system with real coefficients, an expression that relates the fluxes to currents can be obtained and it is given by (D.10) [D2]:

$$\overline{\psi} = \overline{LI} \quad \textbf{(D.10)}$$

where:

$$\overline{\psi} = \begin{bmatrix} \psi_{sd} + j\psi_{sq} \\ \psi_{rd}' + j\psi_{rq}' \end{bmatrix}, \overline{I} = \begin{bmatrix} I_{sd} + jI_{sd} \\ I_{rd}' + jI_{rq}' \end{bmatrix}, \overline{V} = \begin{bmatrix} V_{sd} + jV_{sq} \\ V_{rd}' + jV_{rq}' \end{bmatrix}, L = \begin{bmatrix} l_s & m \\ m & l_r \end{bmatrix}$$

D.5 IM Direct Starting

In this paragraph, the stator currents, the speed and the electromagnetic torque that correspond to a direct start-up for the IM are presented (Figure D.3).

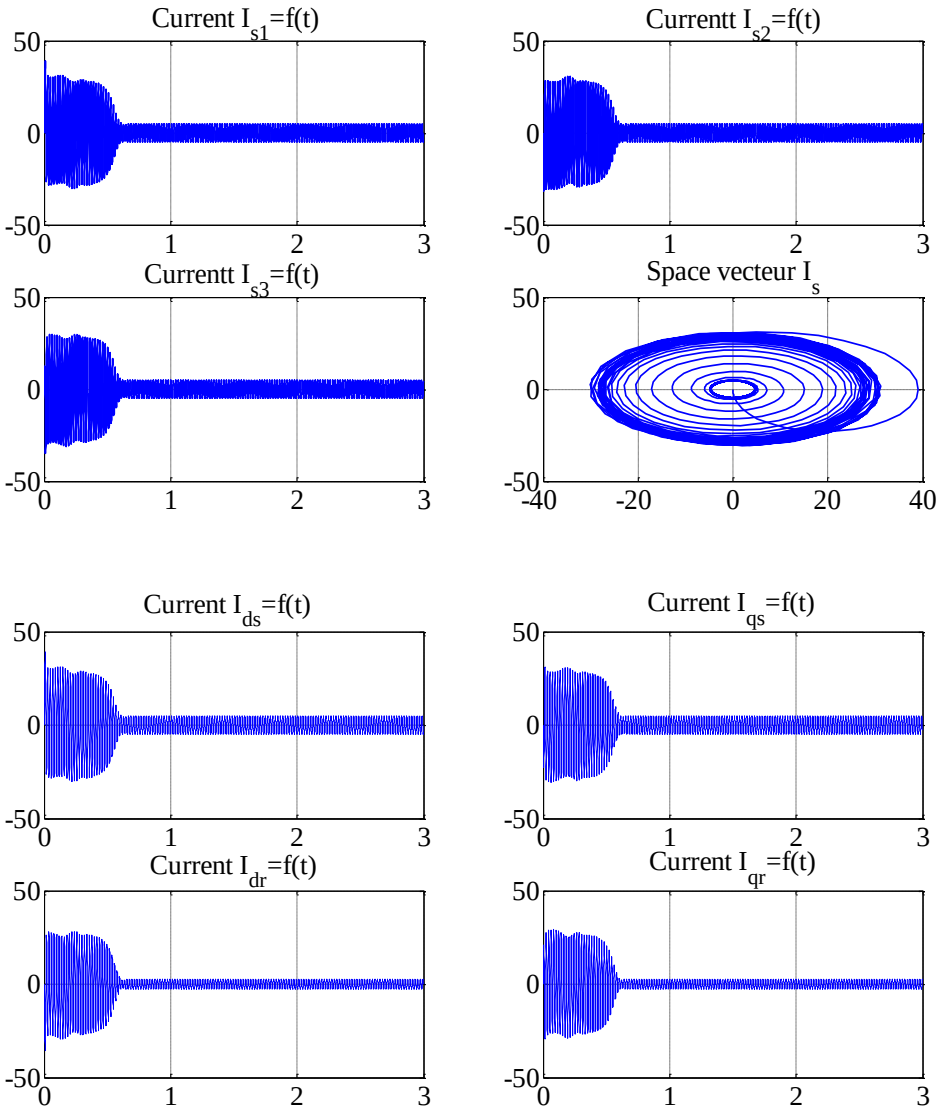

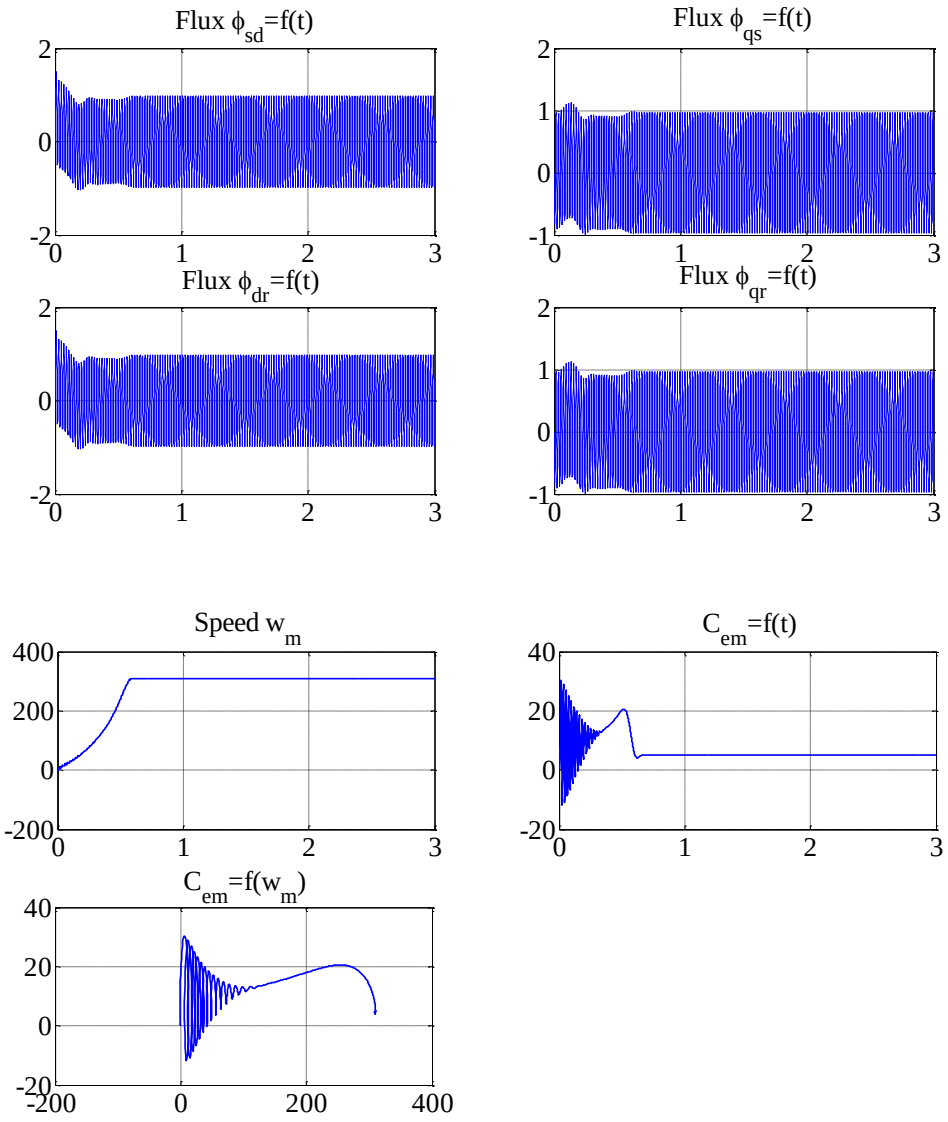

Figure D. 3 IM Direct Start-up results

A direct start-up for the IM shows that the stator current is high and may reach four times the nominal value. Hence, the use of a control method is needed.

D.6 IM Control using the RFOC Method

The IM model is tested using the vector control with the RFOC method. For this, we suppose that the pump is connected to the photovoltaic panel. The IM parameters are given by Table D.1. The simulation results are given in Figure D.3 [D3].

Table D. 1 IM parameters [D1]

Parameters	**Values**
R_{ss}	5.72 Ω
R_{rr}	4.2 Ω
L_s	0.462 H
L_r	0.462 H
M	0.44 H
p	2
J	0.0049 kg.m²

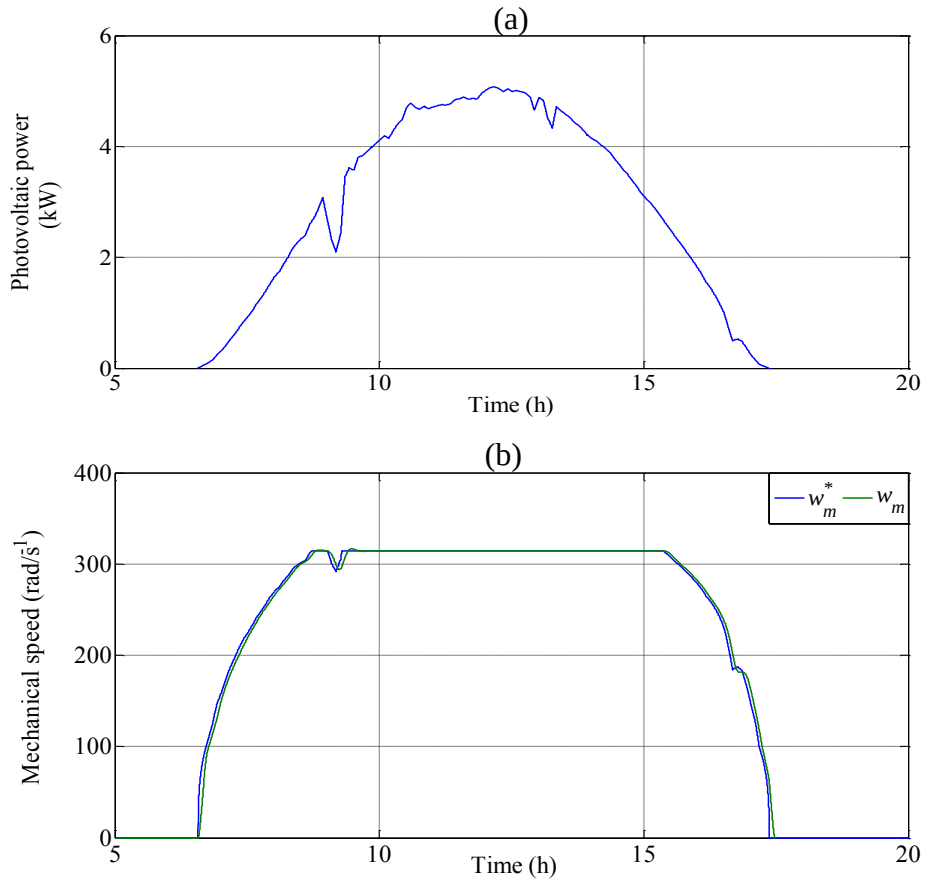

(c)

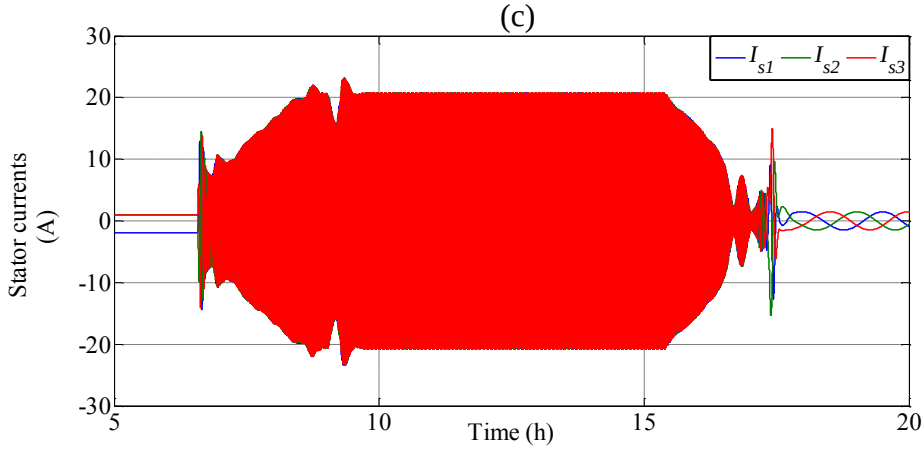
I_{s1} I_{s2} I_{s3}
Stator currents (A)
30
20
10
0
-10
-20
-30
5
10
15
20
Time (h)

(d)

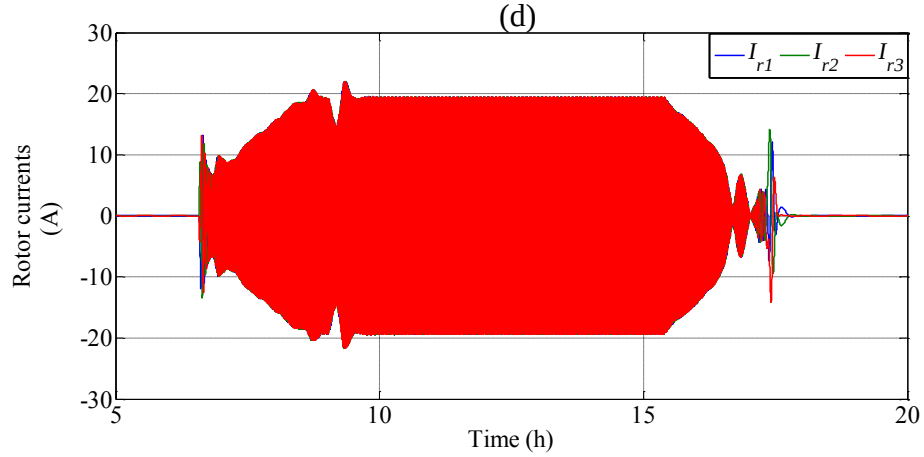
I_{r1} I_{r2} I_{r3}
Rotor currents (A)
30
20
10
0
-10
-20
-30
5
10
15
20
Time (h)

(e)

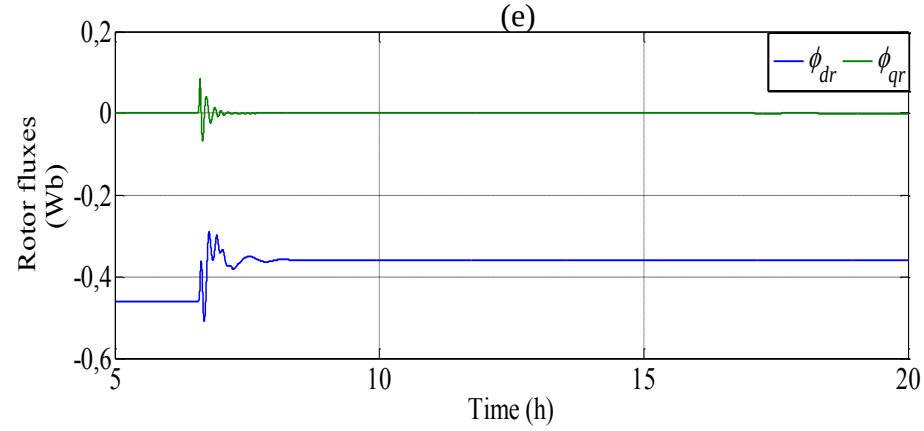
ϕ_{dr} ϕ_{qr}
Rotor fluxes (Wb)
0,2
0
-0,2
-0,4
-0,6
5
10
15
20
Time (h)

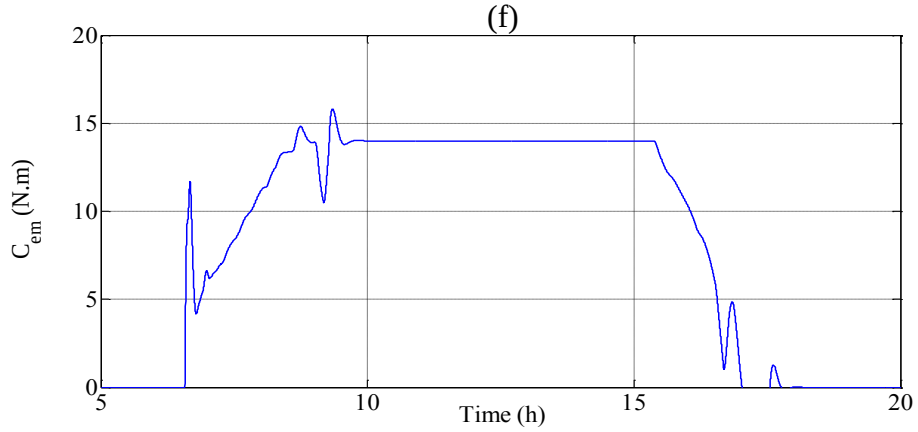

Figure D. 4 RFOC results for an IM, (a): P_{pv}; (b): w_m; (c): I_s; (d): I_r; (e): φ_r; (f): C_{em}

D.7 References

[D1] Sallem, Souhir. (2009). "Contribution à l'integration d'une machine doublement alimentée dans des systems autonomies". Thesis presented at the National School of Engineering of Sfax, Tunisia.

[D2] Kamoun, Mohammed Ben Ali. (2011). "Modeling of electric machnies". Cours at the National School of Engineering of Sfax, Tunisia.

[D3] Yahyaoui, Imene; Sallem, Souhir; Chaabene, Maher; & Tadeo, Fernando. (2012). "Vector control of an induction motor for photovoltaic pumping". In the proceedings of the International Renewable Energy Conference (IREC), 877- 883.

Appendix E: MPPT Techniques and Chopper Modeling and Control

E.1 MPPT Results

In literature, several algorithms for MPPT have been developed and validated [E1, E2], for example, the Look-up Table MPPT [E3], the Neuro-Fuzzy [E4], the Incremental Conductance [E4] and the Perturbation and Observation (P&O) [E5] methods. We now present the results of the MPPT using these methods.

Using measured climatic data (G, T_a) of Medjez El Beb (Northern of Tunisia, latitude: 36.39º; longitude: 9.6º) during a typical day in July, the MPPT algorithms has been compared in terms of the PV power P_{mpp}, current I_{mpp}, voltage V_{mpp} and the duty cycle α deviations. The performance indexes are expressed by the Normalized Mean Bias Error (NMBE) and the Normalized Root-Mean-Square Error (NRMSE), given by (E.1) and (E.2) [E3]:

$$\mathrm{NMBE}(\%) = \frac{\sum_{i=1}^{N} \tilde{X}_i - X_i}{\sum_{i=1}^{N} X_i} * 100 \qquad \textbf{(E.1)}$$

$$\mathrm{NRMSE}(\%) = \frac{\sqrt{\frac{1}{N}\sum_{i=1}^{N}\left(\tilde{X}_i - X_i\right)^2}}{\frac{1}{N}\sum_{i=1}^{N} X_i} * 100 \qquad \textbf{(E.2)}$$

The results comparison of the studied MPP Tracking methods is presented in Figures E.1- E.3 and summarized in Tables E.1-E.3.

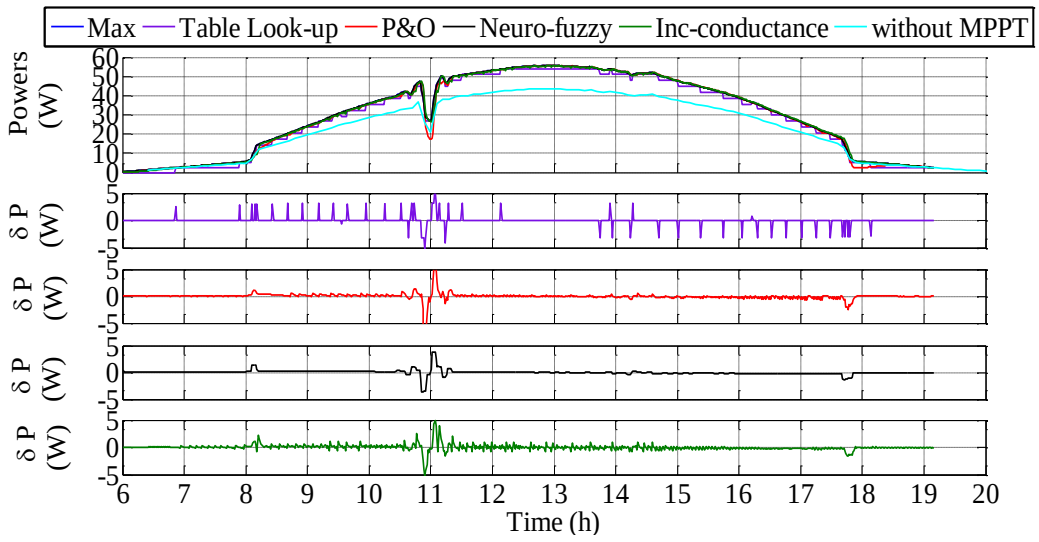

Figure E. 1 MPP Tracking algorithms results for the PV power

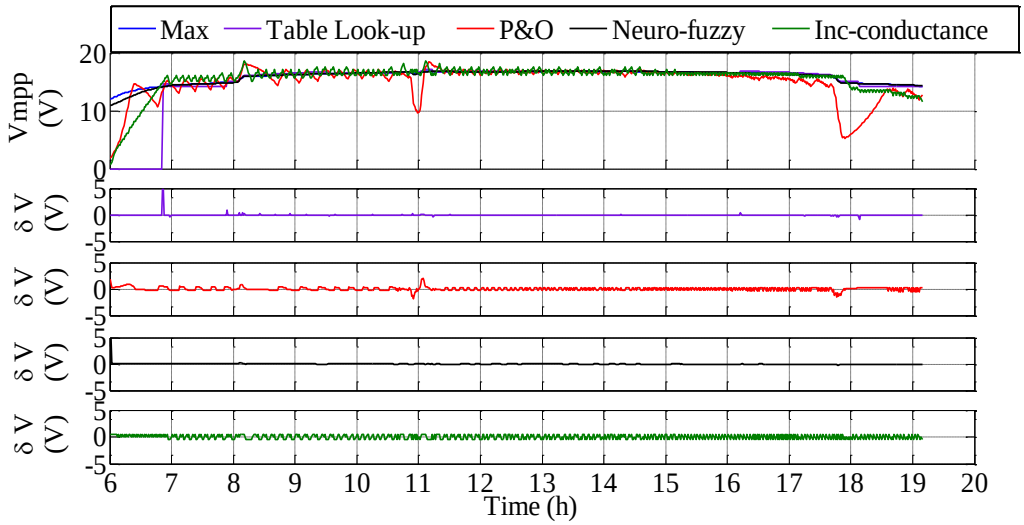

Figure E. 2 MPP Tracking algorithms results for the PV voltage

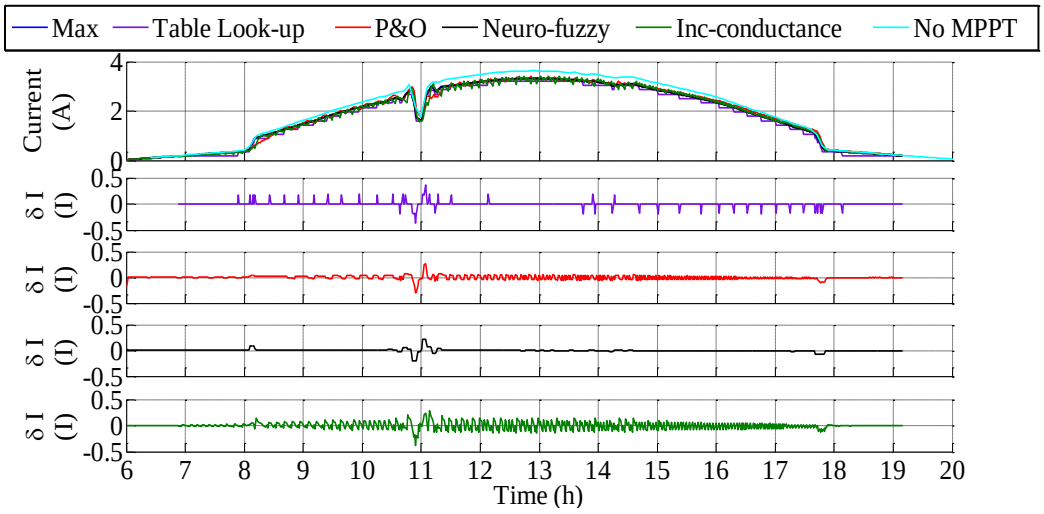

Figure E. 3 MPP Tracking algorithms results for the PV current

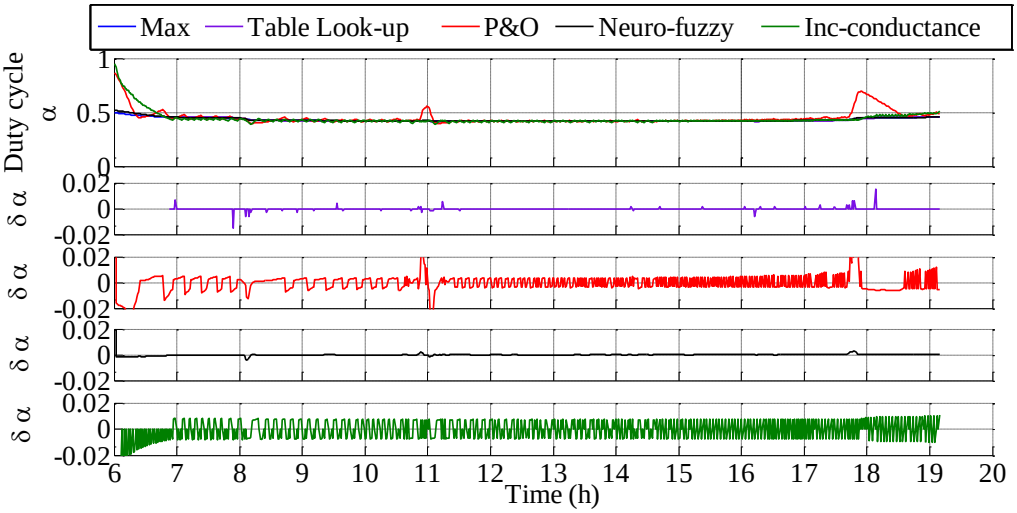

Figure E. 4 MPP Tracking algorithms results for the duty cycle α

TABLE E. 1 MPPT algorithms evaluation for PV power

MPPT method	**Power loss**		
	NMBE	NRMSE	P_{mpp} variation
Look-up Table	-3.8437%	4.9311%	0.0109%
Neuro-fuzzy	-1.0984%	6.5541%	0.0101%
Inc-cond	-0.4235%	1.6241%	0.0106%
P&O	-1.0725%	3.6982%	0.0096%

TABLE E. 2 MPPT algorithms evaluation for PV voltage

MPPT method	**Voltage loss**		
	NMBE	NRMSE	V_{mpp} variation
Look-up Table	0.2592%	1.2872%	0.1174%
Neuro-fuzzy	3.1273%	39.7398%	0.1002%
Inc-cond	-2.6232%	11.2374%	0.1292%
P&O	-4.8122%	13.4396%	0.0917%

Table E. 3 MPPT algorithms evaluation for PV current

MPPT method	**Current loss**		
	NMBE	NRMSE	I_{mpp} variation
Look-up Table	-4.6251%	5.5891%	0.0130%
Neuro-fuzzy	-2.9987%	33.2998%	0.0136%
Inc-cond	-0.0532%	3.3358%	0.0139%
P&O	0.7172%	3.2213%	0.0117%

The obtained results show that the Neuro-Fuzzy MPPT method presents the highest NRMSE error for the power, current, voltage and the duty cycle. This is due to the need of a continuous update for the database used for the data training. Although updated data are used for the Smart MPPT, its NMBE and NRMSE errors are more important than those of the Incremental Conductance or the P&O methods. This is because Smart MPPT uses the minimum values of G and T_a intervals, which makes the working point different from the real MPP.

The Incremental Conductance and the P&O present similar results. For instance, the NRMSE for the Incremental Conductance and the P&O are, respectively, 1.6241% and 3.6982% for the power; 3.3358% and 3.2213% for the current. Hence, the errors values are close. P&O MPPT method is easy in implementation, and characterized by a low cost in installation, compared of the Incremental Conductance [E6]. Since these errors will not cause a great difference for the power and current at the MPP, we choose to use the P&O in our application.

E.2 DC-DC Adaptation

The connection of a photovoltaic generator to a load requires an adaptation system, to ensure the operation at the maximum power point. This consists in varying the duty cycle of the DC-DC converter (chopper), which is interposed between the PV panel and the load. Figure E.5 shows the block diagram of the DC-DC adaptation of the PV generator to a load [E6].

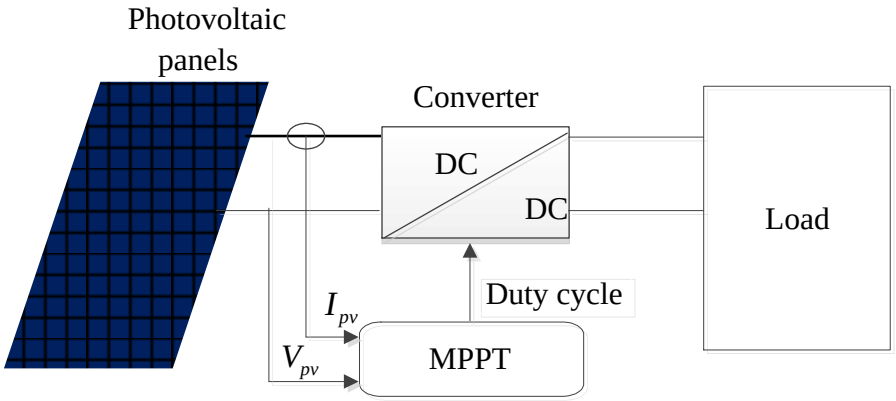

Figure E. 5 DC-DC adaptation of the PV generator to a load

The variation of the duty cycle used to control the chopper is performed by the MPPT algorithm. Hence, three types of choppers are possible: the buck for applications that needs to decrease the photovoltaic voltage, the boost for applications that require increasing the photovoltaic voltage and the buck-boost if the applications require operating in the two modes, buck and boost.

In our applications, the buck is the chopper used since the MPP voltage is higher than the load voltage. This DC-DC converter, characterized by low electric energy consumption and a high efficiency, comprises inductors, capacitors and electronic switches. For the buck choppers, the electronic switch more used is the MOSFET fast switch [E6]. Figure E.6 describes the buck circuit.

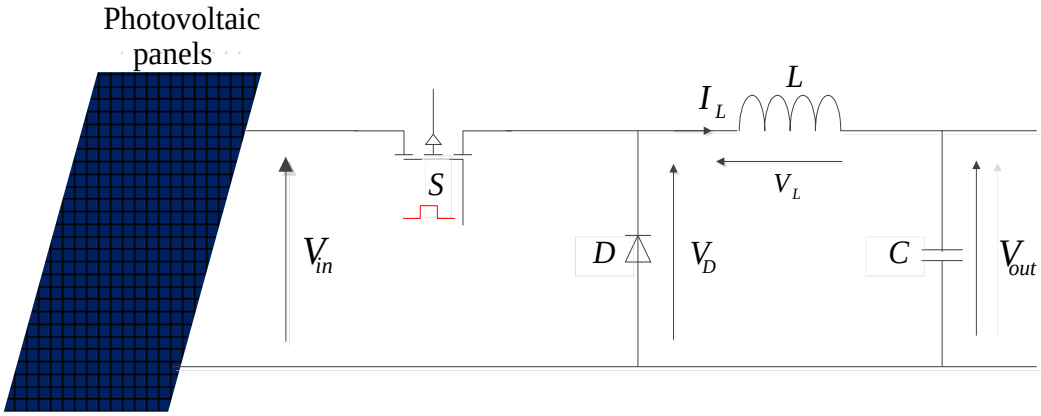

Figure E. 6 Buck circuit

E.3 Function Principle

The adaptation of the load with the solar panel is based in fixing the average voltage V_{out} at the output of the converter that meets the following criteria [E6]:

- $V_{out} \prec V_{pv}$.
- V_{out} is adjustable in the desired range.

The operation of the converter is deduced from the switch *S* behavior analysation. In fact, two operating phases can be distinguished [E6]:

- When the switch *S* is *on* during $0 \prec t \prec \alpha T$, the diode is reverse biased

($V_D = -V_{in}$) and $V_L = V_{in} - V_{out}$.

- When the switch *S* is *off* during $\alpha T \prec t \prec T$, then the diode is directly biased ($V_D = 0$) and $V_L = -V_{out}$.

Two operating modes can be distinguished, following the current $I_L(t)$ in the inductance *L*:

E.3.1 Continuous Operating Mode

During the continuous mode, the current $I_L(t)$ never reaches zero. The operating diagram of the buck chopper in the continuous mode is described by Figure E.7. The variation of $I_L(t)$ is given by [E6]:

$$V_L(t) = L\frac{dI_L(t)}{dt} \qquad \textbf{(E. 3)}$$

- When $0 \prec t \prec \alpha T$, the MOSFET *S* is saturated and the current $I_L(t)$ increases:

$$\Delta I_{L\,on}(t) = \int_0^{\alpha T} \frac{V_{pv} - V_{out}}{L}\,dt = \frac{V_{pv} - V_{out}}{L}\alpha T \qquad \textbf{(E. 4)}$$

- When $\alpha T \prec t \prec T$, the MOSFET *S* is blocked and $I_L(t)$ decreases:

$$\Delta I_{L\,off}(t) = \int_{\alpha T}^{T} \frac{-V_{out}}{L}\,dt = \frac{-V_{out}}{L}(T - \alpha T) \qquad \textbf{(E. 5)}$$

We consider that the current in the inductance when *S* is *on* or *off* is the same. Hence:

$$\Delta I_{L\,on} + \Delta I_{L\,off} = 0 \qquad \textbf{(E. 6)}$$

Using (E.2) and (E.3), we obtain:

$$V_{out} = \alpha V_{pv} \qquad \textbf{(E. 7)}$$

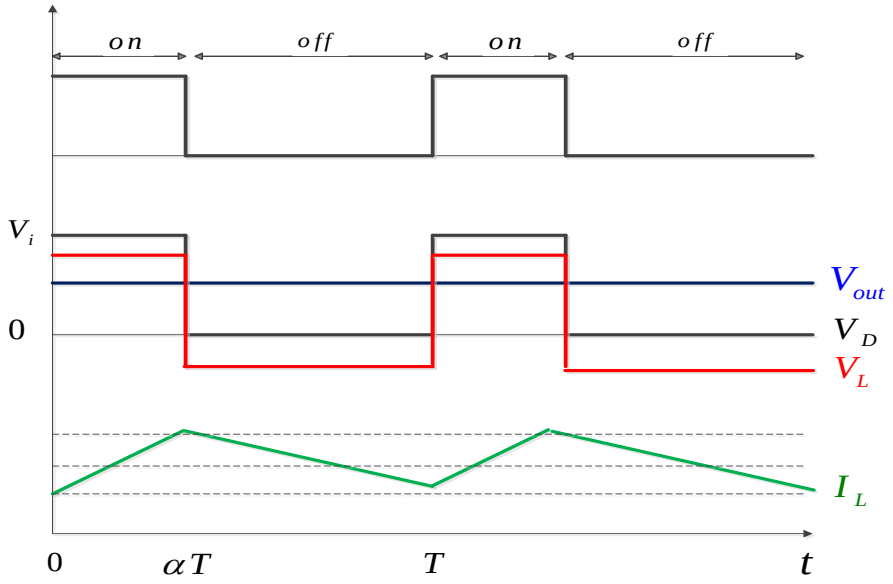

Figure E. 7 Ideal waves forms for the buck converter operating in the continuous mode

E.3.2 Discontinuous Operating Mode

During this mode, the current $I_L(t)$ reaches zero when the MOSFET is blocked (Figure E.8). The energy stocked in the inductance is zero. Using the principle given by (E.4), we have the following relation:

$$\left(V_{pv} - V_{out}\right)\alpha T - V_{out}\delta T = 0 \qquad \textbf{(E. 8)}$$

Thus:

$$\delta = \frac{V_{pv} - V_{out}}{V_{out}}\alpha \qquad \textbf{(E. 9)}$$

We suppose that the value of the capacity C is important that the mean value of the current in the capacity is zero. Hence:

$$\bar{I}_L = I_{out} \qquad \textbf{(E. 10)}$$

Using Figure E.4, the mean value of the inductance current $\bar{I}_L$ is given by:

$$\bar{I}_L = \frac{I_{L\,max}\left(\alpha + \delta\right)}{2} \qquad \textbf{(E. 11)}$$

Knowing that:

$$I_{L\,max} = \frac{V_{pv} - V_{out}}{L} \alpha T \qquad \textbf{(E. 12)}$$

We obtain:

$$V_{out} = V_{pv} \frac{1}{\frac{2LI_{out}}{\alpha^2 V_{pv} T} + 1} \qquad \textbf{(E. 13)}$$

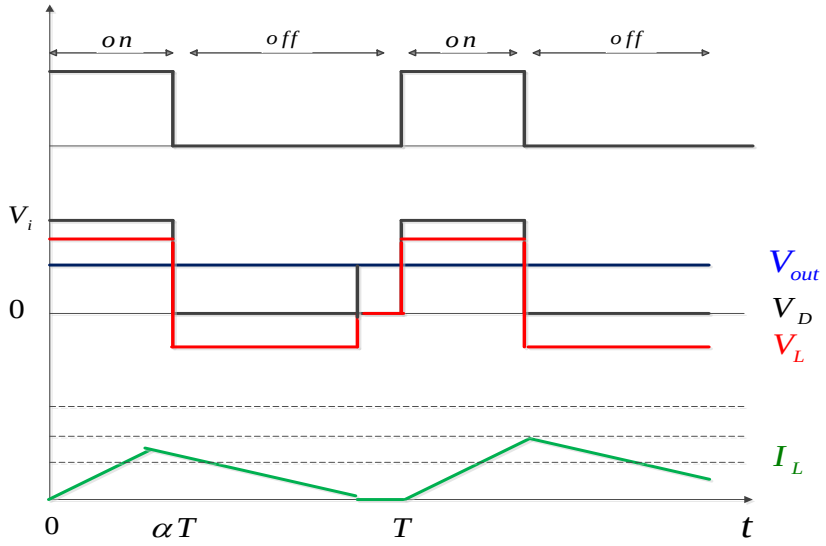

Figure E. 8 Ideal waves forms for the buck converter operating in the discontinuous mode

E.4 Chopper Design

Here, a Buck converter is designed (Table E.4). After the component selection, the design is simulated using SimPower.

Table E. 4 Design specification for the Buck converter

Specifications	**Values**
Input voltage	0-20 (V)
Input current	0-4.5 (A)
Output voltage	12V
Output current	5A
Maximum output power	60W
Switching frequency	50KHz
Duty cycle	$0.1 < \alpha < 0.5$

E.4.1 Inductor Selection

The selection of the inductor size depends on the rate of change in the inductor current. In fact, less than 5% in the current ripple is permitted. This current variation is expressed as follows [E7]:

$$\Delta i_L = \frac{V_{pv}\alpha}{Lf} \quad \textbf{(E. 14)}$$

where:

V_{pv} : the photovoltaic voltage (V),

α : the duty cycle,

f: the switching frequency (Hz).

Hence, the inductance value can be deduced by:

$$L = \frac{V_{pv}\alpha}{\Delta i_L f} \quad \textbf{(E. 15)}$$

E.4.2 Capacitor Selection

The design criterion for the capacitor is that the ripple voltage across it should be less than 5%. The average voltage across the capacitor *C* is given by (E. 14) [E7]:

$$\Delta V_C = 0.05\left(V_{pv} + V_{out}\right) \quad \textbf{(E. 16)}$$

The value of the capacity C is calculated with the following equation:

$$C = \frac{V_{out}\alpha}{Rf\,\Delta V_C} \quad \textbf{(E. 17)}$$

where R is the equivalent load resistance which is given by:

$$R = \frac{{V_{out}}^2}{P_{out}} \quad \textbf{(E. 18)}$$

E.4.3 Diode Selection

Schottky diode is selected since it has a low forward voltage and a good reverse recovery time (typically 5 to 10 ns) [E8]. The recurrent peak reverse voltage

V_{RRM} of the diode is the same as the voltage of the capacity *C*. Generally a 30 % of safety factor is used. The average diode forward current I_F

is the same as the output current. Hence, adding 30 % of safety factor gives the suitable I_F .

E.4.4 Switch Selection

Power-MOSFETs are used in low or medium power applications. The peak voltage of the switch is obtained by KVL on the circuit of Figure E.9.

$$V_{SW} = V_{pv} - \frac{dI_L}{dt} \qquad \textbf{(E. 19)}$$

The voltage of the switch SW reaches 20 V. Adding 30% of safety factor gives the suitable voltage for the SW. The peak current is the same as for the diode.

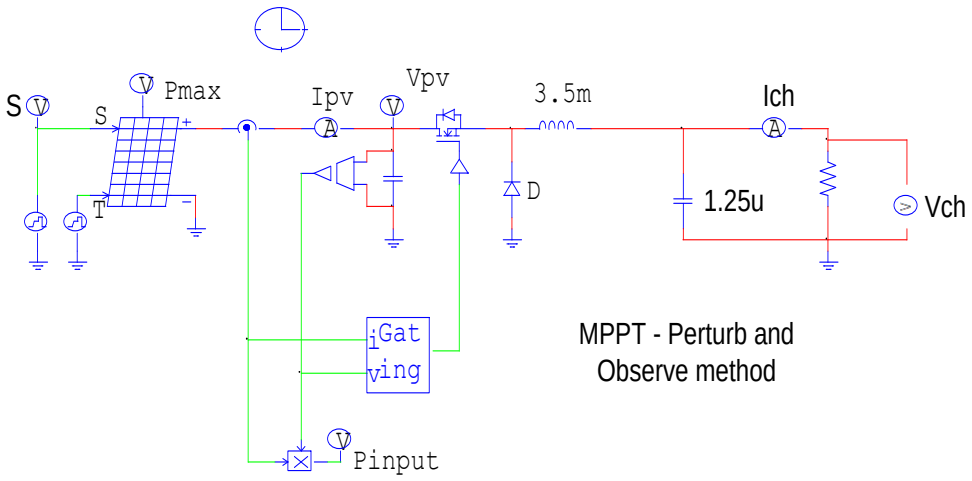

FigureE. 9 Simulation schema of the Buck chopper

E.5 Simulation Results

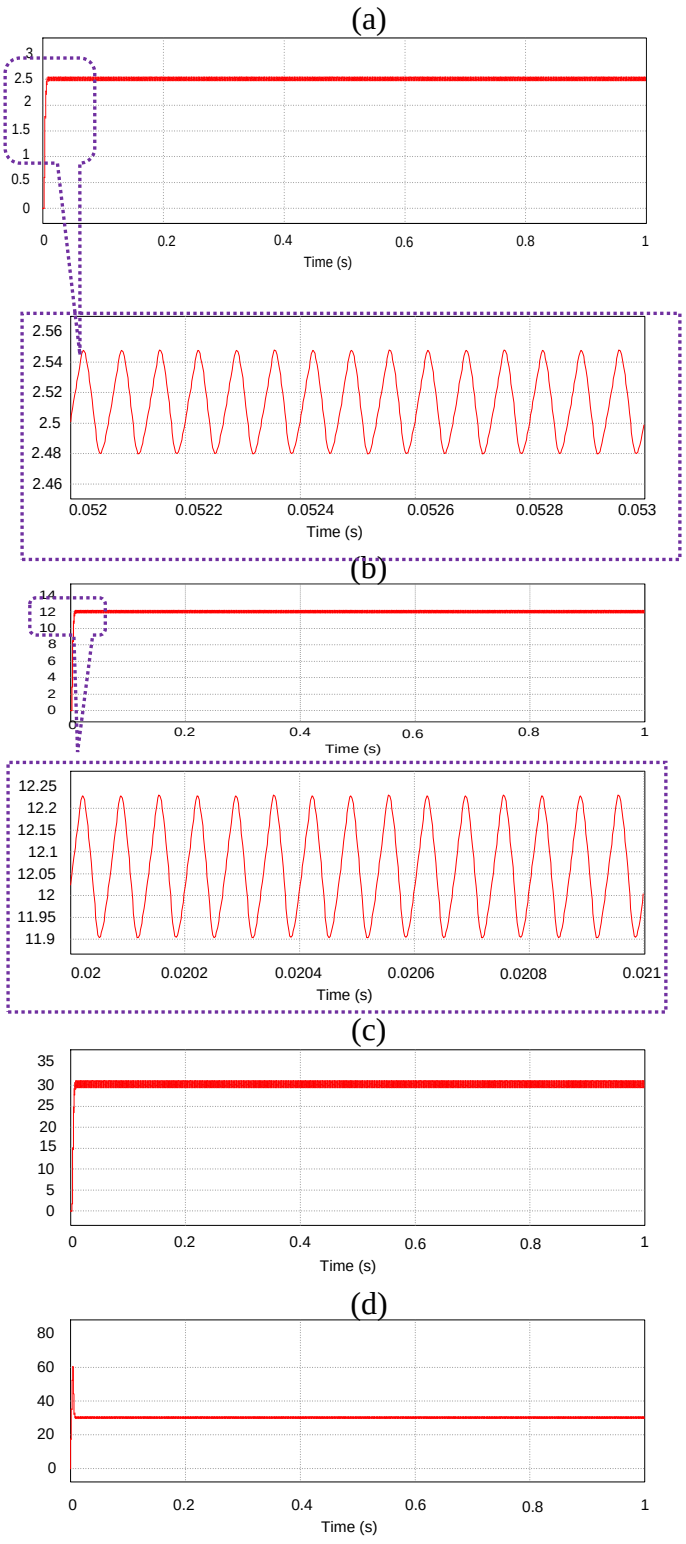

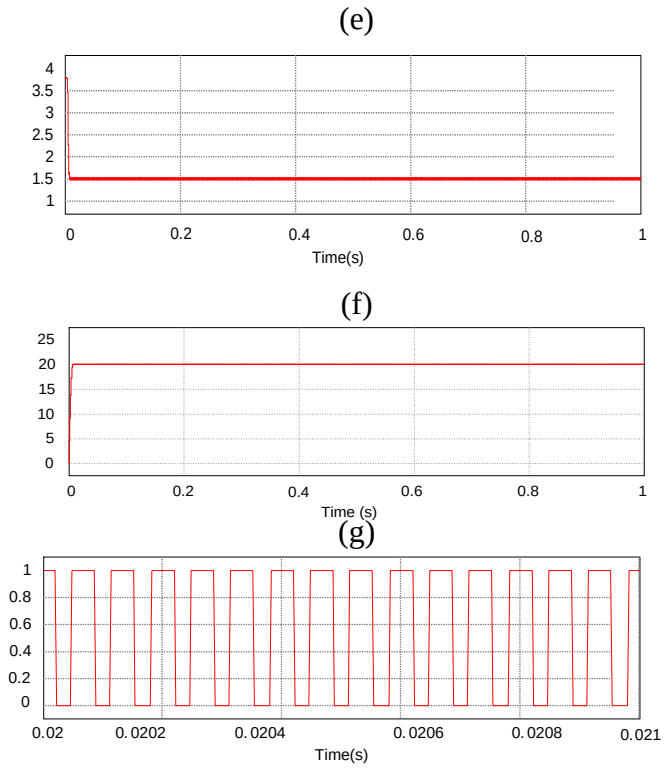

Figure E. 10 Results simulation for G =1000 W/m^2 , T_a =25°C: (a) load current, (b) load voltage, (c) load power, (d) panel power, (e) panel current, (f) panel voltage, (g) duty cycle

E.6 References

[E1] Hohm.D. P; &Ropp.M. E.(2000). "Comparative study of maximum power point tracking algorithms using an experimental, programmable, maximum power point tracking test bed". In the IEEE proceedings of the Photovoltaic specialists conference, 1699.

[E2] Hohm,D. P; & Ropp,M. E.(2000). "Comparative study of maximum power point tracking algorithms," Progress in photovoltaics. Research and Applications, 11, 47-62.

[E3] Charfi,Sana; &Chaabene, Maher. (2014). "A comparative study of MPPT techniques for PV systems".In the IEEE proceedings of the International Renewable Energy Congress (IREC), 22-28.

[E4] Veerachary,M; &Yadaiah,N. (2000). "ANN based peak power tracking for PV supplied DC motors". Solar Energy, 69, 343-350.

[E5] Femia, N; Petrone, G; Spagnuolo, G; &Vitelli, M.(2005)."Optimization of perturb and observe maximum power point tracking method". IEEE Transactions on Power Electronics, 20,963-973.

[E6] Ben Ammar, Mohsen. (2011). "Contribution à l'optimisation de la gestion des systèmes multi-sources d'énergies renouvelables". Thesis presented at the National Engineering School of Sfax (ENIS), Tunisia.

[E7] Akihiro Oi. (2005). "Design and simulation of photovoltaic and IC water pumping system". A master presented at the university of Faculty of California Polytechnic State University, San Luis Obispo, USA.

[E8] Taufik EE410 Power Electronics I - Lecture Note Cal Poly State University, SanLuis Obispo, 2004.

Appendix F: The Sensors

F.1 Current Sensor

LEM

Current Transducers HY 5..25-P

I_{PN} = 5 .. 25 A

For the electronic measurement of currents : DC, AC, pulsed, mixed, with a galvanic isolation between the primary circuit (high power) and the secondary circuit (electronic circuit).

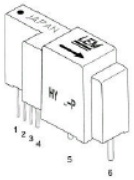

Electrical data

Primary nominal current rms I_{PN} (A)	Primary current, measuring range I_{PM} (A)	Primary conductor (mm)	Type	RoHS since date code
5	± 15	∅ 0.7	**HY 5-P**	45260
10	± 30	∅ 1.1	**HY 10-P**	45286
12.5	± 37.5	∅ 1.4	**HY 12-P**	45264
15	± 45	∅ 1.4	**HY 15-P**	45276
20	± 60	2 x ∅ 1.2 [1]	**HY 20-P**	46097
25	± 75	2 x ∅ 1.4 [1]	**HY 25-P**	45269

V_C	Supply voltage (± 5 %) [6]	± 12 .. 15	V
I_C	Current consumption	± 10	mA
$\hat{I}_P$	Overload capability (1 ms)	50 x I_{PN}	
V_d	Rms voltage for AC isolation test, 50 Hz, 1 min	2.5	kV
V_b	Rated isolation voltage rms	500 [2]	V
R_{IS}	Isolation resistance @ 500 VDC	> 1000	MΩ
V_{OUT}	Output voltage (Analog) @ + I_{PN}, R_L = 10 kΩ, T_A = 25°C	± 4	V
R_{OUT}	Output internal resistance	100	Ω
R_L	Load resistance	> 1	kΩ

Accuracy - Dynamic performance data

X	Accuracy @ I_{PN}, T_A = 25°C (excluding offset)	< ± 1	%
ε_L	Linearity error [3] (0 .. ± I_{PN})	< ± 1	% of I_{PN}
V_{OE}	Electrical offset voltage@ T_A = 25°C	< ± 40	mV
V_{OH}	Hysteresis offset voltage @ I_P = 0; after an excursion of 1 x I_{PN}	< ± 15	mV
TCV_{OE}	Temperature coefficient of V_{OE}	typ. ± 1.5	mV/K
		max. ± 3	mV/K
TCV_{OUT}	Temperature coefficient of V_{OUT} (% of reading)	< ± 0.1	%/K
t_r	Response time to 90% of I_{PN} step	< 3	µs
di/dt	di/dt accurately followed	> 50	A/µs
BW	Frequency bandwidth [4] (- 3 dB)	DC .. 50	kHz

General data

T_A	Ambient operating temperature	- 10 .. + 80	°C
T_S	Ambient storage temperature	- 25 .. + 85	°C
m	Mass	< 14	g
	Standards [5]	EN 50178: 1997	

Notes : [1] Conductor terminals are soldered together.
[2] Pollution class 2, overvoltage category III.
[3] Linearity data exclude the electrical offset.
[4] Please refer to derating curves in the technical file to avoid excessive core heating at high frequency.
[5] Please consult characterisation report for more technical details and application advice.
[6] Operating at ±12V ≤ Vc < ±15V will reduce measuring range.

Features

- Hall effect measuring principle
- Galvanic isolation between primary and secondary circuit
- Isolation voltage 2500 V~
- Compact design for PCB mounting
- Low power consumption
- Extended measuring range (3 x I_{PN})
- Insulated plastic case recognized according to UL 94-V0.

Advantages

- Easy mounting
- Small size and space saving
- Only one design for wide current ratings range
- High immunity to external interference.

Applications

- Static converters for DC motor drives
- Switched Mode Power Supplies (SMPS).
- AC variable speed drives
- Uninterruptible Power Supplies (UPS)
- Battery supplied applications
- General purpose inverters

Application domain

- Industrial

Dimensions HY 5..25-P (in mm. 1 mm = 0.0394 inch)

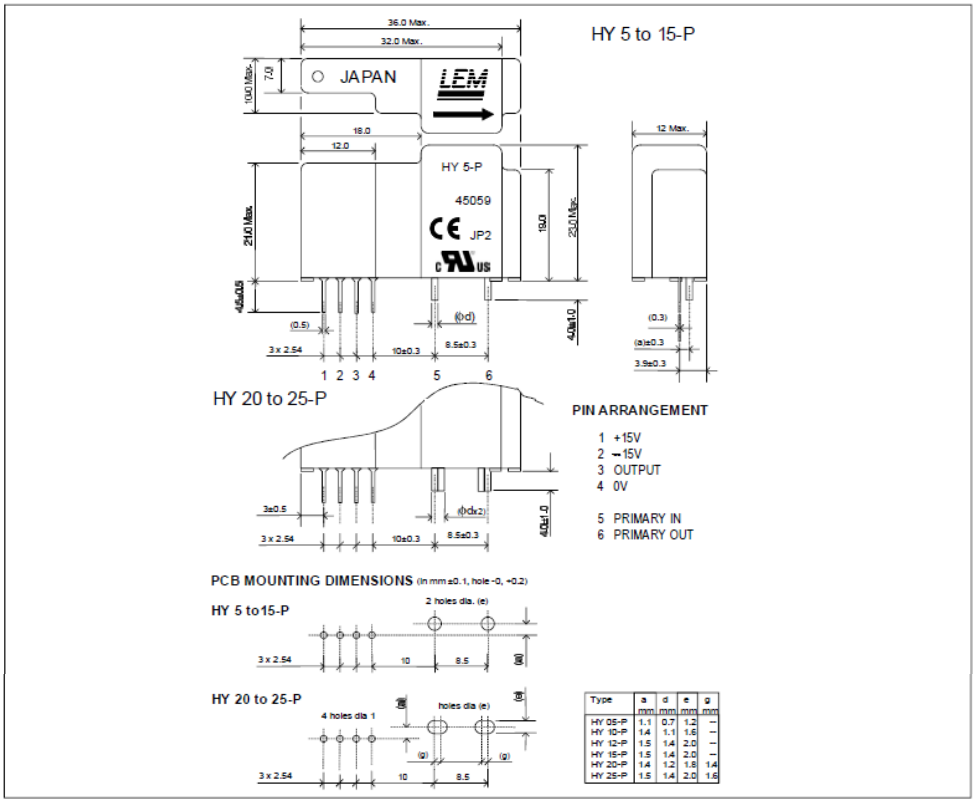

Type	a mm	d mm	e mm	g mm
HY 05-P	1.1	0.7	1.2	--
HY 10-P	1.4	1.1	1.6	--
HY 12-P	1.5	1.4	2.0	--
HY 15-P	1.5	1.4	2.0	--
HY 20-P	1.4	1.2	1.8	1.4
HY 25-P	1.5	1.4	2.0	1.6

Safety

This transducer must be used in electric/electronic equipment with respect to applicable standards and safety requirements in accordance with the following manufacturer's operating instructions.

Caution, risk of electrical shock

When operating the transducer, certain parts of the module can carry hazardous voltage (eg. primary busbar, power supply). Ignoring this warning can lead to injury and/or cause serious damage.
This transducer is a built-in device, whose conducting parts must be inaccessible after installation.
A protective housing or additional shield could be used.
Main supply must be able to be disconnected.

F.2 Pressure Sensor

GRUNDFOS **DATA SHEET**

DPI 0 - 1.0

Differential pressuresensor, Industry, 0 - 1.0 bar

TM04 9034 2909

Fig. 1 DPI sensor

Technical overview

Grundfos Direct Sensors ™ , type DPI, is a series of differential pressure sensors for industry. The DPI sensors are compatible with wet, aggressive media and are available for differential pressure ranges of 0 - 0.6 up to 0 - 10 bar.

The DPI sensor utilises MEMS sensing technology in combination with a novel packaging concept using corrosion-resistant coating on the MEMS sensing element. This makes the DPI sensor very robust and ideal for pump integration and monitoring in harsh environments.

Applications

- Pump and pump control systems
- Filters (monitoring)
- Cooling and temperature control systems
- Water treatment systems
- Boiler control systems
- Renewable energy systems
- Heat exchanger efficiency (monitoring of fouling).

Features

- Pressure ranges: 0 - 0.6; 0 - 1; 0 - 1.2; 0 - 1.6; 0 - 2.5; 0 - 4; 0 - 6 and 0 - 10 bar differential pressure
- Designed for harsh environments
- Analogue output signal
- Compact and well proven design
- MEMS sensing technology
- Approved for the EU, US and Canadian markets.

Benefits

- Compatible with wet, aggressive media
- Accurate, linearised output signal
- Cost-effective and robust design.

Specifications

Pressure	
Measuring range (differential)	1.0 bar
Accuracy (IEC 61298-2)	2 % FS
Response time	< 0.5 s
Static Pressure P_1	16 bar
Static Pressure P_2	10 bar
Max system pressure	16 bar
Media and environment	
Media	Liquids, gasses and air
Media temperature (operation)	–10 to +70 °C
Media temperature (peak)	up to +80 °C
Ambient air temperature	–40 to +70 °C
Ambient air temperature (peak)	–55 to +90 °C
Humidity	0 to 95 % (relative), non-condensing
System burst pressure	25 bar
Electrical data	
Power supply	12-30 VDC
Output signals	4-20 mA
Load impedance	24 V max. 500 kΩ 16 V max. 200 kΩ 12 V max. 100 kΩ
Sensor materials	
Sensing element	Silicon-based MEMS sensor
Seal	FKM rubber
Housing	DIN W.-Nr. 1.4305
Wetted materials	FKM and PPS
Environmental standards	
Enclosure class	IP55
Temperature cycling	IEC 68-2-14
Vibration (non-destructive)	20 to 2000 Hz, 10G, 4h
Immunity	EN 61000-6-2
Emission	EN 61000-6-3
Weight	550 g

Flow compensated differential pressure control

(SPR Reglung)

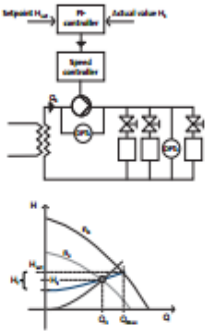

TM03 0311 5004

Fig. 2 SPR Reglung

If the equipment is used in a manner not specified by the manufacturer, the protection provided by the equipment may be impaired.

BE › THINK › INNOVATE ›

GRUNDFOS

Dimensions [mm]

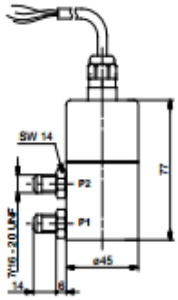

TM03 2059 3505

Fig. 3 Dimensional sketch

Output signals

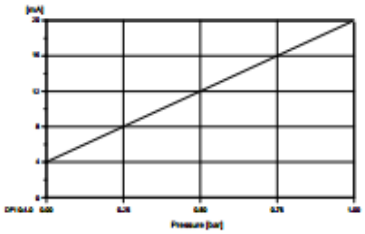

TM00 4510 4609

Fig. 4 Differential pressure response

Electrical connections

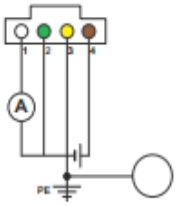

TM04 0570 0808

Fig. 5 Electrical connections

Pin configuration		Colour
1	Test conductor (can be cut off during mounting). Do not connect this conductor to the voltage supply.	White
2	Signal conductor	Green
3	GND (earth conductor)	Yellow
4	12-30 V supply voltage	Brown

Sensor Interface type SI 001 PSU

Power supply and amplifier for cables above 30 m and 2 wire connection of 400 VAC

TM04 4194 0809

Fig. 6 Sensor Interface, SI 001 PSU

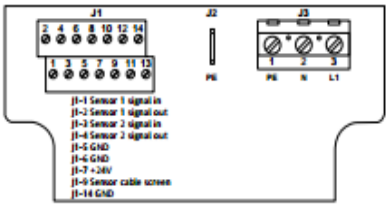

TM04 4131 0809

Fig. 7 Connections for power supply / amplifier

Part
Sensor Interface, SI 001 PSU

Accessories

Pos.	Component		
A	Fitting 6 mm	AISI 316	Tube connection
	Fitting 8 mm		
	Fitting 6 mm		Cutting ring
	Fitting 8 mm		
B	Cable for DPI 5.0 m		
	Cable for DPI 10.0 m		
	Wall bracket for sensor		

Type key

The DPI sensor is labelled with a type designation.

	96573681	- XX	- XXX	XXXXX
Product number				
Version				
Production year and week				
Consecutive number				

For more information, see
http://www.grundfos.com/directsensors.

Subject to alterations.

96985440 1109 GB

Grundfos Sensor A/S
Poul Due Jensens Vej 7. DK-8850 Bjerringbro. Denmark
Telephone: +45 87 50 14 00

www.grundfos.com\directsensors

GRUNDFOS

Appendix G: The Programmable Power Supply

velleman®

PS3005D

PROGRAMMABLE DC LAB POWER SUPPLY 0-30V/5A – DUAL LED DISPLAY
LABORATORIUMVOEDING 0-30V / 5A – DUBBELE LED DISPLAY
ALIMENTATION DE LABORATOIRE 0-30V / 5A – DOUBLE AFFICHEUR LED
FUENTE DE ALIMENTACIÓN PARA LABORATORIO 0-30V / 5A – DOBLE DISPLAY LED
LABORNETZGERÄT 0-30V / 5A – LED-DOPPELANZEIGE

CE

Appendix H: The Inverter

STUDER Innotec SA **AJ**

TECHNICAL DATA

Model		AJ 275-12	AJ 350-24	AJ400-48	AJ 500-12	AJ 600-24	AJ 700-48
Inverter							
Nominal battery voltage		12Vdc	24Vdc	48Vdc	12Vdc	24Vdc	48Vdc
Input voltage range		10.5 – 16Vdc (24Vdc max.)	21 – 32Vdc (44Vdc max.)	42 – 64Vdc (24Vdc max.)	10.5 – 16Vdc (20Vdc max.)	21 – 32Vdc (40Vdc max)	42 – 64Vdc (24Vdc max.)
Continous power at 25ºC		200VA	300VA	300VA	400VA	500VA	500VA
Power 30 min. at 25ºC		275VA	350VA	400VA	500VA	600VA	700VA
Power 5 min. at 25ºC		350VA	500VA	600VA	575VA	675VA	900VA
Power 5 sec.at 25ºC		450VA	650VA	1000VA	1000VA	1200VA	1400VA
Maximum asymmetric load		150VA	150VA	200VA	250VA	300VA	300VA
Max. efficiency (%)		93%	94%	94%	93%	94%	94%
Cos φ max.		0.1 – 1 up to 200VA	0.1 – 1 up to 300VA	0.1 – 1 up to 300VA	0.1 – 1 up to 400VA	0.1 – 1 up to 500VA	0.1 – 1 up to 500VA
Detection of the load		2W (only with the solar option –S)			Adjustable: 1 → 20W		
Current of chort-circuit 2 sec. (exit)		2.3Aac (4.6Aac*)	3.2Aac (6.4Aac*)	4.6Aac (9.2Aac*)	5.2Aac (10Aac*)	5.7Aac (11.4Aac*)	7Aac (14Aac*)
Output voltage		Sine wave 230Vac (120Vac*) ±5%					
Frequency		50Hz (60Hz*) ±0.05% (crystal controlled)					
Distortion THD (resistive load)		< 5% (at Pnom. & Uin nom.)					
Consumption Stand-by		0.3W**	0.5W**	1.1W**	0.4W	0.6W	1.5W
Consumption „ON" no load		2.4W	3.5W	5.2W	4.6W	7.2W	12W
Overheat protection (±5ºC)		Shut down at 75ºC, Auto-restart at 70ºC					
Overload and short circuit protection		Automatic disconnection with 2 restart attempts					
Reverse polarity protection by internal fuse		60A	40A	25A	120A	90A	60A
Deep discharge battery protection		Shut off at 0.87 x Unom, Automatic restart at Unom.					
Max. battery voltage		Shut off at >1.33 x Unom, Automatic restart at < Umax					
Acoustic alarm		Before low battery or overheating disconnection					
General data							
Weight		2.4 kg	2.6 kg		4.5 kg		
Dimensions hxwxl (mm)		142x163x84			142x240x84		
Protection index IP		IP 30 conforms to DIN 40050					
Certification ECE-R 10 (E24)		•	•	Not available	•	•	Not available
EC confirmity		EN 61000-6-1, EN 61000-6-3, EN 55014, EN 55022, EN 60950-1					
Operating temperature		-20ºC up to +50ºC					
Relative humidity in operation		95% without condensation					
Ventilation forced		From 45ºC ±5ºC					
Acoustic level		< 45 dB (with ventilation)					
Warranty		5 years					
Approximate correction of Pnom		-1.5%/ºC as from +25ºC					
Recommended battery capacity		> 5 x Pnom/Unom (recommended value in Ah)					
Length cables (Battery/left AC)		1.2m /1m		1.5m / 1m			
Options		**AJ 275-12**	**AJ 350-24**	**AJ400-48**	**AJ 500-12**	**AJ 600-24**	**AJ 700-48**
Solar regulator	Voltage max	25Vdc	45Vdc	90Vdc	25 Vdc	45Vdc	90Vdc
	Current max.	10Adc			15Adc		
	Principle	3 floating stages (I/U/UO)					
	Absorption voltage	14.4Vdc	28.8Vdc	57.6Vdc	14.4Vdc	28.8Vdc	57.6Vdc
	Floating voltage	13.6Vdc	27.2Vdc	54.4Vdc	13.6Vdc	27.2Vdc	54.4Vdc
Plug for remote control (RCM)		•	•	•	•	•	•

Appendix I: The Acquisition Card

Table 17. 8-channel differential mode

Pin	Signal Name	Pin	Signal Name
1	LLGND	51	FIRSTPORTA Bit 0
2	CH0 HI	52	FIRSTPORTA Bit 1
3	CH0 LO	53	FIRSTPORTA Bit 2
4	CH1 HI	54	FIRSTPORTA Bit 3
5	CH1 LO	55	FIRSTPORTA Bit 4
6	CH2 HI	56	FIRSTPORTA Bit 5
7	CH2 LO	57	FIRSTPORTA Bit 6
8	CH3 HI	58	FIRSTPORTA Bit 7
9	CH3 LO	59	FIRSTPORTB Bit 0
10	CH4 HI	60	FIRSTPORTB Bit 1
11	CH4 LO	61	FIRSTPORTB Bit 2
12	CH5 HI	62	FIRSTPORTB Bit 3
13	CH5 LO	63	FIRSTPORTB Bit 4
14	CH6 HI	64	FIRSTPORTB Bit 5
15	CH6 LO	65	FIRSTPORTB Bit 6
16	CH7 HI	66	FIRSTPORTB Bit 7
17	CH7 LO	67	FIRSTPORTC Bit 0
18	LLGND	68	FIRSTPORTC Bit 1
19	N/C	69	FIRSTPORTC Bit 2
20	N/C	70	FIRSTPORTC Bit 3
21	N/C	71	FIRSTPORTC Bit 4
22	N/C	72	FIRSTPORTC Bit 5
23	N/C	73	FIRSTPORTC Bit 6
24	N/C	74	FIRSTPORTC Bit 7
25	N/C	75	N/C
26	N/C	76	N/C
27	N/C	77	N/C
28	N/C	78	N/C
29	N/C	79	N/C
30	N/C	80	N/C
31	N/C	81	N/C
32	N/C	82	N/C
33	N/C	83	N/C
34	N/C	84	N/C
35	D/A GND 0	85	N/C
36	D/A OUT 0	86	N/C
37	D/A GND 1	87	N/C
38	D/A OUT 1	88	N/C
39	CTR4 CLK	89	GND
40	CTR4 GATE	90	+12 V
41	CTR4 OUT	91	GND
42	A/D EXTERNAL PACER	92	-12 V
43	ANALOG TRIGGER IN	93	N/C
44	D/A EXTERNAL PACER IN	94	N/C
45	A/D EXTERNAL TRIGGER IN	95	A/D INTERNAL PACER OUTPUT
46	N/C	96	D/A INTERNAL PACER OUTPUT
47	N/C	97	EXTERNAL D/A PACER GATE
48	PC +5 V	98	N/C
49	SSH OUT	99	EXTERNAL INTERRUPT
50	GND	100	GND

Appendix J

List of Figures

List of Tables

List of Symbols

❖ ***Capitals:***

A_c : Ammount of clouds per day (%)

C_b : the battery cost (€),

C_{bat} : the nominal capacity for one battery (Ah),

C_{chop} : the chopper cost (€),

C_i : the inverter cost (€),

Cost: the installation cost (€),

C_p : Peukert capacity (A.h),

C_{pv} : the photovoltaic module cost (€),

C_R : the stored charge in the battery (Ah),

DA_i : the ratio between diffuse and global daily solar radiation,

D: the interval of the *dod*,

$\mathcal{D}$: the fuzzified interval of the *dod*,

E_{AM} : the extracted energy in the moring (Wh),

E_c : the charged energy (Wh),

EC_e : the crop salt tolerance (dS. m^{-1}).

EC_w : the electrical conductivity of the irrigation water (dS. m^{-1}),

E_d : the daily consumption (Wh),

E_e : the extracted energy (Wh)

E_{PM} : the extracted energy in the afternoon (Wh),

E_{To}: the monthly reference evapotranspiration average

F: the power difference interval,

$\tilde{F}$: the fuzzified power difference interval,

G_{sc}: the extraterrestal solar constant (W/m²),

G_{ref}: the solar radiation at reference conditions (W/m^2),

H: the hourly global solar radiation (W/m²),

$\overline{H}$: the monthly average of the solar radiation on a horizontal plane (W/ m^2),

$H_b(t,d)$: the direct solar radiation (W/ m^2),

H_d: the hourly diffused solar radiation (W/ m^2),

$\overline{H_d}$: the diffused solar radiation (W/ m^2),

H_h: the head height (m),

H_t: the total daily solar radiation in a tilted panel (W/ m^2),

$\overline{H_{t_i}}$: the solar energy for the month M using the clear database (Wh),

H_0: the extraterrestrial solar radiation (W/ m^2),

I_{bat}: the battery' bank current (A),

$I_c(t)$: the estimated photovoltaic cell current (A),

$I_{ph}(t)$: the generated photo-current at a given irradiance G (A),

I_{pump}: the pump current (A),

$I_r(t)$: the reverse saturation current for a given temperature T_a (A),

$I_{r\_T_{ref}}$: the reverse saturation current for the reference temperature T_{ref} (A),

$I_{sc}(t)$: the short circuit current for a given temperature T_a (A),

$I_{sc\_T_{ref}}$: the short circuit current per cell at the reference temperature (A),

I_{rd} : the rotor current in the direct axe (A),

I_{rq} : the rotor current in the quadrature axe (A),

I_{sd} : the stator current in the direct axe (A),

I_{sq} : the stator current in the quadrature axe (A),

K : the correction factor for the water volume needed for irrigation,

K_t : the clearness index,

K_B : Boltzmann coefficient (J/K),

L: the water volume in the reservoir (m^3)

L_r : the cyclic inductance of the rotor (H),

L_s : the cyclic inductance of the stator (H),

$\mathcal{L}$: the fuzzified interval of the watervolume in the reservoir (m^3),

L_R : the leaching fraction given by the humidity that remains in the soil,

M: the month,

M_{bat} : the maintenance cost for one battery (€),

M_{chop} : the maintenance cost for one chopper (€),

M_{inv} : the maintenance cost for one inverter (€),

M_{pv} : the photovoltaic module maintenance cost (€),

O: the interval for the relays switching ‘control,

$\mathcal{O}$: the fuzzified interval for the relays switching ‘control,

P_{pvi} : the initial photovoltaic power (W),

R_b : the relay that link the panels to the battery’bank,

R'_b : the ratio of the direct radiation on the tilted panel and the direct radiation on the horizontal panel,

R_e: the end resistance (Ω),

R_l: the relay that links the panels to the pump,

R_{lb}: the relay that links the battery'bank to the pump,

R_p: the parallel resistance of the photovoltaic module (Ω),

R_{rr}: the rotor resistance (Ω),

R_s: the serial resistance of the photovoltaic module (Ω),

R_{ss}: the stator resistance (Ω),

R'_s: the surface resistance (Ω).

R_t: the terminal resistance (Ω),

S: the panel surface (m^2),

S_i: the initial panel surface (m^2),

S_M: the optimum panels surface for month M (m^2),

S_{pvopt}: the optimum panel'surface (m^2),

S_{pvm}: the surface of a photovoltaic module (m^2),

S_{std}: the standard panels surface (m²),

T: the mean monthly air temperature T (°C),

$T_a(t)$: the ambient temperature at the panel surface (K),

$T_c(t)$: the cell temperature (ºC),

$T_{max}(d)$: the maximum tempeartue for a day d (°C),

$T_{min}(d)$: the minimum tempeartue for a day d (°C),

T_{ref}: the reference temperature at the panel surface (K),

TF_{annual}: the Annual Transposition Factor (%),

$TF_{monthly}$: the Monthly Transposition Factor (%),

V: the pumped water volume (m^3),

$\mathcal{V}$: the fuzzified water volume interval,

V_{bat} : the battery bank' voltage (V),

$V_c(t)$: the open circuit voltage of the photovoltaic cell (V),

$V_{c\_T_{ref}}$: the open circuit voltage per cell at the reference temperature (V),

V_g : the Gap energy (e. V),

V_n : the daily water volume (m^3),

V_{pumped} : the possible daily water volume pumped in the month M (m^3),

$V_{reservoir}$: the reservoir volume (m^3),

$V_{t\_T_a}$: the thermal potential at the ambient temperature (V),

W_{pv} : the daily solar energy (Wh/ m^2),

W_{pvc_i} : the solar energy for the month M using the clear sky model (Wh),

X: the photovoltaic power interval (W),

$\mathcal{X}$: the fuzzified photovoltaic power interval (W),

❖ ***Lower case:***

a : the temperature coefficient for the short circuit current (K^{-1}),

d: the fuzzy variable assigned for the *dod*,

d_{aut} : the days of the battery bank autonomy,

dod : the battery' bank depth of discharge,

dod_{min} : the minimum *dod* level,

dod_{max} : the maximum *dod* level,

d_{rech} : the days needed to recharge the battery bank,

f: the fuzzy variable assigned for the power difference,

g : the gravity acceleration (m/s^2),

l_f : leaching efficiency coefficient as a function of the irrigation water applied,

k_c : the seasonal crop coefficient,

k_p : Peukert coefficient,

l: the fuzzy variable assigned for the water volume in the reservoir,

m: the fuzzy variable assigned for the month M,

n : the panel' quality factor,

n_{bat} : the batteries number,

$n_{bat_{opt}}$: the optimum battery number,

n_{bat_M} : the batteries' number for the month M,

$n_{bat_{std}}$: the number of batteris with standard sizing algorithms,

n_c : the number of consecutive cloudy days per month,

n_{chop} : the choppers number,

n_{M_i} : the days number in the month M,

n_p : the number of parallel photovoltaic modules,

n_{pv} : the number of photovoltaic modules,

n_s : the number of serial photovoltaic cells,

n_y : the years' number for the installation life time,

p : the total daytime hours in the year,

p: the number of poles pairs of the IM,

q : the electron charge (C),

r_b : the control signal for the relay R_b ,

r_d : the ratio of the hourly to daily total diffuse solar radiation,

r_m : the average monthly rain volume (m^3),

r_l : the control signal for the relay R_l ,

r_{lb} : the control signal for the relay R_{lb} ,

$r_t(t,d)$: the ratio of the hourly to the daily total global solar radiation,

t_{sr} : the time of sunrise (h),

t_{ss} : the time of sunset (h),

t_{on} : the time when the panel produces an excess of energy (h),

t_{ed} : the time when the water extraction ends (h),

t_{sd} : the time when the water extraction starts (h),

v: the fuzzy variable assigned for the fuzzified water volume in the reservoir,

v_{sd} : the stator voltage in the direct axe (V),

v_{sq} : the stator voltage in the quadrature axe (V),

w : the hour angle of the sun (°),

x : the fuzzy variable assigned for the photovoltaic power,

y_{bat} : the number of batteries replace during n_y years,

y_{chop} : the number of chopper replace during n_y years,

y_{inv} : the number of the inverter replace during n_y years,

❖ ***Greek letters:***

ρ : the albedo of the soil,

β : the panel declination (°),

β_{pv} : the temperature coefficient for the panel yield ($°C^{-1}$),

θ : the radiation incidence angle (°),

θ_z : the zenith angle of the sun (°),

η : the quotient between the charged and the extracted energies, fixed in the sizingalgorithm,

η_1 : the quotient between the charged and extracted energies obtained by the sizing algorithm using estimated solar radiation (%),

η_{bat} : the electrical efficiency of the battery bank (%),

η_{erreur} : the coefficient of the error between the estimated and measured values of the photovoltaic power (%),

η_{exp} : the quotient of the charged and the extracted energies using measured solar radiation (%),

η_{inv} : the inverter performance (%),

$\eta_{matching}$: the panel matching performance (%),

η_l : the electrical efficiency of the installation (%),

$\eta_{opt\,ther}$: the panel performance facing to optical and thermal effects (%),

η_p : the pump efficiency (%),

η_{pv} : the efficiency of each photovoltaic panel (%),

η_r : the panel yield at the reference temperature (%),

η_{reg} : the regulator performance (%),

φ_{rd} : the rotor flux in the direct axe (Wb),

φ_{rq} : the rotor flux in the quadrature axe (Wb),

ρ : the water density(Kg/ m^3),

Δt : the pumping duration (h),

Δdod_{max} :the maximum dod variation (%).

Δ_{irg} : the duration of the irrigation (h),

ΔP : the power difference (W),

Δt_{bat} : the duration of discharging totally the battery (h),

$\mu_L(x)$, $\mu_M(x)$ and $\mu_H(x)$ are, respectively, the low, medium and high membership functions at the measured power level*x*.

$\mu_{dL}(d)$, $\mu_{dM}(d)$ and $\mu_{dH}(d)$ are, respectively, the low, medium and high membership functions of the estimated dod d .

$\mu_{vL}(v)$, $\mu_{vM}(v)$ and $\mu_{vH}(v)$ are, respectively, the the low, medium and high membership functions of v,

$\mu_{fL}(f)$ and $\mu_{fH}(f)$ are respectively, the low and highmembership functions of the power difference ΔP

$\mu_{m_i}(m)$ is the membership functions corresponding to the month m,

$\mu_{l_i}(l)$ is the membership function corresponding to l_i evaluated at l.

$\mu_{off\, r_l, r_b, r_{lb}}(o_{0z}), \mu_{on\, r_l, r_b, r_{lb}}(o_{0z})$ are the switching controls given to the relays and evaluated at o.

m: the mutual inductance stator-rotor (H),

w_g : the rotor pulsations (rad. s^{-1}).

List of Acronyms

AC: Alternating Current,

ANN: Artificial Neural Network,

DC: Direct Current,

FMA: Fuzzy Management Algorithm,

IM: Induction Machine,

MPPT: Maximum Power Point Tracking,

NOCT: Nominal Operating Cell Temperature,

NMBE: Normalized Mean Bias Error,

NRMSE: Normalized Root-Mean-Square Error,

PMSG: Permanent Magnet Synchronous Generators,

PPEWPS: Photovoltaic Powered Electric Water Pumping Systems,

PPS: Programmable Power Supply,

PWM: Pulse Widh Modulation,

P&O: Perturb and Observe,

RFOC: Rotor Field Oriented Control,

SPV: Solar Photovoltaic,

WPEWPS: Wind Powered Electric Water Pumping Systems,

List of Websites

COMPASS: www.lorentz1.software.informer.com/

HOMER: www.users.homerenergy.com

NASA: www.eosweb.larc.nasa.gov

PVsyst: www.pvsyst.com/fr

Rapsim: www.sourceforge.net/projects/rapsim/files/latest

Retscreen: www.retscreen.net/fr/home.php